Fall 2013

Top-Down Interrogation And Characterization Of Biological Macromolecules

Yang Gao
Purdue University

Graduate School ETD Form 9
(Revised 12/07)

PURDUE UNIVERSITY
GRADUATE SCHOOL
Thesis/Dissertation Acceptance

This is to certify that the thesis/dissertation prepared

By Yang Gao

Entitled TOP-DOWN INTERROGATION AND CHARACTERIZATION OF BIOLOGICAL MACROMOLECULES

For the degree of Doctor of Philosophy

Is approved by the final examining committee:

Scott A. McLuckey
Chair

Hilkka I. Kenttämaa

Tong Ren

Garth J. Simpson

To the best of my knowledge and as understood by the student in the *Research Integrity and Copyright Disclaimer (Graduate School Form 20)*, this thesis/dissertation adheres to the provisions of Purdue University's "Policy on Integrity in Research" and the use of copyrighted material.

Approved by Major Professor(s): Scott A. McLuckey

Approved by: R. E. Wild 11-4-2013
Head of the Graduate Program Date

TOP-DOWN INTERROGATION AND CHARACTERIZATION OF BIOLOGICAL MACROMOLECULES

A Dissertation

Submitted to the Faculty

of

Purdue University

by

Yang Gao

In Partial Fulfillment of the

Requirements for the Degree

of

Doctor of Philosophy

December 2013

Purdue University

West Lafayette, Indiana

To my parents and my dear wife Biwei (杨碧薇) thank you for your love and support

Special thanks to my beloved Leo (六六), without whom this dissertation could have been finished one month earlier.

ACKNOWLEDGEMENTS

First and foremost, I would like to express my deepest gratitude to my mentor, Dr. Scott A. McLuckey, for bringing me into this wonderful world of biological mass spectrometry. He has been a huge inspiration and role model for me on my way of pursuing to be a good scientist. I am sincerely grateful for his willingness to accept me into his research group and his commitment to provide me with numerous opportunities to develop. Scott has every great attribute of an ideal research advisor that you would ever want in graduate school, and his passion and faith in science will continue to encourage me in my future career.

I am also very lucky to be a member of the family of the McLuckey group. I truly enjoyed working with these many talented people, who were always willing to help and provide useful insights. I would like to thank Dr. Teng-Yi Huang for being so patient in introducing me to the world of nucleic acid mass spectrometry, Dr. Ian K. Webb for the knowledge I gained on the instrumentation of QSTAR, John Stutzman and William Mcgee for their insightful suggestions that benefit a lot of my research projects. I appreciated the help I got from Dr. Ken Chanthamontri, Dr. Kerry Hassel, Dr. Marija Mentinova, Dr. Anastatia Kharlamova, Dr. Boone Prentice and Dr. James Redwine throughout the years I had overlapped with them. It is also a great pleasure to work with Corinne

Demuth, Christine Fisher, Joshua Gilbert, Carl Luongo, Nathan Barefoot, Alice Pilo, Nicole Burke, Stella Betancourt, Jiexun Bu, Zhou Peng and Eric Dziekonski. I would also like to express my sincere gratitude to the McLuckey group alumni, Dr. Xiaorong Liang, Dr. Jian Liu and Dr. Peng Pan in helping me with my research as well as career development. Even though I had no overlapping time with them in the graduate school, they were still very willing to help me and we always enjoyed the get-together during ASMS meetings.

Special thanks to Dr. Frank Londry, Dr. Rishehri Mahmoud and Dr. Min Yang at AB Sciex for the QSTAR instrument troubleshooting and maintenance. Without your help, I could never imagine how I would be able to bring the QSTAR back to live. I also owe my thanks to Dr. James Hager and Dr. Larry Campbell at AB Sciex for baring with my endless questions about troubleshooting the Sciex instrument.

I would also like to acknowledge my collaborators at Merck. Dr. Fanyu Meng, Dr. Jiong Yang and Dr. Mark Cancilla gave me a lot of help and great suggestions on our siRNA collaboration project and shared with me a lot of their valuable experience in the pharmaceutical industry.

Last but not least, I would like to thank Dr. Garth J. Simpson, Dr. Hilkka I. Kenttämaa and Dr. Tong Ren for serving as my thesis committee members. Thank you for sharing your valuable time with me.

TABLE OF CONTENTS

Page

Page

LIST OF TABLES

LIST OF FIGURES

Figure Page

Figure Page

Figure Page

Figure Page

Figure Page

Figure Page

LIST OF SCHEMES

Scheme Page

ABSTRACT

Gao, Yang. Ph.D., Purdue University, December 2013. Top-down Interrogation and Characterization of Biological Macromolecules. Major Professor: Scott McLuckey.

Analytical mass spectrometry has been widely applied in the field of biomolecule identification and characterization. It provides fast, accurate and robust information relevant to the molecular mass, composition and structure of the target analytes.

This thesis is focused on the top-down analysis of various macrobiomolecules, nucleic acids and proteins, in the context of ion/ion reaction and gas-phase unimolecular dissociation. The first part of the thesis deals with gas phase fragmentation behavior of chemically modified oligonucleotides. Factors, such as the observation time-scale, the ion type and the energy deposition method, are explored using a quadrupole/time-of-flight mass spectrometer. Novel fragmentation pathway associated with negative electron transfer dissociation has been investigated and applied to heavily modified siRNA analogues to increase the amount of sequence information that can be derived from the mass spectrum.

The second part of this thesis discusses proximity mapping using chemical crosslinking mass spectrometry coupled with ion/ion reaction. Crosslinkers with various linker arm lengths have been used to probe the proximity between the lysines on the surface of a folded protein. This approach has proved to be a rapid way to generate low-resolution structure information with significantly small sample quantity.

The last part of the thesis is focused on ion manipulation techniques in the mass spectrometer to increase the sensitivity and selectivity of the ion/ion reaction. Ion evaporation mechanism of the dipolar DC mechanism has been studied to understand the effective high mass limitation in the dipolar DC experiment. Efficient ion parking has been implemented in a linear ion trap with the help of axial DC gradient.

CHAPTER 1. INTRODUCTION

1.1 Introduction of Mass Spectrometry as a Structural Characterization

Mass spectrometry (MS) has been used for decades in structure elucidation and characterization via the gas phase fragmentation of ions derived from analytes of interest. The introduction of "soft" ionization methods, such as electrospray ionization (ESI)[1] and matrix assisted laser desorption/ionization (MALDI)[2], allows the formation of intact pseudo-molecular ions ($[M+nH]^{n+}$ or $[M-nH]^{n-}$) as surrogates for the biomolecules. For elucidation of the primary structure of large biopolymers, fragments generated from backbone dissociation have been used to determine the sequence or branching of residues in oligomer.

Fragmentation behavior of biomolecules such as peptides[3,4,5], proteins[6,7,8], oligosaccharides[9,10], and nucleic acids[11,12,13,14] have been extensively studied via tandem MS. Generally, a neutral molecule of interest is introduced into the mass spectrometer in the form of an ion. The ions of interest are then subjected to a tandem MS process that involves at least two stages of mass analysis. A typical tandem MS method is composed of the following steps: (1) mass selection of the ion of interest (parent ion); (2) energy deposition (by collision, photon, electron, etc.) into the isolated parent ion to induce cleavages of the covalent bonds, and (3) mass spectrometric analysis of the product ions. Gas phase fragmentation of

nucleic acids can be generally used in the areas of sequencing, identification of single nucleotide polymorphisms (SNP), identification and location of modified bases and sugar moieties, etc. The dominant dissociation pathways for a particular ion are generally a function of the ion type (e.g., positive ion, negative ion, radical species, etc.), the number of charges, the molecular structure, the energy deposition method, and the fragmentation reaction time-scale. Nucleic acids have both acidic (phosphate backbone) and basic (nucleobase) functionalities, and can therefore be protonated (metalated) or deprotonated to form the pseudo-molecular ions. With the evolution of tandem mass spectrometers, biopolymer ions have been subjected to an increasingly wide range of reaction conditions, including a variety of energy deposition methods, reaction time-frames, and observation time windows ranging over several orders of magnitude.

This chapter summarizes literature describing the gas phase fragmentation of nucleic acid ions under a variety of reaction conditions. Specifically, the phenomenology of gas phase dissociation of nucleic acid ions is determined by ion type, charge state, the energy deposition method and the fragmentation reaction time-scale. Various proposed mechanisms are summarized. The chapter is organized by dissociation method. For the most extensively studied collision-induced dissociation (CID), the literature is sub-categorized by analyte and ion type. In many cases, no single fragmentation mechanism can account for all the reported products. This suggests that multiple dissociation mechanisms can contribute, depending on ion type, ion charge state and reaction conditions.

1.2 Nomenclature of Oligonucleotide Fragment ions

In the early 1980s, Grotjahn and co-workers[15, 16, 17, 18] referred to the fragment ions generated by dissociation of the phosphodiester bond as "sequence ions". Two major fragment ion series were observed for the backbone cleavages of nucleic acid ions upon FAB-MS. The fragment ions containing the 3'-terminus or 5'-terminus of the precursor ion were designated as 5'-sequence ions or 3'-sequence ions, respectively. The detailed fragment notation scheme is shown in Figure 1.1a. Viari et al.[19] suggested an alternative nomenclature in the year 1987, which was later extended by Nordhoff et al.[20] in 1995 (see Figure 1.1b). McLuckey et al.[21] in 1992 proposed a nomenclature scheme that is analogous to the one widely used for peptides and proteins. This nomenclature defines all possible cleavages from the phosphodiester backbone and has been widely adopted by the community. The detailed nomenclature scheme is shown in Figure 1.1c. The four possible cleavages along the phosphodiester linkage are denoted by the lower case letters a, b, c and d for fragments that contain the 5'-terminus of the precursor and w, x, y and z for fragments containing the 3'-terminus of the precursor. The numerical subscripts indicate the number of ribose units from the corresponding termini. Upper case letter B represents a base with the subscript indicating its position in the sequence starting from the 5'-terminus. The identity of the lost base is indicated in parentheses along with the B_n denotation, e.g., B_2(A). The use of B_n(Base), however, has largely been replaced by the use of the base symbol with a subscript indicating location of the nucleotide from which it was lost, e.g., A_2 instead of B_2(A).

1.3 Fragmentation Methods

A variety of methods have been applied to dissociate nucleic acid ions for the purpose of generating sequence information and for localizing modifications. Some are based on depositing energy into the ion via collisions with a gas or surface (ion/neutral interaction) or by some form of photodissociation (ion/photon). Some methods involve either adding or removing an electron to or from an ion derived from ESI to generate a radical ion. In these cases, fragmentation may occur directly as a result of the electronic transition or a subsequent activation step may be used to fragment the radical ion. The energies and time-scales associated with these methods can vary widely. It is beyond the scope of this chapter to describe these methods in detail. The reader is directed to a recent overview of dissociation methods in tandem mass spectrometry [22]. Table 1.1 summarizes many of the methods used for fragmenting nucleic acid ions along with the associated time-scales and instruments often used to implement them. The remainder of the discussion regarding nucleic acid fragmentation is organized according to ion/neutral, ion/photon, and ion/electron(ion) interactions.

1.3.1 Ion/Neutral: CID of Nucleic Acids

CID is the most widely used dissociation method in tandem MS[23]. CID can be effected over a wide range of conditions with collision energies ranging from a few electronvolts to thousands of electronvolts, time-scales ranging from

microseconds to seconds, and pressures ranging from sufficiently low that only single collisions are likely to high enough that hundreds of collisions can occur. The reader is referred to a recent review of CID of peptide and proteins for an in-depth discussion of CID applied to large polyatomic ions[24]. For this discussion, it is useful to point out the distinction between “beam-type CID”, which applies to transmission instruments (e.g., triple quadrupole instruments), and “ion trap” or “sustained off-resonance irradiation (SORI)” CID, which are implemented in quadrupole ion trap and ion cyclotron resonance instruments, respectively. The latter CID approaches CID employ much longer activation times and sample processes that occur over longer time-scales than in beam-type CID. As a result, CID in the ion trapping instruments tends to more strongly favor low energy processes lead to less sequential fragmentation than does beam-type CID.

1.3.1.1 CID of DNA Anions

From the observations made on ion trap CID of a larger set of single-stranded DNA anions under quadrupole ion trap conditions[25,26,27,28,29,30], several tendencies for gas phase decomposition of the multiply deprotonated species emerge:

(1) The loss of a nucleobase is the initiate step of the fragmentation. Depending on the precursor ion charge state, the base can be lost as an anion or neutral. For precursor ions with low charge states, neutral base loss is predominant. As the charge on the precursor ion increases, loss of

charged bases becomes favored and coexists with the neutral base losses. The order of preference for charge base loss is $A^- > T^- > G^-$, C^{-26} or $A^- > G^- > T^- > C^{-27}$. Neither of these orders is consistent with the order for base loss from the 2'-deoxyribonucleoside 3'-monophosphates (dAp, dTp > dCp > dGp) or from the corresponding 5'-monophosphates (pdA, pdT > pdC≫pdG) [31]. The different orders of stability reported can be attributed to higher structural complexity of oligonucleotides and the Coulombic repulsion caused by multiple charges.

(2) Loss of the 3'-terminal base tends to be disfavored. The propensity for base loss has also been reported to be higher for 3'-phosphorylated mononucleotides than for the corresponding 5'-phosphorylated species[18,31,32]. This phenomenon has been attributed to that the base loss is facilitated by the 3'-phosphate. Neither 3'-terminal base nor 5'-phosphorylated mononucleotides have the facilitated 3'-phosphate, and thus such base loss is not favored.

(3) The subsequent cleavage of the 3' C-O bond of the ribose from which the base was lost is a dominant pathway. The dissociation of the 3' C-O bond generally forms complementary (a-B)- and w-type fragments regardless of the base or its charge. This fragmentation channel outcompetes all the other possible cleavages (b/x-, c/y- or d/z-type cleavage) along the phosphodiester linkage and therefore greatly simplifies spectral interpretation for DNA type oligonucleotides.

Base losses from first and second-generation fragments facilitate further backbone cleavages and produce internal fragments. Multiple base losses increase with increasing activation energy and increasing precursor ion charge state. However, loss of a PO_3^- group from 5'-phosphorylated fragment ions, such as w-type products ions, can compete effectively with this base loss channel.

McLuckey and Habibi-Goudarzi[26] proposed a mechanism to account for the formation of the base loss as well as (a-B)/w-fragments (Scheme 1.1). Firstly, a nucleobase is removed by 1,2-elimination on the ribose. For highly charged ions, loss of a nucleobase anion is preferred to relieve electrostatic repulsion. The second step involves another "1,2-elimination reaction" (ribose ring numbering changed due to the abstraction of the nucleobase), which cleaves the 3' C-O bond and forms a furan ring attached to the 5'-carbon. The second 1,2-elimination step is believed to be independent of the identity of the base initially removed and the precursor ion charge state. The formation of a stable aromatic system (furan) is the major driving force in the formation of the second-generation products.

In addition to the observations made ion quadrupole ion traps, CID behaviors of DNAs have been investigated with beam-type instruments, such as triple quadrupoles. The results differ from somewhat from trends observed in quadrupole ion traps. One of the most obvious differences is that no obvious preference for loss of a specific nucleobase is observed in beam-type CID of DNA anions[33,34,35]. Moreover, it has been reported that base loss is not a prerequisite for backbone cleavage[36]. The prominent product ions from beam-

type CID are not limited to (a-B)- and w-ions[34]. The differences in dissociation pattern of DNA anions in ion trap versus beam-type instruments likely arise from the differences in activation time-frames and precursor ion internal energies. Ion trap collisional activation generally favors slow low-energy processes due to its relatively long time-frame, whereas beam-type collisional activation tends to access higher energies that make more dissociation channels competitive. Additionally, ion trap CID uses single-frequency excitation which only affects the precursor ions, whereas, in triple quadrupole instrument, product ions can undergo secondary collision with the bath gas and induce further generations of fragments. It has been reported that beam-type CID generated more extensive sequence information than ion trap CID[35].

1.3.1.2 CID of DNA Cations

Reports for gas phase fragmentation of protonated DNAs are relatively few, presumably due to the fact that the negative mode tends to provide higher ion yields, at least under ESI conditions. Most positive ion studies were performed on small oligomers. Boschenok and Sheil[34] investigated the fragmentation pattern of protonated dinucleotides ($[M+H]^+$) using beam-type collisional activation. They observed both protonated base losses and neutral base losses, as well as w-type ions. Vrkic et al.[37] systematically examined CID patterns of all 64 protonated oligonucleotide trimers and 16 mixed-base tetramers by ESI-MS^n in a quadrupole ion trap. They found that the neutral base loss pathway is related

to the relative proton affinity of the nucleobase. Wang et al.[38] studied the CID behavior of positively charge oligonucleotides up to 20-mer level and found that charging levels of oligonucleotides were largely dependent on base composition. Ni et al.[39] confirmed that positive ion CID generates similar product ion types as negative ion CID, namely (a-B)- and w-type ions. The only exception comes from poly-T, which yields x-2H and z-2H ions exclusively. Weimann et al.[40] examined the high energy CID behavior of oligonucleotides (6- to 10-mers) on a hybrid EBE-TOF mass spectrometer. Some differences from those reported with triple quadrupoles were observed, presumably due to the significant variations in collision energy and time-scale of dissociation. The reader is referred to the studies just mentioned for details of the respective observations.

Several groups[37, 38, 39] have shown that the CID product spectra of DNA cations qualitatively resemble the CID product spectra of the corresponding anions, showing (a-B)/w-fragment ions. Wang and co-workers[38] postulated that the CID fragmentation mechanisms of protonated and deprotonated DNAs may share some commonalities. However, DNA cations are believed to be, in most cases, protonated on the nucleobases, and such protonation appears to facilitate the cleavage of the glycosidic bond resulting in base loss and subsequent formation of (a-B)/w-ions.

Vrkic et al.[37] proposed two possible pathways for the general base loss from a protonated DNA (Scheme 1.2). The first mechanism is similar to the one that was proposed by Beauchamp and co-workers[41], the base is lost via an E1 reaction, in which a carbocation intermediate is generated followed by loss of a

neutral base to form the oxonium ion (Scheme 1.2a). This pathway does not require the previously proposed 3'-phosphate facilitation in the negative ion CID, allowing for the possibility of the 3'-base loss. The second mechanism occurs via an intramolecular E2 reaction, in which the base is lost simultaneously with formation of a furan double bond. 5' or internal base loss can go through either the E1 or E2 mechanism. The authors also proposed a mechanism for the formation of (a-B)/w sequence ions from the $[M+H-BH]^+$ ions (Scheme 1.2a) that involves an ion-molecule complex undergoing either proton transfer or direct dissociation (Scheme 1.3). The instability of the oxonium ion leads to 3' C-O backbone cleavage, forming an ion-molecule intermediate. This complex can either dissociate directly to yield $(a_1\text{-}B_1)^+$ or undergo intermolecular proton transfer to form a w_2^+ ion. Vrkic et al. also postulated a mechanism for the formation of the "$(a_3\text{-}B_3)^+$ ion" that results from water loss from the $[M+H-B_3H]^+$ ion of the trimers. The loss of 3'-base via the E1 mechanism produces an intermediate, which can then lose the 3'-OH as a neural water molecule. The key concepts for the ion trap CID fragmentation mechanisms are summarized as follows: (1) the mechanisms are charged directed; (2) two complementary fragment ions (a-B) and w are competing for the charge via an ion-molecule complex intermediate, and (3) The "mobile proton model"[42,43], in which a labile proton is able to relocate from one potential cleavage site to another to effect fragmentation, may also be applied in explaining the fragmentation of protonated oligonucleotides.

1.3.1.3 CID of RNA Anions

Compared to DNA fragmentation, relatively few observations have been made on the dissociation of RNA, most of which were made in the past decade. The most distinct dissociation pathway of RNA involves backbone fragmentation characterized by the formation of abundant c-ions and their complementary y-ions as the major sequence informative series. Another difference from DNA is that backbone dissociation of RNA is not correlated with base loss. Later findings[44] have established the importance of the 2'-hydroxyl substituent as the structural key element in the fragmentation mechanism of RNA. As opposed to DNA, which preferentially dissociates into (a-B)/w-type ions, the presence of the 2'-hydoxyl group of RNA results in formation of predominant c/y-type ions. They suggested that the electron-withdrawing 2'-substituent induces a stablizing effect on the N-glycosidic bond by impeding the formation of the carbocation at the 1'-position[45], and therefore makes nucleobase loss less prominent. Moreover, the availability of a proton in the vicinity of the phosphate group is necessary for the RNA-typical backbone cleavage.

The proposed fragmentation mechanism is described in Scheme 1.4. Backbone fragmentation is initiated by forming an intramolecular cyclic intermediate with 2'-hydroxyl proton bridged to the 3'-phosphate oxygen. The 2'-hydroxyl proton is abstracted from the oxygen and facilitates the cleavage of the 5' P-O bond, yielding c/y-type fragments. The formation of a 3'-metaphosphoric-acid ester group following subsequent bond rearrangement stabilizes the c-

fragment. The complementary y_1-fragment is released as a neutral molecule, and thus will not be detected.

1.3.1.4 CID of RNA Cations

Kirpekar and Krogh[46] have studied the fragmentation behavior of short, singly protonated oligoribonucleotides generated by with Q-TOF instrument to locate post-transcriptional modifications of RNA molecules. Complex MS/MS spectra were generally observed, showing nearly all types of cleavages along the phosphodiester backbone and of the N-glycosidic bonds (and combinations of these) at different relative abundances. The most prevalent backbone fragment ions were found to be c- and y-ions, whereas the least prevalent ions were b/x-ions. Loss of neutral cytosine and guanine required low-energy deposition and therefore were preferred, whereas neutral loss of adenine was less prevalent. Loss of uracil, either as a neutral or cation, was never observed. By varying the collision energy, ions arising from loss of neutral GH and CH, and of y-sequence ions are typically the first fragments to appear. This fragmentation behavior is distinct from the that of singly protonated DNAs, where loss of a nucleobase is the key initiating step followed by predominant cleavage of the 3' C-O bond, resulting in (a-B)/w-fragments. As suggested by Tang et al.[47], the 2'-hydroxyl stablizes the N-glycosidic bond in RNA, making it less susceptible to cleavage upon protonation of the nucleobase. As a result, the energies required to generate MH^+-GH, MH^+-CH in RNA cations are elevated to the similar level as the c/y-formation channel.

For elucidation of the gas phase unimolecular dissociation behavior of RNA and DNA cations, Andersen et al.[48] performed hydrogen/deuterium exchange on a series of RNA and DNA tetranucleotides and studied their fragmentation patterns on a MALDI TOF-TOF instrument. They observed the loss of a neutral nucleobase as a fully deuterated species for all RNA tetramers, which is consistent with the DNA result reported by Gross et al.[49] They have also found that all y-ions and all c_2- and c_3-ions of the RNA tetramers analyzed are observed as fully deuterated species. Therefore, no carbon-bound hydrogens are transferred to mobile sites in the cleavage reaction. Moreover, nucleobase loss or other hydrogen mobilizing reactions generally do not precede cleavage of the 5' P-O bond. Initial loss of a nucleobase would have induced peak splitting of the c/y-ion fragments due to intramolecular H/D exchange before 5' P-O cleavage. In addition to the significant difference in fragmentation pathways between RNA and DNA (c/y-fragment vs. (a-B)/w-fragments), water loss from the precursor ion is only observed for RNA ions, implying that this water is lost from or by the interaction of 2'-OH. Water loss was not observed in the fragmentation of the 2'-O-methylated UAUC tetramer, further indicating the involvement of 2'-OH in the reaction. Tandem mass spectrometry of the ribonucleosides shows no evidence of water loss, and suggests that the presence of 2'-OH alone is not sufficient to induce the loss of water. Other reactive groups present in RNA, most likely phosphate, are required in the reaction as well.

Andersen et al.[48] have proposed a common RNA-specific mechanism to explain the water loss as well as 5' P-O cleavage (Scheme 1.4). This mechanism

involves an intramolecular nucleophilic attack on the phosphorus atom by the adjoining 2'-OH to yield a phosphorane transition state. The phosphorane transition state is well-documented in the mechanism of RNase[50]. In the gas phase, the deuteron abstracted from the 2'-OD presumably delocalizes between the oxygens of the phosphorane. Two reaction (1 and 2) pathways could occur depending on which oxygen acts as the leaving group: (1) The delocalized deuteron leaves with the –OD group leading to neutral loss of D_2O and formation of an internal 2'-3'-cyclic phosphate (reaction 1 in Scheme 1.4); (2) 5' P-O cleavage and formation of a y-fragment and a c-fragment with a 3'-terminal 2'-3' cyclic phosphate (reaction 2). The mechanism of Scheme 1.4 agrees well with the detecion of all deuterated c- and y-ions from the deuterated precursor, and also accounts for the neutral loss of water observed only for the RNA precursors. Furthermore, this mechanism explains why the water loss from deuterated RNA is a loss of D_2O and not HDO, which would otherwise be expected from a simple dehydration reaction.

1.3.2 Ion/Photon Interactions: Photodissociation of Nucleic Acids

1.3.2.1 Infrared Multiphoton Dissociation

Infrared multiphoton dissociation (IRMPD)[51, 52] involves multiple photon absorption over a relatively long time-frame to induce fragmentation via vibrational excitation. Since low energy CID and IRMPD both give rise

predominantly to vibrational excitation, they are likely to lead to similar fragmentation mechanisms. The typical IRMPD experiment is implemented with a continuous wave CO_2 laser (10.6 μm) in an ICR cell[53]. The precursor ions are isolated and slowly heated to their dissociation threshold. The irradiation time required for fragmentation to occur is dependent upon the ion structure. IRMPD is well-suited to the FT-ICR mass analyzer because it eliminates the need to introduce a collision gas for CID so that there is no pump-down delay, degradation of the high vacuum or subsequent deterioration in analyzer performance. However, IRMPD can also be implemented in quadrupole ion traps[54,55]. A variation of the IRMPD experiment is BIRD, which relies on blackbody radiation as the energy source, which has been far less used in the characterization of oligonucleotide ions.

IRMPD has been widely used in the identification and characterization of nucleic acid ions. McLafferty and co-workers[56,57] applied IRMPD to various DNA and RNA ions ranging in size from 8-mer to 108-mer. Complete sequence information of a 50-mer DNA was achieved[56]. They determined that oligonucleotides are more susceptible to infrared irradiation than peptides or proteins, which was later proved to be due to the strong absorption at 10.6 μm (the typical wavelength used) by backbone phosphate groups[58,59]. Later, Hofstadler et al.[60] demonstrated the use of a peptide as a stable internal mass standard to obtain accurate mass measurements of IRMPD generated phosphorothioate oligonucleotide fragment ions by manipulating the duration and power of the IRMPD event. Sannes-Lowery and Hofstadler[61] examined the

fragmentation behavior of modified oligonucleotides (2'-O-methoxylethyl ribose, phosphorothioate) using IRMPD in an external ion reservoir of an ESI-FT-ICR mass spectrometer. Keller and Brodbelt[62] have compared CID and IRMPD of oligonucleotide cations and anions in a quadrupole ion trap. Yang and Håkansson [63] demonstrated the use of double resonance experiments to interrogate the IRMPD fragmentation mechanism of DNAs. Their results indicated that IRMPD of the relatively low charge state ions examined proceeds through the zwitterionic intermediate mechanism proposed by Gross and co-workers [64] Parr and Brodbelt [65] demonstrated that IRMPD can significantly promote the fragmentation of thymine-rich oligodeoxyribonucleotides. Gardner et al.[66] performed IRMPD on protonated and deprotonated single-stranded small interfering RNA as well as duplexes and compared the IRMPD result with the result from CID in a quadrupole ion trap. Generally, IRMPD of various oligonucleotides (DNA, RNA, modified oligonucleotides) shows significant resemblance to the respective CID results.

1.3.2.2 UltraViolet Photodissociation

UVPD at 193nm [67,68] and electron photodetachment dissociation [69,70] at 260nm, have been applied to multiply charged oligonucleotide anions. McLafferty and co-workers[71] demonstrated for the first time that 193nm photon irradiation can fragment multiply charged dT_{30} via electron photodetachment and formation of d/w-and a/z-ions (which were initially interpreted as w- and a-ions since they have the same masses as d-and z-ions in the sequence dT_{30}). Gabelica et al.[69,70] examined the electron photodetachment of single-stranded oligonucleotide anions and duplexes at 250-285nm. They found that laser irradiation at 260nm results in minimal fragmentation of the DNA anion; generating predominant charge-reduced radical anions. CID of the charge-reduced radical anions arising from the irradiation produced complementary a/w- and d/z-fragment ions. Smith and Brodbelt[68] explored UVPD of a series of modified oligonucleotides (6- to 20-mer) at 193nm, and observed all types of backbone fragments and internal fragments. EPD also resulted in abundant sequence ions in terms of a/(a-B)/w- and d/z-products. Generally, UVPD and EPD are almost identical in fragmentation pathways. The only difference between the two is that EPD uses lower irradiation photon energy and requires further collision activation to fragment the radical species generated via the electron photodetachment process.

To understand the photodetachment mechanism, Gabelica and co-workers[69] have investigated the electron detachment efficiency as a function of irradiation wavelength and found that maximum effect is observed between

260nm and 275nm. The 260nm irradiation mainly gives rise to electron detachment with very low abundance of backbone fragments. They also suggested that electron detachment efficiency of DNA duplexes is correlated with their G/C composition, with higher electron detachment efficiency of G/C-rich duplexes. This phenomenon is attributed to the low ionization potential (IP) of guanine [72]. With further CID on the charge-reduced radical anions, nearly complete a/w- and d/z-ion series were observed. In contrast to fragment ions produced by CID of normal DNA anions, a- and z-ions are suggested to be radicals, which is consistent with the fragment ions observed in the EDD experiment [73]. A mechanism was proposed for the fragmentation pathway observed in EPD (Scheme 1.6). The guanine base absorbs the UV photon energy due to its low oxidation potential and leads to electron detachment from the base. Then the radical delocalizes to the phosphodiester backbone and facilitates the cleavage of the 3' C-O and 5' C-O bonds.

1.4 Conclusions

With the development of mass spectrometry instrumentation and ionization methods, the fragmentation of gaseous nucleic acid ions of both polarities has been investigated with a variety of energy deposition methods and over a wide range of reaction time-frames. Observations made by many laboratories over several decades have been broadly self-consistent. However, some inconsistencies in the literature have been noted, which may arise from differences in instrument platforms, different discrimination effects, and variations

in conditions. For instance, different base loss trends (orders) have been reported for what nominally appear to be similar conditions. Moreover, distinct correlations between electron photodetachment efficiency and nucleobase identity have been reported.

As a tool for the sequencing of oligonucleotides and characterization of modifications, tandem MS has become particularly powerful for small oligomers. Its utility is derived from the ability to generate a variety of ion types, access a wide variety of dissociation conditions, and yield high mass accuracy product analysis [74, 75]. Mass spectrometry is not competitive with conventional sequencing techniques for high throughput sequencing applications. However, it is uniquely suited to the characterization of modified oligmers[76]. These include modified bases, for which there are many in RNA, and modified backbones, which are being explored for therapeutic applications, for example. In terms of the length of oligomers that can be sequenced (i.e., the 'read length'), tandem MS is largely limited to oligomers with a common backbone smaller than a few tens of residues. In a few exceptional cases, high sequence coverages for species greater than about 30 nucleotides have been reported using CID[77]. This performance, however, is hardly routine. Current technology is able to support 'bottom-up" scenarios that employ RNases, for example, to generate oligomers small enough for characterization by CID[78]. The relatively recent introduction of techniques to generate radical ions, however, has enabled the sequencing of mixed backbone oligomers of the size of typical siRNAs and relatively high sequence coverage for natural RNA molecules as large as tRNA[79,80]. These

constitute “top-down” applications. Several factors contribute to limiting the size of oligonucleotides amenable to top-down structural characterization. Among these is the fragmentation chemistry. The introduction of hybrid techniques (e.g., EPD followed by CID) that combine the generation of a new ion type with another structural probe have opened up new possibilities for increasing sequence coverage in oligonucleotide analysis. Such hybrid approaches appear to be promising for improving the state-of-the-art in the primary structural characterization of oligonucleotides by tandem mass spectrometry and will likely see further exploration/development in the coming years.

1.5 References

[1] Fenn, J.; Mann, M.; Meng, C.; Wong, S.; Whitehouse, C. Electrospray ionization for mass-spectrometry of large biomolecules. *Science*. **1989**, *246*, 64-71.

[2] Hillenkamp, F.; Karas, M. Matrix-Assisted Laser Desorption/Ionization Mass Spectrometry of Biopolymers. *Anal. Chem*. **1991**, *63*, A1193-A1202.

[3] Tabb, D.; Smith, L.; Breci, L.; Wysocki, V.; Lin, D.; Yates, J. Statistical characterization of ion trap tandem mass spectra from doubly charged tryptic peptides. *Anal Chem*, **2003**, *75*, 1155-1163.

[4] Breci, L.; Tabb, D.; Yates, J.; Wysocki, V. Cleavage N-terminal to proline: analysis of a database of peptide tandem mass spectra. *Anal. Chem.* **2003**, *75*, 1963-1972.

[5] Huang, Y.; Triscari, J. M.; Pasa-Tolic, L.; Anderson, G. A.; Lipton, M. S.; Smith, R. D.; Wysocki, V. H. Dissociation behavior of doubly-charged tryptic peptides: Correlation of gas phase cleavage abundance with Ramachandran plots. *J. Am. Chem. Soc.* **2004**, *126*, 3034-3035.

[6] McLafferty, F. W. Tandem Mass Spectrometric Analysis of Complex Biological Mixtures. *Int. J. Mass Spectrom.* **2001**, *212*, 81-87.

[7] Stephenson, J. L.; McLuckey, S. A.; Reid, G. E.; Wells, J. M.; Bundy, J. L. Ion/ion chemistry as a top-down approach for protein analysis. *Curr. Opin. Biotechnol.* **2002**, *13*, 57-64.

[8] Reid, G. E.; McLuckey, S. A. 'Top down' protein characterization via tandem mass spectrometry. *J. Mass Spectrom.* **2002**, *37*, 663-675.

[9] Harvey, D. J. Matrix-assisted laser desorption ionization mass spectrometry of oligosaccharides and glycoconjugates. *J. Chromatogr. A.* **1996**, *720*, 429-446.

[10] Zaia, J. Mass spectrometry of oligosaccharides. *Mass Spectrom. Rev.* **2004**, *23*, 161-227.

[11] Nordhoff, E.; Kirpekar, F.; Roepstorff, P. Mass spectrometry of nucleic acids. *Mass Spectrom. Rev.* **1996**, *15*, 67-138.

[12] Murray, K. K. DNA sequencing by mass spectrometry. *J. Mass Spectrom.* **1996**, *31*, 1203-1215.

[13] Muddiman, D. C.; Smith, R. D. Sequencing and characterization of larger oligonucleotides by electrospray ionization fourier transform ion cyclotron resonance mass spectrometry. *Rev. Anal. Chem.* **1998**, *12*, 1-68.

[14] Wu, J.; McLuckey, S. A. Gas phase fragmentation of oligonucleotide ions. *Int. J. Mass Spectrom.* **2004**, *237*, 197-241.

[15] Grotjahn, L.; Frank, R.; Blocker, H. Ultrafast sequencing of oligodeoxyribonucleotides by FAB-MASS spectrometry. *Nucleic Acid Res.* **1982**, *10*, 4671-4678.

[16] Grotjahn, L.; Blocker, H.; Frank, R. Mass spectroscopic sequence-analysis of oligonucleotides. *Biomed. Mass Spectrom.* **1985**, *12*, 514-524.

[17] Cerny, R. L.; Tomer, K. B.; Gross, M. L.; Grotjahn, L. Fast-atom bombardment combined with mass spectrometry for determining structures of small oligonucleotides. *Anal. Biochem.* **1987**, *165*, 175-182.

[18] Cerny, R. L.; Gross, M. L.; Grotjahn, L. Fast-atom bombardment combined with tandem mass spectrometry for the study of dinucleotides. *Anal. Biochem.* **1986**, *156*, 424-435.

[19] Viari, A.; Ballini, J. P.; Vigny, P.; Shire, D.; Dousset, P.; CF-252-Plasma desorption mass-spectrometry of oligonucleotides. 3. Sequence-analysis of unprotected tri-deoxyribonucleoside diphosphates by CF-252-plasma desorption mass-spectrometry. *Biomed. Environ. Mass Spectrom.* **1987**, *14*, 83-90.

[20] Nordhoff, E.; Karas, M.; Cramer, R.; Hahner, S.; Hillenkamp, F.; Kirpekar, F.; Lezius, A.; Muth, J.; Meier, C.; Engels, J. W. Direct mass spectrometric sequencing of low-picomole amounts of oligodeoxynucleotides with up to 21 bases by matrix-assisted laser desorption/ionization mass spectrometry. *J. Mass Spectrom.* **1995**, *30*, 99-112.

[21] McLuckey, S. A.; Van Berkel, G. J.; Glish, G. L. Tandem Mass Spectrometry of Small, Multiply Charged Oligonucleotides. *J. Am. Soc. Mass Spectrom.* **1992**, *3*, 60-70.

[22] McLuckey S. A.; Mentinova, M. “Ion/Neutral, Ion/Electron, Ion/Photon, and Ion/Ion Interactions in Tandem Mass Spectrometry: Do we need them all? Are they enough?” *J. Am. Soc. Mass Spectrom.* **2011**, *22*, 3-12.

[23] McLuckey, S. A. Principles of collisional activation in analytical mass spectrometry. *J. Am. Soc. Mass Spectrom.* **1992**, *3*, 599-614.

[24] Wells, J.M.; McLuckey, S.A. "Collision-induced Dissociation (CID) of Peptides and Proteins." *Methods in Enzymology* **2005**, *402*, 148-185.

[25] McLuckey, S. A.; Stephenson, J. L.; O'Hair, R. A. J. Decompositions of odd- and even-electron anions derived from deoxy-polyadenylates. *J. Am. Soc. Mass Spectrom.* **1997**, *8*, 148-154.

[26] McLuckey, S. A.; Habibi-Goudarzi, S. Decompositions of multiply charged oligonucleotide anions. *J. Am. Chem. Soc.* **1993**, *115*, 12085–12095.

[27] McLuckey, S. A.; Habibi-Goudarzi, S. Ion trap tandem mass spectrometry applied to small multiply charged oligonucleotides with a modified base. *J. Am. Soc. Mass Spectrom.* **1994**, *5*, 740-747.

[28] McLuckey, S. A.; Vaidyanathan, G. Charge state effects in the decompositions of single-nucleobase oligonucleotide polyanions. *J. Mass Spectrom. Ion Process.* **1997**, *162*, 1-16.

[29] Rodgers, M. T.; Campbell, S.; Marzluff, E. M.; Beauchamp, J. L. Low-energy collision-induced dissociation of deprotonated dinucleotides: determination of the energetically favored dissociation pathways and the relative acidities of the nucleic acid bases. *Int. J. Mass Spectrom. Ion Process.* **1994**, *137*, 121-149.

[30] Vrkic, A. K.; O'Hair, R. A. J.; Foote, S. Fragmentation reactions of all 64 deprotonated trinucleotide and 16 mixed base tetranucleotide anions via tandem mass spectrometry in an ion trap. *Aust. J. Chem.* **2000**, *53*, 307-319.

[31] Habibi-Goudarzi, S.; McLuckey, S. A. Ion trap collisional activation of the deprotonated deoxymononucleoside and deoxydinucleoside monophosphates. *J. Am. Soc. Mass Spectrom.* **1995**, *6*, 102-113.

[32] Sidona, G.; Uccella, N.; Weclawek, K. Structure Determination of Isomeric Oligodeoxynucleotide Salts by Fast-Atom Bombardment Mass-Spectrometry. *J. Chem. Res. Synop.* **1982**, *1982*, 184-185.

[33] Barry, J. P.; Vouros, P.; Van Schepdael, A.; Law, S. J. Mass and sequence verification of modified oligonucleotides using electrospray tandem mass spectrometry. *J. Mass Spectrom.* **1995**, *30*, 993-1006.

[34] Boschenok, J.; Sheil, M. M. Electrospray tandem mass spectrometry of nucleotides. *Rapid Commun. Mass Spectrom.* **1996**, *10*, 144-149.

[35] Crain, P.F.; Gregson, J.M.; McCloskey, J.A.; Nelson, C.C.; Peltier, J.M.; Phillips, D.R.; Pomerantz, S.C.; Reddy, D.M. in: A.L. Burlingame, S.A. Carr (Eds.), Mass Spectrometry in the Biological Sciences, Humana Press, Totowa, NJ, 1996, p. 497.

[36] Bartlett, M. G.; McCloskey, J. A.; Manalili, S.; Griffey, R. H. The effect of backbone charge on the collision-induced dissociation of oligonucleotides. *J. Mass Spectrom.* **1996**, *31*, 1277-1283.

[37] Vrkic, A. K.; O'Hair, R. A. J.; Foote, S.; Reid, G. E. Fragmentation reactions of all 64 protonated trimer oligodeoxynucleotides and 16 mixed base tetramer oligodeoxynucleotides via tandem mass spectrometry in an ion trap. *Int. J. Mass Spectrom.* **2000**, *194*, 145-164.

[38] Wang, P. P.; Bartlett, M. G.; Martin, L. B. Electrospray collision-induced dissociation mass spectra of positively charged oligonucleotides. *Rapid Commun. Mass Spectrom.* **1997**, *11*, 846-856.

[39] Ni, J. S.; Mathews, M. A. A.; McCloskey, J. A. Collision-induced dissociation of polyprotonated oligonucleotides produced by electrospray ionization. *Rapid Commun. Mass Spectrom.* **1997**, *11*, 535-540.

[40] Weimann, A.; Iannitti-Tito, P.; Sheil, M. M. Characterisation of product ions in high-energy tandem mass spectra of protonated oligonucleotides formed by electrospray ionization. *Int. J. Mass Spectrom.* **2000**, *194*, 269-288.

[41] Rodgers, M. T.; Campbell, S.; Marzluff, E. M.; Beauchamp, J. L. Site-specific protonation directs low-energy dissociation pathways of dinucleotides in the gas phase. *Int. J. Mass Spectrom. Ion Process.* **1995**, *148*, 1-23.

[42] Dongre, A. R.; Jones, J. L.; Somogyi, A.; Wysocki, V. H. Influence of peptide composition, gas phase basicity, and chemical modification on fragmentation efficiency: Evidence for the mobile proton model. *J. Am. Chem. Soc.* **1996**, *118*, 8365-8374.

[43] Harrison, A. G.; Yalcin, T. Proton mobility in protonated amino acids and peptides. *Int. J. Mass Spectrom. Ion Process.* **1997**, *165*, 339-347.

[44] Tromp, J. M.; Schürch, S. Gas phase dissociation of oligoribonucleotides and their analoges studied by electrospray ionization tandem mass spectrometry, *J. Am. Soc. Mass Spectrom.* **2005**, *16*, 1262-1268.

[45] Tang, W.; Zhu, L.; Smith, L. M. Controlling DNA Fragmentation in MALDI-MS by Chemical Modification. *Anal. Chem.* **1997**, *69*, 302-312.

[46] Kirpekar, F.; Krogh, T. N. RNA fragmentation studied in a matric-assisted laser desorption/ionization tandem quadrupole/orthogonal time-of-flight mass spectrometer. *Rapid Commun. Mass Spectrom.* **2001**, *15*, 8-14.

[47] Tang, W.; Zhu, L.; Smith, L. M. Controlling DNA Fragmentation in MALDI-MS by Chemical Modification. *Anal. Chem.* **1997**, *69*, 302-312.

[48] Andersen, T. E.; Kirpekar, F.; Haselmann, K. F. RNA Fragmentation in MALDI Mass Spectrometry Studied by H/D-Exchange: Mechanisms of General Applicability to Nucleic Acids. *J. Am. Soc. Mass Spectrom.* **2006**, *17*, 1353-1368.

[49] Gross, J.; Leisner, A.; Hillenkamp, F.; Hahner, S.; Karas, M.; Schafer, J.; Lutzenkirchen, F.; Hordhoff, E. Investigations of the metastable decay of DNA under ultraviolet matrix-assisted laser desorption/ionization conditions with post-source decay analysis and hydrogen/deuterium exchange. *J. Am. Soc. Mass Spectrom.* **1998**, *9*, 866-878.

[50] Horton, H. R.; Moran, L. A.; Ochs, R. S.; Rawn, J. D.; Scrimgeour, K. G. *Principles of biochemistry, 3rd ed.*; Prentice-Hall: **2002**, 605-607.

[51] Little, D. P.; Speir, J. P.; Senko, M. W.; O'Connor, P. B.; McLafferty, F. W. Infrared Multiphoton Dissociation of Large Multiply Charged Ions for Biomolecule Sequencing. *Anal. Chem.* **1994**, *66*, 2809-2815.

[52] Woodin, R. L.; Bomse, D. S.; Beauchamp, J. L. Multiphoton dissociation of molecules with low power continuous wave infrared laser radiation. *J. Am. Chem. Soc.* **1978**, *100*, 3248-3250.

[53] Håkansson, K.; Cooper, H. J.; Hudgins, R. R.; Nilsson, C. L. High Resolution Tandem Mass Spectrometry for Structural Biochemistry. *Curr. Org. Chem.* **2003**, *7*, 1503-1525.

[54] Stephenson, J. L. Jr.; Booth, M. M.; Shalosky, J. A.; Eyler, J. R.; Yost, R. A. Infrared multiphoe-photon dissociation in the quadrupole ion trap via a multipass ootical arrangement. *J. Am. Soc. Mass Spectrom.* **1994**, *5*, 886-893.

[55] Hofstadler, S. A.; Sannes-Lowery, K. A.; Griffey, R. H. Infrared Multiphoton Dissociation in an External Ion Reservoir. *Anal. Chem.* **1999**, *71*, 2067-2070.

[56] Little, D. P.; McLafferty, F. W. Sequencing 50-mer DNAs Using Electrospray Tandem Mass Spectrometry and Complementary Fragmentation Methods. *J. Am. Chem. Soc.* **1995**, *117*, 6783-6784.

[57] Little, D. P.; Aaserud, D. J.; Valaskovic, A.; McLafferty, F. W. Sequence Information from 42-108-mer DNAs (Complete for a 50-mer) by Tandem Mass Spectrometry. *J. Am. Chem. Soc.* **1996**, *118*, 9352-9359.

[58] Crowe, M. C.; Brodbelt, J. S. Differentiation of phosphorylated and unphosphorylated peptides by high-performance liquid chromatography-electrospray ionization-infrared multiphoton dissociation in a quadrupole ion trap. *Anal. Chem.* **2005**, *77*, 5726-5734.

[59] Flora, J. W.; Muddiman, D. C. Selective, sensitive, and rapid phosphopeptide identification in enzymatic digests using ESI-FTICR-MS with infrared multiphoton dissociation. *Anal. Chem.* **2001**, *73*, 3305-3311.

[60] Hofstadler, S. A.; Griffey, R. H.; Pasa-Tolic, L.; Smith, R. D. The Use of a Stable Internal Mass Standard for Accurate Mass Measurements of Oligonucleotide Fragment Ions Using Electrospray Ionization Fourier Transform Ion Cyclotron Resonance Mass Spectrometry with Infrared Multiphoton Dissociation. Rapid Commun. Mass Spectrom. **1998**, *12*, 1400-1404.

[61] Sannes-Lowery, K. A.; Hofstadler, S. A. Sequence Confirmation of Modified Oligonucleotides Using IRMPD in the External Ion Reservoir of an Electrospray Ionization Fourier Transform Ion Cyclotron Mass Spectrometer. *J. Am. Soc. Mass Spectrom.* **2003**, *14*, 825-833.

[62] Keller, K. M.; Brodbelt, J. S. Collisionally activated dissociation and infrared multiphoton dissociation of oligonucleotides in a quadrupole ion trap. *Anal. Biochem.* **2004**, *326*, 200-210.

[63] Yang, J.; Håkansson, K. Characterization of oligodeoxynucleotide fragmentation pathways in infrared multiphoton dissociation and electron detachment dissociation by Fourier transform ion cyclotron double resonance. *Eur. J. Mass Spectrom.* **2009**, *15*, 293-304.

[64] Wan, K. X.; Gross, M. L. Fragmentation mechanisms of oligodeoxynucleotides: Effects of replacing phosphates with methylphosphonates and thymines with other bases in T-rich sequences. *J. Am. Soc. Mass Spectrom.* **2001**, *12*, 580-589.

[65] Parr, C.; Brodbelt, J. S. Increased sequence coverage of thymine-rich oligodeoxynucleotides by infrared multiphoton dissociation compared to collision-induced dissociation. *J. Mass. Spectrom.* **2010**, *45*, 1098-1103.

[66] Gardner, M. W.; Li, N.; Ellington, A. D.; Brodbelt, J. S. Infrared Multiphoton Dissociaiton of Small-Interfering RNA Anions and Cations. *J. Am. Soc. Mass Spectrom.* **2010**, *21*, 580-591.

[67] Smith, S. I.; Brodbelt, J. S. Hybrid Activation Methods for Elucidating Nucleic Acid Modifications. *Anal. Chem.* **2011**, *83*, 303-310.

[68] Smith, S. I.; Brodbelt, J. S. Characterization of Oligodeoxynucleotides and Modifications by 193nm Photodissociation and Electron Photodissociation Dissociation. *Anal. Chem.* **2010**, *82*, 7218-7226.

[69] Gabelica, V.; TabarIn, T.; Antolne, R.; Rosu, F.; Compagnon, I.; Broyer, M.; De Pauw, E.; Dugourd, P. Electron Photodetachment Dissociation of DNA Polyanions in a Quadrupole Ion Trap Mass Spectrometer. *Anal. Chem.* **2006**, *78*, 6564-6572.

[70] Gabelica, V.; Rosu, F.; Tabarin, T.; Kinet, C.; Antoine, R.; Broyer, M.; De Pauw, E.; Dugourd, P. Base-dependent electron photodetachment from negatively charged DNA strands upon 260-nm laser irradiation. *J. Am. Chem. Soc.* **2007**, *129*, 4706–4713.

[71] Guan, Z.; Kelleher, N. L.; O'Connor, P. B.; Aaserud, D. J.; Little, D. P.; McLafferty, F. W. 193 nm Photodissociation of Larger Multiply Charge Biomolecules. *Int. J. Mass Spectrom. Ion Processes*. **1996**, *157/158*, 357-364.

[72] Wetmore, S. D.; Boyd, R. J.; Eriksson, L. A. Electron affinities and ionization potentials of nucleotide bases. *Chem. Phys. Lett.* **2000**, *322*, 129-135.

[73] Yang, J.; Mo. J. J.; Adamson, J. T.; Håkansson, K. Characterization of oligodeoxynucleotides by electron detachment dissociation Fourier transform ion cyclotron resonance mass spectrometry. *Anal. Chem.* **2005**, *77*, 1876-1882.

[74] Oberacher, H.; Pitterl, F. On the use of ESI-QqTOF-MS/MS for the comparative sequencing of nucleic acids. *Biopolymers* **2009**, *91*, 401-409.

[75] Flosadóttir, H. D.; Gíslason, K.; Sigurdsson, S. T.; Ingólfsson, O. Mass Spectro-metric Study on Sodium Ion Induced Central Nucleotide Deletion in the Gas Phase. *J. Am. Soc. Mass Spectrom.* **2012**, *23*, 690-698.

[76] Giessing, A. M. B.; Kirpekar, F. Mass spectrometry in the biology of RNA and its modifications. *J. Proteomics.* **2012**, *75*, 3434-3449.

[77] Taucher, M.; Rieder, U.; Breuker, K. Minimizing Base Loss and Internal Fragmentation in Collisionally Activated Dissociation of Multiply Deprotonated RNA. *J. Am. Soc. Mass Spectrom.* **2010,** *21,* 278–285.

[78] Z. Meng, Z.; Limbach, P. A. Shotgun sequencing small oligonucleotides by nozzle-skimmer dissociation and electrospray ionization mass spectrometry. *Eur. J. Mass Spectrom.* **2005**, *11*, 221-229.

[79] Taucher, M; Breuker, K. Top-Down Mass Spectrometry for Sequencing of Larger (up to 61 nt) RNA by CAD and EDD. *J. Am. Soc. Mass Spectrom.* **2010**, *21*, 918-929.

[80] Taucher, M.; Breuker, K. Characterization of modified RNA by top-down mass spectrometry. *Angew. Chemie.* **2012**, *124*, 11451-11454.

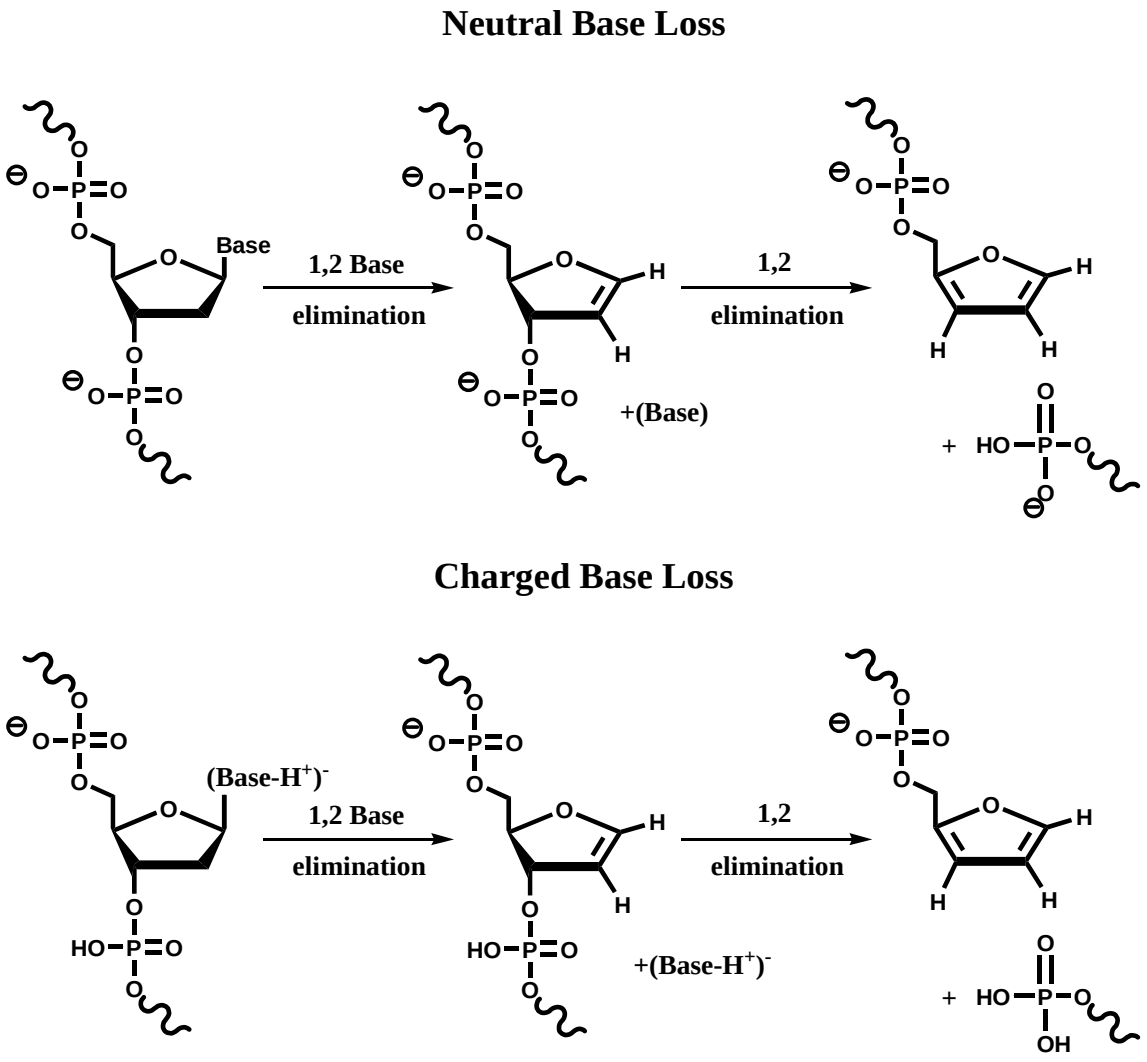

Scheme 1.1 Proposed fragmentation mechanism for DNA anions. Adapted with permission from ref. 26. Copyright 1993 American Chemical Society

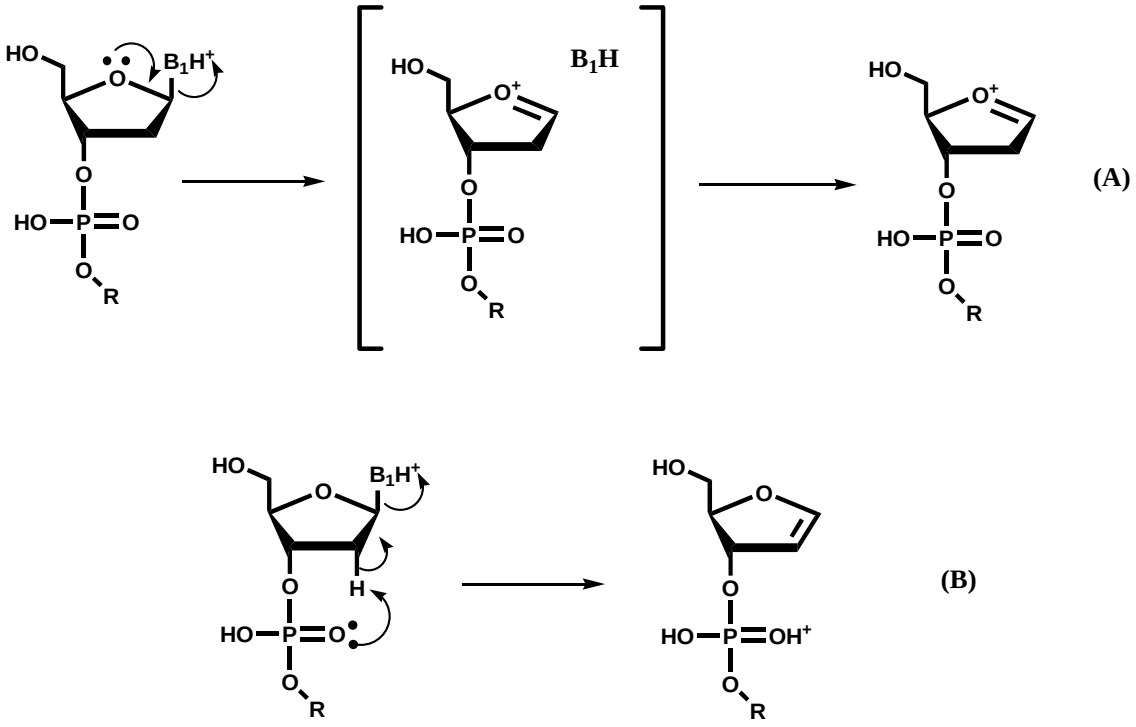

Scheme 1.2 Proposed mechanism for base loss from a protonated oligodeoxyribonucleotide.

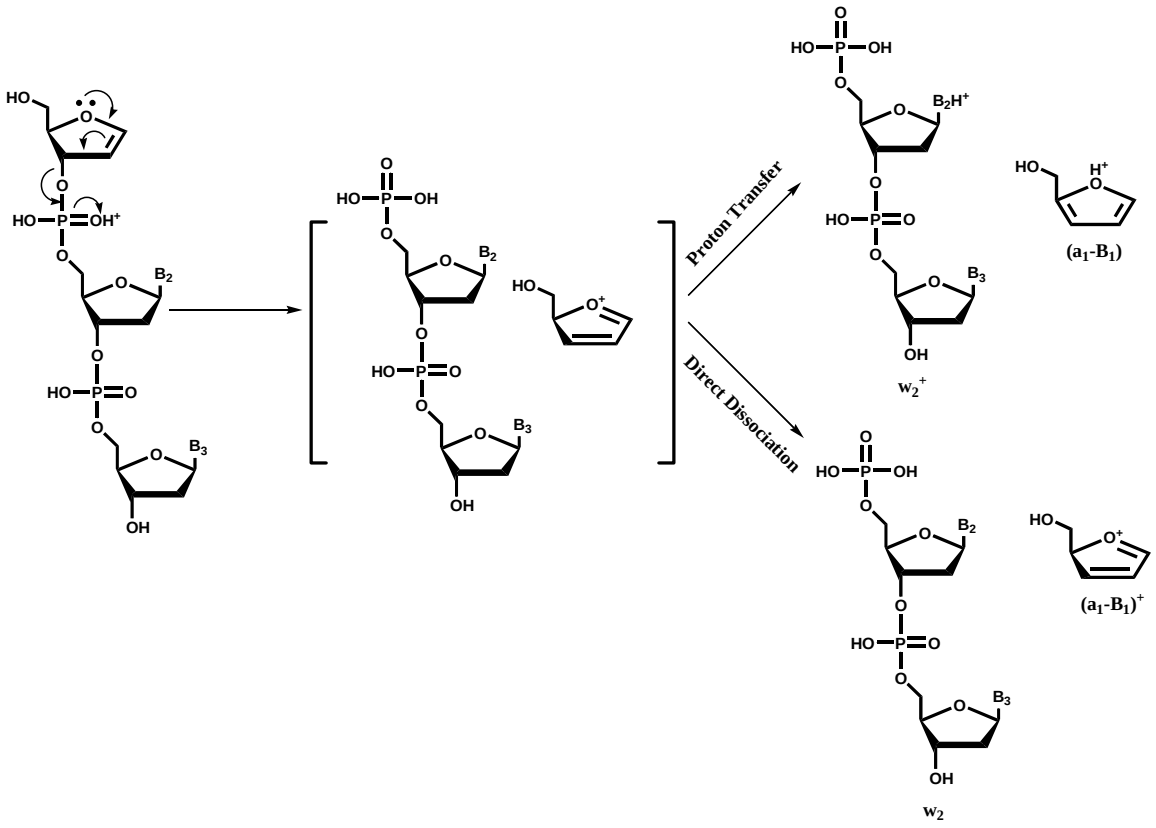

Scheme 1.3 Proposed mechanism for formation of (a-B)/w-fragments from a protonated oligodeoxyribonucleotide.

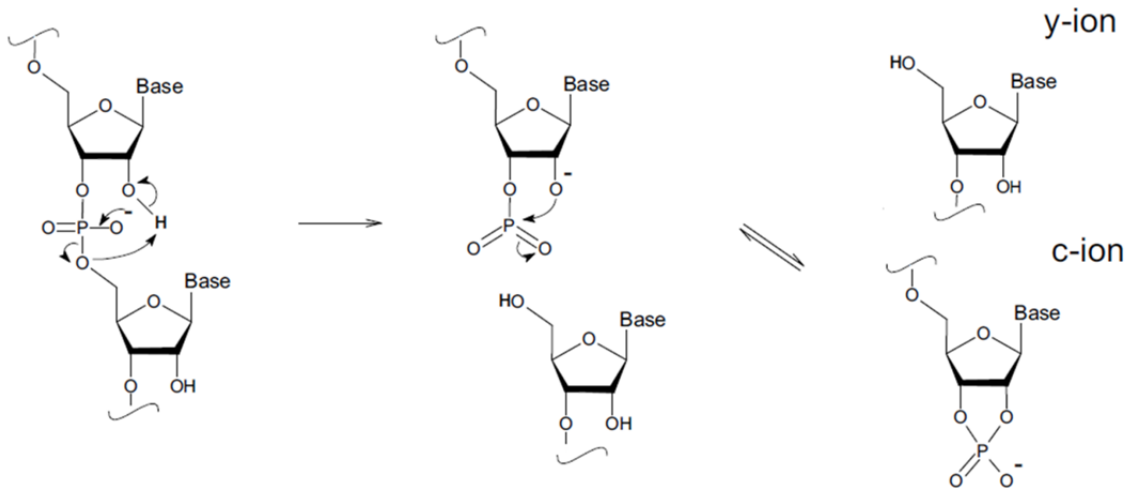

Scheme 1.4 Proposed dissociation mechanisms of RNA. Adapted from ref. 44, Copyright 2005 Elsevier, Inc., with kind permission from Springer Science and Business Media.

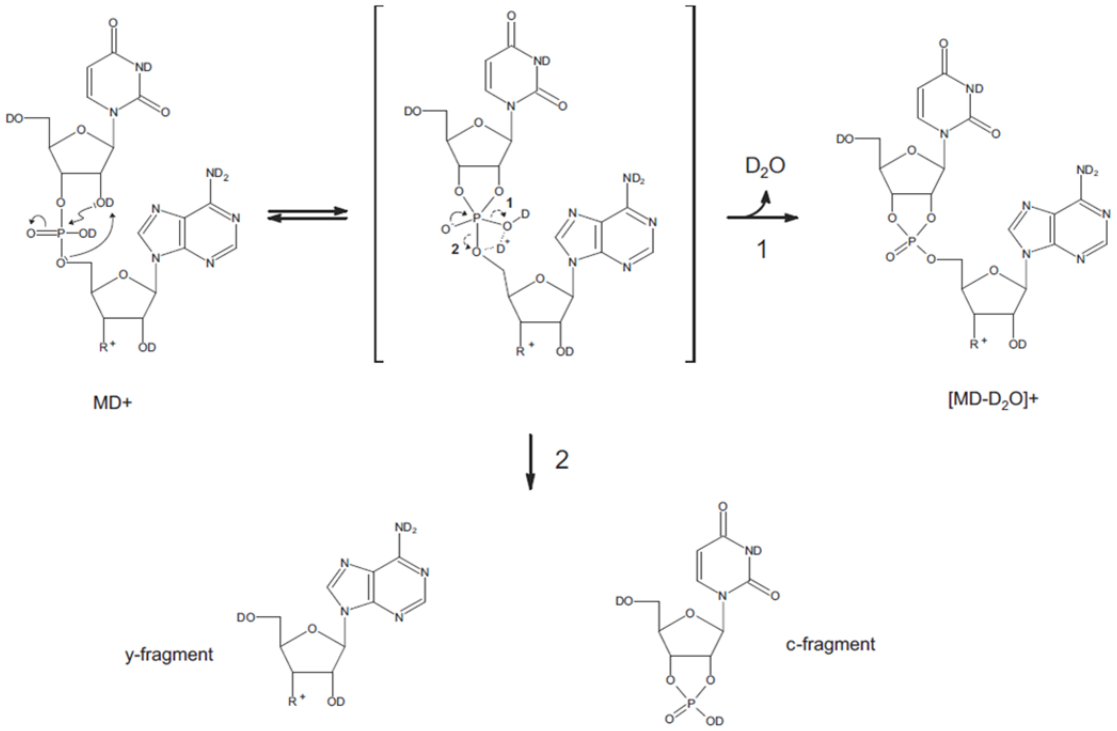

Scheme 1.5 Proposed fragmentation scheme for c- and y-ion formation from a deuterated RNA precursor. Reprinted from ref. 48, Copyright 2005 Elsevier, Inc., with kind permission from Springer Science and Business Media.

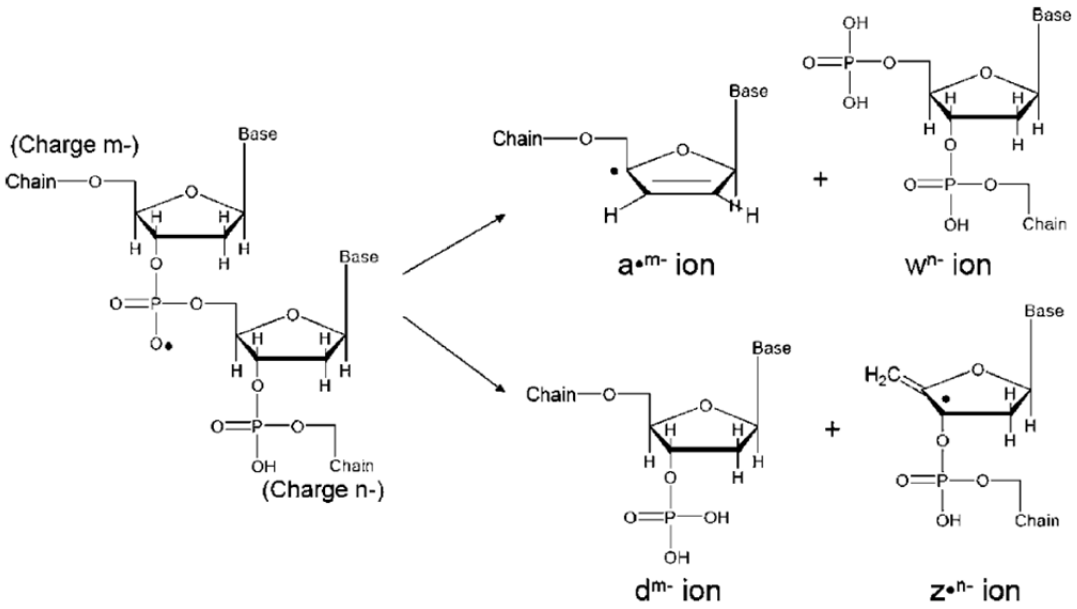

Scheme 1.6 Proposed mechanism for the EPD fragmentation pathways. Reprinted with permission from ref. 69. Copyright 2006 American Chemical Society.

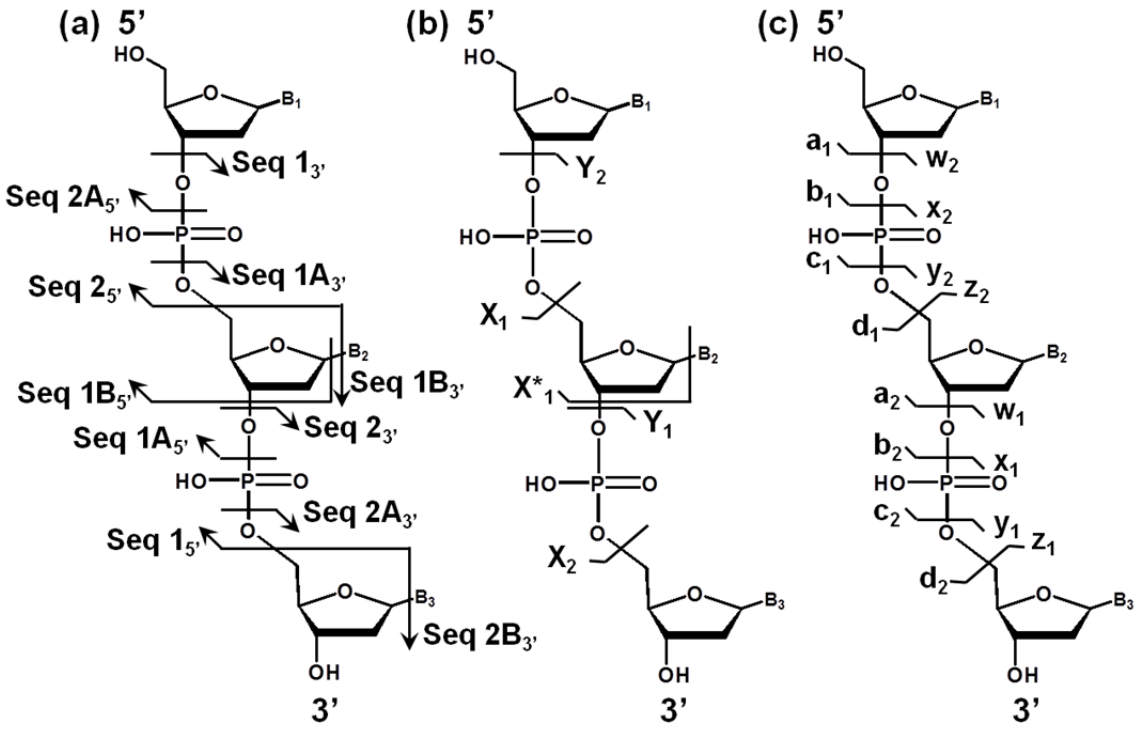

Figure 1.1 Nucleic acid fragment ion nomenclature proposed (a) by Cerny et al.[17] (b) by Nordhoff et al.[20], and (c) by McLuckey et al.[21].

Table 1.1 Summary of methods used to dissociate nucleic acid ions. See abbreviations for definitions of the acronyms.

Interaction	Expt'l time-scale	Main result	Common instruments
Ion/neutral			
Beam-type CID	<100 μs	Fragmentation	QQQ, Q-TOF, TOF/TOF, et al.
Ion trap CID	10-100s ms	Fragmentation	3D, linear ion traps
SORI/CID	10-100s ms	Fragmentation	FT-ICR
Nozzle-skimmer CID	<100 μs	Fragmentation	ESI interface
SID (ion/surface	ns	Fragmentation	Specialized QQQ, Q-TOF
Ion/photon			
BIRD	100 ms-s	Fragmentation	FT-ICR
IRMPD	10-100s ms	Fragmentation	FT-ICR, ion traps
UVPD	ns	Fragmentation	Traps, ICR, TOF/TOF, et al.
EPD	ns	Electron detachment from anion	Traps, ICR, TOF/TOF, et al.
Ion/electron			
ECD	10-100s ms	e^- capture by cation/fragmentation	FT-ICR
niECD	10-100s ms	e^- capture by anion/fragmentation	FT-ICR
EDD	10-100s ms	e^- detachment from anion/fragmentation	FT-ICR

Table 1.1, Continued

Interaction	Expt'l time-scale	Main result	Common instruments
Ion/ion			
ETD	10-100s ms	e^- transfer to cation/fragmentation	Ion traps
NETD	10-100s ms	e^- transfer from anion/fragmentation	Ion traps

CHAPTER 2. COLLISION-INDUCED DISSOCIATION OF OLIGONUCLEOTIDE ANIONS FULLY MODIFIED AT THE 2'-POSITION OF THE RIBOSE: 2'-F/-H AND 2'-F/-H-OME MIXMERS

2.1 Introduction

RNA interference (RNAi) is a regulatory mechanism that uses small double-stranded RNA (dsRNA) molecules, such as small interfering RNAs (siRNA) and micro-RNA (miRNA), to lead to homology-dependent degradation of the target mRNAs.[1,2,3] By delivering the siRNA effector to the cell, the RNA-induced silencing complex (RISC) can be "triggered" in the cell, which results in potent and specific silencing of the targeted mRNA.[4] Therefore, controlling disease-associated genes via RNAi has potential utility for future therapeutics for cancer, immune system diseases, genetic disorders, and viral infections.2,[5] For instance, a 21-mer dsRNA targeting the M-BCR/ABL fusion site was used to kill leukemia cells by depleting the corresponding mRNA and the M-BCR/ABL oncoprotein.[6] *In vivo* RNAi efficacy was first demonstrated by hydrodynamic co-delivery of a hepatitis B replicon and a pol III expression unit encoding an anti-hepatitis B virus (HBV) shRNA in mice.2,[7] Moreover, the feasibility of delivering siRNAs and viral vectors expressing siRNAs to affected regions of the brain makes RNAi potentially useful for treatment of degenerative, neurological diseases.[8]

Exogenous unmodified oligoribonucleotides are limited in therapeutic applications, however, by their inherent susceptibility to rapid degradation by nucleases.[9,10] The introduced siRNA can also bring about immune system responses,[11] which raises safety concerns for the therapeutic use of RNAi. To enhance the performance of dsRNA-mediated gene silencing, various chemical strategies to improve oligoribonucleotide stability have been explored, including modifications of the pentose and the heterocyclic base, as well as modification or replacement of the internucleotide phosphodiester linkage. Chiu et al. have reported that the hydroxyl group of the 2'-carbon of the pentose is not required for siRNA to enter the RNAi pathway and that chemical modification of the 2'-position can enhance the persistence of ribonucleotides both *in vitro* and *in vivo*.[12] Moreover, an *in vivo* model using 2'-F, 2'-O-methyl (2'-OMe) and 2'-H backbone modified siRNA against HBV has demonstrated that the siRNA-mediated immune induction can be avoided while maintaining silencing activity.[13] These studies point to strategies for improving the stability and utility of siRNAs for future *in vivo* therapeutic applications.[12]

For the purpose of therapeutic applications and regulatory filing, the structural characterization of modified siRNA and/or their metabolites is required. The most commonly employed methods for identification of siRNAs are through cloning and sequencing; new methods such as microarray and reverse transcription polymerase chain reaction (RT-PCR) have also been demonstrated.[14] Given the fact that the aforementioned methods detect only the sequence information of the nucleobases on the backbone, modification

information associated with the sugar or backbone is not provided. Thus, it is desirable to establish an approach that is capable of providing both primary nucleobase sequence information as well as the identification and localization of chemical modifications anywhere on the siRNA molecules. [15] Mass spectrometry is a promising candidate for this application.

Analysis of enzymatically digested modified oligonucleotides by tandem mass spectrometry has successfully determined primary structures and modifications.[16] However, the 2'-position modification makes it difficult to confirm the RNA sequences by the currently employed enzymatic digestion assays due to the high resistance it affords against RNases. Therefore, a more efficient way to identify, characterize and sequence oligonucleotides with modifications is needed. One alternative method is to derive structural information by fragmenting the analyte ions in the gas phase as part of a tandem mass spectrometry experiment. This method requires a sufficient understanding of fragmentation patterns for the modified oligonucleotides. CID behavior of intact unmodified duplex and single-stranded siRNA anions has been studied, with complete sequence coverage of c/y ions.[15,17] A recent study has demonstrated the beam-type CID behavior of fully modified (i.e., a methoxyl group was substituted at the 2'-position of each ribose) and platinated RNA oligomer anions and proposed possible fragmentation mechanisms.[18] In this work, we expand observations of the dissociation behaviors of modified RNA species by applying ion trap and beam-type CID to anions of oligomers fully-modified at the 2'-position with a mixture of different modifications (i.e., mix-mers). Of particular interest here is

the scenario in which all residues are modified at the 2'-position with mixtures of 2'-OMe and/or 2'-F and 2'-H (i.e., DNA residues). Such mixtures are of relevance due to their greater resistance to enzymatic degradation relative to unmodified RNA sequences.

2.2 Experimental Section

2.2.1 Materials

Methanol, isopropanol and glacial acetic acid were purchased from Mallinckrodt (Phillipsburg, NJ, USA). Piperidine and imidazole were obtained from Sigma-Aldrich (St. Louis, MO). All oligomers, including the RNA 6-mer 5'-rArCrCrGrArG-3', 2'-OMe fully modified 6-mer 5'-mAmCmCmGmAmG-3', 2'-(F, H) mix-mer 5'-fAdAdCfCdCfCdGfGdAfAdGfG-3', 2'-(F, H, OMe) mix-mer 5'-dAmCdGdTdCdfCdGmAdTdG-3' and the DNA 6-mer 5'-dAdCdCdGdAdG-3', were custom synthesized by Integrated DNA Technologies (Coraville, IA, USA). For the sake of clarity with respect to the nature of the substitution of the 2'-position of the ribose, "r" in the sequence indicates ribonucleotide, "m" represents the 2'-OMe modification, "f" stands for the 2'-fluoro modification, and "d" indicates a deoxyribonucleotide. The sequence was designed to minimize the occurrence of similar or identical masses from different fragment ions. The oligomer samples were used without further purification. Oligonucleotide solutions for negative nano-electrospray (nanoESI) were prepared to ca. 50 μM in 20: 80 (vol:vol)

isopropanol: DEPC-treated water with the addition of 25mM piperidine and 25mM imidazole.

2.2.2 Apparatus and Procedures

All MS/MS experiments were performed using a prototype version of a QqTOF tandem mass spectrometer (QSTAR, AB Sciex, Concord, ON, Canada) modified to allow for ion/ion reaction studies.[19] A home-built pulsed dual nanoESI source was coupled directly to the nanospray interface to produce ions of both polarities. [20] The multiply charged oligonucleotide anions, $[M-nH]^{n-}$, were generated directly via a nanoESI emitter. Nitrogen was used as the curtain gas and as the target gas for CID. To perform ion trap CID, the precursor ions were isolated by Q1 operated in the RF/DC (or resolving) mode and then injected into q2 at a relatively low kinetic energy. Then, a dipolar RF signal with frequency in resonance with the fundamental secular frequency of the precursor ion was applied to one pair of rods of q2 to induce ion trap collisional activation. The fragment ions were cooled in q2 and then subjected to mass analysis by time-of-flight (TOF). The beam-type CID was performed by increasing the potential difference between the q0 and q2 rod offsets, thereby increasing the kinetic energies of the precursor ion injected into q2.

2.3 Results and Discussions

2.3.1 CID of 6-mer Anions with Uniform Substitution at the 2'-Position

In order to evaluate the competition between cleavages along an oligonucleotide backbone with mixtures of substituents at the various 2'-positions, it is instructive to consider the distinct behaviors of oligonucleotides with a common substitution at the 2'-position. The natural substituents are, of course, 2'-OH (RNA) and 2'-H (DNA). A number of other substitutions, such as 2'-F and 2'-OMe, have also been made in the development of RNAi therapeutics. The 2'-OMe modification on the pentose ring, for example, stabilizes the oligonucleotide against degradation by nucleases.[21] Thus, this modification has been applied widely in the study of oligonucleotide based antisense or RNAi therapeutics. The chemical characteristics of 2'-OMe oligomers in the solution phase have been well characterized [12], and the gas phase properties of ions derived from modified oligomers, such as gas phase stabilities and unimolecular dissociation chemistries, have been studied under a limited range of conditions [18,22]. Data were collected here for DNA, RNA, and 2'-OMe versions of the same sequence. These comparisons are useful in interpreting the behavior of oligomers with mixtures of substituents at the various 2'-positions of the riboses. The fragmentation of multiply deprotonated DNA and RNA in the gas phase has been investigated in previous studies.[15,23,24,25,26,27] For the fragmentation of gaseous DNA/RNA, four possible cleavage sites on the phosphodiester backbone could

give rise to four types of characteristic ion pairs, namely a/w-ions, b/x-ions, c/y-ions, and d/z-ions.[17] In the case of the DNA oligomer, the cleavage of an N-glycosidic bond leads to the loss of a nucleobase either as a neutral species (BH) or as an anion (B^-) as the favored first step of fragmentation. Subsequently, cleavage at the 3' C-O bond of the sugar from which the base was lost gives rise to complementary (a-B)/w-ions, as is illustrated in Figure 2.1a. On the other hand, for RNA oligomers, c/y-ions from 5' P-O bond cleavages are more often observed in the CID spectrum (Figure 2.1b). However, when the 2'-position is substituted by a methoxyl group, all types of fragments with nearly full sequence coverage in each channel were present (Figure 2.1c). No preferential dissociation pathway was observed, as was also noted in the beam-type CID of modified triply deprotonated anions of mCmCmGmGmUmU.[18] Although base loss was noted to be a prominent process, it was not as dominant as for the ion trap CID of the same charge state of the DNA version of this sequence. The comparison of the three spectra of Figure 2.1 reflects the competition between the various possible bonds along the phosphodiester linkage when all the 2'-substitutions are the same and clearly shows the dramatic differences in fragmentation behavior of oligonucleotide anions depending upon the nature of the substitution on the 2'-position of the sugar ring.

In order to rationalize the unique fragmentation pattern of the 2'-OMe modified oligomers, it is instructive to refer to the fragmentation mechanisms already examined for unmodified DNA and RNA[28,29]. It has been shown that a facile mechanism for c/y-ion formation is present with the 2'-OH substitution of

RNA that is absent with DNA[30,31,32]. This channel can be favored over formation of (a-B)/w-ions at low ion activation energies, so that the product ion spectrum is dominated by c- and y-ions[26]. The 2'-OMe substitution blocks this facile 5' P-O bond dissociation mechanism. While this does not preclude cleavage of the 5' P-O bond, it apparently makes it less energetically favored such that cleavages at other sites along the phosphodiester linkage can compete. However, the 2'-OMe substitution must also affect the base lose channel. Base loss followed by (a-B)- and w-ion formation is the dominant channel in DNA anions and is the next most energetically favorable process in RNA anions[26]. In the case of DNA, for example, at the threshold for anion dissociation, only base loss is observed[24]. The (a-B)- and w-ions that arise from consecutive cleavage following base loss are observed as the activation energy is increased further. In the case of RNA anions, the c/y-ions, and some base loss fragments, are noted at the onset of dissociation with (a-B)- and w-ions appearing as the activation energy is further increased. In the case of the anions of the 2'-OMe substituted 6-mer, fragments from all dissociation channels were observed at the onset of dissociation and their relative abundances were insensitive to activation amplitude using dipolar resonance excitation ion trap collisional activation (Figure 2.2). This set of observations is consistent with the 2'-OMe substitution inhibiting c/y-ion formation, which has been noted previously[30], and facile base loss, which has not been noted previously, such that formation of b/x- and d/z-ions can compete. However, it is also possible that the 2'-OMe somehow facilitates formation of b/x- and d/z-ions. The mix-mer data discussed below clarifies the situation.

Ion trap CID data were also collected for the $[M-3H]^{3-}$ and $[M-4H]^{4-}$ anions of mAmCmCmGmAmG. The competition between the neutral and charged base loss has been observed to be correlated with charge state for DNA anions[23,24,26] and similar behavior was noted with the 2'-OMe modified anions. The ion trap CID of the doubly deprotonated precursor ion led primarily to neutral base losses (Figure 2.1c). Both neutral and charged base losses were observed from the CID of the triply deprotonated precursor ions (Figure 2.3a) whereas exclusive loss of the deprotonated base was found in the CID product spectrum of 4- charged precursor ions (Figure 2.3b). Aside from base loss, variations in the relative abundances of all other fragment ions were observed as a function of charge state. No single channel was observed to be dominant for all investigated charge states. For instance, the complementary a_5^--B/w_1^- ions were dominant for the $[M-3H]^{3-}$ charge state but were barely seen in the other two charge states. For this limited set of observations, a tendency for increased contributions from fragmentation in the middle of the anion was noted as the precursor ion charge state increased. Overall, the most extensive sequence information was obtained from the doubly charged anion.

Beam-type CID data were also collected for the $[M-2H]^{2-}$, $[M-3H]^{3-}$, and $[M-4H]^{4-}$ charge states of the mAmCmCmGmAmG oligomer (see Figure 2.4) to provide compare the quantity and quality of structural information derived from the slow heating ion trap CID approach to the faster beam-type activation approach. Conventional resonance excitation ion trap collisional activation using helium as the bath gas tends to favor the observation first generation products

due to the fact that first generation product ions, once formed, are not subject to acceleration and can be cooled by collisions with the light bath gas. Exceptional cases, such as the facile formation of (a-B)- and w-type ions after base loss, occur when the first generation product is less stable kinetically than the precursor ion (i.e., when there is a very facile fragmentation mechanism from the first generation product that becomes available only after the initial fragmentation step). Furthermore, dissociation rates in ion trap experiments[33] tend to be on the order of 10^2-10^3 s^{-1} while those for beam-type experiments are generally greater than 10^4 s^{-1}. Hence, the precursor ions in beam-type CID experiments are generally excited to higher energies than in ion trap experiments in order to generate product ions on the time-scale of ion passage through the instrument. Furthermore, first generation products are formed at the same velocity as the precursor ion and can therefore undergo further activating collisions with the nitrogen target gas. Both effects can lead to the observation of dissociation reactions with greater energy requirements than those noted in ion trap experiments and to the observation of sequential fragmentation. For the present comparison, the collision energies and target pressure in the beam-type experiments were chosen to lead to a roughly 80% diminution of the precursor ion signal, which is comparable to that for the ion trap experiments. Note, however, that the dissociation rates for the two approaches are significantly different due to the different experimental time-scales (i.e., tens of microseconds versus tens of milliseconds). Products solely arising from the loss of a single nucleobase were largely absent in the beam-type CID experiments, presumably

due to extensive sequential fragmentation. The appearance of (a-B)-ions is consistent with this interpretation. Internal fragments, which also arise from sequential cleavages, were prevalent in the product spectra. The internal fragments increased in relative abundance as the collision energy was increased, while the abundances of first generation products, such as y_2^-, c_2^-, x_2^-, etc., decreased (data not shown), presumably due to sequential decomposition. Overall, a greater variety of fragments were generated by beam type CID, particularly for the higher (more negative) charge states, compared to ion trap CID, but this increase was largely due to sequential decomposition. However, evidence for contributions from relatively higher energy cleavages is apparent from the appearance of several a-type ions, which must be formed without prior loss of a base. Much less evidence for a-type ions was noted in the ion trap CID experiments. Overall, however, the beam-type CID conditions used here did not provide significantly more structurally diagnostic product ions for the fully modified 6-mer than ion trap CID but did produce many more sequential dissociation products that are difficult to interpret and can possibly complicate *de novo* sequencing.

The dissociation mechanism was further investigated by MS^3 experiments, fragmenting the neutral base loss species, i.e. $[M\text{-}AH]^{2-}$. Although w_1^- and a_5^--A ions, which are generated from the subsequent cleavage of the 3' C-O bond of adenosine, were observed in the product spectrum of the base loss species from the 2'-OMe RNA 6-mer (Figure 2.5a), the other fragmentation pathways also had comparable intensities. The secondary bond cleavages from the $[M\text{-}3H\text{-}A]^{2-}$ ions

also generated fragment ions observed in the MS/MS spectra (a/w, b/x, c/y, d/z) and extensive [fragment-A] ions, such as b_2-A, z_2-A, x_2-A, etc. This data was compared to the ion trap CID of the base loss species from unmodified DNA 6-mer (Figure 2.5b). The CID of the unmodified DNA resulted in almost predominately $(a_5^-$-A)/w_1^- fragments. These MS^3 experiments support the conclusion that the 2'-O-methyl modification hindered the favored fragmentation pathway which generates a-B/w fragments. Additionally, the fragment-A ions, which were not present in the CID spectra of the deprotonated oligonucleotides, demonstrated the high gas phase stability of the base loss species. Beam type CID of the base loss species was performed on the QSTAR by bidirectional ion transfer.[34] The different extents of fragmentation at the same activation energy (200eV for $[$2'-OMe RNA –mer -3H-A$]^{2-}$ vs. 200eV for $[$DNA 6-mer -3H-A$]^{2-}$) confirmed the relatively high gas phase stability of the base loss species of the 2'-OMe RNA 6-mer (Figure 2.6).

2.3.2 CID of 6-mer Cations with Uniform Substitution at the 2'-Position

In order to get a whole picture of the CID behavior of the 2'-O-methyl modified RNA oligomer, ion trap CID was performed in the positive polarity (Figure 2.7) in comparison with the negative polarity. The most significant difference observed in the positive spectra was that the base loss peaks were much more abundant in the positive ion trap CID spectra. Additionally, fragment peaks resulting from the loss of two or three bases were found to be very

abundant. Apparently, the base loss channel is more favorable in the positive mode and the species which lose one or more bases are fairly stable in the gas phase, given the fact that the intensity of fragments other than base losses was low. The product ions from secondary bond cleavage were also observed (y_4-G, d_4-A), indicating that direct backbone cleavage channels are competitive with the subsequent 3' C-O bond cleavages which generate a-B/w ions.

In addition to fragmentation patterns, several phenomena were also noted for oligonucleotide mass spectrometry in positive polarity. Firstly, it is relatively more difficult to ionize oligonucleotide in the positive polarity as opposed to the negative mode, largely due to the relatively lower basicity of the nucleobase and high acidity of the phosphodiester linkage. Secondly, the ESI spectra of oligonucleotide cations tend to be more adducted with metal ions (Na^+, K^+). Thirdly, the stability of the ESI in the positive polarity is much lower than that in the negative mode, the relative spray time is much shorter.

2.3.3 CID of 2'-(F,H) and 2'-(F,H,OMe) Mix-mer Anions

Many chemically synthesized oligoribonucleotides of therapeutic interest are chimeras with different 2'-position modified monomers. The structural characterization of such species is therefore complicated by the competition among various cleavage sites for residues with different modification states at the 2'-carbon. The potential dimensionality (e.g., ion polarity, charge state, dissociation conditions, oligomer composition) associated with the exploration of

the tandem mass spectrometry for the structural characterization of such species is very large and therefore mandates the selection of a subset of studies. A number of studies have been described that have involved mix-mers of one kind or another and in various contexts.[18,22,30,31,35,36] In this work, we employ ion trap CID and beam-type CID of relatively low charge state anions of a few model "mix-mer' species. Specifically, we have examined anions of the 2'-(F, H) mix-mer 5'-fAdAdCfCdCfCdGfGdAfAdGfG-3' and the 2'-(F, H, OMe) mix-mer 5'-dAmCdGdTdCdfCdGmAdTdG-3' due to the lack of mix-mer data involving DNA residues interspersed with the common 2'-F and 2'-OMe substitutions. Figure 2.8 shows the ion trap CID product ion spectra of the $[M-4H]^{4-}$ (Figure 2.8a) and $[M-6H]^{6-}$ (Figure 2.8b) ions of the 2'-(F, H) mix-mer. Cleavages of the 3' C-O bonds of the DNA nucleotides following base losses were the dominant dissociation channel generating a-B/w-ions. There were also some peaks with *m/z* ratios corresponding to the y- and d-ions. However, no fragments from dissociation at the 3'-side of the 2'-F modified nucleotides were observed. As the charge state increased, more y-ions were observed, but no 3'-side dissociation of the 2'-F modified nucleotides was noted. The fact that both 2'-F and DNA residues were present in the same molecule clearly shows that the 2'-modification inhibits dissociation from the 3'-side of the phosphodiester linkage. The fact that all of the sequence related ions are consistent with cleavages at the 3'-sides of the DNA residues strongly suggests that base loss predominantly takes place from the DNA sugars. Like the 2'-OMe substitution, the 2'-F substitution does not allow for the facile formation of c/y-ions noted for RNA anions. Likewise, this

substitution apparently also inhibits the facile base loss followed by (a-B)/w-ion formation process widely noted for DNA anions.

Figure 2.9 shows the ion trap CID product ion spectra of the $[M-3H]^{3-}$, $[M-4H]^{4-}$, and $[M-5H]^{5-}$ ions of the 2'-(F, H, OMe) mix-mer 5'-dAmCdGdTdCdfCdGmAdTdG-3'. Similar to the fragmentation pathways of the 2'-(F, H) mix-mer anions, no backbone bond cleavages from the 3'-sides of either the 2'-F or 2'-OMe nucleotides were observed. The a-B/w-ions corresponding to the dissociation of 3' C-O bond following the base losses were dominant sequence fragments. This mix-mer suggests that both 2'-F and 2'-OMe substitutions have similar effects on oligomer dissociation in that they inhibit c/y-ion formation relative to RNA oligomers and (a-B)/w-ion formation relative to DNA oligomers. The backbone cleavages of the modified oligomer ions were not sensitive to precursor ion charge state with the notable exception of dissociation at the 3'-side of thymidine. In the lower charge state (3-), there was no evidence for cleavage between the thymidine and cytidine residues or between the thymidine and guanosine residues, which would produce a_4-B/w_6 and a_9-B/w_1 ions, respectively (Figure 2.9a). A relatively small w_6-ion signal was observed in the product spectrum of the 4- charge state (Figure 2.9b), while a_4-B/w_6 and a_9-B/w_1-ions were observed in the product spectrum of 5- charge state (Figure 2.9c). The relative contributions from cleavages at thymidine residues clearly increase with the absolute charge of the precursor anion (Figure 2.10). It is well-known that loss of thymine and, as a consequence, the consecutive cleavage at the relevant 3' C-O bond to yield (a-T)/w-ions, is disfavored[26]. This has been

attributed to the strong evidence that, at low anionic charge states, intramolecular proton transfer from a phosphodiester linkage to the nucleobase precedes neutral base loss[37] and that thymine has a proton affinity that is significantly lower than those of the other nucleobases. However, at relatively high charge states, loss of thymine is often observed[26], presumably because the intramolecular proton transfer mechanism becomes energetically unfavorable relative to one or more other mechanisms for base loss.

Beam-type collisional activation was applied to the mix-mer ions to determine if higher activation levels might yield cleavages at the 3'-sides of the 2-F and/or 2'-OMe residues. Figure 2.11a displays the beam type CID product spectrum of the $[M-5H]^{5-}$ of the 2'-(F, H) mix-mer acquired using a collision energy of 100 eV. No evidence for cleavages at the 3'-sides of the 2'-F modified residues was noted under these conditions nor at higher collision energies (data not shown). The beam-type CID of the of the $[M-5H]^{5-}$ of the 2'-(F, H, OMe) mix-mer, on the other hand, yielded relatively low abundance signals from c_2- and x_2-ions indicating backbone dissociation on the 3'-side of the 2'-O-methyl modified nucleotides. Collectively, the results obtained in this work, along with previous studies of DNA and RNA anions, suggest the gas phase stability of the 3'-side backbone linkage follows the order: 2'-F> 2'-OMe> 2'-OH> 2'-H (with the backbone cleavage for the 2'-H cleavage arising from the base loss species). While the low energy beam-type CID conditions accessible on the QqTOF instrument were not able to generate additional primary sequence information

from the 2'-(F, H) mix-mer anions, relative to ion trap CID, such conditions appear to offer some utility for the 2'-(OMe, H) mix-mers.

2.4 Conclusions

In this study, the collision-induced dissociation behavior of oligonucleotide anions with several different substituents at the 2'-carbon of the pentose rings of the oligomer was investigated. The 2'-OMe substitution inhibits the facile mechanism to yield complementary c/y-ions noted for 2'-OH substituted species (i.e., RNA) and stabilizes the oligomer with respect to base loss relative to DNA and RNA anions. As a result, cleavages along each of the four bonds of the phosphodiester linkage in fully substituted 2'-OMe species (i.e., a methoxy substituent is present on the 2'-carbon of all sugars) are observed with no clearly favored dissociation channel. Ion trap CID of the fully modified oligomer therefore provides extensive sequence information. While differences in relative abundances of the various fragments vary with precursor ion charge state, the extent of sequence information present in the CID spectra is similar. Beam-type CID appears to offer little advantage over ion trap CID for sequencing the fully substituted anions and can lead to extensive sequential fragmentation as the collision energy is increased.

Oligomers that do not have the same substituent at the 2'-carbon of each sugar can be difficult to sequence fully via CID due to significant differences in the energetic requirements associated with cleavages of the adjacent

phosphodiester linkage. For example, the presence of DNA nucleotides in the sequence, along with nucleotides with 2'-OMe substituents can lead to a situation where all of the dissociation takes place through the low energy channels associated with DNA with little or no structurally diagnostic cleavages from the 3'-sides of the 2'-OMe substituted nucleotides. In this case, beam-type CID can prove to be beneficial as it may access energies needed to lead to at least some cleavages adjacent to the 2'-OMe nucleotides. This was not observed, however, with 2'-F substitution. This implies that the 2'-F substituent provides even greater stability with respect to fragmentation than the 2'-OMe substitution. Conventional ion trap CID and low energy beam-type CID, such as that commonly effected in quadrupole and other multi-pole collision cells, are therefore expected to be limited in their abilities to provide full sequence information from mix-mers anions comprised of nucleotides with significantly different stabilities towards fragmentation. This was demonstrated here with mix-mers comprised of DNA nucleotides and nucleotides with 2'-OMe and 2'-F substituents.

This chapter was reprinted with permission from Gao, Y., McLuckey, S. A. Collision-induced dissociation of oligonucleotide anions fully modified at the 2'-position of the ribose: 2'-F/-H and 2'-F/-H/-OMe mix-mers. *J. Mass Spectrom.* **2012**, *47*, 364-369. Copyright (2012) John Wiley & Sons, Ltd.

2.5 References

[1] Fire, A.; Xu, S.; Montgomery, M.K.; Kostas, S.A.; Driver, S.E.; Mello, C.C. Potent and specific genetic interference by double-stranded RNA in Caenorhabditis elegans. *Nature*. **1998**, *391*, 806-811.

[2] Aagaard, L.; Rossi, J.J. RNAi therapeutics: Principles, prospects and challenges. *Adv. Drug Delivery Rev*. **2007**, *59*, 75-86.

[3] Bennett, C.F.; Swayze, E.E. RNA targeting therapeutics: Molecular mechanisms of antisense oligonucleotides as a therapeutic platform. *Pharmacology and Toxicology.* **2010**, *50*, 259-293.

[4] Hannon, G.J. RNA interference. *Nature*. **2002**, *418*, 244-251.

[5] Soutschek, A.; Akinc, B.; Bramlage, K.; Charisse, R.; Constien, M.; Donoghue, S.; Elbashir, A.; Geick, P.; Hadwiger, J.; Harborth, M.; John, V.; Kesavan, G.; Lavine, R.K.; Pandey, T.; Racie, K.G.; Rajeev, I.; Rohl, I.; Toudjarska, G.; Wang, S.; Wuschko, D.; Bumcrot, V.; Koteliansky, S.; Limmer, M.; Manoharan, H.; Vornlocher, J. Therapeutic silencing of an endogenous gene by systemic administration of modified siRNAs. *Nature*. **2004**, *432*, 173-178.

[6] Wilda, U.; Fuchs, W.; Wossmann, A.; Borkhardt, M. Killing of leukemic cells with a BCR/ABL fusion gene by RNA interference (RNAi). *Oncogene*. **2002**, *21*, 5716-5724.

[7] McCaffery, A.P.; Nakai, H.; Pandey, K.; Huang, Z.; Salazar, F.H.; Xu, H.; Wieland, S.F.; Marion, P.L.; Kay, M.A. Inhibition of hepatitis B virus in mice by RNA interference. *Nat. Biotechnol*. **2003**, *21*, 639-644.

[8] Davidson, B.L.; Paulson, H.L. Molecular medicine for the brain: silencing of disease genes with RNA interference. *Lancet Neurol*. **2004**, *3*, 145–149.

[9] Cummins, S.R.; Owens, L.M.; Risen, E.A.; Lesnik, S.M.; Freier, D.; McGee, C.J.; Guinosso, P.D.; Cook, L.L. Characterization of fully 2'-modified oligoribonucleotide hetero- and homoduplex hybridization and nuclease sensitivity. *Nucleic Acid Res*. **1995**, *23*, 2019-2024.

[10] Braasch, S.; Jensen, Y.; Liu, K.; Kaur, K.; Arar, M.A.; White, D.R.; Corey, D.A. RNA interference in mammalian cells by chemically-modified RNA. *Biochemistry*. **2003**, *42*, 7967-7975.

[11] Hornung, M.; Guenthner-Biller, C.; Bourquin, A.; Ablasser, M.; Schlee, S.; Uematsu, A.; Noronha, M.; Manoharan, S.; Akira, A.; Fougerolles, S.; Endres, G.; Hartmann, V. Sequence-specific potent induction of IFN-alpha by short interfering RNA in plasmacytoid dendritic cells through TLR7. *Nat. Med*. **2005**, *11*, 263–270.

[12] Chiu, Y.-L.; Rana, T.M. siRNA function in RNA: A chemical modification analysis. *RNA*. **2003**, *9*, 1034-1048.

[13] Morrissey, J.A.; Lockridge, L.; Shaw, K.; Blanchard, K.; Jensen, W.; Breen, K. Hartsough; L.; Machemer, S.; Radka; V.; Jadhav, N.; Vaish; S.; Zinnen, C.; Vargeese; K.; Bowman, C.S.; Shaffer; L.B.; Jeffs, A.; Judge, I.; MacLachlan, B.; Polisky, D.V. Potent and persistent in vivo anti-HBV activity of chemically modified siRNAs. *Nat. Biotechnol*. **2005**, *23*, 1002-1007.

[14] Hüttenhofer, A.; Vogel, J. Experimental approaches to identify non-coding RNAs. *Nucleic Acid Res*. **2006**, *34*, 635-646.

[15] Huang, T.-Y.; Liu, J.; Liang, X.; Hodges, B.D.M.; McLuckey, S.A. Collision-induced dissociation of intact duplex and single-stranded siRNA Anions. *Anal. Chem.* **2008**, *80*, 8501-8508.

[16] Gao, H.; Liu, Y.; Rumley, M.; Yuan, H.; Mao, B. Sequence confirmation of chemically modified RNAs using exonuclease digestion and matrix-assisted laser desorption/ionization time-of-flight mass spectrometry. *Rapid Commun. Mass Spectrom.* **2009**, *23*, 3423-3430.

[17] McLuckey, S.A.; Van Berkel, G.J.; Glish, G.L. Tandem mass spectrometry of small, multiply charged oligonucleotides. *J. Am. Soc. Mass Spectrom.* **1992**, *3*, 60-70.

[18] Nyakas, A.; Stucki, S.R.; Schürch, S. Tandem mass spectrometry of modified and platinated oligoribonucleotides. *J. Am Soc. Mass Spectrom.* **2011**, *22*, 875-887.

[19] Xia, Y. Chrisman, P.A.; Erickson, D.E.; Liu, J.; Liang, X.; Londry, F.A.; Yang, M.J.; McLuckey, S.A. Implementation of ion/ion reactions in a quadrupole/time-of-flight tandem mass spectrometer. *Anal. Chem*. **2006**, *78*, 4146-4154.

[20] Xia, Y.; Liang, X.; McLuckey, S.A. Pulsed dual electrospray ionization for ion/ion reactions. *J. Am. Soc. Mass Spectom*. **2005**, *16*, 1750-1756.

[21] Monia, E.A.; Lesnik, C.; Gonzalez, W.F.; Lima, D.; McGee, C.J.; Guinosso, A.M.; Kawasaki, P.D.; Cook, S.M.; Freier, B.P. Evaluation of 2'-modified oligonucleotides containing 2'deoxy gaps as antisense inhibitors of gene-expression. *J. Bio. Chem*. **1993**, *268*, 14514-14522.

[22] Ivleva, Y.Q.; Yu, M.; Gilar, V.B. Ultra-performance liquid chromatography/tandem mass spectrometry (UPLC/MS/MS) and UPLC/MSE analysis of RNA oligonucleotides. *Rapid Commun. Mass Spectrom.* **2010**, *24*, 2631-2640.

[23] McLuckey, S.A.; Vaidyanathan, G.; Habibi-Goudarzi, S. Charged vs. neutral nucleobase loss from multiply charged oligonucleotide anions. *J. Mass Spectrom.* **1995**, *30*, 1222-1229.

[24] Pan, S.; Verhoeven, K.; Lee, J.K. Investigation of the initial fragmentation of oligodeoxynucleotides in a quadrupole ion trap: Charge level-related base loss. *J. Am. Soc. Mass Spectrom.* **2005**, *16*, 1853-1865.

[25] Wu, J.; McLuckey, S.A. Gas phase fragmentation of oligonucleotide ions. *Int. J. Mass Spectrom.* **2004**, *237*, 197-241.

[26] Huang, T.-Y.; Karlamova, A.; Liu, J.; McLuckey, S.A. Ion trap collision-induced dissociation of multiply deprotonated RNA: c/y-ions versus (a-B)/w-ions. *J. Am. Soc. Mass Spectrom.* **2008**, *19*, 1832-1840.

[27] Monn, S.T.M.; Schürch, S. New Aspects of the Fragmentation Mechanisms of Unmodified and Methylphosphonate-Modified Oligonucleotides. *J. Am. Soc. Mass Spectrom.* **2007**, *18*, 984-990.

[28] Rodgers, M.T.; Campbell, S.; Marzluff, E.M.; Beauchamp, J.L. Low-energy collision-induced dissociation of deprotonated dinucleotides: Determination of the energetically favored dissociation pathways and the relative acidities of the nucleic acid bases. *Int. J. Mass Spectrom.* **1994**, *137*, 121-149.

[29] Habibi-Ghoudarzi, S.; McLuckey, S.A. Ion trap collisional activation of the deprotonated deoxymononucleoside and deoxydinucleoside monophosphates. *J. Am. Soc. Mass. Spectrom.* **1995**, *6*, 102-113.

[30] Tromp, J.M.; Schürch, S. Gas phase dissociation of oligonucleotides and their analogues studied by electrospray ionization tandem mass spectrometry. *J. Am. Soc. Mass Spectrom.* **2005**, *16*, 1262-1268.

[31] Schürch, S.; Bernal-Mendez, E.; Leumann, C.J. Electrospray tandem mass spectrometry of mixed-sequence RNA/DNA oligonucleotides. *J. Am. Soc. Mass Spectrom.* **2002**, *13*, 936-945.

[32] Andersen, T.E.; Kirpekar, F.; Haselmann, K.F. RNA Fragmentation in MALDI mass spectrometry studied by H/D-exchange: Mechanism of general applicability to nucleic acids. *J. Am. Soc. Mass Spectrom.* **2006**, *17*, 1353-1368.

[33] Wells, J.M.; McLuckey, S.A. Collision-induced Dissociation (CID) of Peptides and Proteins. *Methods in Enzymology* **2005**, *402*, 148-185.

[34] Xia, Y.; Thomson, B. A.; McLuckey, S. A. Bidirectional Ion Transfer between Quadrupole Arrays: MSn Ion/Ion Reaction Experiments on a Quadrupole/Time-of-Flight Tandem Mass Spectrometer. *Anal. Chem.* **2007**, *79*, 8199-8206.

[35] Farand, J.; Beverly, M. Sequence Confirmation of Modified Oligonucleotides Using Chemical Degradation, Electrospray Ionization, Time-of-Flight, and Tandem Mass Spectrometry. *Anal Chem.* **2008**, *80*, 7414-7421.

[36] Huang, T.-Y.; Kharlamova, A.; McLuckey, S.A. Ion Trap Collision-Induced Dissociation of Locked Nucleic Acids. *J. Am. Soc. Mass Spectrom.* **2010**, *21*, 144-153.

[37] Wang, Z.; Wan, K. X.; Ramanathan, R.; Taylor, J. S.; Gross, M. L. Structure and fragmentation mechanisms of isomeric T-rich oligodeoxynucleotides: A comparison of four tandem mass spectrometric methods. *J. Am. Soc. Mass Spectrom.* **1998,** *9,* 683–691.

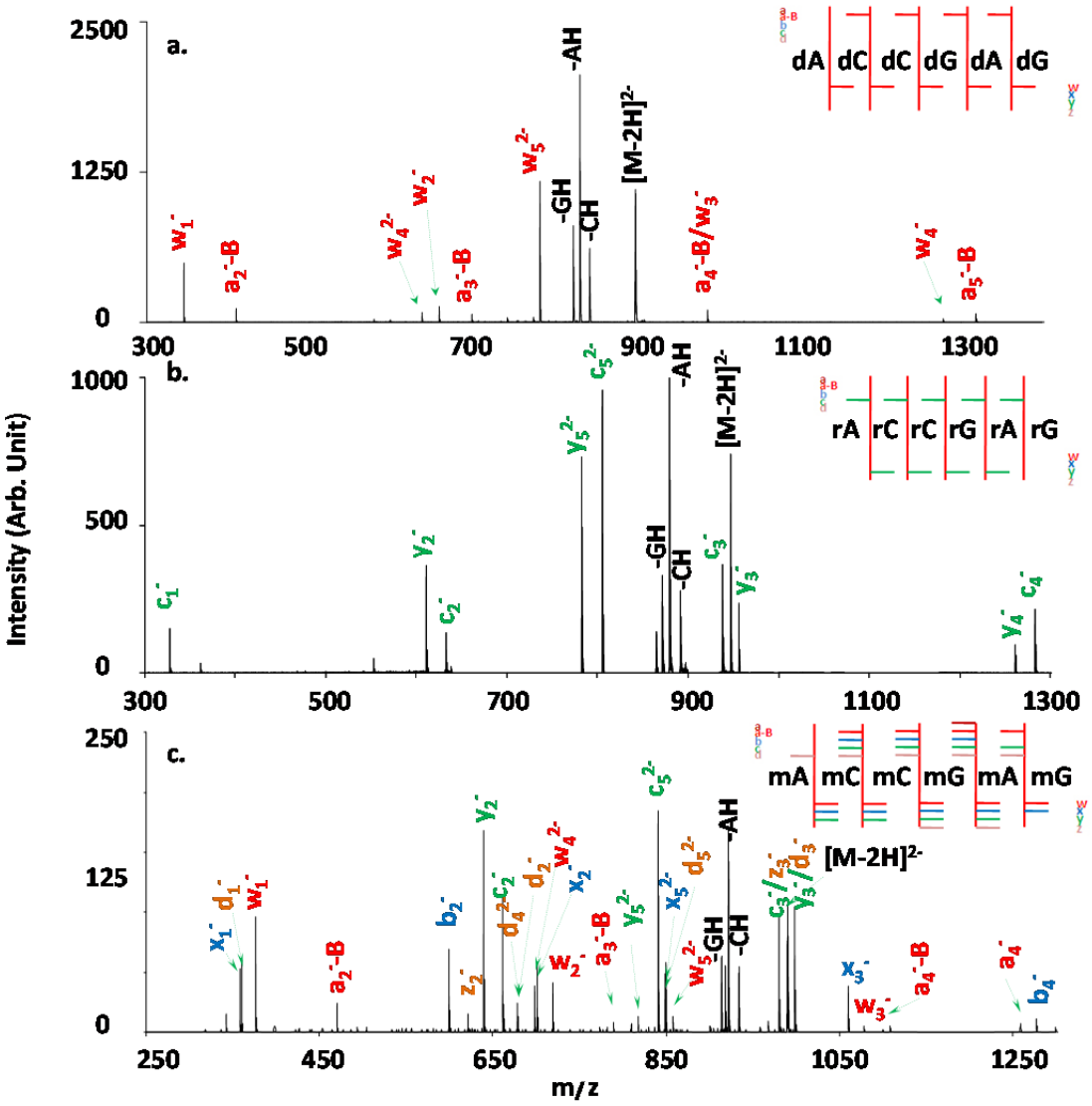

Figure 2.1 Ion trap CID of doubly deprotonated oligonucleotides: (a) DNA 6-mer (dAdCdCdGdAdG), with ion trap CID frequency at 90.5kHz, excitation amplitude at 250mV and excitation time for 100ms; (b) RNA 6-mer (rArCrCrGrArG), 85.5kHz, 250mV and 100ms; (c) 2'-OMe 6-mer (mAmCmCmGmAmG), 82.05kHz, 250mV and 100ms.

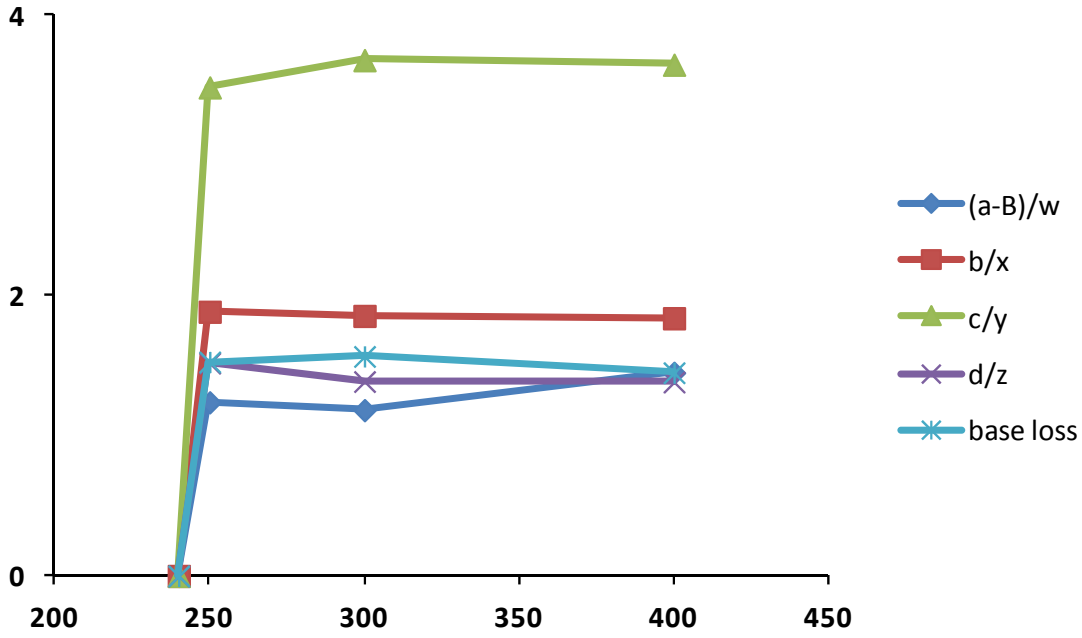

Figure 2.2 Relative abundance versus excitation amplitude for ion trap CID of doubly deprotonated 2'-OMe 6-mer (mAmCmCmGmAmG). The abundances were normalized to the most abundant peak in the spectrum. Excitation amplitude was raised to the point where no precursor ions could be seen in the product spectrum.

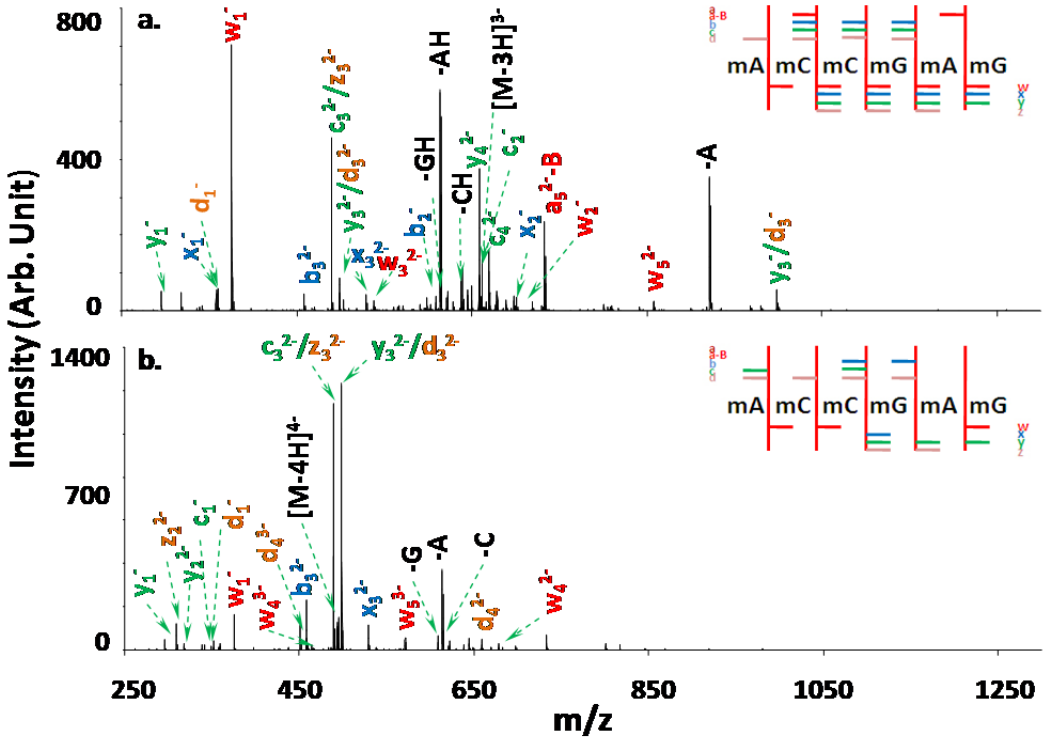

Figure 2.3 Ion trap CID of the 2'-OMe 6-mer (mAmCmCmGmAmG) of different charge states: (a) 3- charge state, 123.257kHz, 220mV and 100ms; (b) 4- charge state, 165.66kHz, 155mV and 100ms. Excitation amplitude was set at the level at which 80% of the precursor ions were fragmented.

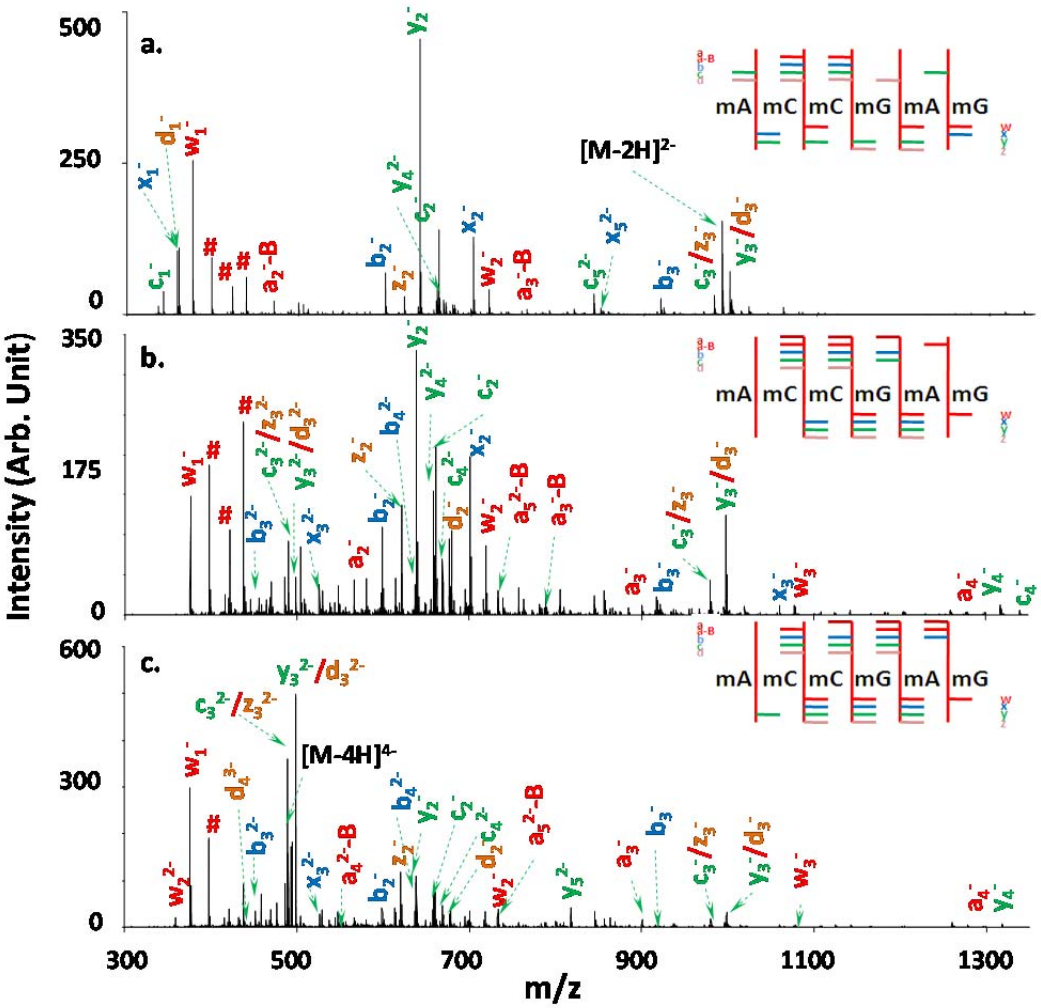

Figure 2.4 Beam type CID spectra of the 2'-OMe 6-mer (mAmCmCmGmAmG) of different charge states: (a) 2- charge state, 90eV; (b) 3- charge state, 99eV, [M-3H]3- peak is between y_4^{2-} and c_2^- but not labeled; (c) 4- charge state, 88eV. "#" represents the internal fragments.

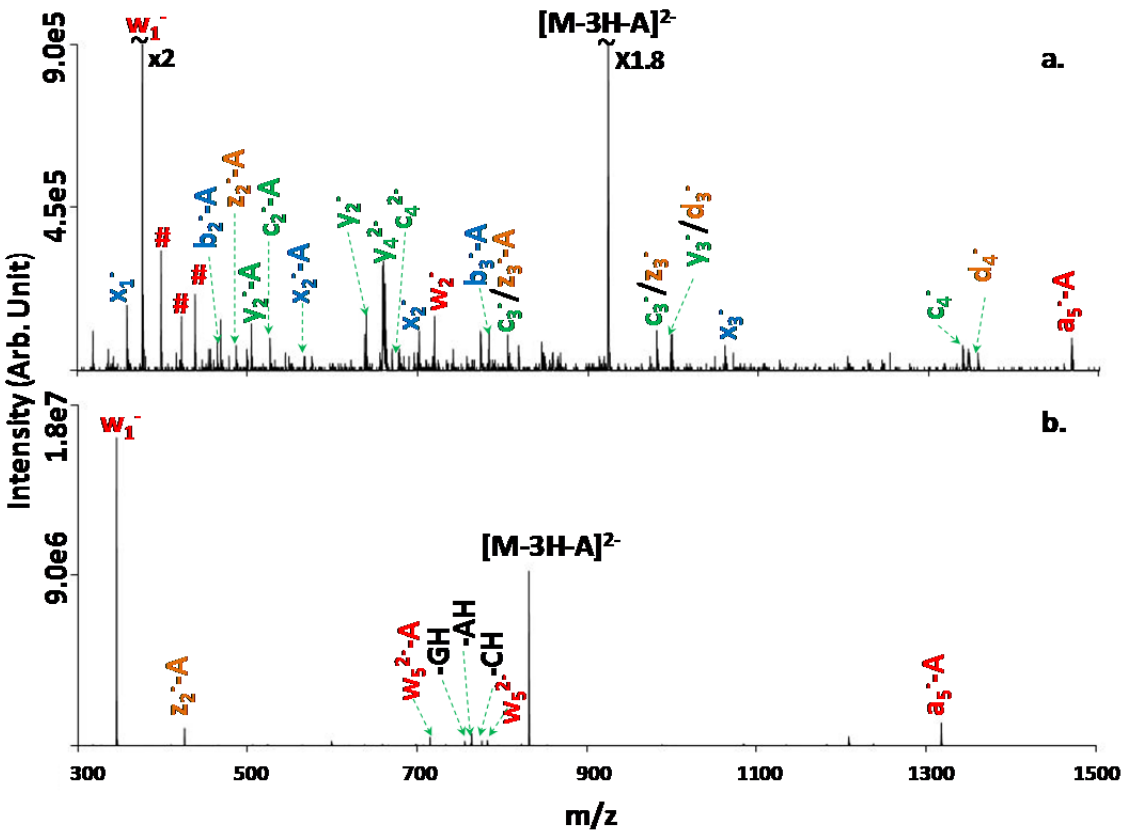

Figure 2.5 Ion trap tandem mass spectra of $[M-3H-A]^{2-}$ of the oligonucleotides: (a) M=2'-OMe RNA 6-mer, 71.139kHz, 130mV and 100ms; (b) M=DNA 6-mer, 71.234kHz, 170mV, 100ms. "#" represents the internal fragments.

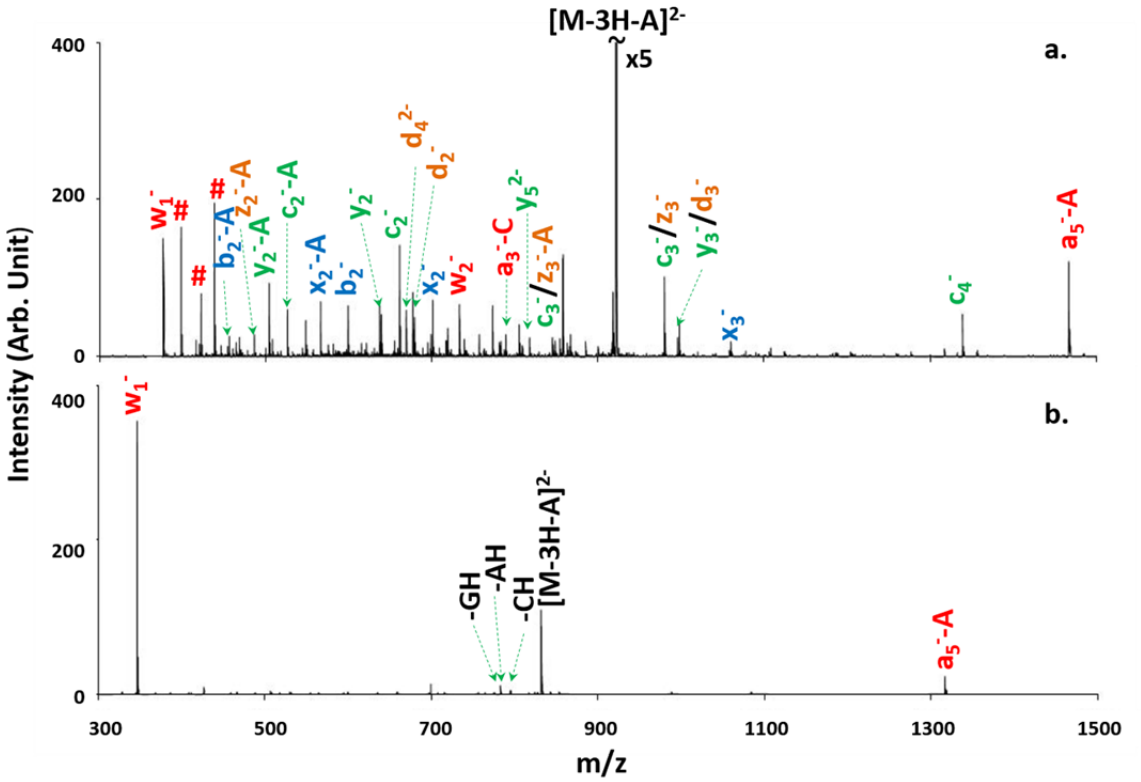

Figure 2.6 Beam-type CID product spectra of $[M-3H-A]^{2-}$ of the oligonucleotides: (a) M=2'-OMe RNA 6-mer, 200eV; (b) M=DNA 6-mer, 200eV. "#" represents the internal fragments.

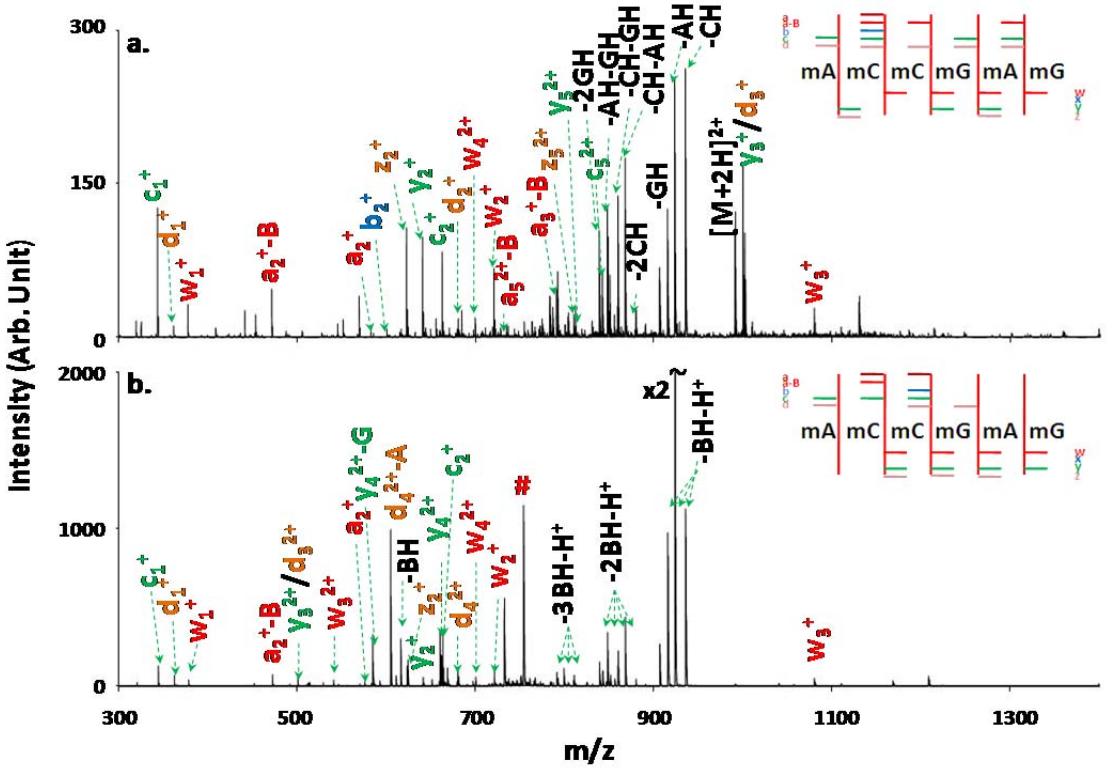

Figure 2.7 Ion trap CID spectra of 2'-OMe RNA 6-mer in positive mode: (a) 2+ charge state, 77.75kHz, 300mV and 100ms; (b) 3+ charge state, 120.63kHz, 230mV and 100ms. "#" represents the internal fragments.

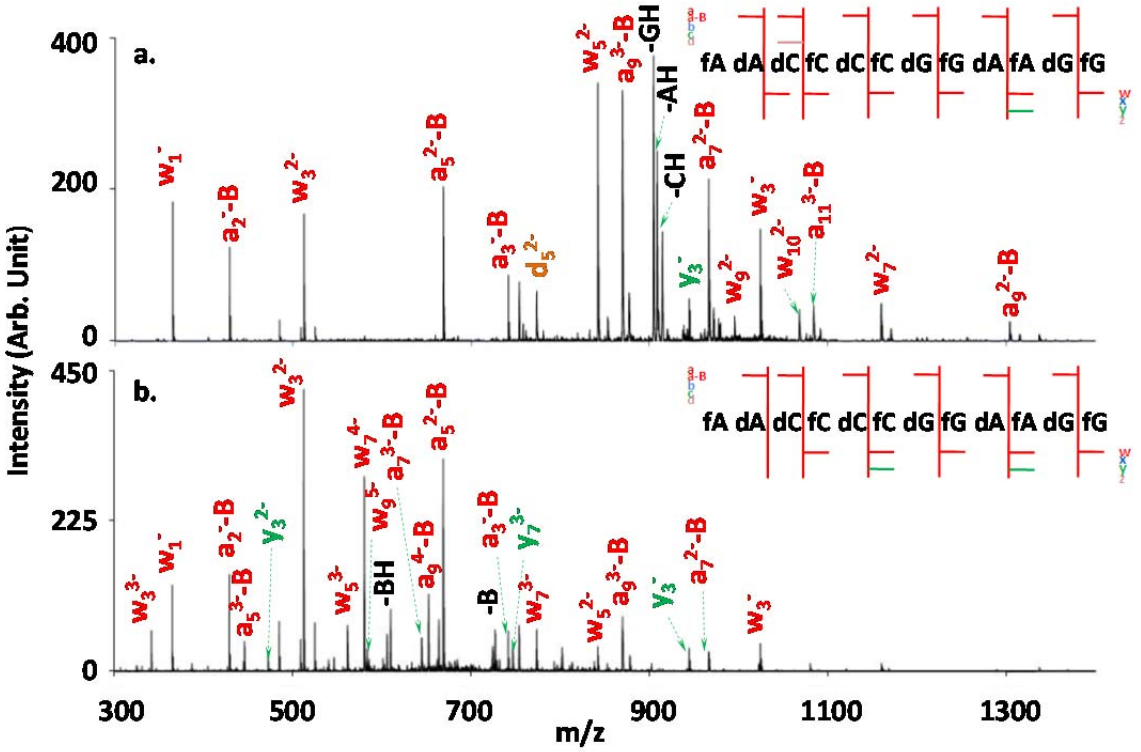

Figure 2.8 Ion trap tandem mass spectra of 2'-(F, H) mix-mer 5'-fAdAdCfCdCfCdGfGdAfAdGfG-3' of different charge states: (a) 4- charge state, 86kHz, 300mV and 100ms; (b) 6- charge state, 130kHz, 300mV and 100ms. The excitation amplitudes were tuned to induce 95% precursor attenuation to generate as many fragment ions as possible. The precursor peaks were not labeled.

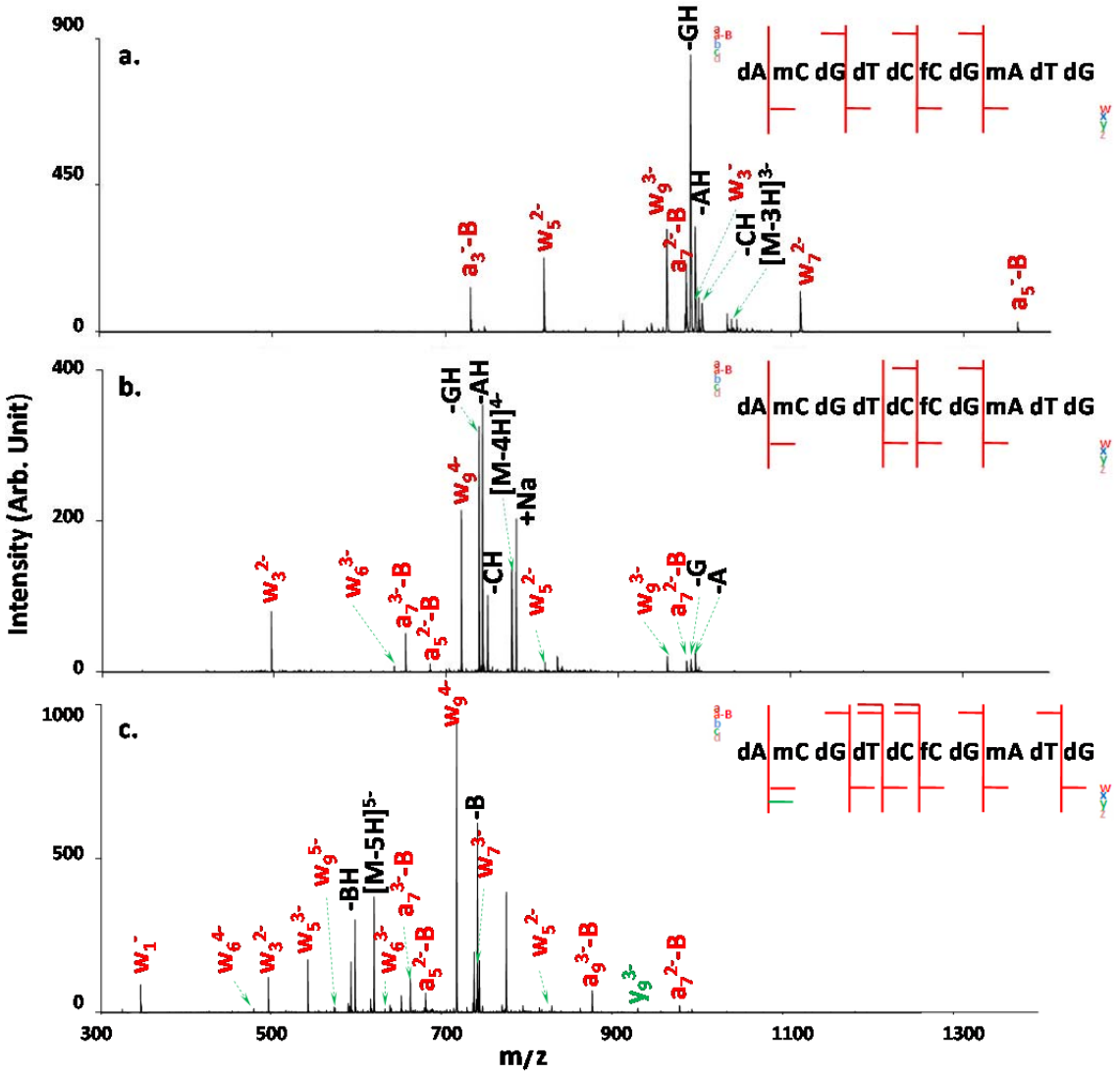

Figure 2.9 Ion trap tandem mass spectra of 2'-(F, H, OMe) mix-mer 5'-dAmCdGdTdCdfCdGmAdTdG-3' of different charge states: (a) 3- charge state, 78.5kHz, 250mV and 100ms; (b) 4- charge state, 104.9kHz, 325mV and 100ms; (c) 5- charge state, 131kHz, 250mV and 100ms. The excitation amplitudes were set to induce 80% precursor attenuation.

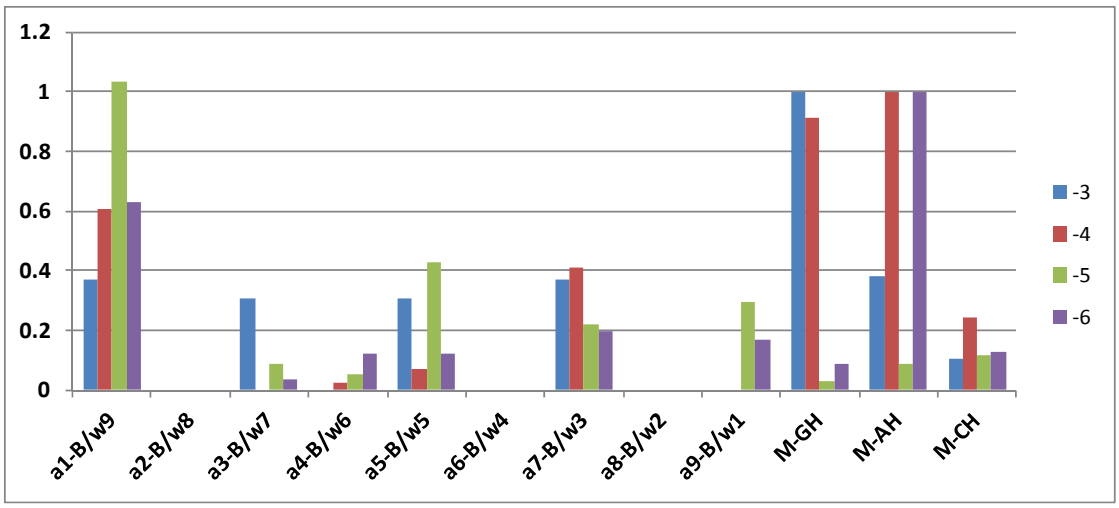

Figure 2.10 Relative intensity of the a-B/w-ion series at various charge states (3- to 6-) under ion trap CID conditions.

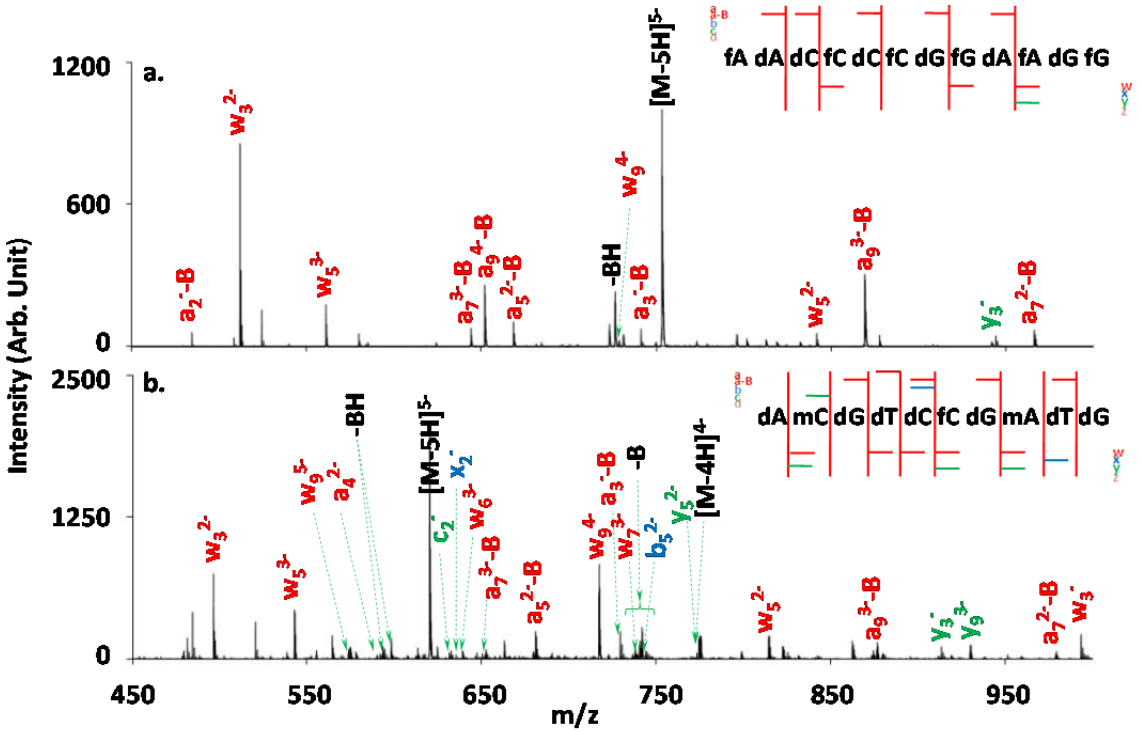

Figure 2.11 (a) Beam type CID of 2'-(F, H) RNA mix-mer $[M-5H]^{5-}$ at a collision energy of 100eV; (b) Beam type CID of 2'-(F, H, OMe) RNA mix-mer $[M-5H]^{5-}$ at a collision energy of 100eV.

CHAPTER 3. ELECTRON TRANSFER FOLLOWED BY COLLISION-INDUCED DISSOCIATION (NET-CID) FOR GENERATING SEQUENCE INFORMATION FROM BACKBONE-MODIFIED OLIGONUCLEOTIDE ANIONS

3.1 Introduction

Oligonucleotide antisense therapies use modified oligonucleotides containing a phosphorothioate (PS) backbones and 2'- modified ribose to improve nuclease resistance and binding affinity[1,2,3,4,5]. Unfortunately, the introduction of the PS modification has resulted in an increased RNase resistance as well as toxicity[6]. Moreover, studies have shown that fully 2'-alkyl modified antisense agents do not induce RNase H activity *in vivo*[7], which is an essential pathway in antisense therapeutics. In practice, antisense oligonucleotides (ASOs) are designed in the form of chimeric oligonucleotide mix-mers to accommodate both toxicity and RNase activity problems[8]. Specifically, a typical chimeric ASO consists of 2'-alkyl or 2'-fluoro nucleotide moieties and deoxynucleotide moieties, the phosphodiester linkages of which are fully or partially modified with PS[9,10]. The complexity of the molecular structures requires analytical tools that are able to distinguish different types of modifications as well as their locations.

Various mass spectrometry methods have been developed for non-modified DNA and RNA characterization, including CID[11,12], photodissociation (PD)[13,14],

electron capture dissociation (ECD)[15,16], electron transfer dissociation (ETD)[17,18], and electron detachment dissociation (EDD)[19,20,21,22,23,24], as well as electron photodetachment dissociation (EPD)[25,26]. However, relatively few efforts have been put into sequencing and characterizing modified oligonucleotide mix-mers. Conventional low energy CID is incapable of providing full sequence information from mix-mer anions comprised of nucleotides with distinct 3'-backbone stabilities towards fragmentation[27]. EPD has been shown to be capable of cleaving PS linkage and generating full sequence coverage for MBO anions[28]. Electron transfer followed by CID or PD has produced almost complete sequence information for chimeric oligonucleotide mix-mer cations with fully PS modified backbone and partially 2'-O-Methyl (2'-OMe) modified ribose[29].

The failure of CID to provide full sequence information for particular oligonucleotide mix-mer anions results from the existing low energy dissociation channels from the deoxynucleotide (base loss channel) or ribonucleotide (5' P-O bond cleavage channel) components[27]. There has been evidence showing that odd-electron oligonucleotide anions do not favor the base loss channel as much as the even-electron species under similar activation conditions[30]. The EPD[28] and ET-CID[29] experiments have shown that supplemental activation of odd-electron oligonucleotide species results in more informative backbone fragmentation. Generally, EPD produces complimentary (a-B)/a/w- and d/z-ions[25,26,28], while ET-CID generates all types of fragments along the backbone[29]. Aiming at producing simple and consistent fragmentation spectra for chimeric oligonucleotide mix-mers, we explored the dissociation patterns of radical anions

of oligonucleotide mix-mers formed via a negative electron transfer reaction with a copper(II) phenanthroline complex. Specifically, an electron is detached from the multiply deprotonated oligonucleotide to form a radical anion (Scheme 3.1). There are also some competing channels such as proton transfer, metal insertion, and metal complex insertion. The odd-electron species that survive the electron transfer process are activated with dipolar resonance excitation in a linear ion trap. This process is termed NET-CID[18].

3.2 Experimental Section

3.2.1 Materials

Methanol, isopropanol and glacial acetic acid were purchased from Mallinckrodt (Phillipsburg, NJ, USA). Copper(II) chloride, 1,10-phenanthroline, piperidine and imidazole were obtained from Sigma-Aldrich (St. Louis, MO). All oligomers, including the 2'-(F, H) mix-mer 5'-fAdAdCfCdCfCdGfGdAfAdGfG-3', 2'-(F, H, OMe) mix-mer 5'-dAmCdGdTdCdfCdGmAdTdG-3', PS 6-mer 5'-dA*dCdC*dGdA*dG-3' ,and PS 2'-OMe 6-mer 5'-mA*mCmC*mGmA*mG-3', were custom synthesized by Integrated DNA Technologies (Coraville, IA, USA). For the sake of clarity with respect to the nature of the modification on the 2'-carbon as well as the backbone, "m" represents the 2'-OMe modification, "f" stands for the 2'-fluoro modification, "d" indicates a deoxyribonucleotide, and "*" represents

the phosphorothioate linkage. The sequence was designed to minimize the occurrence of similar or identical masses from different product ions.

Preparation of oligonucleotide solutions: The oligomer samples were used without further purification. Oligonucleotide solutions for negative nano-electrospray (nanoESI) were prepared to ca. 50 μM in 20: 80 (vol:vol) isopropanol: Diethylpyrocarbonate (DEPC)-treated water with the addition of 25mM piperidine and 25mM imidazole.

Preparation of the metal complex solution: The preparation of the metal complex simply involved mixing copper(II) chloride with three equivalents of 1,10-phenanthroline in a methanol solution to afford a final concentration of 0.1mg/mL. The metal complex solution provided both the bis- and tris-complexes, $[Cu^{II}(phen)_x]^{2+}$ (x=2, 3), upon nanoESI. The bis-complex, $[Cu^{II}(phen)_2]^{2+}$, was selected as the NET reagent.

3.2.2 Apparatus and Procedures

All MS/MS experiments were performed using a prototype version of a QqTOF tandem mass spectrometer (QSTAR, AB Sciex, Concord, ON, Canada) modified to allow for ion/ion reaction studies.[31] A home-built pulsed dual nanoESI source was coupled directly to the nanospray interface to produce ions of both polarities. [32] The multiply charged oligonucleotide anions, $[M-nH]^{n-}$, were generated directly via a nano-ESI emitter. Nitrogen was used as the curtain gas and as the target gas for CID.

In a typical NET-CID experiment, oligonucleotide anions were introduced into mass spectrometer via the negative nano-ESI source and the ions of interest were isolated with Q1 RF/DC and then injected into the Q2 linear ion trap (LIT) at a relatively low kinetic energy. Reagent cations of interest were similarly isolated from the positive nano-ESI of the metal complex solution and introduced into the Q2 LIT, where ions of both polarities were mutually trapped by applying dipolar AC on both exist lenses of Q2. The reaction efficiency was optimized by adjusting the linear accelerator (LINAC) potential [33, 34] to allow maximum overlapping of the cations and anions. Ion/ion reaction time was set to 300ms for all experiments. To perform further ion trap CID, the products of the ion/ion reaction were sent back to Q1 to isolate the charge reduced species[35]. Then, the isolated radical anions were introduced to Q2 for ion trap CID. A dipolar RF signal with frequency in resonance with the fundamental secular frequency of the precursor ion was applied to one pair of rods of Q2 to induce ion trap collisional activation. The product ions were cooled in Q2 and then subjected to mass analysis by time-of-flight (TOF).

3.3 Results and Discussions

3.3.1 NET-CID of 2'-Modified Mix-mers with Phosphodiester Backbones

The structural characterization of 2'-modified mix-mers is inherently complicated due to the competition among different dissociation channels from different modification states at the 2'-carbon. A number of studies have been described that have involved even-electron species of 2'-modified mix-mers of one kind or another and in various contexts.[36,37,38,39,40,41] For even-electron oligodeoxynucleotide species, the facile dissociation pathway is base loss and subsequent 3' C-O bond cleavage[42,43]. However, this pathway is affected by the 2'-alkyl or 2'-F modification[27]. Therefore, ion trap CID of mix-mer anions comprised of DNA residues interspersed with the common 2'-F and 2'-OMe residues, leads to limited backbone fragmentation restricted largely to the DNA residues. In this work, we employ ion trap CID and NET- CID of a few model "mix-mer" species. Specifically, we have examined anions and radical anions of the 2'-(F, H) mix-mer 5'-fAdAdCfCdCfCdGfGdAfAdGfG-3' and the 2'-(F, H, OMe) mix-mer 5'-dAmCdGdTdCdfCdGmAdTdG-3' to allow direct comparison of the fragmentation patterns of even- and odd-electron species.

Figure 3.1a illustrates that 2'-F modification inhibits the facile base loss pathway, as reflected by the lack of 3'-side backbone fragmentation observed for any of the the 2'-F substituted residues as a result of the CID of the $[M-4H]^{4-}$ ion, where M = 5'-fAdAdCfCdCfCdGfGdAfAdGfG-3'. Backbone cleavages were observed only at the 3'-side of the DNA residues. The insets in Figure 1

represent the summary of backbone cleavages, with color coded fragment information (Scheme 3.2). Figure 3.1b shows the ion trap CID product ion spectrum of the $[M\text{-}5H]^{4-\bullet}$ radical anion. The excitation amplitude was set 100mV higher that that used for the $[M\text{-}4H]^{4-}$ ion to induce similar diminution of the precursor ion signal. Backbone fragmentation was observed at almost every phosphodiester linkage with non-complementary d/w-ion pairs. Fragment peaks corresponding to a- and z-ions also appear, with exception of a_6- and z_6-ions, but at far lower abundances Figure 3.2 shows the summary of the contributions of the various ion-types to the spectrum of Figure 3.1b. The d/w-ion formation is consistent with the findings in previous EDD[19-24], EPD[25,26,28] and NETD[18] experiments. The fact that both 2'-F and DNA residues gave rise to backbone cleavages indicates that the 2'-modification does not play a key role in the main sequence-informative fragmentation mechanism(s) of the odd-electron species.

Figure 3.3 shows the ion trap CID product ion spectra of the $[M\text{-}3H]^{3-}$and $[M\text{-}4H]^{3-\bullet}$ ions of the 2'-(F, H, OMe) mix-mer 5'-dAmCdGdTdCdfCdGmAdTdG-3'. This comparison is similar to that of Figure 1 in that the sequence informative fragments from the radical precursor are largely d- and w-ions (see Figure 3.4 for a summary of the contributions of the various backbone fragment ion-types to the spectrum of Figure 3.3b). Base loss is noted in all of the spectra of Figures 3.1 and Figure 3.3. There is little evidence for loss of an even-electron base from the charge-reduced radical anion. For example, very little evidence for $[M\text{-}4H\text{-}BH]^{3-\bullet}$ is observed in the spectrum of Figure 3.3b (see Figure 3.5 for an expansion of the base loss region of Figure 3.3b). We note that proton transfer competes with

electron transfer in generating charge-reduced ions such that some $[M-3H]^{3-}$ ions are present with the $[M-4H]^{3-\bullet}$ ions. Under the resonance excitation conditions used here, the frequency is tuned to activate the $[M-4H]^{3-\bullet}$ ions but $[M-3H]^{3-}$ ions are also activated to some extent. Most of the base loss ions are believed to arise from the off-resonance activation of the $[M-3H]^{3-}$ ions generated from proton transfer. Much of the base loss observed for the CID spectrum of 2'-(F, H) mix-mer radical anion (Figure 3.1b) is also expected to arise from CID of the proton transfer product. The spectra of the ion/ion reaction products collected with higher activation amplitudes, which gives rise to even greater off-resonance excitation, showed increased relative contributions from a-B-ions. An example is provided in Figure 3.6, which shows the product ion spectrum from the 450 mV activation of the ion/ion reaction products from the $[M-5H]^{5-}$ precursor of the 2'-(F,H) mix-mer (compare with the 400 mV activation shown in Figure 3.1b).

The fragmentation mechanism of oligonucleotide radical anions has been proposed by different groups in various contexts.[25,25, 44] The removal of an electron from a multiply-deprotonated oligonucleotide anion via photo-excitation, as in EPD, via electron excitation, as in EDD, and via electron transfer, as in an ion/ion reaction with a cation, all generate radical anion species and are therefore might be expected to lead to similar dissociation behaviors. However, the initial site(s) of electron removal may not be the same for all of these techniques. Evidence for initial radical site formation at the nucleobases in EPD and EDD has been presented. For example, the observation of relatively abundant d-ions at the 3'-side of purine residues, which have relatively low ionization energies (IE)

(i.e., adenine IE = 8.3-8.5 eV; guanine IE = 8.0-8.3 eV[45]), and low d-ion abundances at the 5'-side of the pyrimidine residues, which have relatively high IEs (i.e., thymine IE = 9.0-9.2 eV; uracil = 9.4-9.6; cytosine = 8.8-9.0[45]) has been reported under EDD conditions. On the other hand, w-ions tend to most abundant at the 5'-side of low IE residues and less abundant at the 5'-side of high IE residues. No such tendency is apparent in the electron transfer data described here, however. The recombination energy of the reagent anions used here has been calculated to be 8.4 eV[46], which is too low for removal of an electron from the pyrimidines. We therefore offer in Scheme 3.3 a mechanism for fragment ion formation that begins with electron removal from the backbone rather than from a nucleobase. The radical site then re-locates to the 4'-C on the sugar ring. Subsequent β-cleavage generates a/w$^{\bullet}$, d$^{\bullet}$/z-ions. However, taking the rest of the strand into consideration, the newly formed radical can undergo an intermolecular hydrogen transfer process and transfer the radical to its complimentary fragment. In this way, a mixture of both even- and odd-electron fragments is generated. A close examination of the isotopic distribution of the fragment peaks confirms that hydrogen transfers can occur to generate both even- and odd-electron fragments. This mechanism does not involve the 2'-position substituents, and therefore is consistent with the fact that fragmentation does not appear to be affected by the 2'-modification.

Scheme 3.3 rationalizes the generation of a/w and d/z complementary pairs. All ions types have been observed but non-complementary w- and d-ions dominate the spectra. All complementary ion types are presumed to be

generated initially in equal numbers. However, the a- and z-ions are apparently less stable than their complementary w- and d-ions and, based on the dearth of any other clearly recognizable products, likely fragment to w- and d-ions. Scheme 3.4 provides possible pathways for initially formed a_n- and z_n-ions to fragment further to generate d_{n-1}- and w_{n-1}-ions, respectively. In both cases, the formation of a very stable neutral derived from the pentose ring is generated. An alternative to the structure drawn in Scheme 3.4 is a substituted furan. In either case, neutral product stability may be a primary factor in the facility with which the initially formed a- and z-ions fragment further.

3.3.2 NET-CID of Mixed-Backbone Oligonucleotides

Mixed-backbone oligonucleotides (MBOs) have been designed to reduce side effects while maintaining high stability8[9,10]. Generally, MBOs are oligonucleotides with backbones comprised of a mixture of phoshodiester (PO) and phosphorothioate (PS) linkages. Specifically, PS is utilized as an alternative for the common PO linkages by replacing a non-bridging oxygen with a sulfur atom, which renders *in vivo* resistance to endonuclease degradation[47,48]. In order to evaluate the capability of NET-CID to identify the sequence and modification sites of MBOs, the ion trap CID fragmentation patterns of anions and radical anions of the PS 6-mer 5'-dA*dCdC*dGdA*dG-3'and the PS 2'-OMe 6-mer 5'-mA*mCmC*mGmA*mG-3' with mixed backbones comprised of PS (indicated by "*") and PO were explored. Figure 3.7a shows the ion trap CID product spectrum

of the doubly deprotonated PS 6-mer anion. Full sequence coverage consisting of a-B/w-ion pairs was observed, indicating that the backbone cleavage follows the DNA fragmentation pattern. However, multiple dissociation channels were observed for the PS linkages, including b/x- and c/y-fragments, suggesting that the PS modification alters the competition between the various backbone dissociation channels such that more are observed. In contrast, the NETD product spectrum of the same model sequence (Figure 3.7b) gives rise to a/d/w-fragments, as was also noted for the PO backbone 2'-modified mix-mers. For this sequence, supplemental CID was not applied because spontaneous NETD provided ample sequence information. The fragmentation is dominated by formation of d- and w-ions, consistent with the processes depicted in Schemes 3.3 and 3.4. No clear preferential cleavage along the backbone is noted in this case, which is desirable for sequencing.

The a_3-ion in Figure 3.7b generated from ion/ion reaction between $[M-3H]^{3-}$ of PS 6-mer (A*CC*GA*G) and $Cu^{II}(phen)_2$ complex was isolated and subjected to MS^3 (Figure 3.8). a_3-B, d_2 and internal fragments were observed. The fact that a_3-ions do not fully convert to d_2-ions seems not to support the proposed mechanism. However, it is still ambiguous that whether the a_3 we probe has the same structure/stability as the a-ions that do convert to d-ions. Actually, the a-ions we can probe have significant abundance that is comparable to other d/w-ions, indicating that these surviving a-ions might have relatively higher stability than those not seen. Then it might be the situation where we cannot probe the "labile" a-ions that give rise to d-ions.

Molecular systems bearing both mixed backbone and 2'-sugar modifications pose potentially greater structural characterization challenges due to the greater diversity of factors that could impact the dissociation behavior. As shown in Figure 3.9a, backbone dissociation was found to be limited to the PS linkages under CID conditions as a result of a combination of two effects: (1) 2'-OMe modification strengthens the 3'-side backbone by eliminating the low-energy dissociation pathways; and (2) the cleavages leading to b/x- and c/y-ions are relatively more facile at the PS linkages. As a result, the sequence related fragments are b/x- and c/y-ions, which is consistent with the behavior observed in Figure 3.7a. CID of higher charge states gave rise to greater sequence coverage (Figure 3.10a). However, increasing the precursor ion charge state further leads to limited fragmentation (Figure 3.10b). NET-CID of the PS 2'-OMe 6-mer produced nearly full sequence information with a/w/d-ion fragments. We note that c_3/y_3-fragments are also observed in Figure 3.8b, which are likely to arise from off-resonance excitation of the proton transfer species (i.e., $[M-2H]^{2-}$).

It was observed that radical anions of mixed-backbone oligonucleotides formed via electron transfer appear more likely to undergo backbone cleavages than those of exclusively PO-backbone oligonucleotides. The negative electron transfer reaction of the PS 6-mer, for example, generates backbone fragmentation information without further CID (Figure 3.7b). Likewise, the negative electron transfer reaction of the PS 2'-OMe 6-mer also produces backbone cleavages in addition to reducing the charge (Figure 3.11). To rule out variables other than the backbone composition, the completely 2'-OMe modified

PO-backbone oligonucleotide 5'-mAmCmCmGmAmG-3' (2'-OMe 6-mer) was tested under both NET and NET-CID conditions (Figure 3.12). The 2'-OMe 6-mer barely fragments upon electron detachment. CID of the electron transfer product is required to generate rich fragment information. Thus, the phosphorothioate backbone cleavage appears to be more favorable in a negative electron transfer reaction than cleavage of a phosphodiester linkage. More studies are required to be able to draw firm conclusions regarding differences and similarities associated with PO and PS oligomers under NET conditions. We note, however, that the PS linkages are expected to have lower gas phase acidities than the PO linkages[49], which would tend to favor the negative charge residing on the PS groups. Assuming electron detachment from the charge site, the initial radical site formation at the PS linkages would be expected. This could have a significant effect on the mechanism (see Scheme 3.3) by altering the radical migration steps associated with backbone cleavage (i.e., hydrogen transfer reactions to a sulfur radical site versus to an oxygen radical site).

3.4 Conclusions

In this study, NET-CID behavior of oligonucleotide anions with several different substituents at the 2'-carbons of the pentose rings of the oligomers as well as mixed backbones was investigated. The main dissociation processes follow radical mediated mechanisms that do not involve base loss or the 2'-position substituents. As a result, cleavages on the 5' and 3' C-O bonds of the

phosphodiester linkage in mix-mers with 2'-H, 2'-F or 2'-OMe modification are observed, generating non-complementary d/w-ion pairs. Certain a/z-fragments were observed for each specific sequence, while most a/z-fragments were barely above the noise. The d/w-ions were noted to be a mixture of both even- and odd-electron species, which result from an intermolecular hydrogen transfer process. Complete sequence information was obtained regardless of the substitution on the 2'-carbon.

Oligomers that do not have uniform backbone compositions have different CID fragmentation behavior for both the even- and odd-electron anions. Ion trap CID of both the doubly deprotonated PS 6-mer and PS 2'-OMe 6-mer results in extensive backbone cleavages on the PS bonds, with production of b/x- and c/y ions. PS bonds appear to be more labile to the electron detachment process and can give rise to a/w/d-type fragments under NETD conditions. Supplemental CID generates product ions corresponding to the cleavages of PO bonds, indicating there is a relatively low energy barrier for the cleavage of PS bonds. Ultimately, dissociation can be observed between each residue, giving rise to diagnostic sequence information. In conclusion, nearly full sequence information can be obtained by either NETD or NET-CID of oligomers containing various modifications on the 2'-ribose carbon. The presence of phosphorothioate linkages appears to have a greater effect on the radical anion dissociation behavior than modifications of the 2'-ribose carbon, probably due to the role that the sulfur plays in localizing the radical site. Nevertheless, NET-CID generated full sequence coverage for the PS-containing mix-mer studied here. Ion-ion

electron transfer and electron detachment either via electron irradiation or photodetachment are all means for generating radical anions from multiply deprotonated oligonucleotides. The results reported here suggest that there may be differences in fragmentation behavior resulting from these various approaches, possibly due to differences in the locations of initial electron detachment (i.e., backbone versus nucleobase). In any case, NET-CID is promising as a dissociation method that complements CID of even-electron anions derived from backbone modified oligonucleotides.

This chapter was reprinted with permission from Gao, Y., McLuckey, S. A. Electron Transfer Followed by Collision-Induced Dissociation (NET-CID) for Generating Sequence Information from Backbone Modified Oligonucleotide Anions. *Rapid Comm. Mass Spectrom.* **2013**, *27*, 249-257.

3.5 References

[1] Chan, J.H.P.; Lim, S.; Wong, W.S.F. Antisense Oligonucleotides: From Design to Therapeutic Application. *Clin. Exp. Pharmacol. Physiol.* **2006**, *33*, 533-540.

[2] Altmann, K.; Dean, N.M.; Fabbro. D.; Freier, S.M.; Geiger, T.; Häner, R.; Hüsken, D.; Martin, P.; Monia, B.P.; Müller, M.; Natt, F.; Nicklin, P.; Phillips, J.; Pieles, U.; Sasmor, H.; Moser, H.E. Second Generation of Antisense Oligonucleotides: From Nuclease Resistance to Biological Efficacy in Animals. *Chimia.* **1996**, *50*, 168-176.

[3] Stein, C.A.; Cheng, Y.C. Antisense Oligonucleotides as Therapeutic Agents – Is the Bullet Really Magical? *Science*, **1993**, *261*, 1004-1012.

[4] Eckstein, F. Phosphorothioate oligonucleotides: What is Their Origin and What is Unique about Them? *Antisense Nucleic Acids Drug Dev.* **2000**, *10*, 117–121.

[5] Kurreck, J. Antisense Technologies: Improvement Through Novel Chemical Modifications. *Eur. J. Biochem.* **2003**, *270*, 1628-1644.

[6] Levin, A.A. A Review of Issues in the Pharmacokinetics and Toxicology of Phosphorothioate Antisense Oligonucleotides. *Biochimica et Biophysica Acta.* **1999**, *1489*, 69-84.

[7] Dean, N.M.; McKay, R.; Condon, T.P.; Bennett, C.F. Inhibition of Protein Kinase C-alpha Expression in Human A549 Cells by Antisense Oligonucleotides Inhibits Induction of Intercellular Adhesion Molecule 1 (ICAM-1) mRNA by Phorbol Esters. *J. Bio. Chem.* **1994**, *269*, 16416-16424.

[8] Zhang, R.; Wang, H.; Agrawal, S. Novel Antisense Anti-MDM2 Mixed-Backbone Oligonucleotides: Proof of Principle, In Vitro and In Vivo Activities, and Mechanisms. *Curr. Cancer Drug Targets.* **2005**, *5*, 43-49.

[9] Zhou, W.; Agrawal, S. Mixed-Backbone Oligonucleotides as Second-Generation Antisense Agents with Reduced Phosphorothioate-Related Side Effects. *Bioorg. Med. Chem. Lett.* **1998**, *8*, 3269-3274.

[10] Agrawal, S.; Jiang, Z.; Zhao, Q.; Shaw, D.; Cai, Q.; Roskey, A.; Channavajjala, L.; Saxinger, C.; Zhang, R. Mixed-Backbone Oligonucleotides as Second Generation Antisense Oligonucleotides: In vitro and in vivo studies. *Proc. Natl. Acad. Sci. USA.* **1997**, *94*, 2620-2625.

[11] McLuckey, S.A.; Van Berkel, G.J.; Glish, G.L. Tandem Mass Spectrometry of Small, Multiply Charged Oligonucleotides. *J. Am. Soc. Mass Spectrom.* **1992**, *3*, 60-70.

[12] Huang, T.-Y.; Karlamova, A.; Liu, J.; McLuckey, S.A. Ion Trap Collision-Induced Dissociation of Multiply Deprotonated RNA: c/y-ions versus (a-B)/w-ions. *J. Am. Soc. Mass Spectrom.* **2008**, *19*, 1832-1840.

[13] Keller, K.M.; Brodbelt, J.S. Collisionally Activated Dissociation and Infrared Multiphoton Dissociation of Oligonucleotides in a Quadrupole Ion Trap. *Anal. Biochem.* **2004**, *326*, 200-210.

[14] Guan, Z.; Kelleher, N.L.; O'Connor, P.B.; Aaserud, D.J.; Little, D.P.; McLafferty, F.W. 193 nm Photodissociation of Larger Multiply-Charged Biomolecules. *Int. J. Mass Spectrom.* **1996**, *157*, 357-364.

[15] Schultz, K.N.; Hakansson, K. Rapid Electron Capture Dissociation of Mass-Selectively Accumulated Oligodeoxynucleotide Dications. *Int. J. Mass Spectrom.* **2004**, *234*, 123-130.

[16] Hakansson, K.; Hudgins, R.R.; Marshall, A.G.; O'Hair, R. A. J. Electron Capture Dissociation and Infrared Multiphoton Dissociation of Oligodeoxynucleotide Dications *J. Am. Soc. Mass Spectrom.* **2003**, *14*, 23–41.

[17] Smith, S.I.; Brodbelt, J.S. Electron Transfer Dissociation of Oligonucleotide Cations. *Int. J. Mass Spectrom.* **2009**, *283*, 85-93.

[18] Huang, T.-Y.; McLuckey, S.A. Gas phase Ion/Ion Reactions of Rubrene Cations and Multiply Charged DNA and RNA Anions. *Int. J. Mass Spectrom.* **2011**, *304*, 140-147.

[19] Yang, J.; Mo, J. J.; Adamson, J. T.; Håkansson, K. Characterization of Oligodeoxynucleotides by Electron Detachment Dissociation Fourier Transform Ion Cyclotron Resonance Mass Spectrometry. *Anal. Chem.* **2005,** *77,* 1876.

[20] Yang, J.; Håkansson, K. Fragmentation of Oligoribonucleotides from Gas phase Ion-Electron Reactions. *J. Am. Soc. Mass Spectrom.* **2006,** *17,* 1369.

[21] Mo, J. J.; Håkansson, K. Characterization of Nucleic Acid Higher Order Structure by High-Resolution Tandem Mass Spectrometry. *Anal. Bioanal. Chem.* **2006,** *386,* 675.

[22] Kinet, C.; Gabelica, V.; Balbeur, D.; De Pauw, E. Electron Detachment Dissociation (EDD) Pathways in Oligonucleotides. *Int. J. Mass Spectrom.* **2009,** *283,* 206.

[23] Yang, J.; Håkansson, K. Characterization of Oligodeoxynucleotide Fragmentation Pathways in Infrared Multiphoton Dissociation and Electron Detachment Dissociation by Fourier Transform Ion Cyclotron Double Resonance. *Eur. J. Mass Spectrom.* **2009,** *15,* 293.

[24] Taucher, M.; Breuker, K. Top-Down Mass Spectrometry for Sequencing of Larger (up to 61 nt) RNA by CAD and EDD. *J. Am. Soc. Mass Spectrom.* **2010**, *21*, 918.

[25] Gabelica, V.; Tabarin, T.; Antoine, R.; Rosu, F.; Compagnon, I.; Broyer, M.; De Pauw, E.; Dugourd, P. Electron Photodetachment Dissociation of DNA Polyanions in a Quadrupole Ion Trap Mass Spectrometer. *Anal. Chem.* **2006**, *78*, 6564-6572.

[26] Gabelica, V.; Rosu, F.; Tabarin, T.; Kinet, C.; Antoine, R.; Broyer, M.; De Pauw, E.; Dugourd, P. Base-Dependent Electron Photodetachment from Negatively Charged DNA Strands upon 260-nm Laser Irradiation. *J. Am. Chem. Soc*. **2007**, *129*, 4706-4713.

[27] Gao, Y.; McLuckey, S.A. Collision-Induced Dissociation of Oligonucleotide Anions Fully Modified at the 2'-Position of the Ribose: 2'-F/-H and 2'-F/-H/-OMe Mix-mers. *J. Mass Spectrom.* **2012**, *47*, 364-369.

[28] Smith, S.I.; Brodbelt, J.S. Characterization of Oligodeoxynucleotides and Modifications by 193 nm Photodissociation and Electron Photodetachment Dissociation, *Anal. Chem.* **2010**, *82*, 7218-7226.

[29] Smith, S.I.; Brodbelt, J. S. Hybrid Activation Methods for Elucidating Nucleic Acid Modifications. *Anal. Chem.* **2011**, *83*, 303-310.

[30] McLuckey, S.A.; Stephenson Jr, J.L.; O'Hair, R.A.J. Decompositions of Odd- and Even-Electron Anions Derived from Deoxy-Polyadenylates. *J. Am. Soc. Mass Spectrom.* **1997**, *8*, 148-154.

[31] Xia, Y.; Chrisman, P. A.; Erickson, D. E.; Liu, J.; Liang, X.; Londry, F. A.; Yang, M. J.; McLuckey, S. A. Implementation of Ion/Ion Reactions in a Quadrupole/Time-of-Flight Tandem Mass Spectrometer. *Anal. Chem*. **2006**, *78*, 4146.

[32] Xia, Y.; Liang, X.; McLuckey, S. A. Pulsed Dual Electrospray Ionization for Ion/Ion Reactions. *J. Am. Soc. Mass Spectom*. **2005**, *16*, 1750.

[33] Loboda, A.; Krutchinsky, A.; Loboda, O.; McNabb, J.; Spicer, V.; Ens, W.; Standing, K. Novel Linac II electrode geometry for creating an axial field in a multipole ion guide. *Euro. J. Mass Spectom.* **2000**, *6*, 531.

[34] Liu, J.; Huang, T. -Y.; McLuckey, S. A. Simultaneous Transmission Mode Collision-Induced Dissociation and Ion/Ion Reactions for Top-Down Protein Identification/Characterization Using a Quadrupole/Time-of-Flight Tandem Mass Spectrometer. *Anal. Chem.* **2009**, *81*, 2159.

[35] Xia, Y.; Thomson, B. A.; McLuckey, S. A. Bidirectional Ion Transfer between Quadrupole Arrays: MSn Ion/Ion Reaction Experiments on a Quadrupole/Time-of-Flight Tandem Mass Spectrometer. *Anal. Chem.* **2007**, *79*, 8199.

[36] Nyakas, A.; Stucki, S. R.; Schürch, S. Tandem Mass Spectrometry of Modified and Platinated Oligoribonucleotides. *J. Am Soc. Mass Spectrom.* **2011**, *22*, 875.

[37] Ivleva, V. B.; Yu, Y. Q.; Gilar, M. Ultra-Performance Liquid Chromatography/Tandem Mass Spectrometry (UPLC/MS/MS) and UPLC/MSE Analysis of RNA Oligonucleotides. *Rapid Commun. Mass Spectrom.* **2010**, *24*, 2631.

[38] Tromp, J. M.; Schürch, S. Gas phase Dissociation of Oligonucleotides and Their Analogues Studied by Electrospray Ionization Tandem Mass Spectrometry. *J. Am. Soc. Mass Spectrom.* **2005**, *16*, 1262.

[39] Schürch, S.; Bernal-Mendez, E.; Leumann, C.J. Electrospray Tandem Mass Spectrometry of Mixed-Sequence RNA/DNA Oligonucleotides. *J. Am. Soc. Mass Spectrom.* **2002**, *13*, 936.

[40] Farand, J.; Beverly, M. Sequence Confirmation of Modified Oligonucleotides Using Chemical Degradation, Electrospray Ionization, Time-of-Flight, and Tandem Mass Spectrometry. *Anal Chem.* **2008**, *80*, 7414.

[41] Huang, T. -Y.; Kharlamova, A.; McLuckey, S. A. Ion Trap Collision-Induced Dissociation of Locked Nucleic Acids. *J. Am. Soc. Mass Spectrom.* **2010**, *21*, 144.

[42] Rodgers, M. T.; Campbell, S.; Marzluff, E. M.; Beauchamp, J. L. Low-energy Collision-Induced Dissociation of Deprotonated Dinucleotides: Determination of the Energetically Favored Dissociation Pathways and the Relative Acidities of the Nucleic Acid Bases. *Int. J. Mass Spectrom.* **1994**, *137*, 121.

[43] Habibi-Ghoudarzi, S.; McLuckey, S. A. Ion Trap Collisional Activation of the Deprotonated Deoxymononucleoside and Deoxydinucleoside Monophosphates. *J. Am. Soc. Mass. Spectrom.* **1995**, *6*, 102.

[44] Zheng, Y.; Cloutier, P.; Hunting, D. J.; Sanche, L.; Wagner, J. R. Chemical Basis of DNA Sugar-Phosphate Cleavage by Low-Energy Electrons. *J. Am. Chem. Soc.* **2005**, *127*, 16592.

[45] Roca-Sanjuán, D.; Rubio, M.; Merchán, M.; Serrano-Andrés, L. Ab Initio Determination of the Ionization Potentials of DNA and RNA Nucleobases. J. Chem. Phys. 2006, 125, 084302.

[46] Crizer, D. M.; Xia, Y.; McLuckey, S. A. Transition Metal Complex Cations as Reagents for Gas phase Transformation of Multiply Deprotonated Polypeptides. *J. Am. Soc. Mass Spectrom.* **2009**, *20*, 1718.

[47] Eckstein, F. Stabilization of DNA by Incorporation of Phosphothioate Groups. *Nucleosides Nucleotides.* **1985**, *4*, 77.

[48] Guga, M.; Boczkowska, M.; Janicka, A.; Maciaszek, B.; Nawrot, S.; Antoszczyk, W. J.; Stec, P. Enhanced P-Stereodependent Stability of Complexes Formed by Phosphorothioate Oligonucleotides Due to Involvement of Sulfur as Strong Hydrogen Bond Acceptor. *Pure Appl. Chem.* **2006**, *78*, 993.

[49] Remko, M.; Liedl, K. R.; Rode, B. M. Gas phase Acidities of HM(=X)XH (M=C, Si; X=O, S) Acids Calculated by *ab initio* Molecular Orbital Methods at the G2 Level of Theory. *Chem. Phys. Lett.* **1996**, *263*, 379.

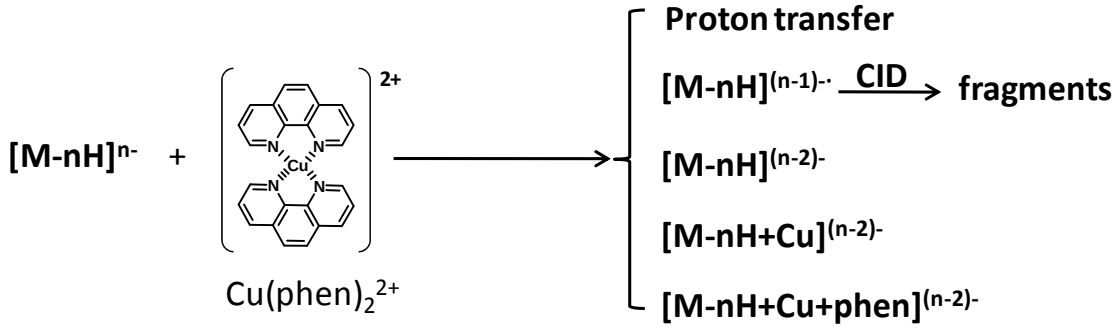

Scheme 3.1 Negative electron transfer reaction and other competing channels.

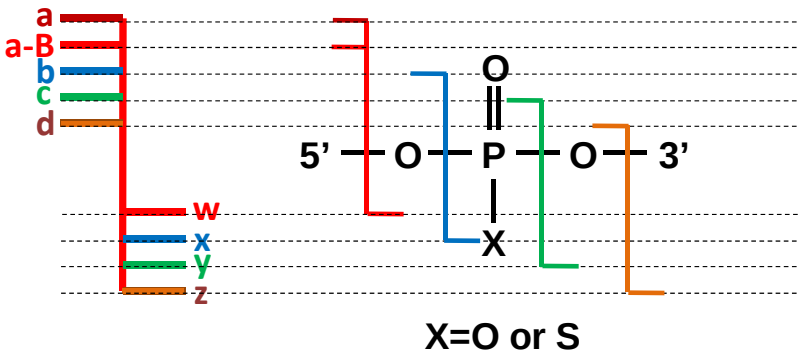

Scheme 3.2 Oligonucleotide fragmentation nomenclature and color coding.

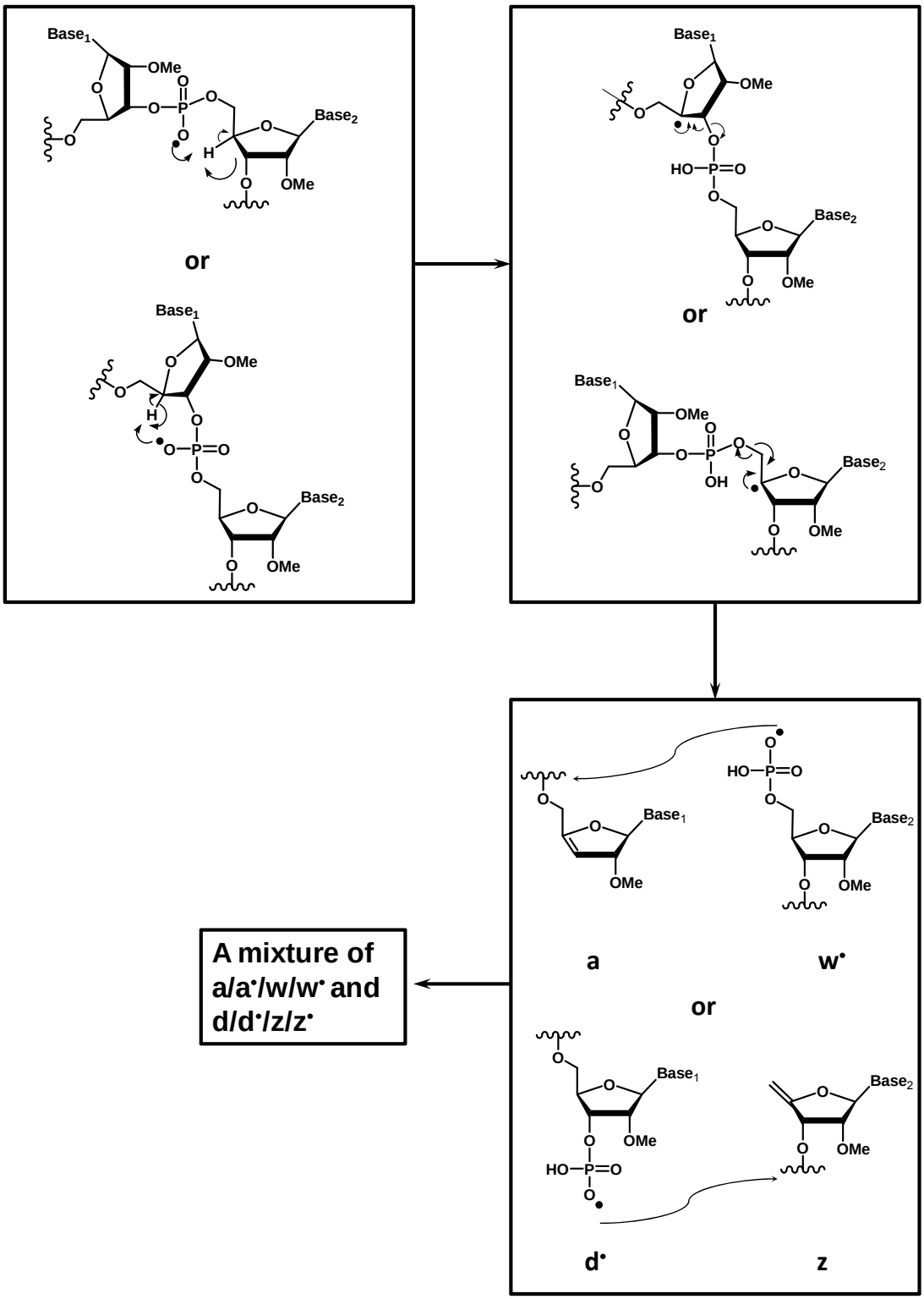

Scheme 3.3 Proposed pathways for phosphodiester bond cleavage following initial electron removal from the phosphodiester linkage.

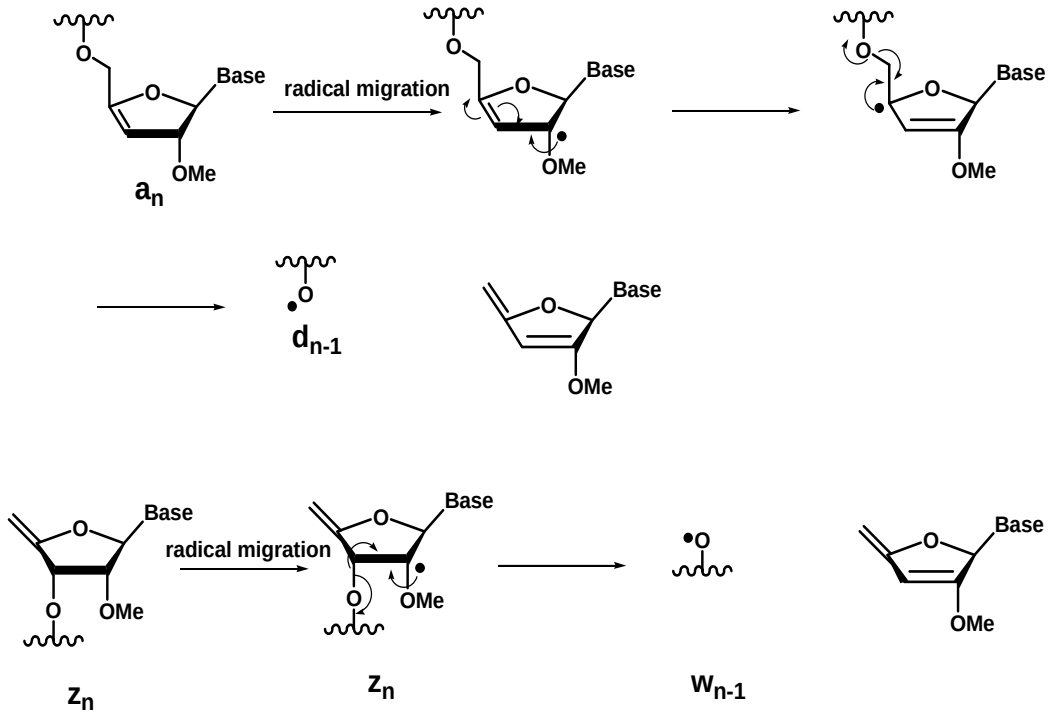

Scheme 3.4 Proposed pathways for the further decomposition of initially formed a- and z-ions.

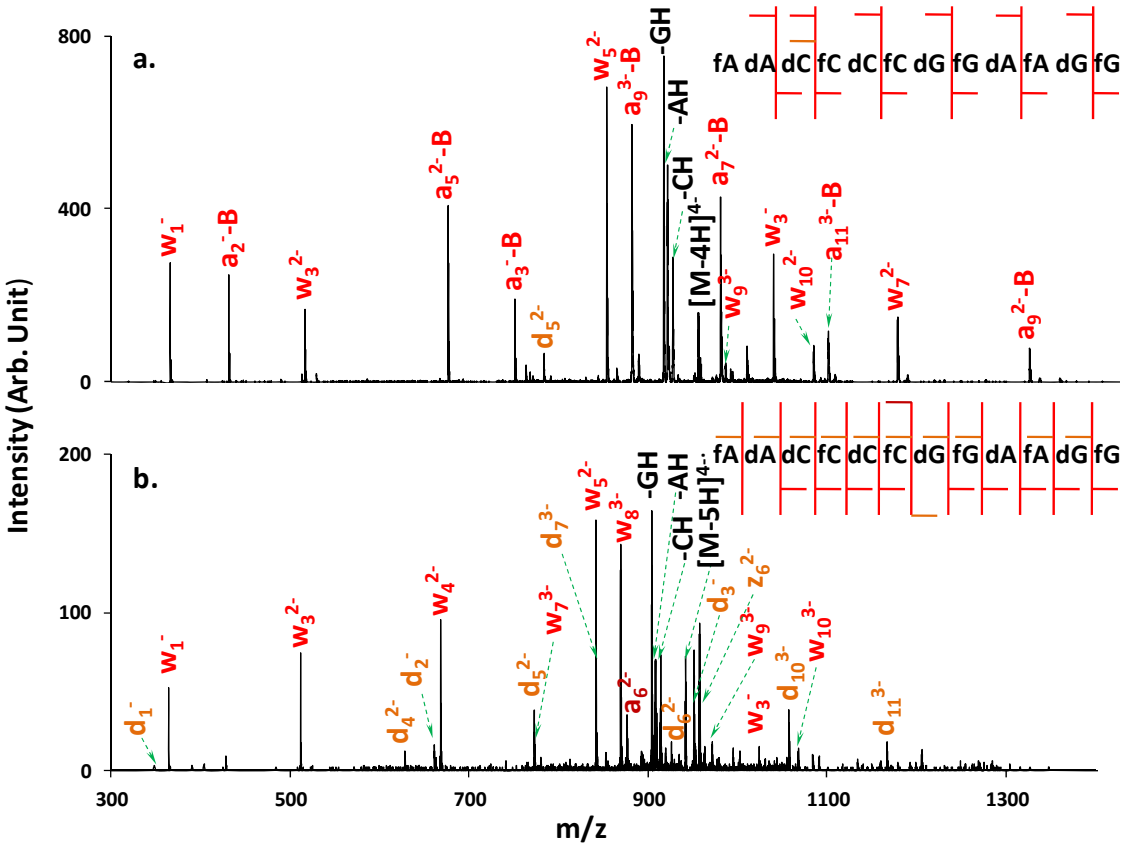

Figure 3.1 MS/MS product ion spectra of 2'-(F, H) mix-mer. (a) Ion trap CID of $[M-4H]^{4-}$, 115kHz dipolar excitation frequency, and the trapping time of 100ms for all , if not otherwise indicated, 300mV excitation amplitude. (b) Ion trap CID of $[M-5H]^{4-\bullet}$ formed from negative electron transfer reaction between $[M-4H]^{4-}$ and $Cu(phen)^{2+}$, 400mV excitation amplitude. (A relatively broad ion isolation window was used for the charge reduced radical anion to avoid any ejection of precursor ions Peaks between *m/z* 943-960, which correspond to Na^+, K^+, O_2 and Cu^{2+} adduction, also appeared within the isolation window. These ions did not contribute to the product ion spectrum, however, due to the mass-selective nature of single frequency ion trap resonance excitation.)

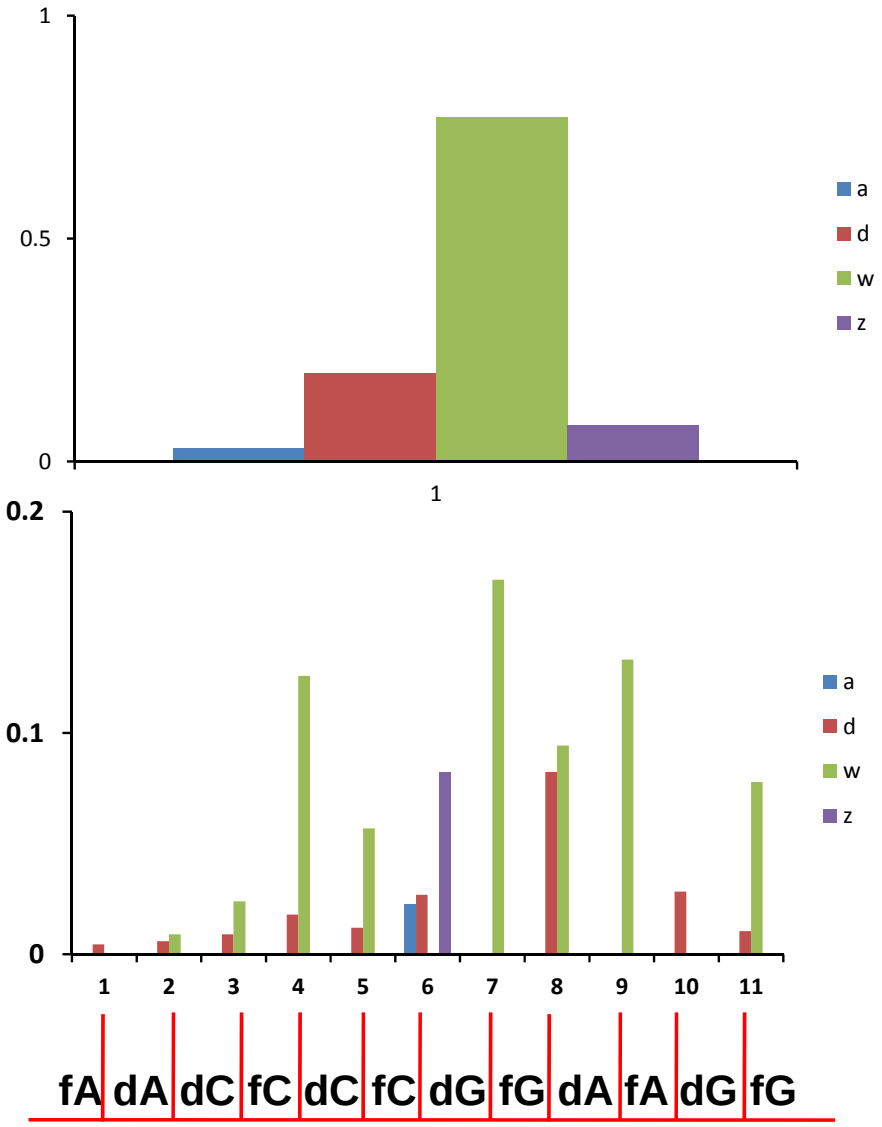

Figure 3.2 (a) Summary of the total contributions from a-, d-, w-, and z-ions to the product ion spectrum of Figure 3.1b of the main text. (b) Breakdown of contributions of the various ion types according to linkage site.

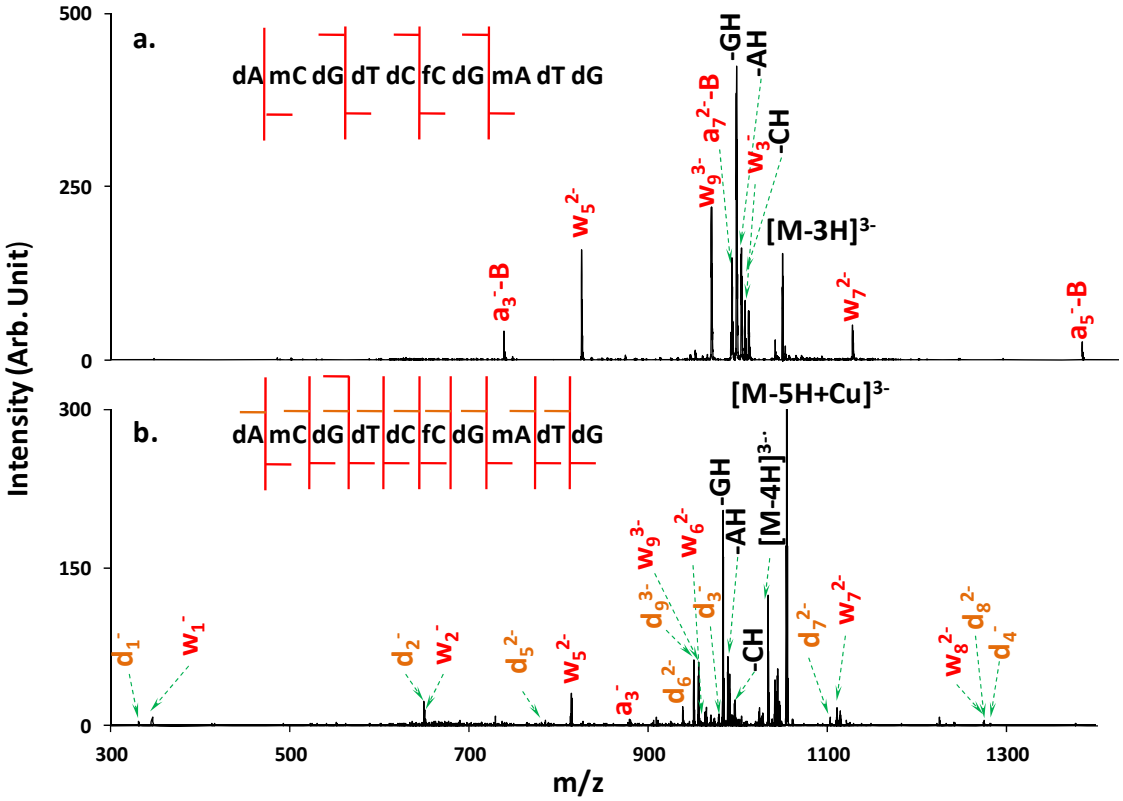

Figure 3.3 MS/MS product ion spectra of 2'- (F, H, OMe) mix-mer. (a) Ion trap CID of $[M-3H]^{3-}$, 250mV excitation amplitude. (b) Ion trap CID of $[M-4H]^{3-\bullet}$ formed from negative electron transfer reaction between $[M-4H]^{4-}$ and $Cu(phen)^{2+}$, 350mV excitation amplitude. The isolation window of the charge reduced radical anion was broad to allow sufficient precursor ions being isolated, allowing for the peaks between *m/z* 1040-1060, which correspond to Na, K, O_2 and Cu adduction.

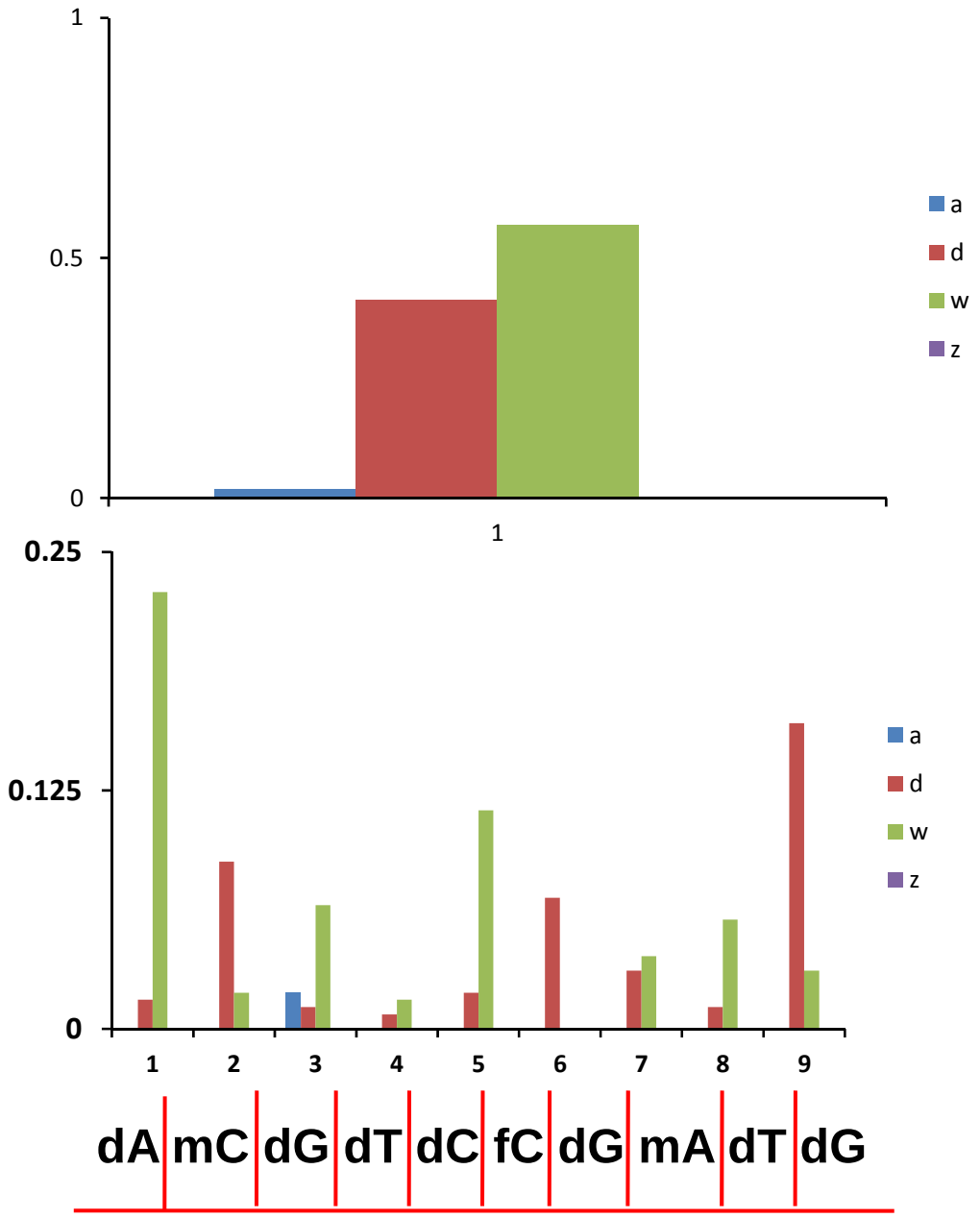

Figure 3.4 (a) Summary of the total contributions from a-, d-, w-, and z-ions to the product ion spectrum of Figure 3.3b of the main text. (b) Breakdown of contributions of the various backbone ion types according to linkage site.

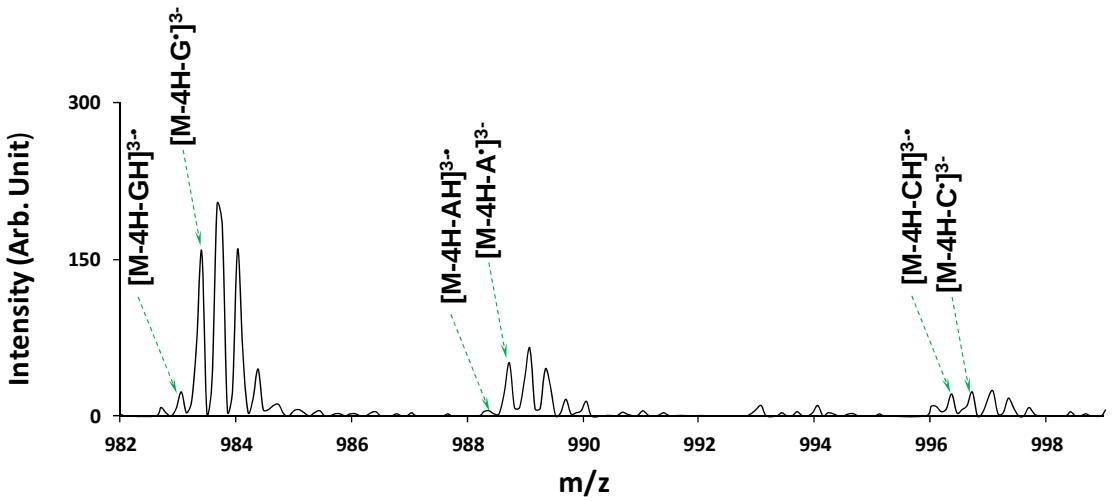

Figure 3.5 Isotopic distribution of base loss peaks from ion trap CID of $[M-4H]^{3-\bullet}$ of 2'-(F, H,OMe) mix-mer.

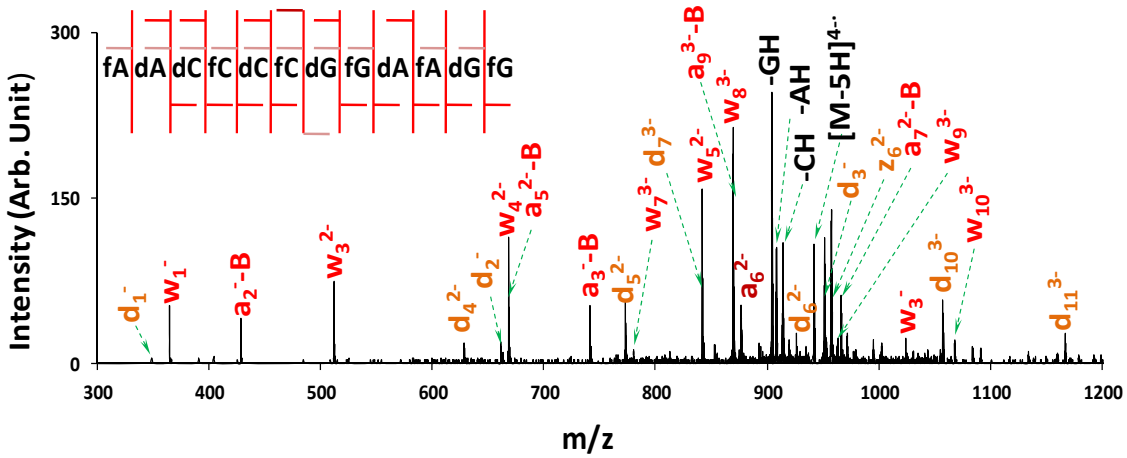

Figure 3.6 MS/MS product ion spectrum of 2'- (F, H) mix-mer. Ion trap CID of $[M-5H]^{4-\bullet}$, excitation amplitude was set to 450mV.

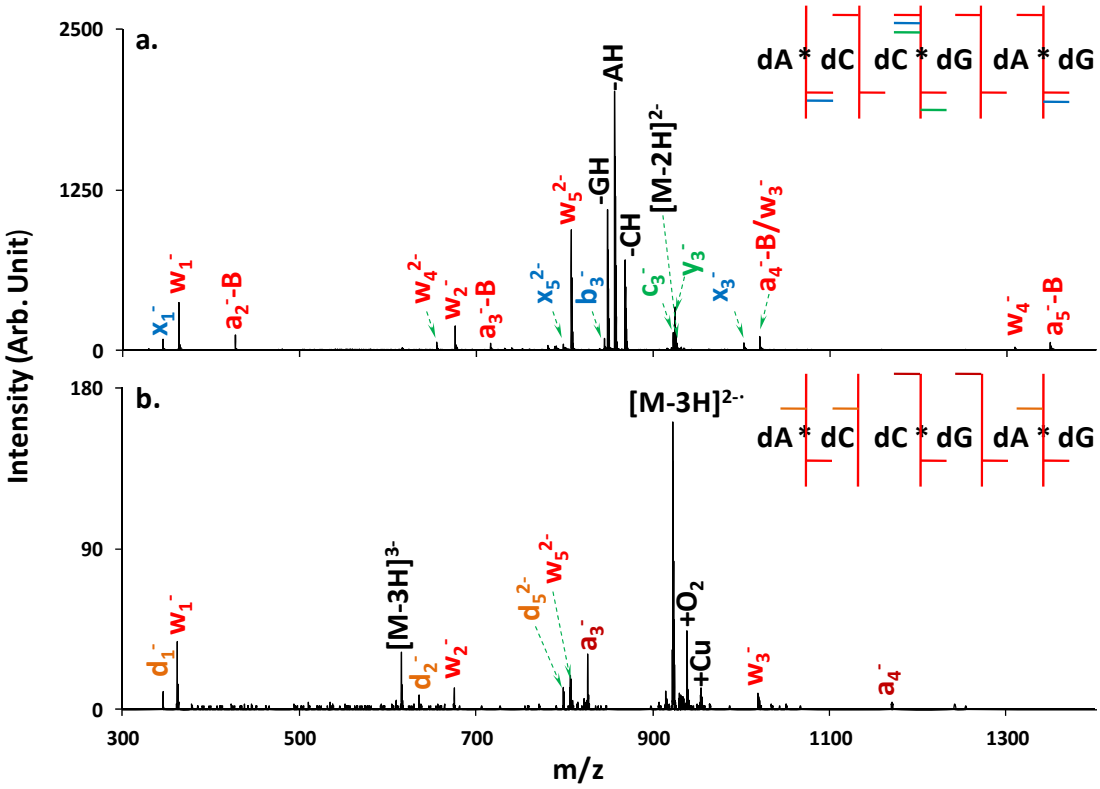

Figure 3.7 MS/MS product ion spectra of PS 6-mer. (a) Ion trap CID of $[M-2H]^{2-}$, 250mV excitation amplitude; (b) Product spectrum of $[M-3H]^{3-}$ reacting with $[Cu^{II}(phen)_2]^{2+}$.

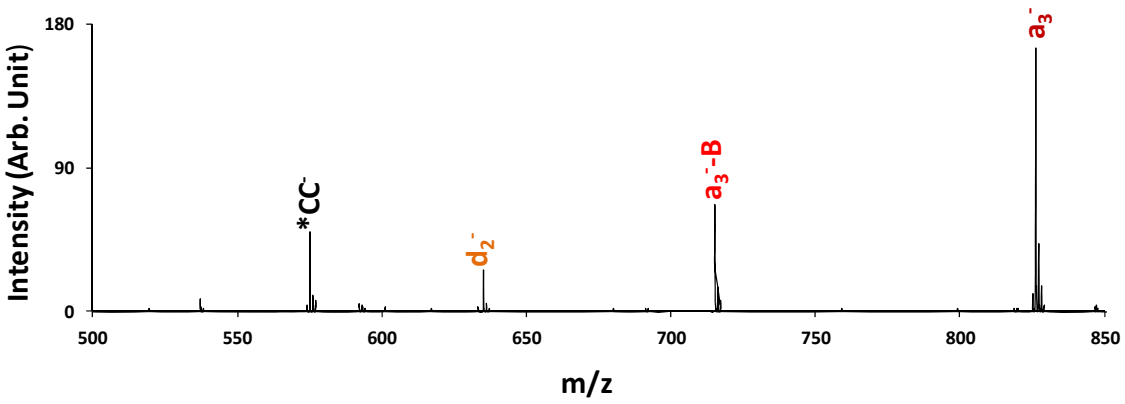

Figure 3.8 MS^3 product ion spectrum of a_3-ions (A*CC) from generated from ion/ion reaction between $[M-3H]^{3-}$ of PS 6-mer (A*CC*GA*G) and $[Cu^{II}(phen)]^{2+}{}_2$.

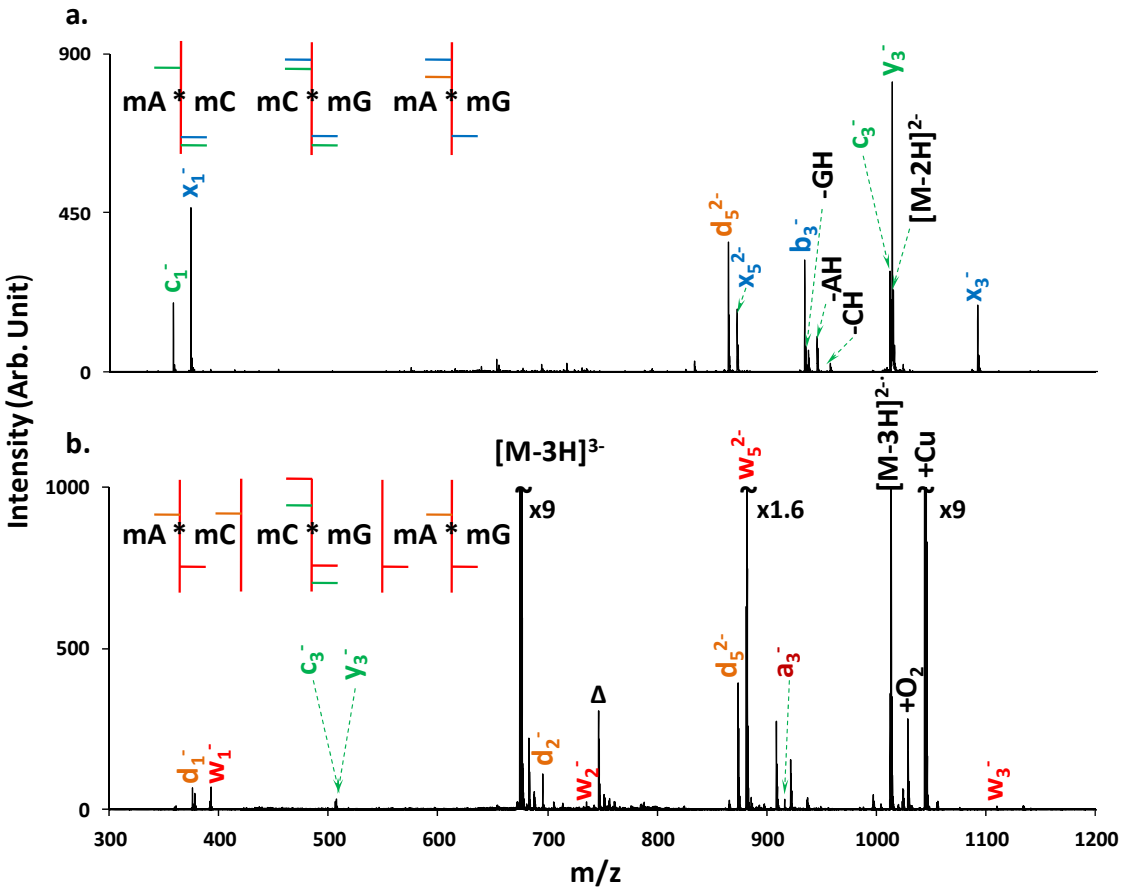

Figure 3.9 MS/MS product ion spectra of PS 2'-OMe 6-mer. (a) ion trap CID of $[M-2H]^{2-}$, 220mV excitation amplitude; (b) ion trap CID of $[M-3H]^{2-\bullet}$ formed from negative electron transfer reaction between $[M-4H]^{4-}$ and $Cu(phen)^{2+}$, 450mV excitation amplitude. Δ represents the triply deprotonated anion with the plasticizer adduct that is commonly seen in an ion trap. Spectrum (b) was obtained without isolating the radical anions due to the low gas phase stability of this species.

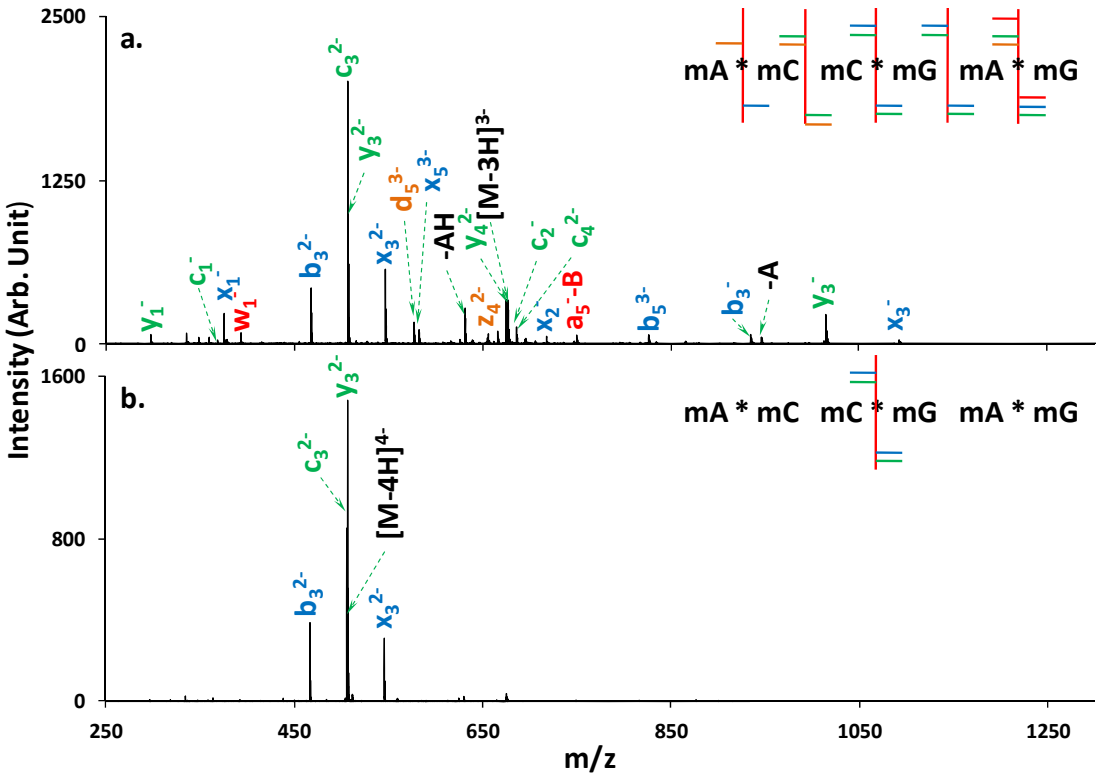

Figure 3.10 Ion trap CID of the PS 2'-OMe 6-mer (mA*mCmC*mGmA*mG) of different charge states: (a) 3- charge state, 120.45kHz, 180mV; (b) 4- charge state, 161.85kHz, 180mV. Excitation amplitude was set at the level at which 80% of the precursor ions were fragmented.

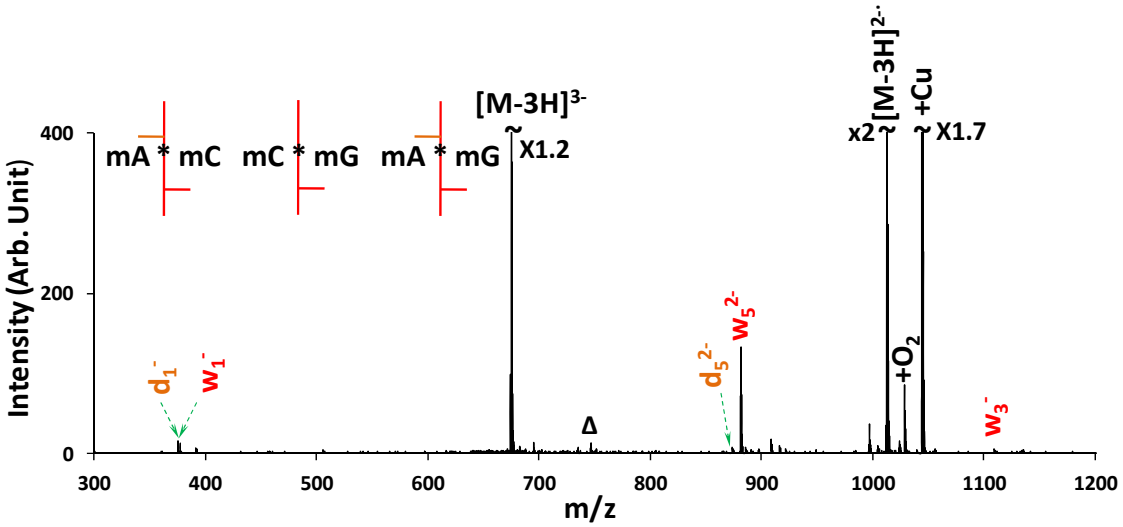

Figure 3.11 MS/MS product ion spectrum of PS 2'-OMe 6-mer ($[M-3H]^{3-}$) reacting with $[Cu^{II}(phen)]^{2+}$. Δ represents the triply deprotonated anion with the plasticizer adduct that is commonly seen in an ion trap.

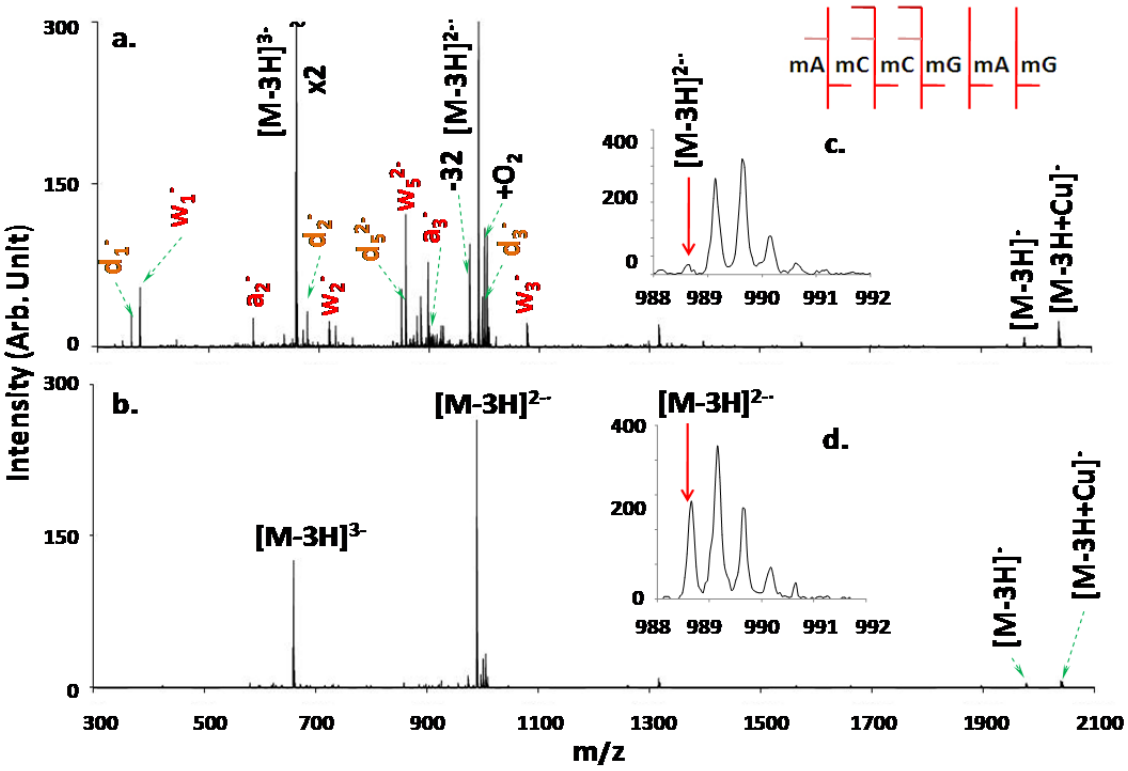

Figure 3.12 MS/MS product ion spectrum of 2'-OMe 6-mer. (a) ion trap CID of $[M-3H]^{2-\bullet}$, excitation amplitude was set to 550mV; (b) product ion spectrum of $[M-3H]^{3-}$ reacting with $[Cu^{II}(phen)]^{2+}$. (c) and (d) are the zoomed-in spectra at the $[M-3H]^{2-\bullet}$ peak showing that the fragments come from the radical anion species.

CHAPTER 4. TOP DOWN INTERROGATION OF CHEMICALLY MODIFIED OLIGONUCLEOTIDES BY NEGATIVE ELECTRON TRANSFER AND COLLISION INDUCED DISSOCIATION

4.1 Introduction

Synthetic oligonucleotides have been extensively researched as drug candidates[1,2,3)]and diagnostic agents[4]. Various chemical modifications have been introduced into such molecules to improve their stability and efficacy as well as minimize toxicity[5,6,7]. Among them, modification of the 2' positionon the pentose ring is widely applied in numerous synthetic oligonucleotides and has proved to be reliable and robust[8]. However, the introduction of modifications in the sugar moietyof oligonucleotide also complicates its characterization, an important part of the quality control foroligonucleotides as therapeutics[9]. And specifically for the chemically modified oligonucleotides, thestructures of base and sugar groups, as well as the order the nucleosides are arranged,will need to be demonstrated.

To address this analytical challenge, both enzymatic digestion [10] and chemical degradation procedure[11] have been described, where both of them showed good success towards confirming the primary structure of purified synthetic oligonucleotide materials. Overall, these approaches are analogous to the bottom-up method used in proteomics, where a large biomolecule is first chemically or enzymatically degraded into smaller components before

characterization by mass spectrometry. An alternative way to address such challenge is the ever more popular top-down strategy, where an oligonucleotidepseudo-molecular cation or anion is subjected to fragmentation in the mass spectrometer and sequence information is derived from the masses of fragment ions. In principle, direct sequencing of oligonucleotides by tandem mass spectrometry is favored over a digestion approach because of its potential advantages in speed, sensitivity, as well as its capability to analyze minor components in a complex mixture. However, in a previous study of the collision-induced dissociation (CID) patterns of 2'-modified mix-mer models, we observed strong differences in the gas phase fragmentation behavior that arise from the various modification sites[12]. Fragmentation of the phosphodiester linkage at the 3'-side of the modified pentose, for example, was not observed with collisional activation when present with DNA residues. Rather, fragmentation tended to dominate at the DNA residue sites. This represents a complicating factor for use of the top-down method to characterize the primary structure of oligonucleotides. Therefore, dissociation approaches that generate sequence information that are not affected by the 2'-modifications are highly desirable.

It has been demonstrated that the 2'-modification plays an important role in the oligonucleotide CID process[12]. The gas phase unimolecular dissociation of DNA gives rise to a-B/w-ions[13], which are generated by a facile base loss process followed by the 3' C-O bond cleavage[14,15,16]. This pathway is favored because the base loss channel requires lower activation energy as opposed to any other backbone cleavages. The mechanism involves a 1,2-elimination step

that requires the 2'-position to be a hydrogen. Once the 2'-position is substituted with other functional groups, this low energy pathway is inhibited. For the CID of RNA, the low-energy base loss channel is inhibited, but there is a c/y-fragmentation channel that arises from 5' P-O bond cleavage involving the 2'-OH functionality[17,18,19]. Likewise, this channel is no longer preferred if the 2'-OH is replacedby other functional groups[17]. According to the previous study of model oligonucleotide mix-mers, fragmentation at the DNA residues outcompetes fragmentation at the phosphodiester linkage to the 3'-side of the 2'-modified ribose to the point that the latter is not observed[12]. When there are no DNA residues, backbone cleavages from the 2'-modified residues are observed even when RNA residues are present[17]. Therefore, chemically modifiedoligonucleotides containing DNA residues are particularly challenging for sequencing and characterization.

A fragmentation method for which the base-loss pathway is not favored may provide non-preferential backbone cleavages for the heavily modifiedoligonucleotides. It has been demonstrated that fragmentation of odd-electron (radical) oligonucleotide anions does not favor the base loss channel under similar activation conditions[20]. Therefore, the gas phase dissociation of the radical species is promising in generating more informative backbone fragmentation. The electron photodetachment dissociation (EPD)[21], electron transfer followed by CID (ET-CID)[22] andnegative electron transfer followed by CID (NET-CID)[23] experiments have shown that supplemental activation of odd-electron (radical) oligonucleotide species is effective in the sequence

determination of 2'-modified model oligonucleotides. There is also evidence that electron detachment dissociation (EDD) [24] generates similar fragmentation patterns as EPD and NET-CID, namely d/w-ions.

In this study, we set out to develop and evaluate a procedure for the identification and characterization of heavily modified oligonucleotides. We have applied the ion trap CID (ion trap CID) and NET-CID to analyze a series of oligonucleotidewith different combinations of modifications at the 2' positions of the sugar moiety. Firstly, a set of oligonucleotideswith a single type of sugar moiety were subjected to ion trap CID to identify the fragmentation patterns for the corresponding even-electron anions. Then, a set of even-electron oligonucleotide mix-mers was studied by ion trap CID to identify how fragmentations at the different modified sites compete with one another. Finally, NET-CID was applied to these mix-mers to demonstrate the utility of using NET-CID to generate high sequence coverage for these highly modified oligonucleotide molecules.

4.2 Experimental Section

4.2.1 Materials

Methanol, isopropanol and glacial acetic acid were purchased from Mallinckrodt (Phillipsburg, NJ, USA). Rubrene, acetonitrile, dichloromethane, piperidine, and imidazole were obtained from Sigma-Aldrich (St. Louis, MO). All oligonucleotides were synthesized in house (Rahway, NJ). For the sake of clarity

with respect to the nature of the modification on the 2' of sugar moiety, "m" represents the 2'-O-methyl modification, "f" stands for the 2'-fluoro modification, "d" indicates a deoxyribonucleotide (Table 4.1 and Figure 4.1). The oligonucleotides are based on two complementary sequences (55664 and 55665) and different 2'-modifications are incorporated along the backbone.

Preparation of solutions: Synthetic oligonucleotide samples were desalted before mass spectrometry analysis. Desalting was carried out using a cation exchange resin. Desalting of oligonucleotides by the cation exchange resin (Amberlite IRN77 hydrogen form) was carried out as described below. The cation exchange resin was rinsed with DEPC-H_2O and then mixed with 100 µL oligonucleotide stock solution of about 200µM at room temperature for 10 min to reduce the cation adducts (Na^+ or K^+). Oligonucleotide solutions for negative nano-electrospray (nanoESI) were prepared to ca. 50 µM in 20: 80 (vol:vol) isopropanol: water with the addition of 25mM piperidine and 25mM imidazole. Rubrene was dissolved in dichloromethane to a concentration of ca. 4 mM and then diluted to ca. 80 µM in 20: 80 (vol:vol) dichloromethane:acetonitrile.

4.2.2 Apparatus and Procedures

All MS/MS experiments were performed using a prototype version of a QqTOF tandem mass spectrometer (QSTAR, AB Sciex, Concord, ON, Canada) modified to allow for ion/ion reaction studies.[25] A home-built pulsed dual nanoESI source was coupled directly to the nanospray interface to produce ions of both

polarities. [26] The multiply charged oligonucleotide anions, $[M-nH]^{n-}$, were generated directly via a nanoESI emitter. Nitrogen was used as the curtain gas as well as the target gas for CID.

In a typical ion trap CID experiment, the oligonucleotide anions were generated via nanoESI and the precursor ions were isolated with Q1 RF/DC and directed into the q2 linear ion trap (LIT) at a relatively low kinetic energy. During the trapping time in q2, an RF amplitude was applied in a dipolar manner to one pair of the rods with frequency in resonance of the fundamental secular frequency of the ion of interest. Excitation of the ion of interest led to an increase in orbited trajectory, resulting in higher energy collisions with the N_2 cooling/bath gas. Conversion of kinetic energy to internal energy subsequently resulted in dissociation. The fragment ions were cooled in q2 and then subjected to mass analysis by time-of-flight (TOF).

In a typical NET-CID experiment, oligonucleotide anions were introduced into the mass spectrometer via the negative nESI source and the ions of interest were isolated and then injected into the q2. Reagent cations of interest were similarly isolated from the positive nano-ESI of the metal complex solution and introduced into the q2 LIT, where ions of both polarities were mutually trapped by applying AC on both entrance and exist lenses of q2. The reaction efficiency was optimized by adjusting the linear accelerator (LINAC) potential [27, 28] to allow maximum overlapping of the cations and anions. To perform further ion trap CID, the products of the ion/ion reaction were sent back to Q1 to isolate the charge

reduced species[29]. Then, the isolated radical anions were introduced to q2 for ion trap CID.

4.3 Results and Discussions

4.3.1 Ion trap CID of Oligonucleotides with Uniformly Modified Backbones.

Previous studies have shown that the 2'-modification can considerably alter the gas phase fragmentation patterns of the short-strand oligonucleotide anions[12,18]. To extend this knowledge based on the short oligomers[12] to the longer oligonucleotides, i.e., 21- and 23-mers, we have synthesized eight oligonucleotides (Table 4.1) that are based on 2 basic sequences (named 55664 and 55665) with 4 different types ofsugarcompositions (2'-H, 2'-OH, 2'-F, 2'-OMe). These molecules were analyzed using a modified QqTOF instrument and their gas phase fragmentation behaviors were studied. Ion trap CID was performed on all eight samples with multiply charged anions ($[M-9H]^{9-}$) as precursors. For 55664 samples, CID of 2'-H oligomers gives rise to a-B/w fragments (Figure 4.2a), CID of 2'-OH oligomers generates c/y fragments (Figure 4.2b), CID of 2'-F (Figure 4.2c) and 2'-OMe (Figure 4.2d) oligomers produces all possible types of backbone cleavages resulting in a/w, b/x, c/y and d/z-fragments. And similar fragmentation was observed for the 55665 samples (Figure 4.3). These data suggest that the gas phase dissociation of the oligonucleotide 21-mers follow the same patterns as those noted for a short

model oligomer system[12]. Briefly, the (a-B)/w fragmentation pattern of the all-DNA oligomer is predicated on the facile base loss channel that involves the 2'-H on the ribose ring[30,31]; the c/y product formation of the all-RNA oligomer results from the 5' P-O bond cleavages due to a rearrangement mechanism involving the 2'-OH substitution[17]. It is noteworthy that ion trap CID of 2'-H 55664 generates relatively poor sequence coverage (defined as the number of cleaved linkage between nucleoside residues divided by the total number of applicable linkages, e.g., 11/22=50% in this case). This is likely due to relatively little sequential fragmentation following base loss, so we performed supplemental activation on the base loss peaks, and successfully improved the sequence coverage to 86% (Figure 4.4). When the 2'-position on the pentose ring is substituted by other functional groups, such as 2'–fluoro (2'-F) or 2'–o-methyl (2'-OMe), the low energy channels are inhibited and therefore other backbone cleavage pathways become competitive. Various fragmentation channels were observed as demonstrated in Figures 4.2c and 4.2d. At least 70% sequence coverage is achieved by ion trap CID for all of the modification states of 55664 and 55665 samples (Figure 4.5), indicating that ion trap CID may be fairly effective in characterizing oligonucleotides with only one type of sugar moiety.

4.3.2 Ion Trap CID of Oligonucleotide Mix-mers

It is relatively straightforward to characterize uniformly 2'-modified oligonucleotides due to the simplicity of the backbone. When the oligonucleotide sequences have more than one type of functional sugar groups, it can be expected that preferential cleavages will happen at the modification sites with the most facile dissociation pathways. To confirm this type of cleavage preference, three oligonucleotide mix-mers with DNA moieties and one oligonucleotide mix-mer with no DNA moieties were subjected to ion trap CID under the same experimental conditions. Figure 4.6 shows the fragment ion maps from ion trap CID of the four oligonucleotide mix-mers. Backbone cleavages are almost exclusively limited to the 3'-side of the DNA residues when DNA residues are present in the sequence (Figure 4.6a-c), and the sequence coverage are 41%, 32% and 32%, respectively. For the oligonucleotide mix-mer with no DNA residues, dissociation is more evenly distributed across the backbone (Figure 4.6d). 16 out of the 20 applicable linkages are cleaved, generating a sequence coverage of 80% for this molecule. This experiment suggests that 2'-OH, 2'-F and 2'-OMe modified backbones have comparable fragmentation threshold during the ion trap CID event, where the 2'-H backbone is less stable and thus gives rise to a more competitive dissociation pathway. As a summary, we have found that the ion trap CID of multiply deprotonated anions is very effective in characterizing oligonucleotides that do not contain any DNA moieties. And for oligonucleotide mix-mers with DNA moieties, ion trap CID might not be able to provide good sequence coverage.

4.3.3 NET-CID and Ion Trap CID of Oligonucleotide Mix-mers

Previous studies have shown that CID of modified oligonucleotide radical anions generates sequence information with little apparent preference for modification state[12], and the radical-directed dissociation mechanism does not involve the 2'-substitution. Therefore, we proceed to examine the utility of NET-CID in characterizing oligonucleotide mix-mers, especially for those that contain DNA moieties. Specifically in this study, we generated radical anions by reacting multiply-charged oligonucleotide anions with rubrene radical cations in the gas phase. Rubrene was chosen as the negative electron transfer reaction reagent because it can be generated as a radical cation via electrospray. This significantly simplifies the instrument set-up by having both ion sources being nano-electrospray.

Two representative oligonucleotide mixers, 2'- (F, H) 55664 and 2'- (F, OH, OMe) 55665 (Table 4.1) were selected to demonstrate the universal fragmentation pattern of NET-CID process. When 200 ms reaction time was used for the 9- charge state of sequence 55665 that contain 2'-OH, 2'-F, and 2'-OMe in sugar moiety, we observed multiple charge reduced products ($[M-9H]^{8-\cdot}$, …) and rubrene adducted peaks (Figure 4.7). The radical anion generated via single electron transfer ($[M-9H]^{8-\cdot}$) was selected for collisional activation, and the resulting MS/MS is shown in the Figure 4.8d. In this case, we observed 102 fragment peaks for NET-CID, where 26 peaks matched theoretical gas phase fragment ions within 100 ppm (Table 4.2), and 23 of them matched to the d and w typed ions. It is noted that c/y-fragments are also observed in the NET-CID

spectrum (Figure 4.8d), which are most likely generated by exciting the even-electron species from proton transfer processes. Therefore, d/w fragments constitutes the major channel for NET-CID fragmentation.

As shown in Figure 4.8a, the sequence coverage obtained from ion trap CID of $[M-8H]^{8-}$ 55665 is 80%. This number can increase to 85% if multiple charge states are investigated. However, if information from both CID spectra of the even-electron (Figure 4.8a) and radical species (Figure 4.8b) are combined, 100% sequence coverage can be achieved. These data suggested that the NET-CID provides additional fragment channels that are complementary to ion trap CID. When combining both techniques, we are able to achieve very high (in this case 100%) sequence coverage.

The NET-CID method was also applied to the 2'-(F, H) 55664 oligonucleotide, where only 27% sequence coverage has been achieved when performing IT-CID study alone (Figure 4.9a). Totally, 48 peaks were observed in the NET-CID (Figure 4.9d), and 26 peaks matched theoretical gas phase fragment ions within 100 ppm (Table 4.3), and 14 of them matched expected d/w-ions. As shown in Figure 4.9d, d/w-fragments constitute the main dissociation products with randomly distributed a/z-fragments also present, and no preferential backbone fragmentation channel is observed. The sequence coverage was improved from 27% (Figure 4.9a) to 64% (Figure 4.9b) for the same charge state. Interestingly, the NET-CID of $[M-7H]^{7-}$, $[M-8H]^{8-}$ and $[M-9H]^{9-}$ of 2'-(F, H) 55664 generate 59%, 64%, 64% sequence coverage, respectively, and we found that their cleavage sites are located on different phosphodiester

linkages (Figure 4.10). This indicates that the NET-CID is affected by the precursor ion charge state, and therefore performing NET-CID on more than one charge states may provide even greater sequence information. To confirm this, we examined the NET-CID of charge states 5- to 9-, and found that combining the information from the 7- to 9- charge states results in a total sequence coverage of 95% (Figure 4.10). The 5- and 6- charge states do not provide any additional sequence information.

From the NET-CID of the studied oligonucleotides, it is apparent that the entire sequence of the oligomer usually cannot be generated by simply performing one experiment with a single charge state, despite the lower sensitivity to 2'-modification states in the odd-electron ions. Other variables, such as gas phase secondary structure and charge site location, may also play important roles. The fact that complementary information is obtained from different charge states strongly suggests that such variables are in play. As there are many variables associated with the size of oligonucleotides, it is hardly surprising that the examination of several ion-types (e.g., odd-electron, even-electron or different charge states) leads to the greatest opportunity for generating higher sequence coverage.

4.4 Conclusions

The identification and complete sequence characterization of highly modified oligonucleotides remains a challenging problem largely due to the

diversity of modification states along the backbone. IT-CID, an extensively utilized activation approach for mass spectrometric sequencing, has proved to be limited to some specific modification combinations in even-electron anions, and the achievable sequence coverage is particularly low when DNA residues are present (largely due to the highly favorable base loss channel associated with deoxyribose). In this report, we have shown that the NET-CID (that entails IT-CID of odd-electron anions) is less sensitive to modification states in oligonucleotides with modified sugars. In the case of oligonucleotides mix-mers with DNA residues (55664), NET-CID can serve as an efficient method to break the DNA as well as non-DNA backbone. Although NET-CID on a single charge state only provides 56-64% sequence coverage, we are able to achieve 95% sequence coverage when combining the MS/MS data from 7-, 8-, and 9- charge states. Indeed, our data suggest that it is desirable to probe different charge states for both even-electron and odd-electron precursor ions to generate the most complete sequence coverage. In summary, we found that the even-electron and odd-electron ions fragment along the backbone by distinct mechanisms that showed distinct sensitivities to the 2'-modification states. This work demonstrates the NET-CID can serve as a part of valuable toolkits to provide high sequence coverage for heavily modified synthetic oligonucleotides. And we believe that such detailed characterization will serve as an important assay to control the quality of therapeutic oligonucleotides, especially for those that are produced under GMP regulations and will eventually be used in clinical studies.

4.5 References

[1] Goodchild, J. Oligonucleotide therapeutics: 25 years agrowing. *Curr.Opin. Mol. Ther.* **2004**, *6*, 120–128.

[2] Opalinska, J.B.; Gewirtz, A.M. Nucleic Acid Therapeutics: Basic Principles and Recent Applications. *Nat. Rev. Drug Discovery.***2002**, *1*, 503–514.

[3] Raal F.J.; Santos, R.D.; Blom, D.J.; Marais, A.D.; Charng, M.J.; Cromwell, W.C.; Lachmann, R.H.; Gaudet, D.; Tan, J.L.; Chasan-Taber, S.; Tribble, D.L.; Flaim, J.D.; Crooke, S.T. Mipomersen, an Apolipoprotein B Synthesis Inhibitor, for Lowering of LDL Cholesterol Concentrations in Patients with Homozygous Familial Hypercholesterolaemia: a Randomised, Double-Blind, Placebo-Controlled Trial. *Lancet*. **2010**, *375*, 998-1006.

[4] Brody, E.N.; Gold, L. Aptamers as therapeutic and diagnostic agents.*J Biotechnol.* **2000**, 74, 5-13.

[5] Chiu, Y.-L.; Rana, T.M. siRNA function in RNA: A chemical modification analysis. *RNA*.**2003**, *9*, 1034-1048.

[6] Morrissey, D.V.; Lockridge, J.A.; Shaw, L.; Blanchard, K.; Jensen, K.; Breen, W.; Hartsough, K.; Machemer, L.; Radka, S.; Jadhav, V.; Vaish, N.; Zinnen, S.; Vargeese, C.; Bowman, K.; Shaffer, C.S.; Jeffs, L.B.; Judge, A.; MacLachlan, I.; Polisky, B. Potent and persistent in vivo anti-HBV activity of chemically modified siRNAs.*Nat. Biotechnol*. **2005**, *23*, 1002-1007.

[7] Manoharan, M. RNA interference and chemically modified small interfering RNAs. *Curr.Opin. Chem. Biol.* **2004**, 8, 570–579.

[8] Chan, J.H.P.; Lim, S.; Wong, W.S.F. Antisense Oligonucleotides: From Design to Therapeutic Application. *Biol.* **2004**, 8, 570–579.

[9] Capaldi, D.; Ackley, K.; Brooks, D.; Carmody, J.; Draper, K.; Kambhampati, R.; Kretschmer, M.; Levin, D.; McArdle, R.; Noll, B.; Raghavachari, R.; Roymoulik, I.; Sharma, B.P.; Thürmer, R.; Wincott, F. Quality Aspects of Oligonucleotide Drug Development: Specifications for Active Pharmaceutical Ingredients. *Drug Information Journal.* **2012***.* 46, 5 611-626.

[10] Cummins,L.L.; Owens, S.R.; Risen, L.M.; Lesnik, E.A.; Freier, S.M.; McGee, D.; Guinosso, C.J.; Cook, P.D. Characterization of fully 2'-modified oligoribonucleotide hetero- and homoduplex hybridization and nuclease sensitivity. *Nucleic Acid Res*. **1995**, *23*, 2019-2024.

[11] Farand, J., Beverly, M. Sequence Confirmation of Modified Oligonucleotides Using Chemical Degradation, Electrospray Ionization, Time-of-Flight, and Tandem Mass Spectrometry. *Anal. Chem.* **2008**, 80, 7414–7421.

[12] Gao, Y, McLuckey, S.A. Collision-induced dissociation of oligonucleotide anions fully modified at the 2 '-position of the ribose: 2 '-F/-H and 2 '-F/-H/-OMe mix-mers. *J. Mass Spectrom.***2012**, *47*, 364-369.

[13] McLuckey, S.A.; Van Berkel, G.J.; Glish, G.L. Tandem Mass Spectrometry of Small, Multiply Charged Oligonucleotides.*J. Am. Soc. Mass Spectrom.* **1992**, *3*, 60-70.

[14] McLuckey, S.A.; Vaidyanathan, G.; Habibi-Goudarzi, S. Charged vs. Neutral Nucleobase Loss from Multiply Charged Oligonucleotide Anions.*J. Mass Spectrom.* **1995**, *30*, 1222-1229.

[15] Pan, S.; Verhoeven, K.; Lee, J.K. Investigation of the Initial Fragmentation of Oligodeoxynucleotides in a Quadrupole Ion Trap: Charge Level-Related Base Loss. *J. Am. Soc. Mass Spectrom.* **2005**, *16*, 1853-1865.

[16] Wu, J.; McLuckey, S.A. Gas phase Fragmentation of Oligonucleotide Ions.*Int. J. Mass Spectrom.* **2004**, *237*, 197-241.

[17] Tromp, J.M.; Schürch, S. Gas phase Dissociation of Oligonucleotides and their Analogues Studied by Electrospray Ionization Tandem Mass Spectrometry. *J. Am. Soc. Mass Spectrom.* **2005**, *16*, 1262-1268.

[18] Schürch, S.; Bernal-Mendez, E.; Leumann, C.J. Electrospray Tandem Mass Spectrometry of Mixed-Sequence RNA/DNA Oligonucleotides.*J. Am. Soc. Mass Spectrom.* **2002**, *13*, 936-945.

[19] Andersen, T.E.; Kirpekar, F.; Haselmann, K.F. RNA Fragmentation in MALDI Mass Spectrometry Studied by H/D-Exchange: Mechanism of General Applicability to Nucleic Acids. *J. Am. Soc. Mass Spectrom.* **2006**, *17*, 1353-1368.

[20] McLuckey, S.A.; Stephenson Jr, J.L.; O'Hair, R.A.J. Decompositions of Odd- and Even-Electron Anions Derived from Deoxy-Polyadenylates. *J. Am. Soc. Mass Spectrom.* **1997**, *8*, 148-154.

[21] Smith, S.I.; Brodbelt, J.S. Characterization of Oligodeoxynucleotides and Modifications by 193 nm Photodissociation and Electron Photodetachment Dissociation, *Anal. Chem.***2010**, *82*, 7218-7226.

[22] Smith, S.I.; Brodbelt, J. S. Hybrid Activation Methods for Elucidating Nucleic Acid Modifications. *Anal. Chem.***2011**, *83*, 303-310.

[23] Gao, Y, McLuckey, S.A. Electron transfer followed by collision-induced dissociation (NET-CID) for generating sequence information from backbone-modified oligonucleotide anions. *Rapid Comm. Mass Spectrom.* **2013**, *27*, 249-257.

[24] Yang, J.; Håkansson, K. Characterization of Oligodeoxynucleotide Fragmentation Pathways in Infrared Multiphoton Dissociation and Electron Detachment Dissociation by Fourier Transform Ion Cyclotron Double Resonance. *Eur. J. Mass Spectrom*. **2009**, 15, 293-304.

[25] Xia, Y.; Chrisman, P.A.; Erickson, D.E.; Liu, J.; Liang, X.; Londry, F.A.; Yang, M.J.; McLuckey, S.A. Implementation of Ion/Ion Reactions in a Quadrupole/Time-of-Flight Tandem Mass Spectrometer. *Anal. Chem*. **2006**, *78*, 4146-4154.

[26] Xia, Y.; Liang, X.; McLuckey. S.A. Pulsed Dual Electrospray Ionization for Ion/Ion Reactions. *J. Am. Soc. Mass Spectom*. **2005**, *16*, 1750-1756.

[27] Loboda, A.; Krutchinsky, A.; Loboda, O.; McNabb, J.; Spicer, V.; Ens, W.; Standing, K. Novel Linac II electrode geometry for creating an axial field in a multipole ion guide.*Euro. J. Mass Spectom.***2000**, *6*, 531-536.

[28] Liu, J.; Huang, T,-Y.; McLuckey, S.A. Simultaneous Transmission Mode Collision-Induced Dissociation and Ion/Ion Reactions for Top-Down Protein Identification/Characterization Using a Quadrupole/Time-of-Flight Tandem Mass Spectrometer.*Anal. Chem.***2009**, *81*, 2159-2167.

[29] Xia, Y.; Thomson, B.A.; McLuckey, S.A. Bidirectional Ion Transfer between Quadrupole Arrays: MS^n Ion/Ion Reaction Experiments on a Quadrupole/Time-of-Flight Tandem Mass Spectrometer. *Anal. Chem.***2007**, *79*, 8199-8206.

[30] Rodgers, M.T.; Campbell, S.; Marzluff, E.M.; Beauchamp, J.L. Low-energy Collision-Induced Dissociation of Deprotonated Dinucleotides: Determination of the Energetically Favored Dissociation Pathways and the Relative Acidities of the Nucleic Acid Bases. *Int. J. Mass Spectrom.***1994**, *137*, 121-149.

[31] Habibi-Ghoudarzi, S.; McLuckey, S.A. Ion Trap Collisional Activation of the Deprotonated Deoxymononucleoside and Deoxydinucleoside Monophosphates. *J. Am. Soc. Mass. Spectrom.* **1995**, *6*, 102-113.

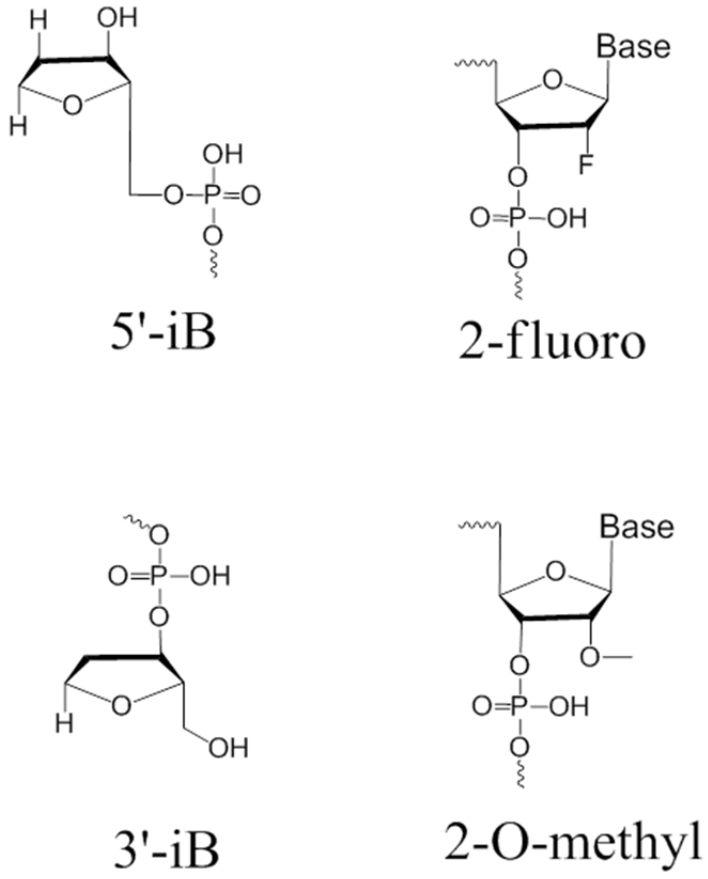

Figure 4.1 Chemically modified nucleotide residues.

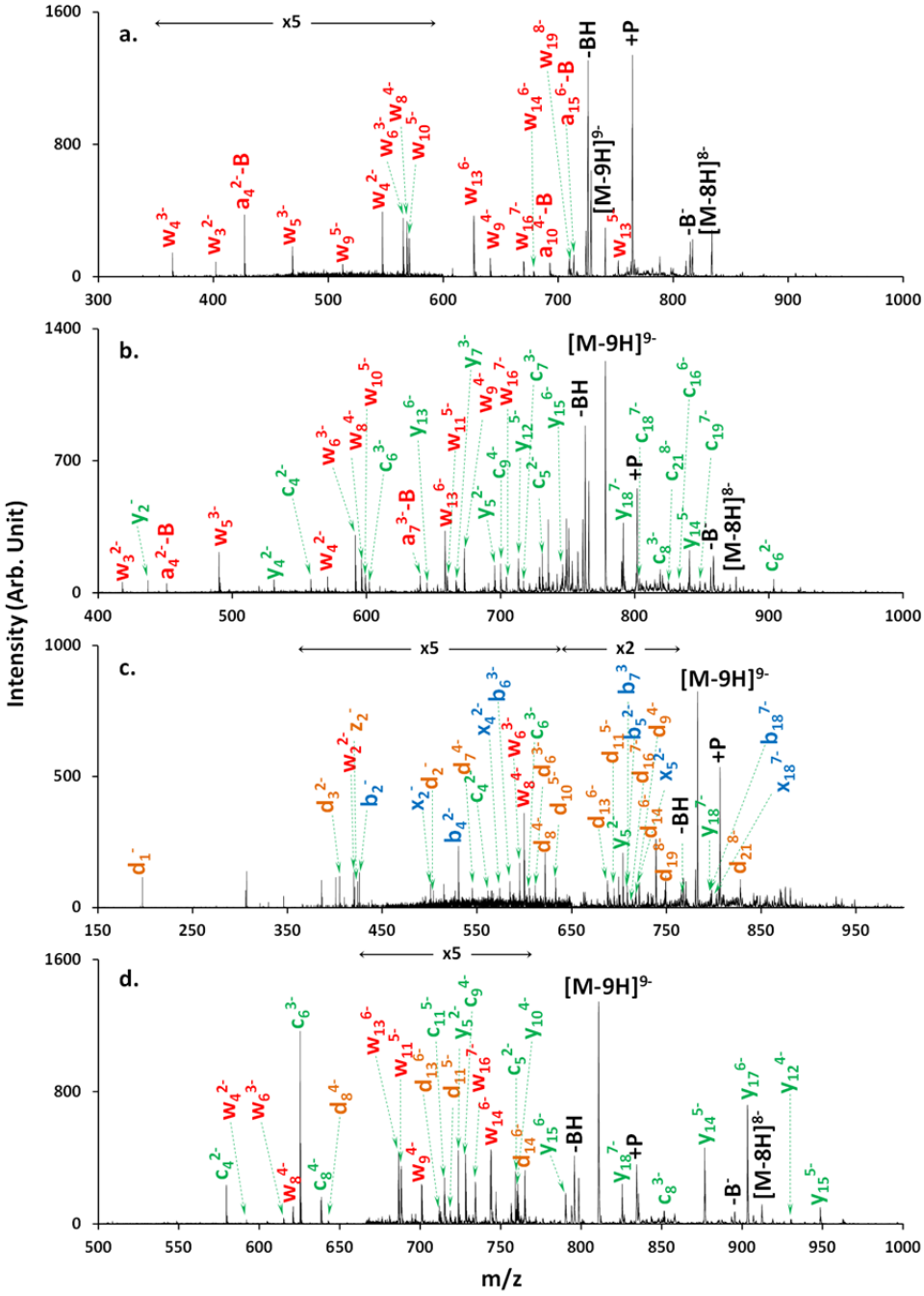

Figure 4.2 Product spectra from ion trap CID of (a) 2'-H 55664; (b) 2'-OH 55664; (c) 2'-F 55664; (d) 2'-OMe 55664 with 475mV dipolar excitation at 115kHz frequency. –BH and $-B^-$ peaks represent neutral and charged base losses. +P peaks indicate $[M-9H+plasticizer]^{9-}$, which is formed by ion/molecule reactions when the oligonucleotide anions are exposed to the plasticizer present in the vacuum housing.

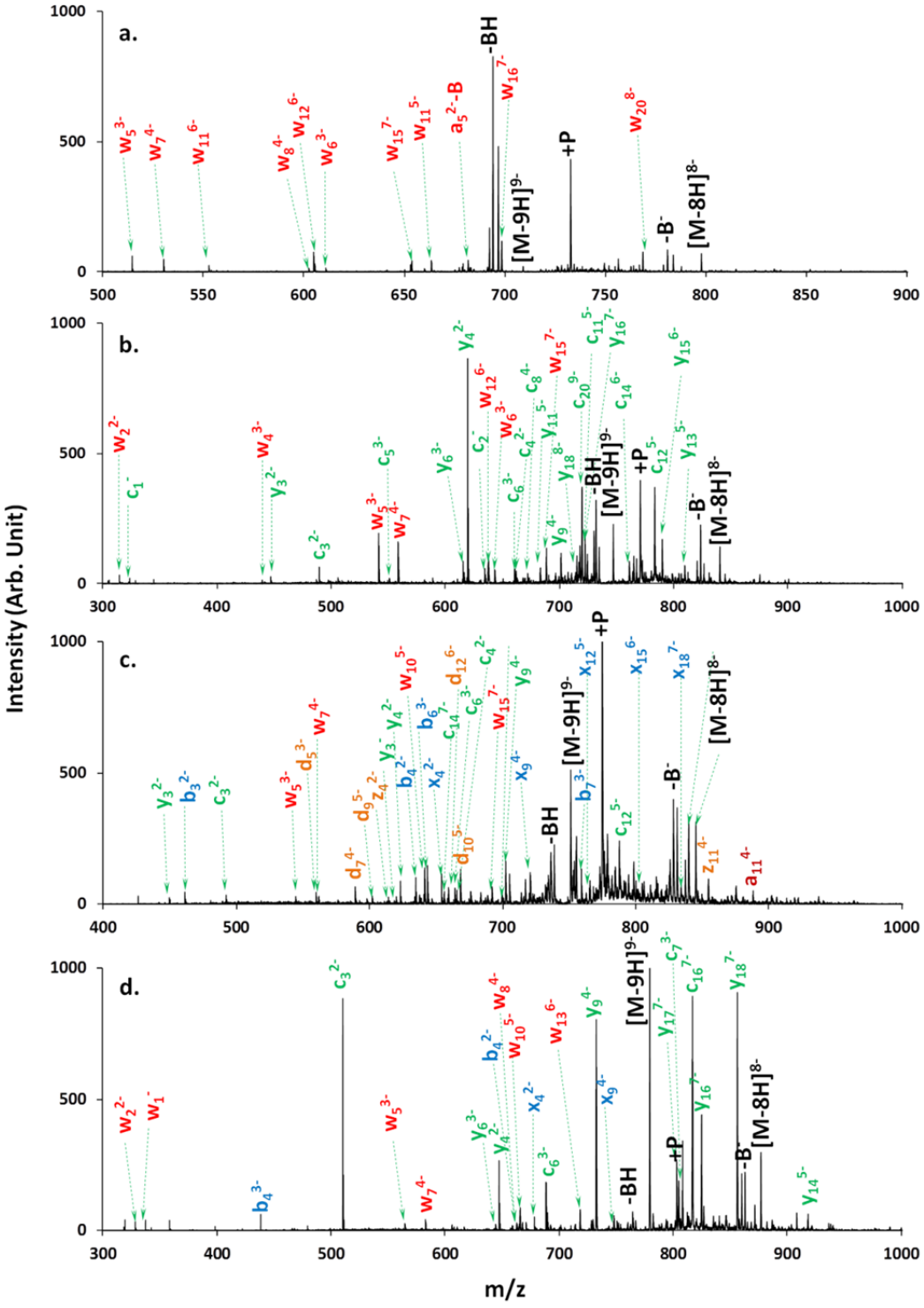

Figure 4.3 Product spectra from ion trap CID of (a) 2'-H 55665; (b) 2'-OH 55665; (c) 2'-F 55665; (d) 2'-OMe 55665 with 475mV dipolar excitation at 115kHz frequency.

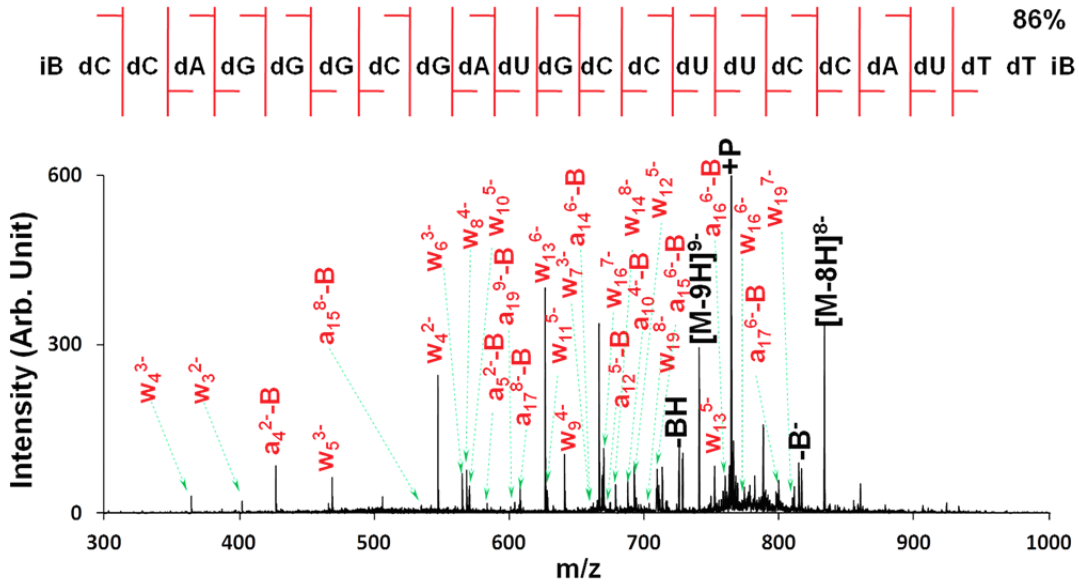

Figure 4.4 Ion trap CID of 2'-H 55664 with supplemental activation applied to the base loss peaks.

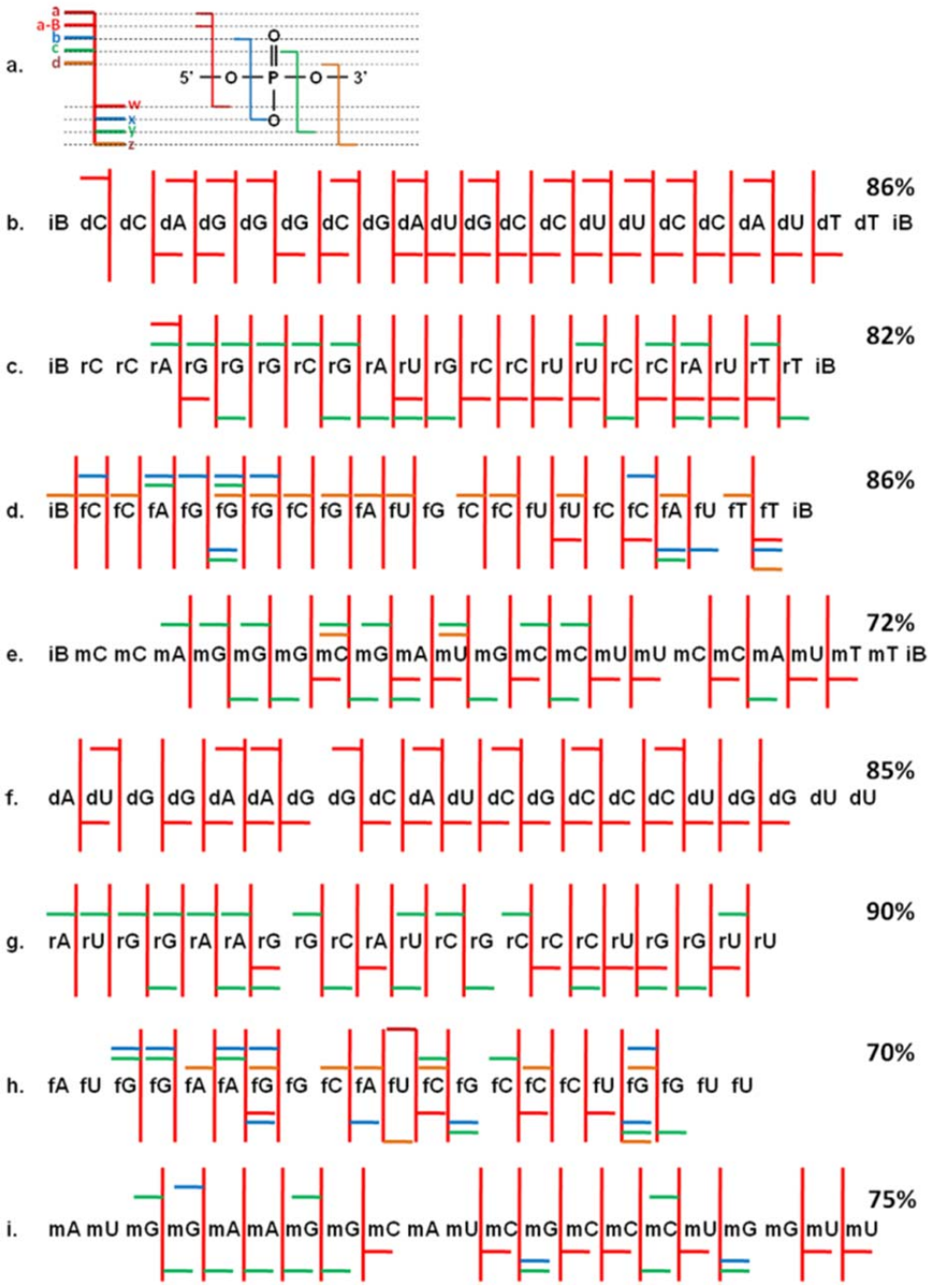

Figure 4.5 Backbone fragmentation summary for the ion trap CID of uniformly 2'-modified oligonucleotides. (a) Fragment nomenclature with color coding. Fragmentation summary for (b) 2'-H 55664; (c) 2'-OH 55664; (d) 2'-F 55664; (e) 2'-OMe 55664; (f) 2'-H 55665; (g) 2'-OH 55665; (h) 2'-F 55665; (i) 2'-OMe 55665. The percentages are calculated sequence coverage.

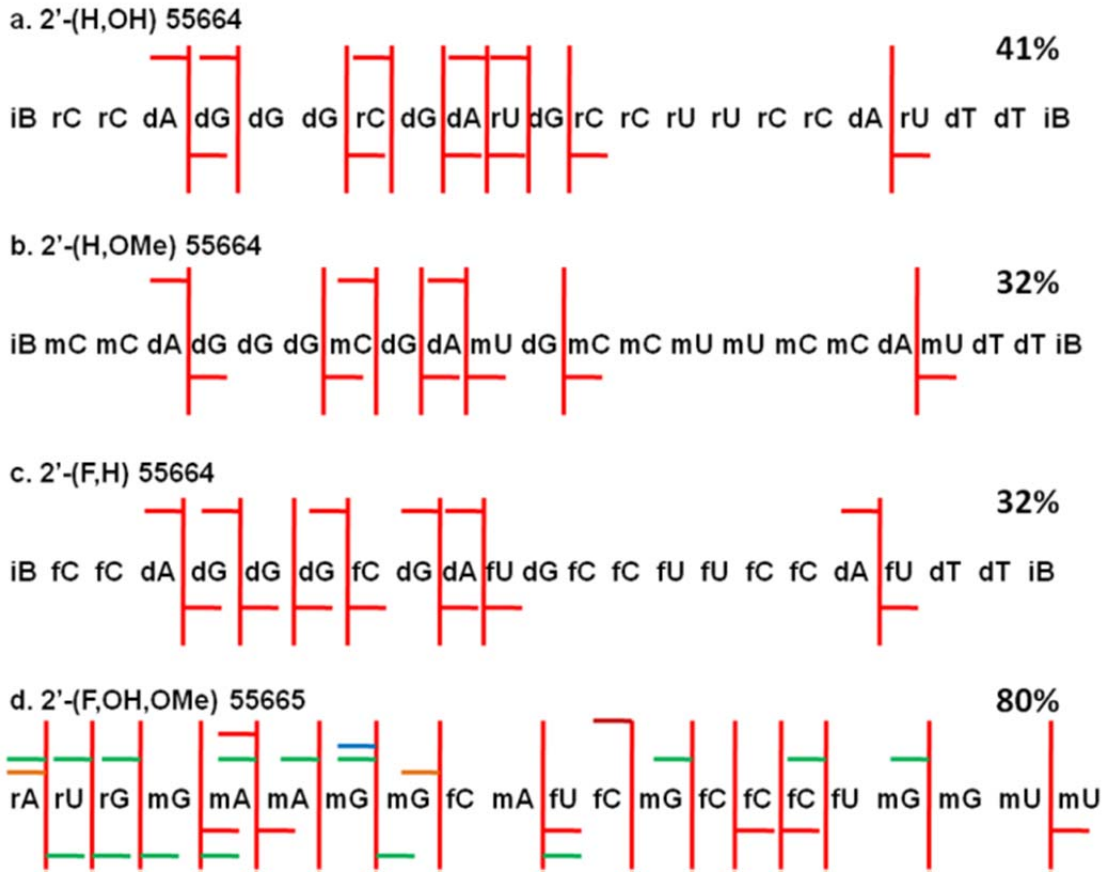

Figure 4.6 Fragment ion map from IT-CID of $[M-9H]^{9-}$ of (a) 2'-(H,OH) 55664; (b) 2'-(H,OMe) 55664; The percentages are calculated sequence coverage. (c) 2'-(F,H) 55664 and (d) 2'-(F,OH,OMe) 55665 with 475mV dipolar excitation at 115kHz frequency. (See key in Figure 4.5 for the fragment types.)

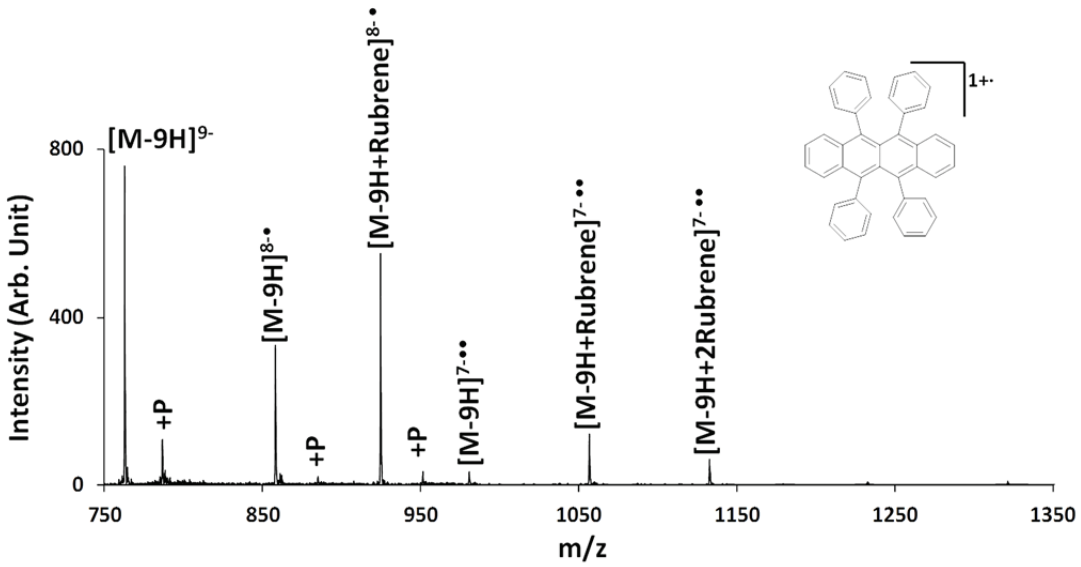

Figure 4.7 Product spectrum from ion/ion reaction between [(2'-(F,H) 55664)-9H]$^{9-}$ and [rubrene]$^{+\bullet}$. +P represents plasticizer adduction to the peak on the left.

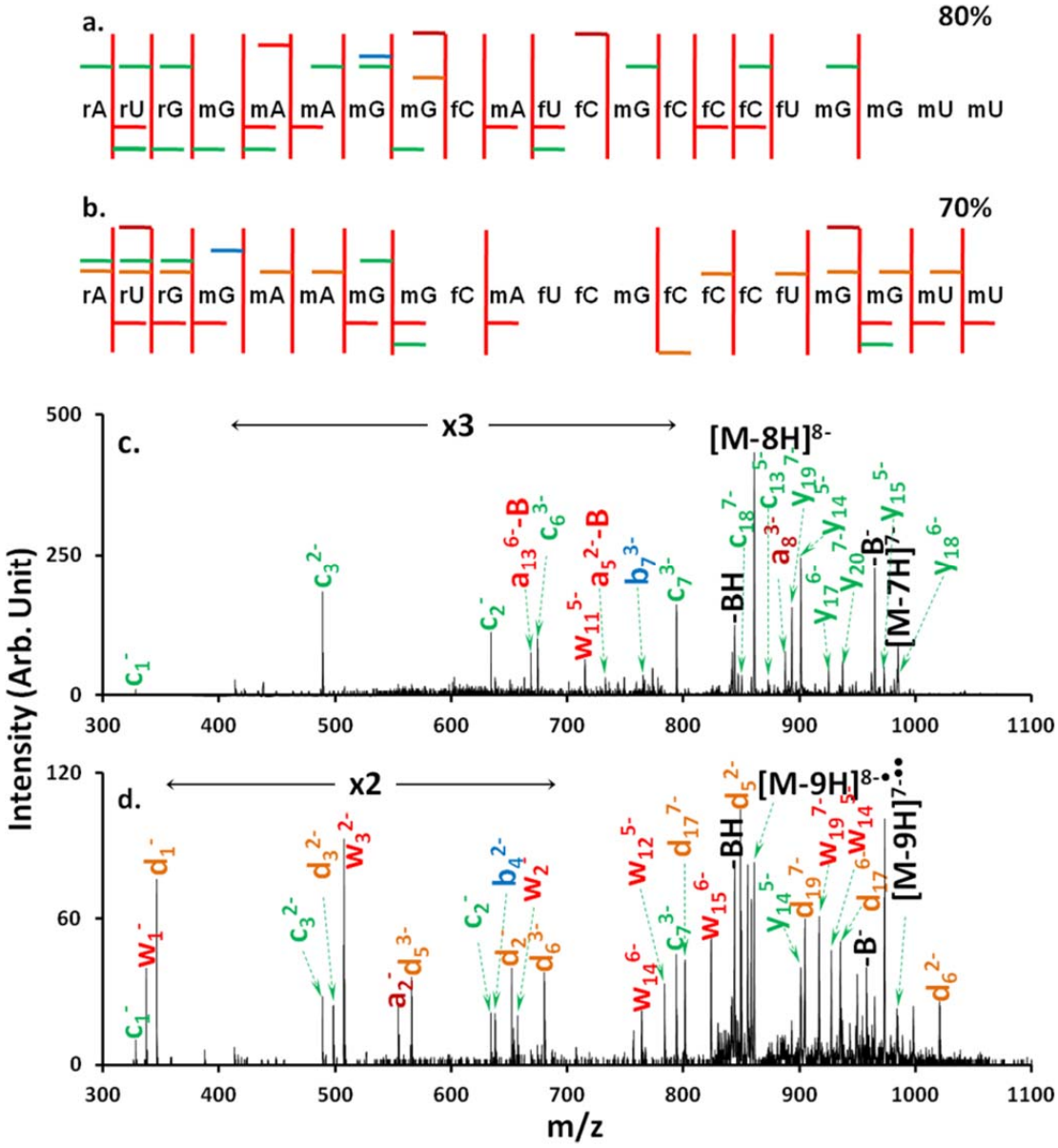

Figure 4.8 Fragment ion map from IT-CID of (a) $[M-8H]^{8-}$ and (b) $[M-9H]^{8-\bullet}$ of 2'-(F,OH,OMe) 55665with 475mV dipolar excitation at 115kHz frequency. The percentages are calculated sequence coverage. (c) Product spectrum of $[M-8H]^{8-}$ of 2'-(F,OH,OMe) 55665. (d) Product spectrum of $[M-9H]^{8-\bullet}$ of 2'-(F,OH,OMe) 55665. (See key in Figure 4.5 for the fragment types in a and b.)

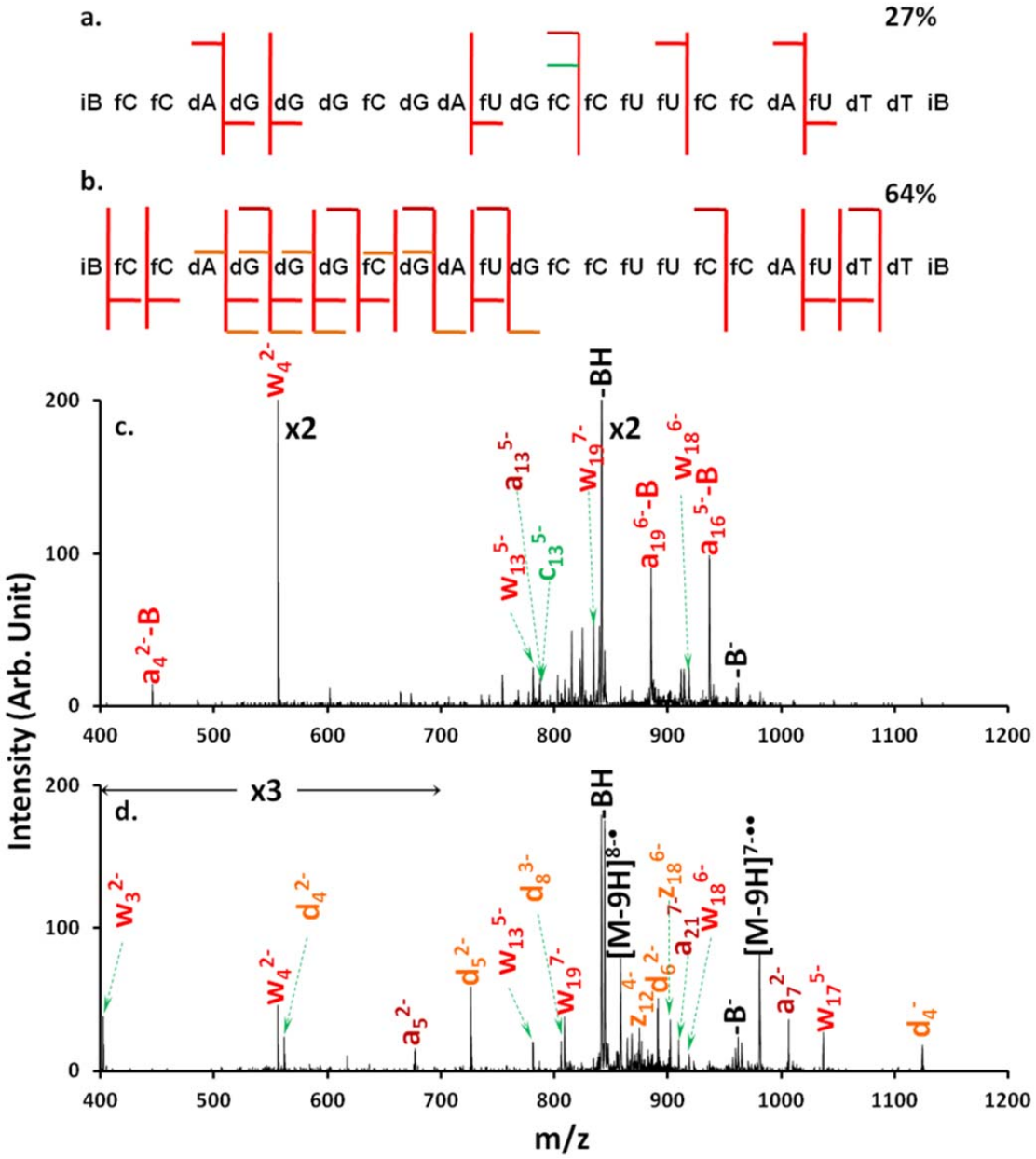

Figure 4.9 Fragment ion map from ion trap CID of (a) $[M-8H]^{8-}$ and (b) $[M-9H]^{8-\bullet}$ of 2'-(F, H) 55664 with 475mV dipolar excitation at 115kHz frequency. The percentages are calculated sequence coverage. Product spectra from IT-CID of (c) $[M-8H]^{8-}$ and (d) $[M-9H]^{8-\bullet}$ of 2'-(F,H) 55664.

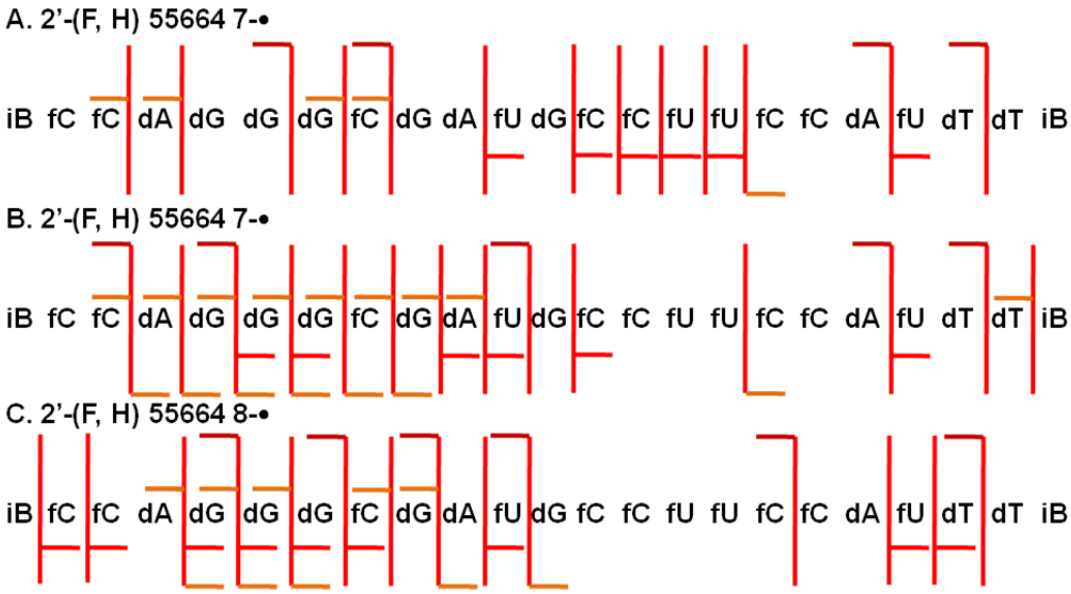

Figure 4.10 Backbone fragmentation summary for the NET-CID of 2'-(F, H) 55664. Charge state 5-• and 4-• were also investigated but did not provide further information.

Table 4.1 Summary of the oligonucleotide sequences used in this study.

Name	Sequence[a]
2'-H 55664	5'-iBdCdCdAdGdGdGdCdGdAdUdGdCdCdUdUdCdCdAdUdTdTiB-3'
2'-OH 55664	5'-iBrCrCrArGrGrGrCrGrArUrGrCrCrUrUrCrCrArUrTrTiB-3'
2'-F 55664	5'-iBfCfCfAfGfGfGfCfGfAfUfGfCfCfUfUfCfCfAfUfTfTiB-3'
2'-OMe 55664	5'- iBmCmCmAmGmGmGmCmGmAmUmGmCmCmUmUmCmCmAmUmTmTiB-3'
2'-H 55665	5'-dAdUdGdGdAdAdGdGdCdAdUdCdGdCdCdCdUdGdGdUdU-3'
2'-OH 55665	5'-rArUrGrGrArArGrGrCrArUrCrGrCrCrCrUrGrGrUrU-3'
2'-F 55665	5'-fAfUfGfGfAfAfGfGfCfAfUfCfGfCfCfCfUfGfGfUfU-3'
2'-OMe 55665	5'-mAmUmGmGmAmAmGmGmCmAmUmCmGmCmCmCmUmGmGmUmU-3'

Table 4.1, continued

Name	Sequence[a]
2'-(F,H) 55664	5'-iBfCfCdAdGdGdGfCdGdAfUdGfCfCfUfUfCfCdA fUdTdTiB-3'
2'-(H, OH) 55664	5'-iBrCrCdAdGdGdGrCdGdArUdGrCrCrUrUrCrCdA rUdTdTiB-3'
2'-(H, OMe) 55664	5'-iBmCmCdAdGdGdGmCdGdAmUdGmCmCmUmU mCmCdAmUdTdTiB-3'
2'-(F,OH, OMe) 55665	5'-rArUrGmGmAmAmGmGfCmAfUfCmGfCfCfCfU mGmGmUmU-3'

a.The modifications on the 2' of sugar moiety are indicated: "m" represents the 2'-O-methyl modification, "f" stands for the 2'-fluoro modification, "d" indicates a deoxyribonucleotide, and "r" indicates a ribonucleotide, iB stands for inverted abasic (Supplementary figure 4).

Table 4.2 Comparison of experimental fragment data with theoretical fragments (Figure 4.9d in the main body)

ion-type	Charge state	exp.	cal.	accuracy (ppm)
c1	1-	328.0232	328.0445	64.93021526
c2	1-	634.0265	634.0698	68.28901171
c3	2-	489.0119	489.0546	87.31131452
c7	3-	793.7327	793.7879	69.53998669
y3	1-	936.1033	936.1751	76.69505416
y14	5-	900.6833	900.7255	46.85112168
d1	1-	346.0330	346.0551	63.86266233
d2	1-	652.0332	652.0804	72.38371219
d3	2-	498.0266	498.0599	66.85942795
d5	2-	849.0702	849.1256	65.24358705
d6	3-	680.0388	680.1038	95.57364626
d15	5-	998.8531	998.9444	91.39647812
d17	6-	934.7052	934.7953	96.38473792
d18	7-	852.4801	852.4038	-89.51156717
d19	7-	903.6687	903.6986	33.08625243
d20	7-	949.4686	949.4187	-52.55847604
w1	1-	337.0375	337.0430	16.31839261
w2	1-	657.0252	657.0840	89.48627573
w3	2-	507.5475	507.5969	97.32131934
w12	5-	783.5355	783.4999	-45.43714683
w14	5-	916.6509	916.7199	75.26835623
w15	5-	988.4503	988.5325	83.15356349
w18	6-	997.9018	997.8090	-93.00377126
w19	7-	904.3737	904.4134	43.89585559
w20	7-	948.1752	948.1313	-46.30160401
a2	1-	554.1001	554.1035	6.136037762
a18	6-	978.2584	978.3097	52.43738256
z8	3-	834.8205	834.7812	-47.07820444

Table 4.3 Comparison of experimental fragment data with theoretical fragments (Fig. 4.9d in the main body).

ion-type	Charge state	exp.	cal.	accuracy (ppm)
d4	**1-**	1124.066	1124.153	77.12473302
d4	**2-**	561.5204	561.5725	92.77519822
d5	**2-**	726.042	726.0988	78.22626893
d6	**2-**	890.5583	890.625	74.89122807
d8	**3-**	805.3988	805.4438	55.86981984
d9	**3-**	915.0933	915.128	37.91819286
a5	**2-**	677.0945	677.1103	23.33445526
a7	**2-**	1006.09	1006.1628	72.75164616
a9	**3-**	882.4257	882.469	49.0668794
a11	**4-**	816.8537	816.8694	19.2197186
a17	**6-**	855.2673	855.2779	12.39363253
a21	**7-**	908.9881	908.9744	-15.07193162
w3	**2-**	402.0511	402.0524	3.233409376
w4	**2-**	556.0249	556.0629	68.33759274
w13	**5-**	780.6377	780.6846	60.07547734
w16	**5-**	970.4782	970.514	36.88766983
w17	**5-**	1036.277	1036.3245	45.54557959
w18	**6-**	918.2047	918.2778	79.60553985
w19	**7-**	833.891	833.9588	81.29898024
w21	**7-**	922.5198	922.5437	25.90663185
w22	**8-**	845.4901	845.4794	-12.65554193
z12	**4-**	874.549	874.6068	66.0868404
z14	**5-**	823.6838	823.6996	19.18175024
z17	**6-**	847.0562	847.1053	57.96209751
z18	**6-**	901.8632	901.9474	93.3535592
z19	**6-**	956.7684	956.7895	22.0529176

CHAPTER 5. INTRAMOLECULAR GAS PHASE CROSSLINKING OF UBIQUITIN ANALOGUES GENERATED BY SITE-DIRECTED MUTAGENESIS

5.1 Introduction

Mass spectrometry has long been applied to the study of protein structure characterization ever since the advent of electrospray ionization (ESI) [1, 2] and matrix assisted laser desorption ionization (MALDI) [3, 4]. Generally, primary protein structures can be probed by various collisional, photon-based, and electron-based activation methods, generating sequence-informative fragment ions. Specifically, collision-induced dissociation (CID) [5, 6, 7], surface-induced dissociation (SID) [8, 9], infrared multiphoton dissociation (IRMPD) [10, 11], ultraviolet photodissociation (UVPD) [12, 13, 14], electron capture dissociation (ECD) [15, 16, 17] and electron transfer dissociation (ETD)[18, 19, 20] have been extensively applied in the field of protein/peptide sequencing, characterization and top-down proteomics.

Comparing to the well-established application in primary structure characterization, using mass spectrometry to unravel higher order structure of protein and protein complexes is still a challenging area in this field[21]. Most A number of approaches have been used to obtain information from the mass spectrometry data, i.e. fragmentation pattern[22, 23, 24, 25, 26], hydrogen/deuterium

exchange (HDX)[27, 28, 29], ion mobility spectrometry (IMS)[30, 31, 32, 33, 34, 35, 36, 37, 38], and chemical crosslinking[39, 40, 41, 42], etc. Comparing to the traditional methods like X-ray crystallography and nuclear magnetic resonance spectroscopy (NMR), these mass spectrometric approaches provide relatively lower resolution and regional information[43]. However, they are more tolerant in terms of sample concentration and purity, providing low-resolution structure information with significantly less sample (2-3 orders of magnitude lower than NMR or crystallography by using chemical crosslinking mass spectrometry) and faster experimental turnaround times[44].

Among the aforementioned techniques, chemical crosslinking mass spectrometry has become increasingly popular in the past decade. Various chemical crosslinkers have been developed to map 3D protein structures and protein-protein interactions[39, 43, 44]. Many of the crosslinkers are designed to be reactive towards particular amino acid residues, i.e. amine, sulfhydryl or under photoactivations. Generally, chemical crosslinking analysis of a protein or protein complex involved formation of covalent bonds between the protein and the crosslinker so that the interaction between two amino acid residues close in space is preserved. After locking in the distance between two amino acid residues, two alternative strategies are available in principle, which are commonly referred to as bottom-up and top-down approaches, to obtain the proximity information from mass spectrometry data. In the bottom-up procedure, the crosslinked protein is enzymatically digested and mass spectrometric identification of the crosslinked peptides is performed. MS/MS study of the

crosslinked peptides allows for the localization of the crosslinking sites. Since the chemical crosslinkers have distance constraints and can bind specifically to certain functional groups, 3D structure information can therefore be deduced from the identified crosslinking sites [45]. The alternative top-down approach analyzes intact crosslinked proteins or protein complexes [46]. Gas phase unimolecular dissociation of the crosslinked products gives rise to fragment ions that may or may not carry the crosslinks. Similarly to the bottom-up approach, the crosslinking sites can be deduced from the fragment mass shifts comparing to the fragments from non-crosslinked counterparts, and the 3D structural information can thus be obtained.

We have recently demonstrated the chemical crosslinking mass spectrometry study of ubiquitin using gas phase ion/ion reaction with homobifunctional sulfo-NHS esters[42]. The results provided evidence of crosslinking, and thus proximity, of lysine 27- lysine 29 (K27-K29) and lysine 48-lysine 63 (K48-K63). However, the proximity analysis of K33 and the other lysines are still not clear due to information redundancy in the crosslinked fragment ions. In order to acquire information from the redundant fragment ions, ubiquitin mutants have been used in this study, in which a known crosslinking site is selectively mutated to a non-reactive residue. Moreover, chemical crosslinkers with various arm lengths have been used to obtain more accurate measurement of the proximity between certain lysine residues.

5.2 Experimental Section

5.2.1 Materials

Glacial acetic acid and methanal were purchased from Mallinckrodt (Phillipsburg, NJ, USA). Ubiquitin from bovine erythrocytes and ubiquitin mutant (Ub_K29R) were purchased from Sigma-Aldrich (St. Louis, MO, USA). All other ubiquitin mutants (Ub_K27R, K48R and K63R) were obtained from Boston Biochem (Cambridge, MA, USA). The chemical crosslinkers (ethylene glycol bis[sulfosuccinimidylsuccinate] (sulfo-EGS), bis[sulfosuccinimidyl] suberate (BS_3), and bis[sulfosuccinimidyl] glutarate (BS2G)) were purchased as the sodium salt from Thermo Fisher Scientific Inc. (Rockford, IL, USA). Amberlite cation exchange resin was obtained from Supelco (Bellefonte, PA, USA). The crosslinkers were treated with cation exchange resin to replace the sodium counterions with protons. Ubiquitin/mutant solutions were made 20 μM in 50/50/1 water/methanol/acetic acid (vol/vol/vol). The reagent was dissolved in water at a concentration of approximately 1mM.

5.2.2 Apparatus and Procedures

All gas phase crosslinking reactions were performed using a QTRAP 4000 hybrid triple quadrupole/linear ion trap mass spectrometer (AB Sciex, Concord, ON, Canada) modified to allow for ion/ion reaction studies[47]. A home-built pulsed dual nano-electrospray (nESI) source was coupled directly to the nanospray interface to produce ions of both polarities. The NHS chemistry in the gas phase

has been previously described[48,49] and has been adapted on the QTRAP 4000 instrument. In a typical gas phase crosslinking experiment, ubiquitin or mutant cations and reagent anions were sequentially introduced and trapped in the q2 collision trap, followed by a 200ms mutual storage period to allow ion/ion reaction, forming electrostatic complexes between the protein cation and crosslinker anion. The products were transferred to Q3 for RF/DC isolation as well as further ion trap CID. The crosslinking reaction was noted by a sequential loss of two neutral sulfo-NHS moieties, each one of which indicates an amide bond formation between the linker arm and the basic residue on the protein. Then, the crosslinked protein was subjected to further fragmentation via ion trap CID, giving rise to the crosslinked fragment ions and pinpointing the possible crosslinking sites. All ion trap CID were performed at q=0.2 with an amplitude of 50-100 mV_{p-p} over a period of 200 ms.

The solution phase crosslinking reaction was performed following the procedure provided by ProteoChem Inc[50]. (Denver, CO, USA). Sample desalting was performed using PD-10 desalting columns (GE Healthcare, Pittsburgh, PA, USA). The reaction mixtures were separated using a reverse-phase HPLC (Agilent 1100, Palo Alto, CA) equipped with an Aquapore RP-300 (7μm pore size, 100mm×4.6mm i.d.) column (Perkin-Elmer, Wellesley, MA). Tandem MS/MS of the crosslinked proteins were performed using a modified QqTOF mass spectrometer (QSTAR, AB Sciex, Concord, ON, Canada).

5.3 Results and Discussions

Gas phase intramolecular crosslinking of ubiquitin has been previously demonstrated using a homobifunctional NHS crosslinker – sulfo-EGS[42] (Scheme 5.1). The general procedure and findings have been summarized as follows: (1) CID product spectrum of crosslinked ubiquitin is compared with the one of unmodified species. Any fragment ion with the crosslinker modification will have a +226 Da (+[sulfo-EGS]$^-$-2[sulfo-NHS]) mass shift comparing to the unmodified fragment ion. (2) For the crosslinked fragment ions, reactive residues (lysines, N-terminus and possibly arginines) are identified. For instance, crosslinked b_{32} (Scheme 5.2 and Figure 5.1) indicates Lys 27 and Lys 29 (K27 and K29) are crosslinked (Previous data suggested that N-terminus, K6 and K11 are not reactive towards NHS chemistry in the gas phase [42]). (3) Consequently, K27-K29 and K48-K63 have been identified as being crosslinked by sulfo-EGS, indicating that K27-K29 and K48-K63 residues are within 16.1 Å range in the 3D configuration of 7+ ion of ubiquitin.

However, this approach has its limitations that most crosslinked fragment ions are redundant and therefore not informative on the crosslinking sites. For example, crosslinked b_{34} ion has three reactive residues (K27, K29 and K33). It has already been demonstrated that K27 and K29 can be crosslinked. Thus, there is no direct evidence to determine whether or not K27-K33 or K29-K33 are crosslinked. Similarly, the distance between K33 to K48 or K63 cannot be justified using the crosslinked fragments due to the redundancy of the data. In order to eliminate the ambiguity in the information derived from the crosslinked

fragment ions, site-directed mutagenesis was applied to selectively swap an ambiguous lysine residue (i.e. K29) with an arginine residue (i.e. R29). For the charge states examined in this study, all arginines are protonated and therefore not reactive towards NHS chemistry. Thus, the previously non-informative crosslinked fragment ions (i.e. b_{34}) can become informative due to the fact that there are only two reactive sites within b_{34} (K27 and K33).

5.3.1 Gas Phase Intramolecular Crosslinking of Ubiquitin Mutants

Fragmentation pattern shown in Scheme 5.2 suggested that the relationship between K33 and the other lysines (K27, K29, K48 and K63) are unclear due to the fragment redundancy. To measure the proximity between K33 and other lysines, K27, K29, K48 and K63 are substituted with arginines, respectively. Two assumptions are made here: (1) the substitution of a lysine residue by arginine does not significantly alter the gas phase configuration of the protein at given charge state. (2) The fragmentation pathways do not change as a result of the site-directed mutagenesis. The first assumption was confirmed by the similarity between the charge state distributions in the nESI spectra of ubiquitin and the mutants. The second was supported by the identical ion trap CID spectra of the natural and mutant proteins. For each mutant, b_{32}/y_{44}, b_{34}/y_{42}, b_{39}/y_{37} fragment ion pairs are monitored to localize the crosslinks.

Figure 5.2 shows the product ion spectra resulting from ion trap CID of crosslinked 6+ ions of ubiquitin and ubiquitin K29R mutant. Most of the fragment

ions are identical, including modified and unmodified b_{34}/y_{42} and b_{39}/y_{37} fragment ion pairs. However, both modified and unmodified b_{32}/y_{44} fragments were observed for crosslinked ubiquitin ions ($[Ubiq+6H^+ +*]^{6+}$) (Figure 5.2a), whereas only modified y_{44} and unmodified b_{32} were seen in the product ion spectrum of $[Ubiq\_K29R+6H^+ +*]^{6+}$ ions (Figure 5.2b). Because K29 is replaced by R29 in this mutant, b_{32} only contains one reactive site (K27) and therefore cannot be crosslinked. The absence of crosslinked b_{32} also confirms the previous finding that K6, K11 and the N-terminus of ubiquitin are not available for gas phase NHS chemistry in the charge states investigated. The facts that b_{34}, b_{36}, and b_{39} still show up in the form of crosslinked species indicate that K33 and K27 are crosslinked by sulfo-EGS, suggesting that K33 and K27 are within 16.1 Å range in the 3D configuration. The absence of an unmodified y_{44} ion further confirmed that there is no crosslink occurring N-terminal to K33.

To narrow down the distances between the lysines, chemical crosslinkers with shorter linker arms are used (Scheme 5.1). Specifically, BS_3 (11.4 Å) and BS_2G (7.7 Å) are introduced to effect ion/ion reactions with ubiquitin (Figure 5.3). For the BS_3 crosslinker, the modified fragment ions show a mass shift of 138 Da from the unmodified counterparts, whereas for the BS_2G crosslinker, there is a 95 Da mass difference between the crosslinked and non-crosslinked fragment ions. In all cases, the ion trap CID of the crosslinked protein cations showed no significant differences by using difference crosslinkers. The product spectra are almost identical in terms of backbone cleavages as well as the modifications on the fragments. The fragment b_{32}, appears in both crosslinked and unmodified

forms, indicating the presence of a mixture of structures. The crosslinked b_{32} ion indicates that K27 and K29 are within 7.7 Å range in the 3D configuration of ubiquitin 7+ ion. Similarly, the crosslinked y_{37} ion suggests that K48 and K63 are within the distance that can be crosslinked with BS_2G. This further restricts the dimensions of the ubiquitin ion and provide more precise measurement of its 3D structure.

For other ubiquitin mutants, BS_2G was used as crosslinker in order to achieve higher measurement sensitivity towards the structure. Figure 5.4 shows the ion trap CID product ion spectra from ubiquitin mutants crosslinked by BS_2G. For ubiq_K48R, no crosslinked y-ions are observed up to y_{42} (Figure 5.4a). Similarly, b_{34} and b_{39} are only detected in crosslinked form. This indicates that two crosslinking anchors are not available C-terminal to K33 (cleavage of the amide bond C-terminal to K33 gives rise to b_{34}/y_{42} fragment ion pair). Because K48 is replaced with R48 in this mutant, the only possible reactive site is the remaining K63, making y_{42} not able to be crosslinked. The first crosslinked y-ion (counting from the C-terminus) is y_{44}, and b_{32} is the first b-ion (counting from the N-terminus) that has both crosslinked and unmodified forms. The difference between y_{44} and y_{42} is K33-E34 (Scheme 5.2). Since glutamic acid is known as not reactive towards NHS chemistry, the additional lysine residue is where the crosslinking takes place. Thus, K33 and the remaining K63 are crosslinked by BS_2G as indicated by the crosslinked y_{44}. Similarly, no crosslinked y_{37} and y_{42} are both observed in crosslinked and unmodified form in the CID spectrum of crosslinked ubiquitin_K27R (Figure 5.4b), whereas y_{44} only shows as crosslinked

species. The solely crosslinked y_{44} can be rationalized in that there is only one reactive lysine N-terminal to K33, and therefore, it is impossible to have a crosslinked b_{32}/unmodified y_{44} fragment ion pair. The crosslinked b_{34} and unmodified y_{42} suggest that K33 and K29 are within 7.7 Å range in the 3D protein structure. Likewise, the crosslinked b_{32} and unmodified y_{42} in Figure 5.4c provide evidence that K33 and K48 are crosslinked by BS_2G.

Based on the information provided by gas phase intramolecular crosslinking the ubiquitin mutants, together with the result from ubiquitin crosslinking[42], 18 of the 28 unique potential crosslinking combinations can be eliminated while 6 specific crosslinks mentioned above are strongly indicated. Results for the 7+ charge state are summarized in Table 5.1.

5.3.2 Solution Phase Intramolecular Crosslinking of Ubiquitin

Solution phase crosslinking of ubiquitin has been performed as a comparison to the gas phase crosslinking experiments. As shown in Figure 5.5, the fragmentation patterns (crosslinked and unmodified) in both cases are almost identical except for a few fragments. The fragment ions are not only identical in mass-to-charge ratios but also similar in relative intensities. The indications of the crosslinks on the protein cations are also the same, suggesting similarity in the 3D structures of solution phase ubiquitin and 7+ ubiquitin cation.

It is noted that the crosslinked y_{18}^{2+} ion is the outlier in the gas phase crosslinking spectrum (Figure 5.5a), which is not seen in the solution phase

crosslinking spectrum. The y_{18} fragment sequence has primary amine sites including two arginines, one lysine, one histidine and the N-terminus. Since it has two charges, the arginines are most likely to be solvated by protons. Because the histidine has significantly lower reactivity towards NHS chemistry than lysine and N-terminus, the possibility that it acts as a crosslink anchor is very low. Ion trap CID of the crosslinked y_{18} ion shows crosslinked b_{14} and b_{16} fragments, whereas y_{12} and y_4 fragments are not crosslinked (Figure 5.6). The unmodified y_{12} and y_4 indicate that neither arginine nor histidine is crosslinked. Additionally, the crosslinked b_{14} and b_{16} fragments suggest that the crosslinking occurs between the lysine and the newly formed N-terminus. The mechanism for crosslinking between a lysine and an N-terminus formed in the process of CID is shown in Scheme 5.3. During the ion/ion reaction, an electrostatic complex is formed between the protein cation and crosslinker anion. The first step CID results in the covalent bond formation between the lysine and the crosslinker, with the signature loss of neutral sulfo-NHS, and the amide bond cleavage between the aspartic acid (D) and the tyrosine (Y). However, the two peptide fragments (b_{58} and y_{18}) still stick together due to the electrostatic interaction between the sulfonate and the basic residue. The second step CID drives the reaction between the newly formed N-terminus of the y_{18} and the other end of the crosslinker. Then, the third step CID separate the crosslinked y_{18} ion and the unmodified b_{58} ion. This process is only possible in the gas phase reaction because the NHS chemistry is driven by the collisional activation, which can also lead to backbone cleavages. The solution phase reaction, on the other hand, is

driven by basic solution environment which does not disrupt the protein primary structure.

5.4 Conclusions

Intramolecular crosslinking of ubiquitin muntant cations in the gas phase has been demonstrated using several homobifunctional crosslinking reagents with different linker arm length. Ion/ion reactions have been performed using a multiply charged protein cation with singly deprotonated sulfo-NHS crosslinking reagent, which lead to the formation of an electrostatic complex that can form covalent crosslinks between reactive sites (i.e., unprotonated primary amines and guanidine groups) located within distance constraint of the crosslinker. Ubiquitin mutants generated by site directed mutagenesis are used to extract information from the redundant fragment ions. For the 7+ charge state examined in this study, 18 of 28 possible crosslinking combinations could be ruled out and crosslinks between K27-K29 as well as K48-K63 are confirmed. Moreover, there is strong evidence supporting four additional crosslinks (K27-K33, K29-K33, K48-K33 and K63-K33) on the basis of ion trap CID of the ubiquitin mutants. These results indicate that in combination with site-directed mutagenesis, gas phase intramolecular covalent crosslinking of protein ions is able to provide specific proximity information with respect to the surface basic residues. This approach may therefore provide information that complements the information provided by other approaches, such as ion mobility, H/D exchange, etc.

5.5 References

[1] Whitehouse, C.M.; Dreyer, R.N.; Yamashita, M.; Fenn, J.B. Electrospray interface for liquid chromatographs and mass spectrometers. *Anal. Chem*. **1985**, *57*, 675–679.

[2] Fenn, J.B.; Mann, M.; Meng, C.K.; Wong, S.F.; Whitehouse, C.M. Electrospray ionization for mass spectrometry of large biomolecules. *Science*. **1989**, *246*, 64–71.

[3] Karas, M.; Bachmann, D.; Bahr, U.; Hillenkamp, F. Matrix-assisted ultraviolet laser desorption of non-volatile compounds. *Int. J. Mass Spectrom. Ion Processes*. **1987**, *78*, 53–68.

[4] Karas, M.; Hillenkamp, F.H. Laser desorption ionization of proteins with molecular masses exceeding 10,000 daltons. *Anal. Chem*. **1988**, *60*, 2299–2301.

[5] Steen, H.; Mann, M. The ABC's (and XYZ's) of peptide sequencing. Nature Rev. Mol. Cell Biol. **2004**, *5*, 699-711.

[6] Aebersold, R., Goodlett, D. R.: Mass Spectrometry in Proteomics. Chem. Rev. **2001**, *101*, 269-296.

[7] Beimann, K. Sequence of Peptides by Tandem Mass-Spectrometry and High-Energy Collision-Induced Dissociation. *Methods Enzymol.* **1990**, *193*, 455-479.

[8] Zhou, M.; Dagan, S.; Wysocki, V. H. Impact of Charge State on Gas phase Behaviors of Noncovalent Protein Complexes in Collision Induced Dissociation and Surface Induced Dissociation. *Analyst*, **2013**, *138*, 1352-1362.

[9] Dongre, A.R.; Somogyi, A.; Wysocki, V.H. Surface-induced dissociation: An effective tool to probe structure, energetics and fragmentation mechanisms of protonated peptides. *J. Mass Spectrom.* **1996**, *31*, 339–350.

[10] Little, D.P.; Speir, J.P.; Senko, M.W.; O'Connor, P.B.; McLafferty, F.W. Infrared multiphoton dissociation of large multiply charged ions for biomolecule sequencing. *Anal. Chem.* **1994**, *66*, 2809–2815.

[11] Payne, A. H.; Glish, G. L. Thermally Assisted Infrared Multiphoton Photodissociation in a Quadrupole Ion Trap. *Anal. Chem*. **2001**, *73*, 34542-3548.

[12] Madsen, J. A.; Boutz, D. R.; Brodbelt, J. S. Ultrafast Ultraviolet Photodissociation at 193 nm and its Applicability to Proteomic Workflows. *J. Proteome Res.* **2010**, *9*, 4205-4214.

[13] Wilson, J.J.; Brodbelt, J.S. MS/MS simplification by 355 nm ultraviolet photodissociation of chromophore-derivatized peptides in a quadrupole ion trap. *Anal. Chem*. **2007**, *79*, 7883–7892.

[14] Reilly, J.P. Ultraviolet photofragmentation of biomolecular ions. *Mass Spectrom. Rev*. **2009**, *28*, 425–447.

[15] Zubarev, R.A.; Kelleher, N.L.; McLafferty, F.W. Electron capture dissociation of multiply charged protein cations. A nonergodic process. *J. Am. Chem. Soc.* **1998**, *120*, 3265–3266.

[16] Zubarev, R.A.; Kruger, N.A.; Fridricksson, E.K.; Lewis, M.A.; Horn, D.M.; Carpenter, B.K.; McLafferty, F.W. Electron capture dissociation of gaseous multiply-charged proteins is favored at disulfide bonds and other sites of high hydrogen atom affinity. *J. Am. Chem. Soc.* **1999**, *121*, 2857–2862.

[17] Mann, M.; Jensen, O. N. Proteomic Analysis of Post-Translational Modifications. *Nature Biotechnol.* **2003**, *21*, 255-261.

[18] Syka, J.E.; Coon, J.J.; Schroeder, M.J.; Shabanowitz, J.; Hunt, D.F. Peptide and protein sequence analysis by electron transfer dissociation mass spectrometry. *Proc. Natl. Acad. Sci. U.S.A.* **2004**, *101*, 9528–9533.

[19] Pitteri, S.J.; Chrisman, P.A.; Hogan, J.M.; McLuckey, S.A. Electron transfer ion/ion reactions in a three-dimensional quadrupole ion trap: reactions of doubly and triply protonated peptides with $SO_2^{\bullet-}$. *Anal. Chem*. **2005**, *77*, 1831–1839.

[20] Reid, G. E.; McLuckey, S. A. 'Top Down' Protein Characterization via Tandem Mass Spectrometry. *J. Mass Spectrom.* **2002**, *37*, 663-675.

[21] Kaltashov, I.A.; Eyles, S.J. Mass Spectrometry in Biophysics. Wiley-Interscience, Hoboken (2005). ISBN 0-471-45602-0

[22] Breuker, K.; Oh, H.; Horn, D.M.; Cerda, B.A.; McLafferty, F.W. Detailed unfolding and folding of gaseous ubiquitin ions characterized by electron capture dissociation. *J. Am. Chem. Soc.* **2002**, *124*, 6407–6420.

[23] Breuker, K.; Oh, H.; Cerda, B.A.; Horn, D.M.; McLafferty, F.W. Hydrogen atom loss in electron-capture dissociation: A Fourier transform-ion cyclotron resonance study with single isotopomeric ubiquitin ions. *Eur. J. Mass Spectrom*. **2002**, *8*, 177–180.

[24] Oh, H.; Breuker, K.; Sze, S.K.; Ge, Y.; Carpenter, B.K.; McLafferty, F.W. Secondary and tertiary structures of gaseous protein ions characterized by electron capture dissociation mass spectrometry and photofragment spectroscopy. *Proc. Natl. Acad. Sci. U.S.A.* **2002**, *99*, 15863–15868.

[25] Skinner, O.S.; McLafferty, F.W.; Breuker, K. How ubiquitin unfolds after transfer into the gas phase. *J. Am. Soc. Mass Spectrom*. **2012**, *23*, 1011-1014.

[26] Ly, T.; Julian, R.R. Elucidating the tertiary structure of protein ions in vacuo with site specific photoinitiated radical reactions. *J. Am. Chem. Soc.* **2010**, *132*, 8602–8609.

[27] Freitas, M.A.; Hendrickson, C.L.; Emmet, M.R.; Marshall, A.G. Gasphase bovine ubiquitin cation conformations resolved by gas phase hydrogen/deuterium exchange rate and extent. *Int. J. Mass Spectrom.* **1999**, *185/186/187*, 565–575.

[28] Evans, S.E.; Lueck, N.; Marzluff, E.M. Gas phase hydrogen/deuterium exchange of proteins in an ion trap mass spectrometer. *Int. J. Mass Spectrom*. **2003**, *222*, 175–187.

[29] Hoerner, J.K.; Xiao, H.; Kaltashov, I.A. Structural and dynamic characteristics of a partially folded state of ubiquitin revealed by hydrogen exchange mass spectrometry. *Biochem.* **2005**, *44*, 11286–11294.

[30] Koeniger, S.L.; Merenbloom, S.I.; Sevugarajan, S.; Clemmer, D.E. Transfer of structural elements from compact to extended states in unsolvated ubiquitin. *J. Am. Chem. Soc.* **2006**, *128*, 11713–11719.

[31] Wyttenbach, T.; Bowers, M.T. Structural stability from solution to the gas phase: native solution structure of ubiquitin survives analysis in a solvent-free ion mobility-mass spectrometry environment. *J. Phys. Chem. B*. **2011**, *115*, 12266–12275.

[32] Shi, H.; Pierson, N.A.; Valentine, S.J.; Clemmer, D.E. Conformation types of ubiquitin $[M + 8H]^{8+}$ ions from water:methanol solutions: evidence for the N and A states in aqueous solution. *J. Phys. Chem. B*. **2012**, *116*, 3344–3352.

[33] Myung, S.; Badman, E.R.; Lee, Y.J.; Clemmer, D.E. Structural transitions of electrosprayed ubiquitin ions stored in an ion trap over 10 ms to 30 s. *J. Phys. Chem. A*. **2002**, *106*, 9976–9982.

[34] Li, J.; Taraszka, J.A.; Counterman, A.E.; Clemmer, D.E. Influence of solvent composition and capillary temperature on the conformations of electrosprayed ions: unfolding of compact ubiquitin conformers from pseudonative and denatured solutions. *Int. J. Mass Spectrom.* **1999**, *185/186/187*, 37–47.

[35] Valentine, S.J.; Counterman, A.E.; Clemmer, D.E. Conformer-dependent proton-transfer reactions of ubiquitin ions. *J. Am. Soc. Mass Spectrom.* **1997**, *8*, 954–961.

[36] Segev, E.; Wyttenbach, T.; Bowers, M.T.; Gerber, R.B. Conformational evolution of ubiquitin ions in electrospray mass spectrometry: molecular dynamics simulations at gradually increasing temperatures. *Phys. Chem., Chem. Phys*. **2008**, *10*, 3077–3082.

[37] Koeniger, S.L.; Clemmer, D.E. Resolution and structural transitions of elongated states of ubiquitin. *J. Am. Soc.Mass Spectrom*. **2007**, *18*, 322–331.

[38] Badman, E.R.; Hoaglund-Hyzer, C.S.; Clemmer, D.E. Dissociation of different conformations of ubiquitin ions. *J. Am. Soc. Mass Spectrom.* **2002**, *13*, 719–723.

[39] Sinz, A. Chemical cross-linking and mass spectrometry to map threedimensional protein structures and protein–protein interactions. *Mass Spectrom. Rev*. **2006**, *25*, 663–682.

[40] Chakravarti, B.; Lewis, S.J.; Chakravarti, D.N.; Raval, A. Three dimensional structures of proteins and protein complexes from chemical cross-linking and mass spectrometry: a biochemical and computational overview. *Curr. Proteom*. **2006**, *3*, 1–21.

[41] Singh, P.; Panchaud, A.; Goodlett, D.R. Chemical cross-linking and mass spectrometry as a low-resolution protein structure determination technique. *Anal. Chem*. **2010,** *82*, 2636–2642.

[42] Webb, I. K.; Mentinova, M.; McGee, W. M.; McLuckey, S. A. Gas phase Intramolecular Protein Crosslinking via Ion/Ion Reactions: Ubiquitin and a Homobifunctional sulfo-NHS Ester. *J. Am. Soc. Mass Spectrom.* **2013**, *24*, 733-743.

[43] Chakravarti, B.; Lewis, S.J.; Chakravarti, D.N.; Raval, A. Three dimensional structures of proteins and protein complexes from chemical cross-linking and mass spectrometry: a biochemical and computational overview. *Curr. Proteom*. **2006**, *3*, 1–21.

[44] Singh, P.; Panchaud, A.; Goodlett, D.R. Chemical cross-linking and mass spectrometry as a low-resolution protein structure determination technique. *Anal. Chem*. **2010**, *82*, 2636–2642.

[45] Dihazi, G.H., Sinz, A.: Mapping low-resolution three-dimensional protein structures using chemical cross-linking and Fourier transform ion-cyclotron resonance mass spectrometry. *Rapid Commun. Mass Spectrom*. **2003**, *17*, 2005–2014.

[46] Kruppa, G.H.; Schoeniger, J.; Young, M.M. A top-down approach to protein structural studies using chemical cross-linking and Fourier transform mass spectrometry. *Rapid Commun. Mass Spectrom*. **2003**, *17*, 155–162.

[47] Xia, Y.; Wu, J.; Londry, F.A.; Hager, J.W.; McLuckey, S.A. Mutual storage mode ion/ion reactions in a hybrid linear ion trap. *J. Am. Soc. Mass Spectrom.* **2005**, *16*, 71–81.

[48] Mentinova, M.; McLuckey, S.A. Covalent modification of gaseous peptide ions with n-hydroxysuccinimide ester reagent ions. *J. Am. Chem. Soc.* **2010**, *132*, 18248–18257.

[49] Mentinova, M.; McLuckey, S.A.: Intra- and intermolecular crosslinking of peptide ions in the gas phase: Reagents and conditions. *J. Am. Soc. Mass Spectrom.* **2011**, *22*, 912–921.

[50] ProteoChem, Retrieved from: http://www.proteochem.com/protocols/BS2G-Product-Information-Sheet.pdf.

sulfoEGS, 16.1 Å linker arm

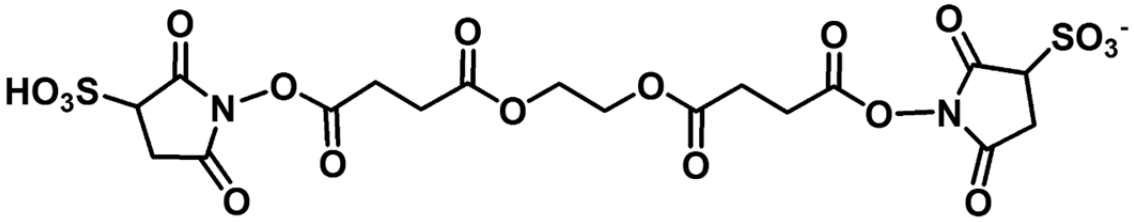

BS_3, 11.4 Å linker arm

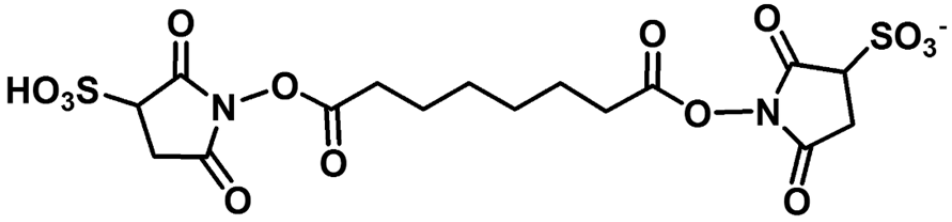

BS_2G, 7.7 Å linker arm

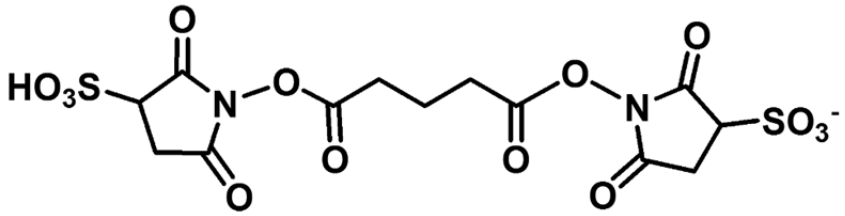

Scheme 5.1 Structure and linker arm lengths of the crosslinker anions.

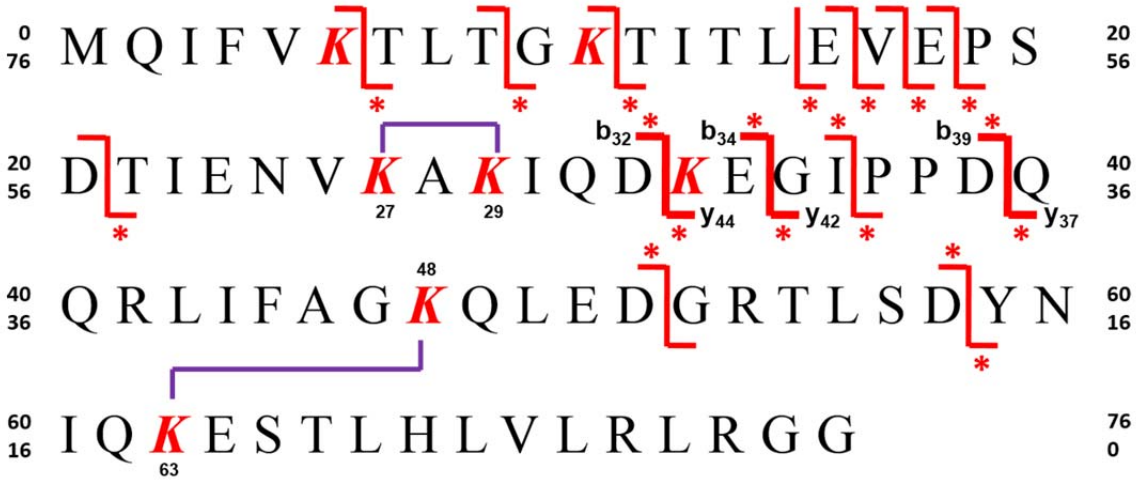

Scheme 5.2 Summary of major amide bond cleavages from the 7+ ions of ubiquitin crosslinked by [sulfo-EGS]$^{1-}$. The asterisk (*) indicates crosslinked fragment ions. The purple traces indicate that K27-K29 and K48-K63 are proved to be crosslinked by sulfo-EGS.

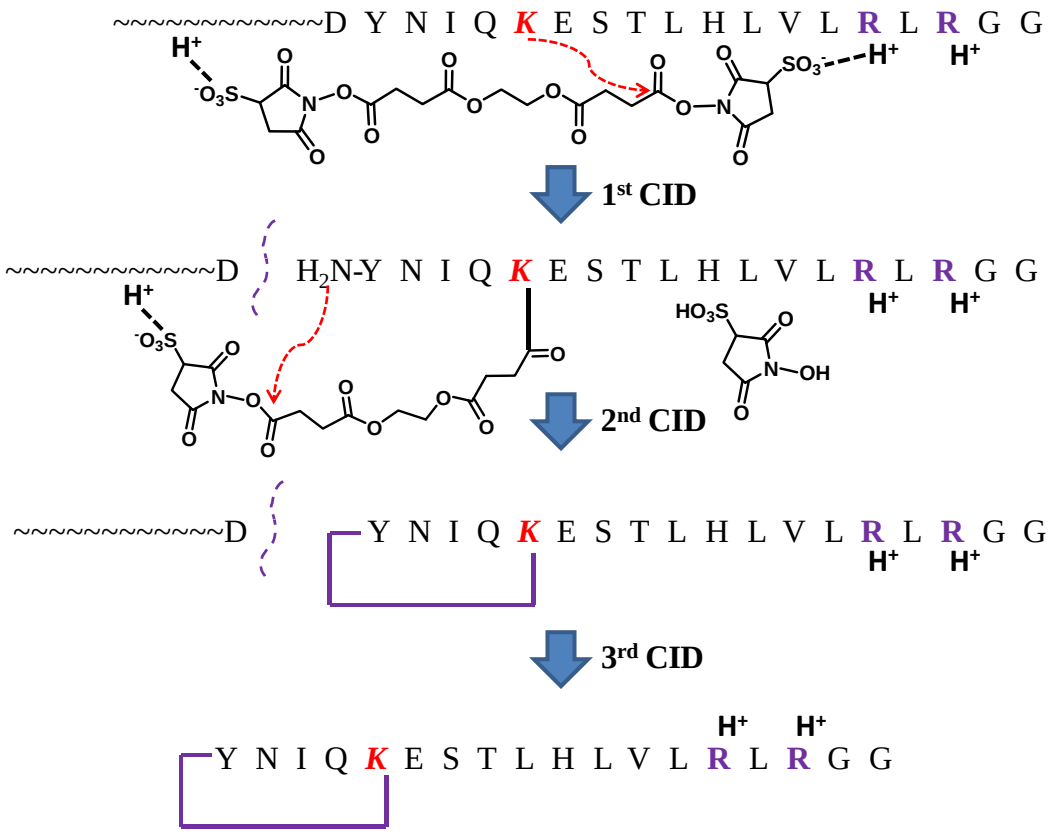

Scheme 5.3 Mechanism of crosslinking between the lysine residue (labeled in red) and the N-terminus formed via CID.

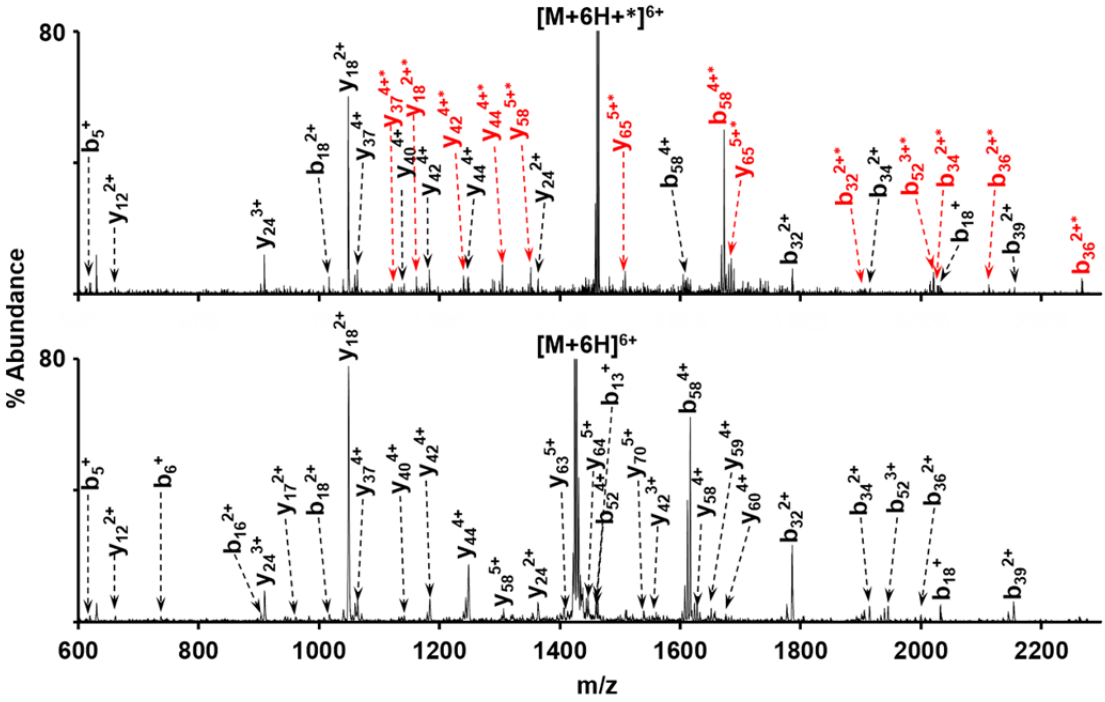

Figure 5.1 Unimolecular dissociation to determine crosslinked sites. +* Indicates a covalently attached crosslinker (+ $[sulfo\text{-}EGS]^{1-}$ - 2[sulfo-NHS]). (a) CID of $[M + 7H^{+} +*]^{6+}$. (b) CID of $[M + 6H]^{6+}$.

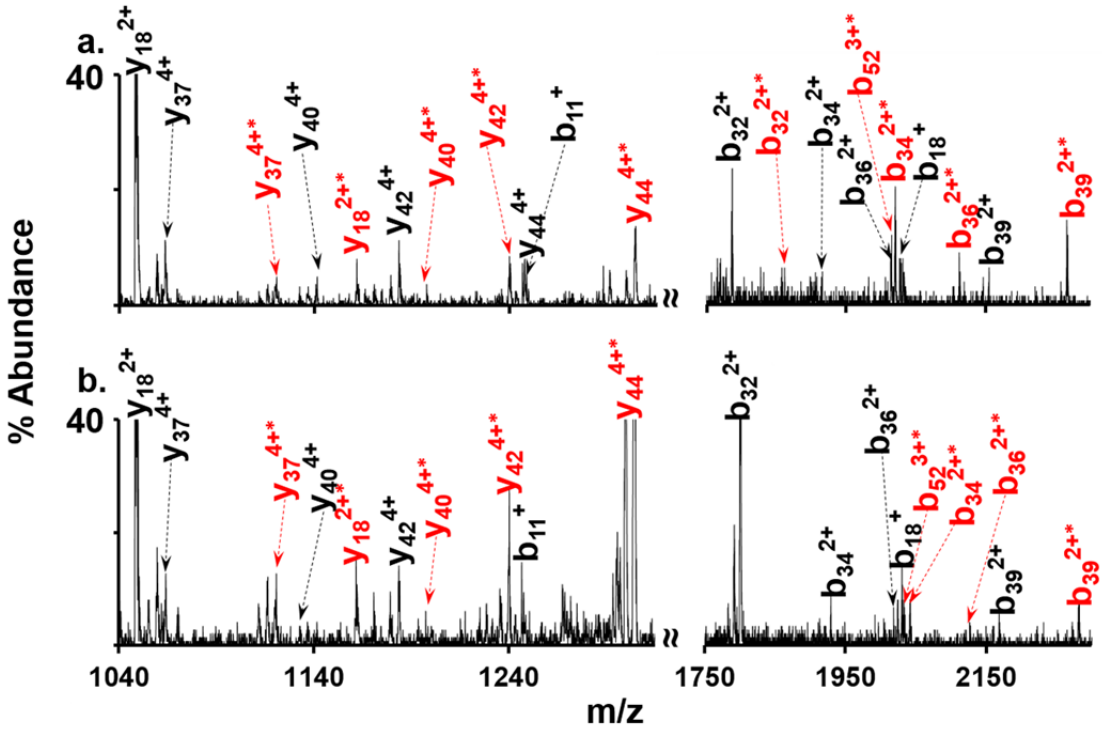

Figure 5.2 Ion trap CID product spectra of (a) $[Ubiq+6H^{+}+*]^{6+}$ and (b) $[Ubiq\_K29R+6H^{+}+*]^{6+}$. +* indicates a covalent attached crosslinker (+[sulfo-EGS]-2[sulfo-NHS]). The crosslinked fragment ions are noted in red.

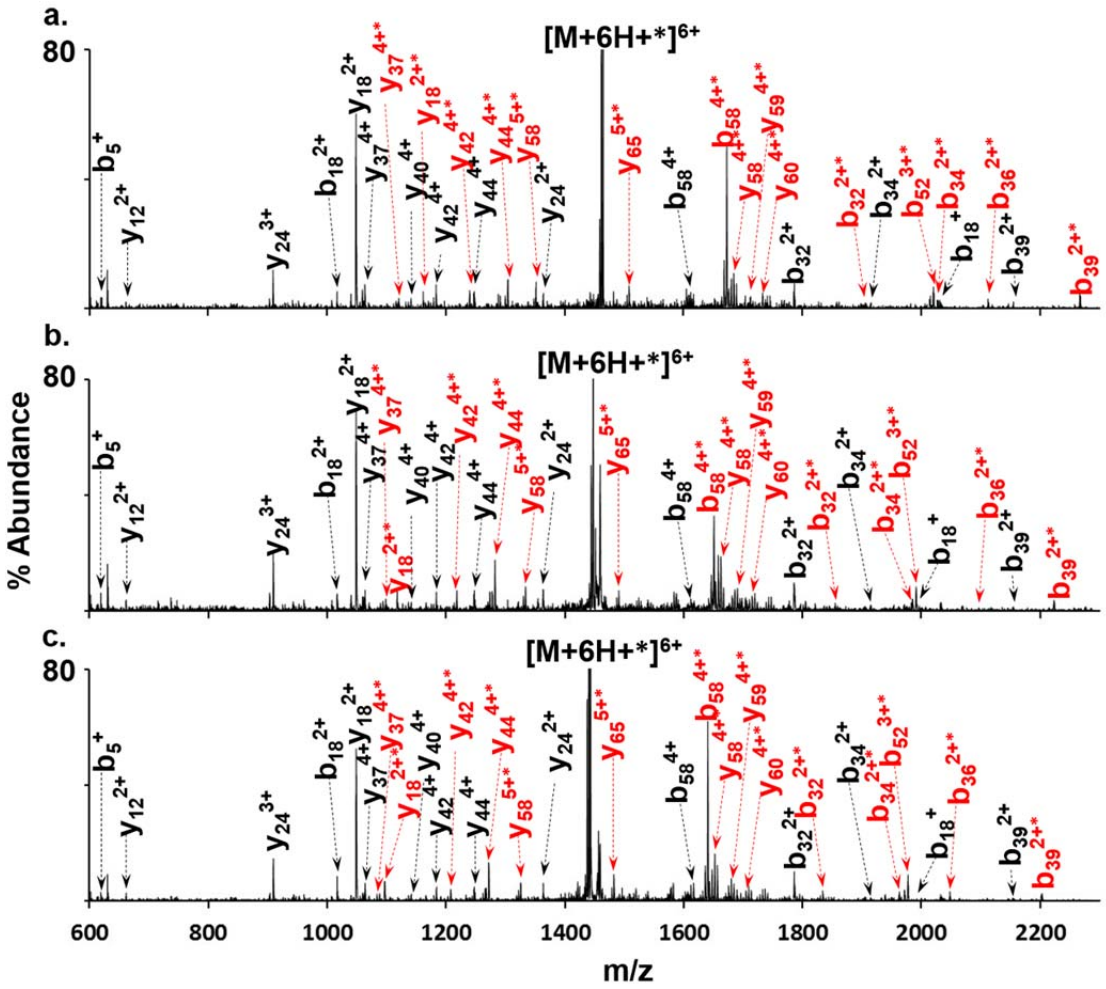

Figure 5.3 Ion trap CID product spectra of (a) [Ubiq+7H$^+$+[sulfo-EGS]$^-$-2[sulfo-NHS]]$^{6+}$, (b) [Ubiq+7H$^+$+[BS$_3$]$^-$-2[sulfo-NHS]]$^{6+}$ and (c) [Ubiq+7H$^+$+[BS$_2$G]$^-$-2[sulfo-NHS]]$^{6+}$. +* indicates a covalent attached crosslinker. The crosslinked fragment ions are noted in red.

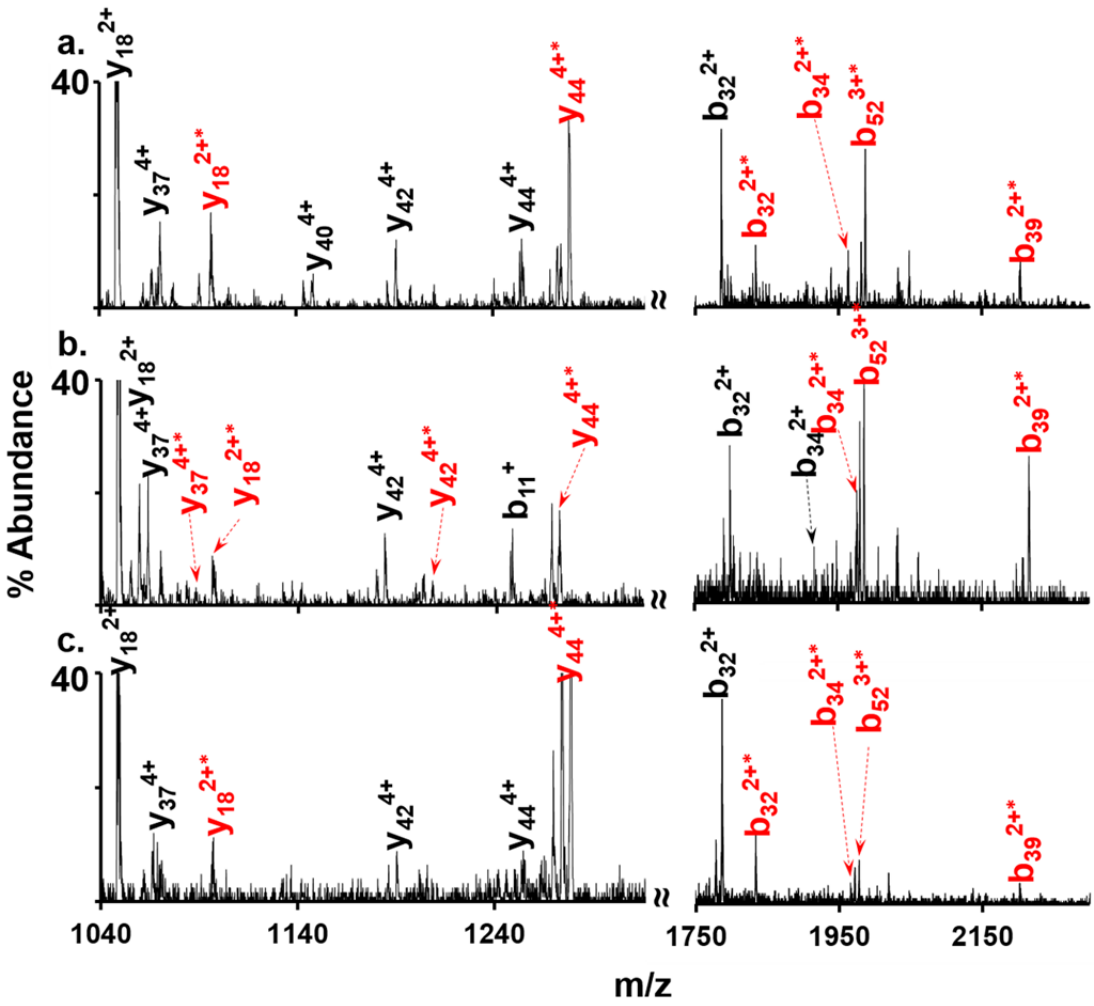

Figure 5.4 Ion trap CID product spectra of (a) $[Ubiq\_K48R+6H^{+}+*]^{6+}$, (b) $[Ubiq\_K27R+6H^{+}+*]^{6+}$ and (c) $[Ubiq\_K63R+6H^{+}+*]^{6+}$. +* indicates a covalent attached crosslinker (+[BS_2G]-2[sulfo-NHS]). The crosslinked fragment ions are noted in red.

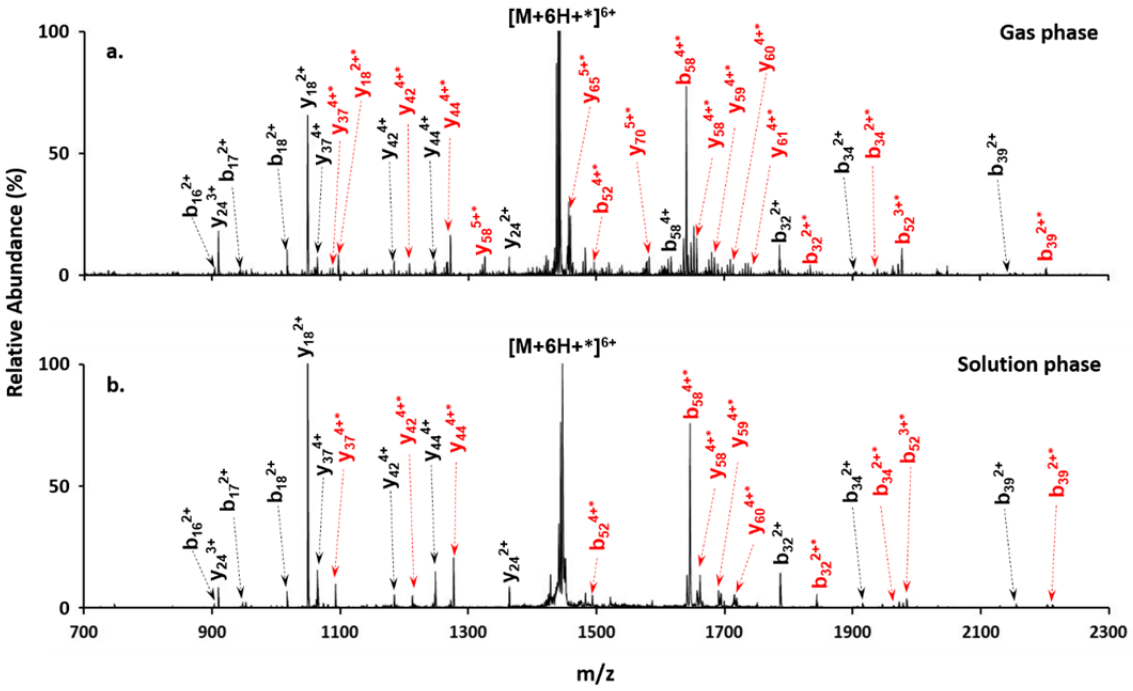

Figure 5.5 Ion trap CID product spectrum of BS_2G crosslinked ubiquitin ion $[M+6H^+{+}*]^{6+}$ formed via (a) gas phase reaction; (b) solution phase reaction.

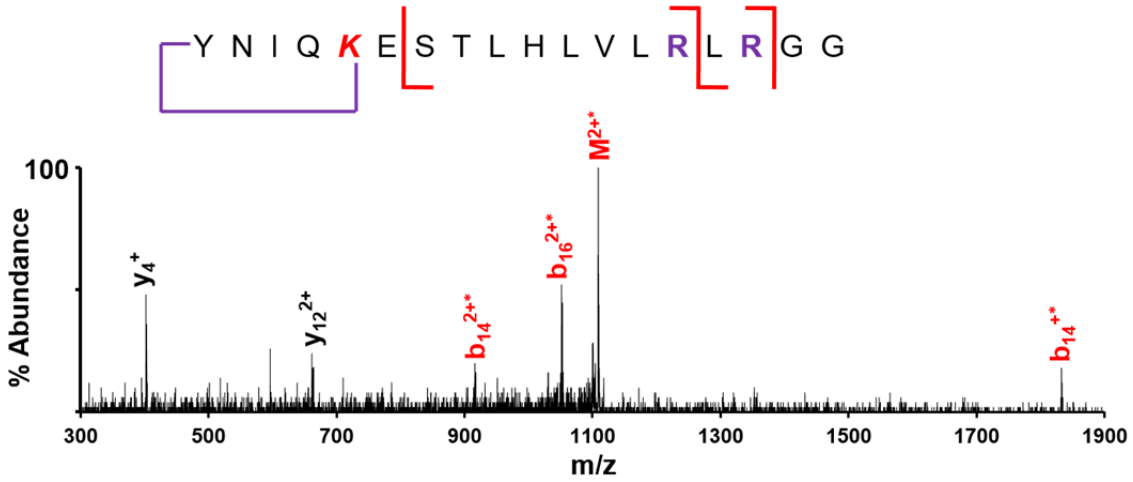

Figure 5.6 Ion trap CID product ion spectrum of crosslinked y_{18}^{2+} ion. The crosslinked fragments are labeled in red. The inset ladder structure shows the cleavage sites the proposed crosslinking sites.

Table 5.1 Possible locations of crosslinkers. Half of the possibilities are removed due to redundancy (--). X indicates links ruled out due to experimental results. K27-K29, K48-K63, K27-K33, K29-K33, K48-K33 and K63-K33 have been experimentally determined by the given modified sequence ions. Question marks represent possibilities that cannot be ruled out by the gas phase crosslinking approach.

	NT	**K6**	**K11**	**K27**	**K29**	**K33**	**K48**	**K63**
NT	--	--	--	--	--	--	--	--
K6	X	--	--	--	--	--	--	--
K11	X	X	--	--	--	--	--	--
K27	X	X	X	--	--	--	--	--
K29	X	X	X	**b_{32}***	--	--	--	--
K33	X	X	X	**b_{34}***	**b_{34}***	--	--	--
K48	X	X	X	**?**	**?**	**y_{44}***	--	--
K63	X	X	X	**?**	**?**	**y_{44}***	**y_{37}***	--

CHAPTER 6. THE EFFECTIVE HIGH MASS CUTOFF OF THE DIPOLAR DC EXPERIMENT AND ION EVAPORATION KINETICS

6.1 Introduction

Mass spectrometry has been widely applied in the field of analysis of large biomolecules, including proteins and nucleic acids, due to the advent of electrospray ionization (ESI)[1]. Accurate mass determination of the molecular weights of the biomolecules can be achieved with high resolution mass analyzers, i.e. time-of-flight (TOF), Fourier transform ion cyclotron resonance (FT-ICR) and orbitrap. Ions generated by electrospray can sampled by various mass spectrometer interfaces such as heated capillary[2] or nozzle-skimmer[3] interfaces. The interfaces are designed in such ways that can sample ions from the supersonic jet expansion[4] between atmospheric pressure and the intermediate vacuum. Specifically, the solvent in ESI droplets rapidly evaporates during the passage through the instrument interface, and ions are thus formed from complete desolvation.[5], [6] However, the particles are cooled within the expansion, allowing for clustering to occur if there are any solvent molecules present in the expansion region. Therefore, if the ESI droplets are not completely desolvated before introduction into vacuum, clusters of analyte ions, solvent and other components in the sample solution can form during the supersonic expansion period, resulting in heavily adducted and poorly resolved peaks in the mass

spectrum. This will inevitably hinder accurate mass determination and poor sensitivity because the ions signal is spread over a broad mass-to-charge (*m/z*) range.

Several approached have been developed to eliminate the clustering effects. Among them, counter-current flow of dry gases[7] and in source heating capillary[8] are two most commonly used methods on commercial instruments. Recently, we have implemented dipolar DC collisional activation in the RF-only ion guide of a linear ion trap/TOF instrument for gaseous bio-ion declustering.[9] The dipolar DC (DDC) heating technique has been demonstrated to be an effective means of declustering protein and nucleic acid samples prior to mass analysis. However, there is in theory a limitation at higher *m/z* associated with this method. In a typical DDC experiment, the ions are displaced away from the center of the trap and therefore be activated due to the exposure to the quadrupole RF field. The displacement is proportional to the *m/z* of the ions, so ions with higher mass-to-charge ratio have greater displacement from the center. There is a certain limit where the high m/z ions are moved so far that they can no longer be trapped by the RF field. This constitutes the so-called high mass cut off (HMCO), which potentially limits the application of the dipolar DC declustering for large biomolecules. The displacement for a given *m/z* ion is related to both quadrupole RF amplitude and the DDC applied. Theoretically, the parameters can be tuned to increase the high *m/z* limit while compromising the low *m/z* limit. Such hypothesis is tested with ion evaporation kinetics of Cs^+ ions and HMCO measurement of Ubiquitin carboxy-terminal hydrolase L1 (UCH-L1) ions.

6.2 Experimental Section

6.2.1 Materials

Cesium iodide (CsI) and leucine encephalin acetate salt hydrate (YGGFL) were purchased from Sigma-Aldrich (St. Louis, MO). Ubiquitin carboxy-terminal hydrolase L1 (UCH-L1) was provided by Chittaranjan Das Research Group. Methanol and glacial acetic acid were purchased from Mallinckrodt (Phillipsburg, NJ, USA). 10 μM solutions of UCH-L1 and YGGFL were made in 50/50/1 water/methanol/acetic acid (vol/vol/vol). 1 mM CsI solution was used in 50/50 water/methanol.

6.2.2 Apparatus and Procedures

All MS/MS experiments were performed on a QqTOF mass spectrometer modified to allow for application of dipolar DC in X direction of the quadrupole collision cell.[10] (QStar XL, AB Sciex, Concord, ON, CA). The instrument geometry is comprised of a transmission quadrupole operated in RF-only mode (q0), a mass resolving quadrupole (Q1), and a quadrupole collision cell (q2). Software control over the instrument was provided by Daetalyst 3.14, developed by AB Sciex. Precursors were preheated in q0 by DDC, mass selected via RF/DC isolation in Q1, and transferred to q2 and trapped. 20 V DC potentials were applied to the entrance and exit lenses of q2 to allow for efficient trapping during the DDC activation segment in storage mode.

For DDC experiment, q0 and q2 of the mass spectrometer were modified to provide for a DC dipolar field in the X-dimension. The rod offset leads to one rod pair were uncoupled, while those of the other rod pair were left coupled. The DC offset for each uncoupled rod was supplied by individual power supplies, and a third supply provided the offset for the remaining pair. This allowed an offset voltage of +/- x to be set on one pair of rods. The voltages were controlled through the Daetalyst software. The experiments performed in this work used DC dipolar potentials in q2 only. The basic parameters for q2 operation were r_0 = 4.17 mm and Ω = 1.8*2π*10^6 rad/s and V_{RF} (listed as 0-p) and V_{DDC} values listed in the text below.

6.3 Results and Discussions

The ion heating effect by dipolar DC excitation in an electrodynamic ion trap has been described by Tolmachev et al.[11]. The main objective is to use the dipolar DC field to delocalize the ions from the center of the ion trap to new equilibrium position where the ions are affected by the higher RF electric field, resulting in an increase in ion velocity due to RF-heating. The extent to which an ion of a given mass-to-charge ratio (*m/z*) is activated is determined by the point at which the ion displacement from the DDC electric field is counter-balanced by the trapping electric field. The latter is estimated from the negative gradient of the effective pseudopotential, V_{eff}:

$$V_{eff}(x,y) = D(\frac{x^2+y^2}{r_0^2}) \quad (6.1)$$

where x and y are displacements from the center of the trap, r_0 is the inscribed radius of the rod set, and D is the pseudo potential well-depth[12]:

$$D = \frac{qV_{RF}}{4} \tag{6.2}$$

V_{RF} is the quadrupole RF amplitude and the q is the Mathieu parameter given by

$$q = \frac{4zeV_{RF}}{m\Omega^2 r_0^2} \tag{6.3}$$

where z is the ion unit charge, m is the ion mass, and Ω is the RF frequency in radian-s^{-1}. The electric field, E_{DDC}, due to the DDC voltage, V_{DDC}, for round rods in a quadrupole array has been estimated to be:[13]

$$E_{DDC} = \frac{(0.8)V_{DDC}}{2r_0} \tag{6.4}$$

0.8 is the correction coefficient for the DDC field between a rod pair as opposed to a pair of parallel plate. The equilibrium point is reached when the electric force provided by the DDC field equals that of the trapping field. Using Equation 6.4 for E_{DDC}, the equilibrium displacement is given by:

$$r_e = \frac{(0.8)V_{DDC}}{qV_{RF}} r_0 \tag{6.5}$$

Substituting q with Equation 6.3:

$$r_e = \frac{m}{z}\left(\frac{{r_0}^3\Omega^2 V_{DDC}}{5e{V_{RF}}^2}\right) \tag{6.6}$$

Given certain V_{DDC} and V_{RF} conditions, the ion cloud displacement (r_e) is proportional to the *m/z* of the ions. There is a certain limit where the ions are no

longer trapped by the RF field and be lost by radial ejection. The maximum value for this limit is given by Equation 6.7 when the ions hit the rod ($r_e = r_0$):

$$(m/z)_{max} = \frac{5eV_{RF}^2}{\Omega^2 r_0^2 V_{DDC}} \quad (6.7)$$

However, this relationship simply determines the point at which the average equilibrium displacement reaches a rod surface and does not take into account the size of the ion cloud, the position spread due to the secular motion and micro-motion, and losses due to scattering. These effects are expected to lead to a decrease in trapping efficiency as r_e increases from zero to r_0. Thus, the ion storage lifetime is expected to be dependent on r_e, particularly as r_e becomes a substantial fraction of r_0, the practical useful *m/z* range over which DDC can be used is expected to be dependent upon the DDC time over the range of r_e values where there is a roll-off in trapping efficiency.

6.3.1 Effective High Mass Cutoff with Dipolar DC Activation

The protein UCH-L1 is used as a model system for the study of effective high mass cutoff in the DDC experiment for its stability towards collision activation in the gas phase. The ESI spectrum of UCH-L1 has a wide envelop of charge states spreading from 1000 to 7000 *m/z* range. The UCH-L1 ions are trapped in q2, where various DDC potentials are applied. The effective high mass cutoff is determined as the signal-to-noise ratio of a substantial peak gets down below 3. The heating effect should also be considered because the ions can also be lost via collision-induced dissociation (CID). Ideally, the HMCO should be

measured under the same heating effect (ΔT). Tolmachev et al.[11] described an "effective temperature" approach to estimate the increase in polyatomic ion temperatures subjected to DDC. The change in temperature, ΔT, due to the DDC voltage, assuming purely quadrupolar fields, the mass of the ion to be much greater than that of the background gas, m_g, and that changes in internal temperatures reflect increases in micro-motion velocity is given by:

$$\Delta T = \frac{(0.64)m_g\Omega^2 r_0^2}{24k}\left(\frac{V_{DDC}}{V_{RF}}\right)^2 \tag{6.8}$$

where k is the Boltzmann constant, 0.64 is the correction coefficient for the DDC field between a rod pair. The change in internal temperature can be maintained constant by locking the ratio between V_{DDC} and V_{RF}. Figure 6.1 shows the measured HMCO of DDC experiments using UCH-L1 ESI spectra under different temperature change scenarios. In all cases, the measured HMCO is approximately 50% of the theoretical value, suggesting the ions are lost completely when they are displaced $\frac{1}{2}r_0$ from the center of the trap. Controlled experiment shows that the change in pseudo potential well depth (from the change in V_{RF}) does not affect the trapping efficiency in all cases investigated.

According to Equation 6.7, if the ratio between V_{DDC} and V_{RF} is constant, the theoretical HMCO is only proportional to the V_{RF} applied to the quadrupole. As a result, the operational HMCO can be changed by increasing the V_{RF} while keeping the V_{DDC}/V_{RF} ration constant. The hypothesis has been supported by Figure 6.1, where in three different heating conditions, the experimentally measured HMCO increase as the V_{RF} or V_{DDC} increases. However, the low mass

cutoff (LMCO) is increase accordingly as described in Equation 6.3 when $q = 0.908$. More importantly, the ratio between the experimental and theoretical HMCO remain constant regardless of the V_{RF} and V_{DDC} applied.

6.3.2 Ion Evaporation Kinetics with Dipolar DC Activation

Given the difference between the experimental and theoretical HMCO, it is desirable to understand the ion evaporation kinetics with DDC activation in a linear ion trap. It is most straightforward to rationalize that the ion losses in the DDC experiment follow pseudo first order kinetics, because the ions are eventually lost by collisional scattering with the bath gas, whose number density is significantly higher than the analyte ions. However, since the ion cloud has a finite size, different ions in the cloud experience different electric fields and thus different collisional scattering effects. This effect was demonstrated using Cs^+ ions generated by electrospray to eliminate the effect of fragmentation. Generally, Cs^+ and $Cs^+(CsI)_n$ clusters are introduced to q2 and trapped. A preheating process is effected by applying a DDC field to break all the clusters down to Cs^+ ion. Then, the Cs^+ ions are cooled before a second step DDC activation is applied to move the ion cloud to the boundary where the Cs^+ signal starts to drop. The holding time of the second DDC period is varied to get an intensity vs. holding time plot that can be used to determine ion depletion rate constant (Figure 6.2). Figure 6.2a illustrates the shielding effect when there are a large number of ions, the ion depletion rate tends to be lower than that of a small ion

cloud (Figure 6.2b). Even in the case when the ion injection time is minimized, the initial ion depletion pattern is still affected by the ion cloud shielding effect (Figure 6.2b). In practicality, only the last few data points were used to determine the depletion rate constant.

Assuming pseudo first order kinetics for the ion depletion in the DDC experiment, the experimental conditions (i.e. pressure and temperature) of the ions should fit into Arrhenius equation:

$$k = Ae^{-\frac{E_a}{RT}} \tag{6.8}$$

where k is the rate constant, E_a is the activation energy, R is the universal gas constant, T is the temperature, A is the pre-exponential factor, which represents the total number of collisions between the analyte ion and the ambient gas and can be calculated using Equation 6.9[11]:

$$A = n\sigma v_r \tag{6.9}$$

where n is the number density of the ambient gas, σ is the cross section of the two colliding particles, and v_r is the relative velocity of the two colliding particles. Substituting A in Equation 6.8 by Equation 6.9, the relationship between the depletion rate constant and the experimental conditions can be depicted as:

$$k = n\sigma v_r e^{-\frac{E_a}{RT}} \tag{6.10}$$

In Equation 6.10, n can be measured as the pressure in the trap, T can be calculated using Equation 6.8 with given experimental conditions, σ, E_a and R are constant for a given colliding pair. In order to test the first order kinetics

hypothesis, we need to investigate the relationship of depletion rate constant with pressure as well as with ion temperature.

Figure 6.3a shows the depletion constant measured under different trap pressures. The numbers P=3, 6, 9, 12 and15 are arbitrary values of trap pressure set by the instrument software. As shown in Figure 6.3b, the depletion rate constant (k) has a linear relationship with trap pressure (P), with a correlation coefficient as 0.9783. Similarly, the relationship between k and T is measured in the same manner (Figure 6.4). However, the relationship between ln(k) and $1/T$ is not a straight line. It is noted that there is a v_r factor in the pre-exponential factor, which is also related to ion temperature. Therefore, the relationship between k and T cannot be mathematically derived. The fact that most solution phase first order reaction shows linear relationship between ln(k) and $1/T$ is because the contribution of temperature in the pre-exponential factor can be neglect since the solution phase reaction happens at relatively low temperature.

6.3.3 Efficient CID Using a Combination of DC Field and Resonance Excitation

The knowledge of ion evaporation mechanism in DDC experiment can be applied to unimolecular dissociations that are difficult to perform in a linear ion trap. For instance, some large biomolecules, i.e. protein complexes with many disulfide linkages, are difficult to dissociate in the gas phase by ion trap CID because the resonance excitation amplitude applied either eject the precursor ions radially or is not high enough to fragment the ions. It is desirable for a

fragmentation approach that can deposit more energy into the target ion population without losing them by radial or axially ejection.

Dipolar DC excitation, as one of the ion activation methods, is implemented by applying a DC field between a rod pair. In our instrumental setup, the DC field is applied between the rod pair in X-dimension. At the same time, the ion trap CID is implemented by applying a single frequency dipolar RF excitation between the rod pair in Y-dimension. As a result, an orthogonal activation approach can be performed by effect DDC CID in one dimension and ion trap CID in another.

Figure 6.5 shows the orthogonal activation of protonated YGGFL ions using a combination of DDC CID and ion trap CID. Firstly, the YGGFL ions are activated by DDC to a point when the $[M+H]^+$ ions start fragment and give rise to b_4 ions (Figure 6.5a). Then, resonance excitation amplitude from the ion trap CID is gradually increased from 250mV to 350mV. With low excitation amplitude (Figure 6.5b), the precursor ion signal goes down without giving rise to more fragment ions. This is presumable due to the fact that orthogonal excitation by resonance ejects the precursor ions because it effects ion oscillation close to the ejection boundary. With higher excitation amplitude, the precursor ions are even more suppressed and fragment ions start to increase in absolute intensity (Figure 6.5c and d). In the case of higher excitation amplitude, more energy is deposited into the peptide ions and thus they fragment promptly in the first few oscillations. The fragment ions are then cooled down and trapped by the quadrupolar field. However, since the amplitude of the oscillation gets larger, the loss of precursor ions via radial ejection becomes more significant. As a result, the orthogonal

activation by combining DDC CID and ion trap CID cannot be achieved due to the poor trapping efficiency at the boundary.

Figure 6.6 describes the combination of quadrupolar DC field and ion trap CID, which gives rise to more efficient fragmentation for YGGFL ions. The resonance excitation amplitude of the ion trap CID is held at 285mV to induce maximum fragmentation without losing the precursor ion by ejection (Figure 6.6b). Then, the q2 rod offset for the rod pair B (RO2B) (inset of Figure 6.6) is changed while keeping the q2 rod offset for the rod pair A (RO2A) constant at 0V. With RO2B being more positive relative to RO2A, the fragmentation efficiency is decreased, whereas the more negative RO2B leads to more efficiency fragmentation. However, if the RO2B is too negative, both precursor ion and the product ion signal are suppressed presumable due to poor trapping efficiency. The enhanced fragmentation efficiency can be rationalized with increased a (the Mathieu parameter) value. The change in quadrupolar DC field leads to change in the a parameter, which delocalize the ions in the Mathieu stability diagram. Once the ions are moved to the boundary of the stability diagram, they can be activated. As a result, more energy deposition can be achieved by activating ions with a combination of quadrupolar DC field and dipolar resonance excitation.

6.4 Conclusions

Effective high mass cutoff is determined to be approximately 50% of the theoretical value in the UCH-L1 experiment. The relative ratio is not affected by

the ion internal temperature or pseudo potential well depth. The ion losses in the DDC experiment follows pseudo first order kinetics. The relationship between the depletion rate constant and trap pressure has proved to be linear. However, relationship between the ion temperature and the depletion rate constant is complicated and need more sophisticated mathematical model to analyze. Orthogonal ion activation using DDC CID and ion trap CID cannot be achieved because of the poor trapping efficiency at the boundary region. However, it has been demonstrated that the combination of quadrupolar DC field and ion trap CID can increase the amount of energy that can be deposited into the target ion population without ejecting the ions.

6.5 References

[1] Fenn, J.; Mann, M.; Meng, C.; Wong, S.; Whitehouse, C. Electrospray ionization for mass-spectrometry of large biomolecules. *Science*. **1989**, *246*, 64-71.

[2] Whitehouse, C.M.; Dreyer, R.N.; Yamashita, M.; Fenn, J.B. Electrospray interface for liquid chromatographs and mass spectrometers. *Anal. Chem.* **1985**, *57*, 675-679.

[3] Yamashita, M.; Fenn, J.B. Electrospray ion source. Another Variation on the Free-Jet Theme. *J. Phys. Chem.* **1984**, *88*, 4451-4459.

[4] Reis, V,H,; Fenn, J. B. Separation of Gas Mixtures in Supersonic Jets. *J. Chem. Phys.* **1963**, *39*, 3240.

[5] Chowdhury, S. K.; Katta, V.; Chait, B. T. An electrospray-ionization mass spectrometer with new features. *Rapid. Commun. Mass Spectrom.* **1990,** *4,* 81-87.

[6] Guo, X.; Bruins, A. P.; Covey, T. R. Characterization of typical chemical background interferences in atmospheric pressure ionization liquid chromatography-mass spectrometry. *Rapid Commun. Mass Spectrom.* **2006,** *20,* 3145-3150.

[7] Covey, T. R.; Bonner, R. F.; Shushan, B. I.; Henion, J. D. Determination of protein, oligonucleotide and peptide molecular weights by ion spray mass spectrometry. *Rapid Commun. Mass Spectrom.* **1988,** *2,* 249-256.

[8] Loo, J. A.; Udseth, H. R.; Smith, R. D. Peptide and protein analysis by electrospray ionization-mass spectrometry and capillary electrophoresis-mass spectrometry. *Anal. Biochem.* **1989,** *179,* 404-412.

[9] Webb, I. K.; Gao, Y.; Londry, F. A.; McLuckey, S. A. Dipolar DC Collisional Activation in the RF-Only Ion Guide of a Linear Ion Trap/Time-of-Flight Instrument for Gaseous Bio-Ion Declustering. *J. Mass Spectrom.* **2013**, *48,* 1059-1065.

[10] Xia, Y.; Chrisman, P. A.; Erickson, D. E.; Liu, J.; Liang, X.; Londry, F. A.; Yang, M. J.; McLuckey, S. A. Implementation of Ion/Ion Reactions in a Quadrupole/Time-of-Flight Tandem Mass Spectrometer. *Anal. Chem.* **2006**, *78*, 4146-4154.

[11] Tolmachev, A.V.; Vilkov, A.N.; Bogdanov, B.; Păsa-Tolić, L.; Masselon, C.D.; Smith, R.D. Collisional activation of ions in RF ion traps and ion guides: the effective ion temperature treatment. *J .Am. Soc. Mass Spectrom.* **2004**, *15***,** 1616-1628.

[12] March, R.E.; Todd, J.F.J. *Quadrupole Ion Trap Mass Spectrometry, Second Edition.* John Wiley & Sons, Inc.: Hoboken, NJ, **2005**.

[13] Michaud, A.L.; Frank, A.J.; Ding, C.; Zhao, X.-Z.; Douglas, D.J. Ion excitation in a linear quadrupole ion trap with an added octopole field. *J. Am. Soc. Mass Spectrom.* **2005**, *16*, 835-849.

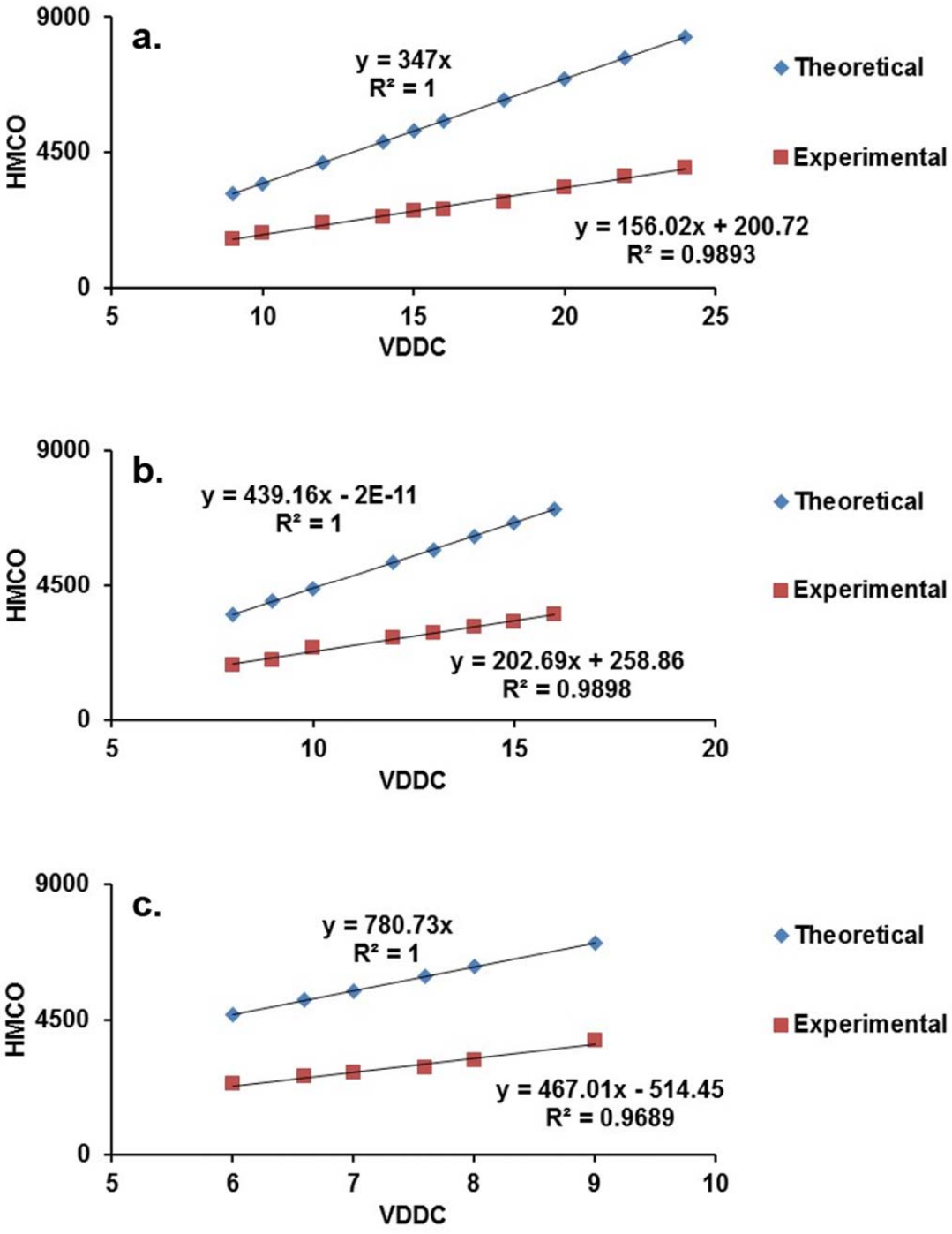

Figure 6.1 Experimental vs. theoretical high mass cutoff of UCH-L1 ESI spectra within a range of dipolar DC activation. For each data point within a line, the ratio of V_{DDC} and V_{RF} is kept constant in order to maintain constant heating effect: (a) ΔT=124.85K; (b) ΔT=98.64K; (c) ΔT=55.49K.

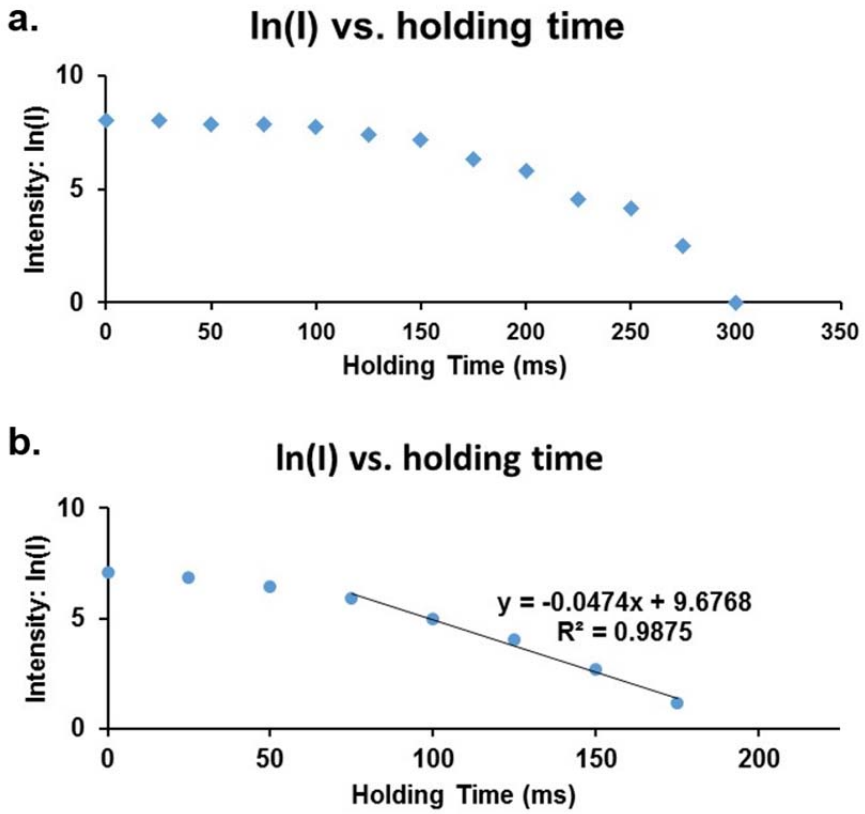

Figure 6.2 First order kinetics of ion evaporation from the ion trap via dipolar DC excitation. (a) 200ms Cs^+ injection; (b) 8ms Cs^+ injection. All data points are collected under the condition: V_{DDC}=8.2V, V_{RF}=30.16V, ΔT=887.23K.

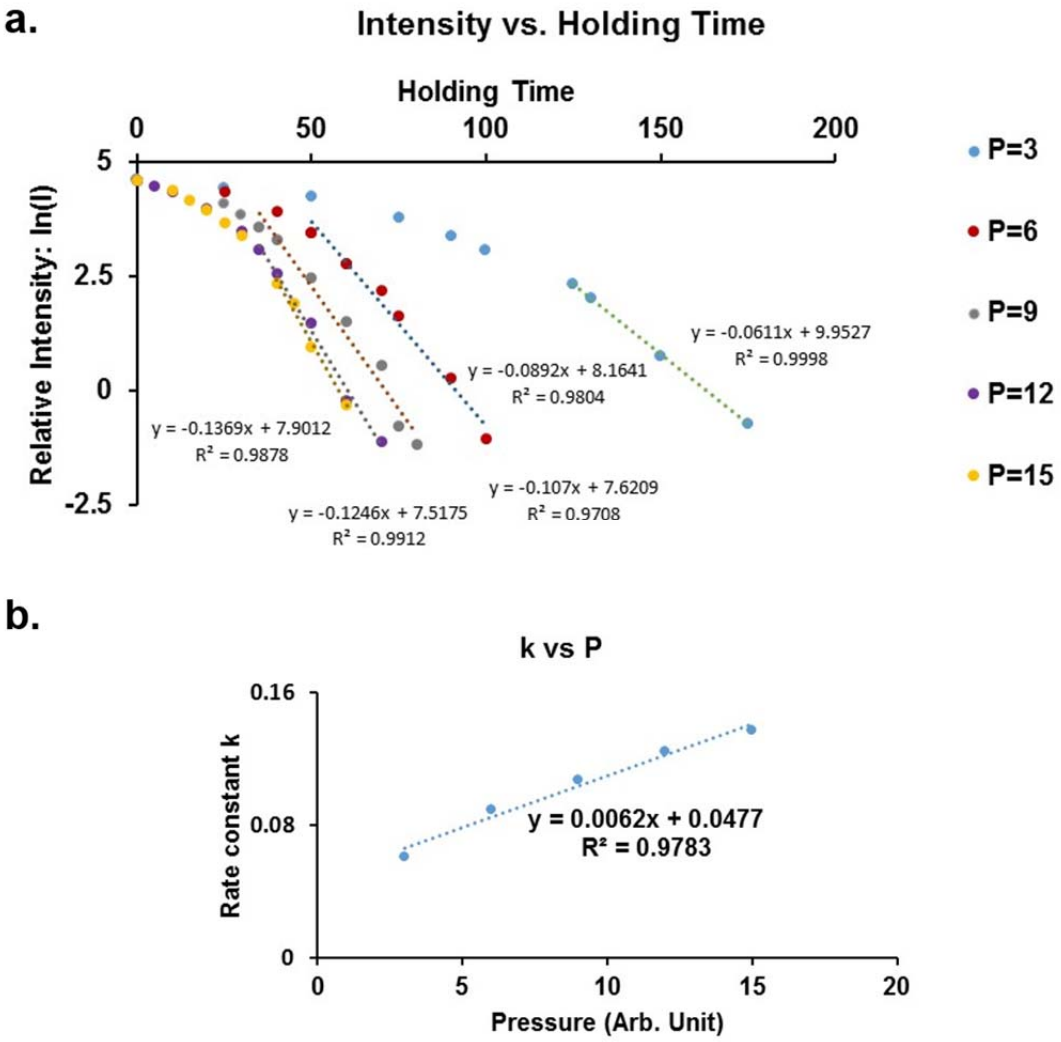

Figure 6.3 (a) First order ion evaporation kinetics under different trap pressure; (b) Linear relationship between pressure and evaporation rate constant.

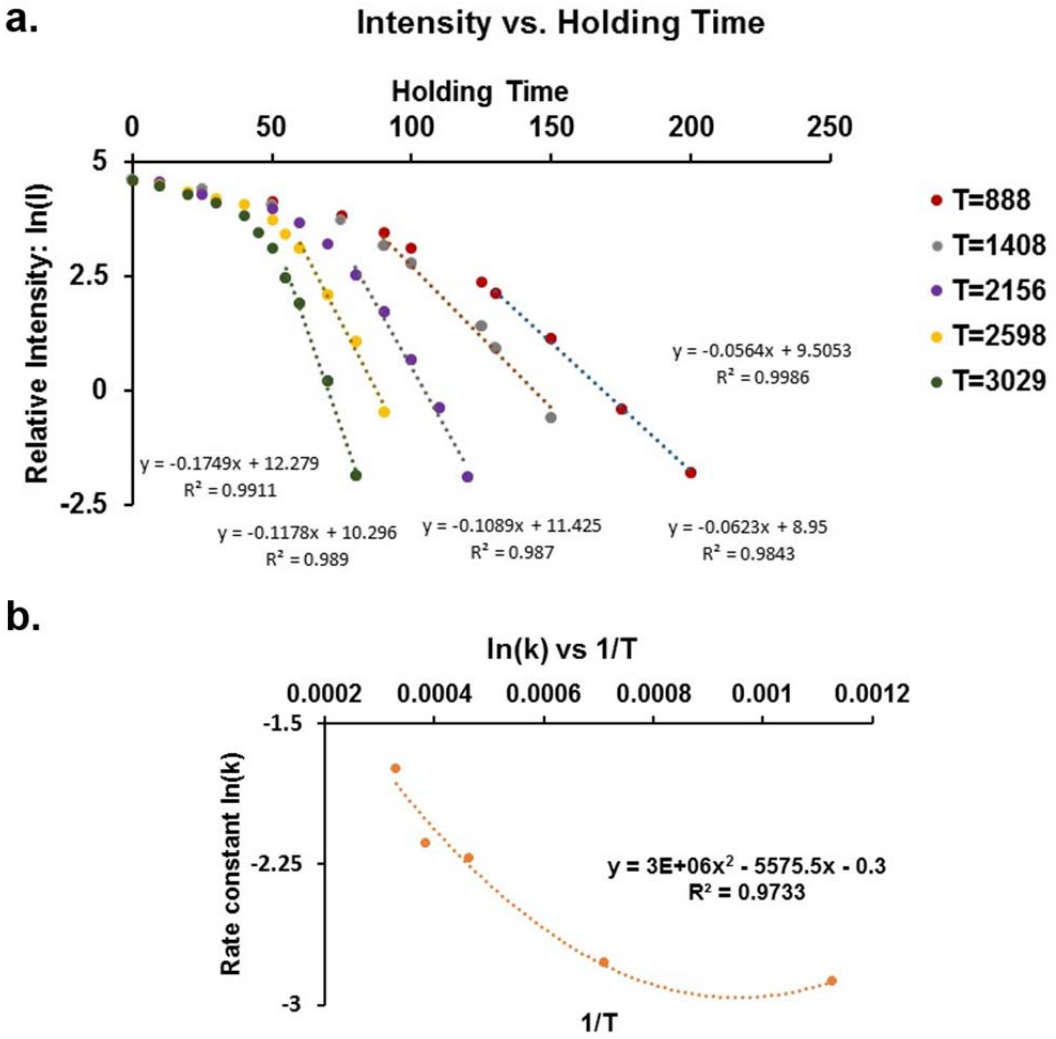

Figure 6.4 (a) First order ion evaporation kinetics under different temperature increase; (b) Fitting temperature increase and evaporation rate constant into Arrhenius equation.

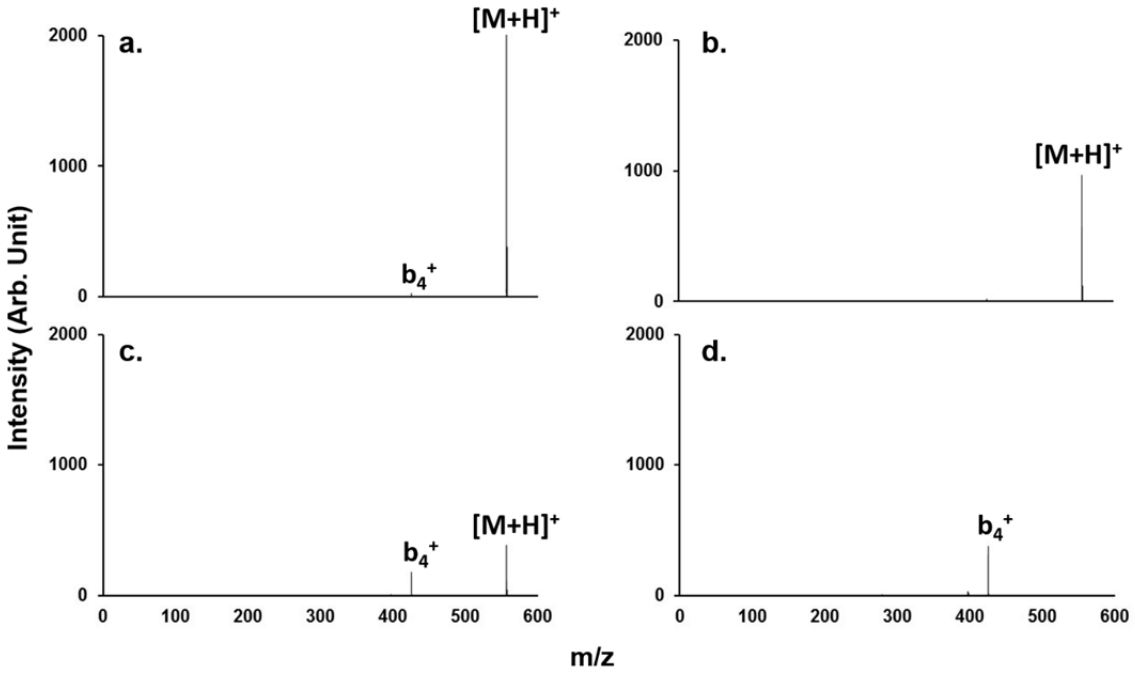

Figure 6.5 Orthogonal activation of protonated YGGFL ions. DDC is held at 6V. Resonance excitation amplitude is at (a) 0mV; (b) 250mV; (c) 300mV; (d) 350mV, respectively.

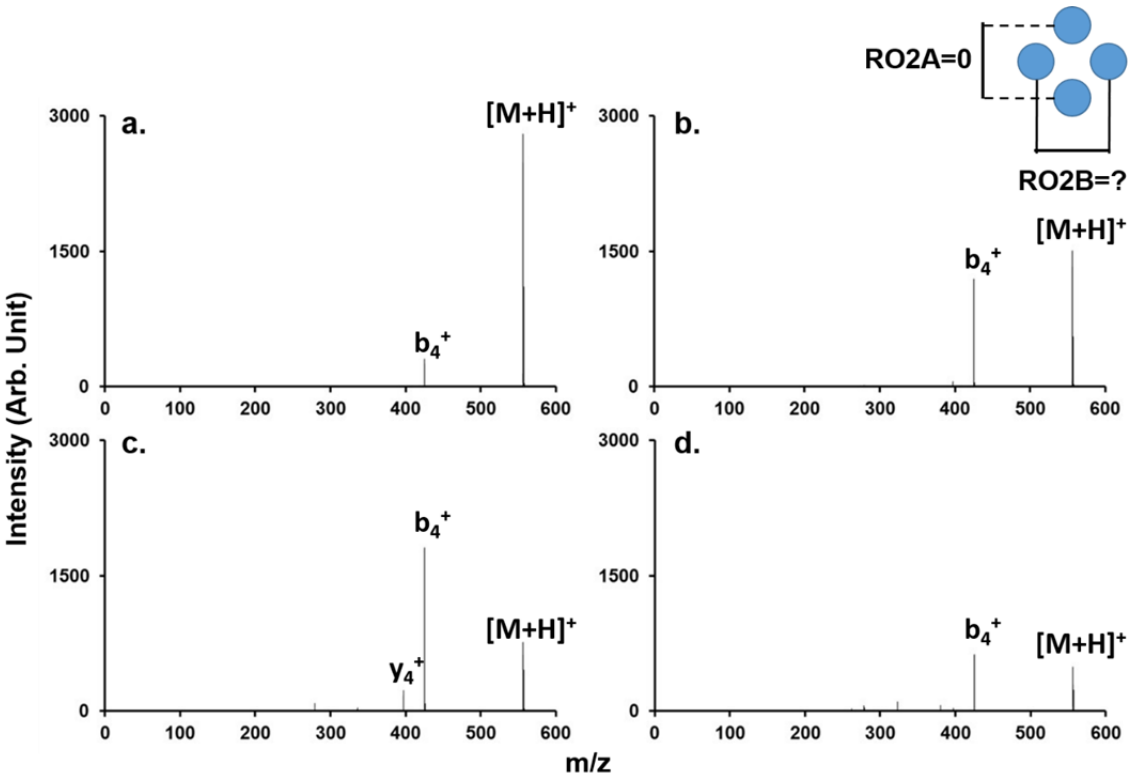

Figure 6.6 Orthogonal activation of protonated YGGFL ions. Resonance excitation amplitude is held at 285 mV. Rod offset B is held at (a) 5V; (b) 0V; (c) -2V; (d) -6V, respectively. The inset describes the wiring for two rod pairs of q2 quadrupole.

CHAPTER 7. ION/ION REACTION PRODUCT ENRICHMENT IN LINEAR ION TRAP

7.1 Introduction

Ion/ion reaction has been significantly developed in the past decades targeting various mass spectrometric applications.[1, 2, 3, 4, 5, 6] Specifically, proton transfer reactions have been used to reduce the charges of complex mixtures that are generated by ESI;3, [7, 8, 9, 10] electron transfer reactions have been applied to change the precursor ion type or induce alternative fragmentation pathways;[11] and gas phase covalent bond formation have been studied in terms of gas phase derivatization and labeling.[12,13]

The efficiencies and rates of the reactions vary based on different reagents, reaction conditions, analyte properties as well as stoichiometry of reactants. In terms of application, there are only certain types of reaction products that are of interest whereas the rest are considered as byproducts. Efforts have been made to optimize the reagents such that the desired products are more abundant than the byproducts[14, 15]. There are also techniques, i.e. ion parking[16], developed to change the reaction conditions so that certain products can be enriched. Typically, ion parking has been developed to allow for an entire charge state envelope to be concentrated into an individual charge state by resonantly exciting the desired *m/z* with the application of AC across the endcap electrodes.

The resonance excitation of the desired *m/z* can delocalize the target ion population from the reaction pool and thus prohibit them from further reaction with the excess reagent ions. The experiment has also been implemented in parallel parking mode by applying DC across the end caps to spatially spread out the cation and anion clouds in the axial direction[17, 18]. Traditionally, ion parking has been implemented in the 3D ion trap, in which 80% efficiency can be achieved. However, given the prevalence of hybrid mass spectrometers with linear ion traps, it is desirable to explore the feasibility of ion parking in a linear ion trap instrument. In this work, efficient ion parking of protein charge states as well as reaction complex formation is demonstrated using a QqTOF mass spectrometer.

7.2 Experimental Section

7.2.1 Materials

Ubiquitin from bovine erythrocytes, benzoic acid, 1-Ethyl-3-(3-dimethylaminopropyl)carbodiimide (EDC), sulfo-NHS acetate (SA) and N-Hydroxysulfosuccinimide sodium salt (sulfo-NHS) were purchased from Sigma-Aldrich (St. Louis, MO). 1H,1H-Pentadecafluoro-1-octanol (PFO) was obtained from Fisher Scientific (Waltham, MA). Methanol and glacial acetic acid were purchased from Mallinckrodt (Phillipsburg, NJ, USA). 10 μM solution of ubiquitin was made in 50/50/1 water/methanol/acetic acid (vol/vol/vol). 2 mM PFO solution was used in 50/50 water/methanol. Sulfosuccinimidyl benzoate (BSN)

was synthesized by add 1 equivalent of sulfo-NHS to a mixture of 1:1 (equiv.) benzoic acid and EDC to a final concentration of 1mM.

7.2.2 Apparatus and Procedures

All MS/MS experiments were performed using a prototype version of a QqTOF tandem mass spectrometer (QSTAR, AB Sciex, Concord, ON, Canada) modified to allow for ion/ion reaction studies.[19] A home-built pulsed dual nanoESI source was coupled directly to the nanospray interface to produce ions of both polarities.[20] The collision cell quadrupole q2 has been modified to allow dipolar DC application across one rod pair.[21] Briefly, one pair of q2 rods is wired together, floated to the same rod offset, while the other pair of rods are not connected, allowing the rod offsets of each rod to be controlled separately. The offsets on the dipolar pair have their potentials set symmetrically above and below the rod offset of the other pair. The total dipolar potential is the difference between the two equal and opposite potentials. Ion/ion reactions were implemented by first storing the cations in q2, followed by mutually storing anions with cations in q2. Ion parking was achieved by applying dipolar resonance excitation of the target product *m/z* or a dipolar potential during the anion introduction step, the mutual storage step or both.

7.3 Results and Discussions

The selective enrichment of a certain product of an ion/ion reaction relies on the exploitation of the fundamental motion of an ion in the electrodynamic trap[16]. Ions trapped by electrodynamic field have characteristic oscillatory motions that are *m/z* dependent.[22, 23, 24] The *m/z*-dependent oscillation frequency is given by Equation 7.1:

$$\omega_{n',u} = (2n \pm \beta_u)\frac{\Omega}{2} \tag{7.1}$$

where u denotes either radial or axial dimension, n is an integer, Ω represents driving frequency of the quadrupolar field, and β_u is given approximately by Equation 7.2:

$$\beta_u \approx (a_u + \frac{{q_u}^2}{2})^{\frac{1}{2}} \tag{7.2}$$

where a_u is given by Equation 7.3:

$$a_u = \frac{8zeU}{m{r_0}^2\Omega^2} \tag{7.3}$$

and the q_u is given by Equation 7.4:

$$q_u = \frac{4zeV}{m{r_0}^2\Omega^2} \tag{7.4}$$

where U is the quadrupolar DC potential on the rods ($U = 0$ in all ion parking experiments), V is the RF amplitude applied to the quadrupole, r_0 is the inscribed radius of the quadrupole (distance from the center to one of the rods), and m/z is the mass-to-charge ratio of the ion. The most important frequency is the fundamental secular frequency when $n = 0$. The application of a single-frequency waveform to one pair of the rods (i.e. X/Y-dimension) which is in

resonance with the X/Y-dimension fundamental secular frequency of ions of a particular *m/z* results in the X/Y-dimension acceleration of the ions. This is the common approach to induce collisional activation of ions in a linear ion trap[25] or to selectively eject ions radially within the context of precursor ion isolation[26].

In a typical ion parking experiment, the resonance frequency waveform is applied with the amplitude high enough to excite the target ions and delocalize them from the center of the trap but not so high as to cause collision-induced fragmentation or radial ejection. The rate of ion/ion reaction for the excited target ion can be diminished relative to its rate in the absence of excitation due either to an increase in the relative velocity of the collision pair[16] or a decrease in the physical overlap of the positive and negative ion clouds. Note that Equation 7.1-7.4 apply to a pure quadrupolar field, which is impossible to achieve in an actual device, i.e. quadrupole rods are not perfectly parallel and result in imperfect quadrupolar field along the Z-dimension. Ion parking was well established in the 3D quadrupole ion trap due to the perfect overlap between the two reactant ions (compact ion cloud in the XYZ-dimensions). However, for linear ion trap, the ion cloud is constrained radially (XY-dimensions) but spreads axially (Z-dimension). Ion parking by radially activating the target *m/z* does not work as efficiently because same *m/z* ions spreading out in the Z-dimension have slightly different fundamental secular frequency due to the imperfection in the quadrupolar field and thus cannot be activated by the RF excitation. To resolve this problem associated with linear ion trap, we utilize the linear accelerator (LINAC)[27] function

of the Sciex mass spectrometer to axially constrain ion clouds of both polarities and effect ion parking with radial resonance excitation.

7.3.1 Resonance Excitation Ion Parking during Ion/Ion Reactions

Ion parking has proved to be useful in a number of analytical applications due to its selective inhibition of ion/ion reaction rates. For instance, it is capable of stopping or slowing a reaction at a selected product ion and essentially converting all precursor ion signal into the target *m/z*. Such an experiment is demonstrated using complex formation reaction between a multiply charge ubiquitin ion and a deprotonated reagent ion (Figure 7.1). Sulfosuccinimidyl benzoate (BSN) is a gas phase derivatization reagent that can covalently attached a benzoate functional group (+104 Da) to a primary amine containing residue (N-terminus, lysine, arginine). The first step of the derivatization involves electrostatic complex formation between the protein cation and the BSN anion. Further activation of the long-live complex results in amide bond formation with signature loss of neutral sulfo-NHS (195 Da). The complex formation step is essential since it determines the final product yield in this reaction. However, more than one BSN can be attached to the protein cation and therefore the precursor ion (7+) (Figure 7.1a) is converted into several product species (Figure 7.1b). Figure 3c shows ion parking on the $[M+6H+BSN]^{6+}$ species by apply dipolar RF excitation in resonance to the *m/z* 1477. The actual applied frequency (81.77kHz) is several kHz off the theoretical fundamental secular frequency (90.77kHz), suggesting the imperfection of the quadrupolar RF field. The ion

intensity in the $[M+6H+BSN]^{6+}$ species (Figure 7.1c) was 85% of the precursor ion $[M+7H]^{7+}$ (Figure 7.1a). Comparing to the ion intensity of $[M+6H+BSN]^{6+}$ without ion parking (Figure 7.1b), the absolute intensity of the ion parking experiment shows an increase of over a factor of 2, suggesting that the acceleration of the $[M+6H+BSN]^{6+}$ species inhibits its reaction to more BSN adductions.

Effective ion parking experiments have been demonstrated for 1 to 3 BSN adduction species (Figure 7.2). In all cases, significant concentration of signal in the ions resonantly excited was observed. The intensity of the species that were accumulated were 85%, 86% and 71%, respectively, of the precursor ion, suggesting that the majority of the precursor signal is converted into target product signal. A variety of ion parking experiments more sophisticated than illustrated in Figure 7.2 can be envisioned. For instance, the “stars” in Figure 7.2 represent first neutral sulfo-NHS losses from the electrostatic complexes. Generally in such experiments, the “star” peaks are the next generation products, which are desirable to be maximized in signal. However, the sulfo-NHS loss can happen simultaneously upon complex formation reaction (Figure 7.2a), and the $[M+6H+BSN-[sulfo-NHS]]^{6+}$ ions can react further with the excess of $[BSN-H]^-$ ions in the trap (generating the two stars on the right in Figure 7.2a) and dilute the target product signal. Even with ion parking on the first generation product, i.e. $[M+6H+BSN]^{6+}$, the sulfo-NHS loss species can still react to form more BSN adductions (the two stars on the right in Figure 7.2b) because the star peaks are not resonantly excited and therefore are cooled down into the center to react with

the excess of $[BSN-H]^-$. The use of double resonance excitation frequencies simultaneously in the mutual storage period of the ion/ion reaction allows for concentration on both $[M+6H+BSN-[sulfo-NHS]]^{6+}$ ions and $[M+6H+BSN]^{6+}$ ions, which maximize the signal intensity in the final product.

7.3.2 The Factors Relative to Resonance Excitation Ion Parking Efficiency

In order to improve the ion parking efficiency in the linear ion trap, linear accelerator (LINAC) was used to manipulate two ion clouds of opposite polarities in the mutual storage period. Specifically, LINAC is an axial DC gradient applied along the q2 collision cell. The potential is relative to the q2 DC rod offset. In all ion parking experiments, q2 DC rod offset was held at 0V. The negative LINAC potential drives cations to the entrance lenses direction and anions to the exist lenses direction, whereas the positive LINAC does the opposite. The LINAC potential helps either to increase or decrease the overlap of two ion clouds. When it has an effect in merging two ion clouds, the LINAC also helps to axially constrain the ion distribution in the Z-dimension, resulting in more homogeneous quadrupolar field.

Figure 7.3 demonstrates the effect of LINAC potential on the efficiency of ion parking. The highest ion parking efficiency is noted in Figure 7.3b where LINAC is equal to 0V. In this particular case, the ubiquitin cations and PFO anions overlap perfectly based on their injection conditions. Resonance activation of the 5+ charge state result in more than 80% of the signal recovery. Without ion parking, the ion/ion reaction proceed up to 1+ charge state or

neutralization since the total ion intensity in Figure 7.3e is lower than those in the other four spectra. The abundant precursor charge state (6+) in Figure 7.3a suggests that negative LINAC potential separate the two ion clouds and therefore retard the proton transfer reaction. Other than the overlap issue, Z-dimensional spreading is another factor that determines the ion parking efficiency. Figure 7.3a, c and d all show more abundant 4+ and 3+ charge states than Figure 7.3b, suggesting less efficiency ion parking because some portion of the 5+ charge state ions react further into lower charge states. This phenomenon is presumably due to the fact that Figure 7.3b is not only the best overlapped scenario, but also the most compact. Increasing or decreasing the LINAC potential results in spreading of the ion clouds in the Z-dimension, causing both precursor and product ions to experience different quadrupolar field. Thus, signal frequency excitation will only accelerate a portion of 5+ charge state ions, resulting in spectra with both enhanced 5+ charge state signal and some lower charge state ions. The portion of 5+ charge state ions that are not affected by the signal frequency excitation become greater as the LINAC potential increases (Figure 7.3c to d), resulting in more lower charge state ions and less efficiency ion parking.

It is always essential to find the optimal LINAC potential for different ion/ion reactions. The LINAC potential is correlated to the starting position of both ion clouds in the mutual storage period. Figure 7.4 demonstrates ion parking on different product charge states for the same reaction $[ubiquitin]^{7+}+PFO^{-}$. Note that the amount of PFO ions introduced via electrospray is different in two scenarios

due to the different extents of reaction required for two parking experiments. Because of the variations in the amounts of negative ions, different LINAC potentials (5V vs. 15V) are required to obtain the optimum parking efficiency. The effect of the excitation amplitude seems to be incremental to the ion parking efficiency before it exceeds the fragmentation/ejection threshold. Generally, increasing excitation amplitude increases the oscillation velocity of the target ion, and thus diminishes its reaction rate towards the opposite charge. However, when the excitation amplitude exceeds a certain threshold, the target ions signal drops due to loss from collision-induced fragmentation or radial ejection from the trap.

7.3.3 Parallel Ion Parking Using Dipolar DC Excitation

The application of dipolar DC (DDC) during ion/ion reactions diminishes the ion/ion reaction rates in a similar fashion to using auxiliary AC waveforms. The DDC potential separate the oppositely charged ion clouds by displacing them radially in opposite directions (+X/Y vs –X/Y). Moreover, Displacement from the center of the trap increases the velocity of the ions' micromotions as they are activated by the RF field from regions closer to the rods.[28], [29] Thus, the application of dipolar DC field, in theory, can selectively enhance certain reaction product signal by reducing its reaction rate. This process is termed parallel ion parking[17,18].

The selective ion enrichment in the context of parallel parking is more elusive than the resonance excitation. The whole ion population is affected by the

dipolar DC field, causing radial displacement relative to the *m/z* of the ions (Equation 7.5)[30, 31, 32]:

$$r_e = \frac{r_0}{q}\frac{0.8V_{DDC}}{V_{RF}} \quad (7.5)$$

where r_e is the ion cloud displacement from the center, r_0 is the inscribed radius of the q2 quadrupole, V_{DDC} is the dipolar DC potential applied to one pair of the rods, V_{RF} is the RF amplitude applied to the q2 quadrupole, q is the Mathieu parameter which can be calculated by Equation 7.4, 0.8 is the correcting coefficient for the DC field between a rod pair[31, 32]. Substitute q in Equation 7.5 with Equation 7.4, the relationship between r_e and *m/z* can be demonstrated as Equation 7.6:

$$r_e = \frac{m}{z}\left(\frac{{r_0}^3\Omega^2 V_{DDC}}{5e{V_{RF}}^2}\right) \quad (7.6)$$

The parameters in the parentheses are constant at a given experimental condition, i.e. constant V_{DDC} and V_{RF}. Therefore, r_e is direct proportional to *m/z* at any given condition. Ions with higher *m/z* are displaced further from the center, and thus be exposed to stronger RF field and activated more. Since most of the ion/ion reactions result in mass addition to the reactants, the reaction rates of the products should be reduced more as opposed to that of the reactants. Note that the reagent ions (in the opposite polarity) are displaced in the opposite direction, so the overall reaction rate is also diminished due to the ion cloud separation. Theoretically, for low V_{DDC}, only high *m/z* ions are displaced far enough to reduce the reaction rate, so ion parking can be achieved for these high *m/z* products; for

high V_{DDC}, both high *m/z* and low *m/z* ions are separated from the reaction pool and low *m/z* products can be accumulated.

The effect ion parallel parking in a linear ion trap has been illustrated using ion/ion reaction between $[M+7H]^{7+}$ ions of ubiquitin and deprotonated sulfo-NHS acetate (SA) (Figure 7.5). Without application of dipolar DC potential, up to 3 SA adductions to the ubiquitin cation can be observed (Figure 7.5a). With 2V dipolar DC applied, the intensities of $[M+4H+3SA]^{4+}$ and $[M+5H+2SA]^{5+}$ ions decrease by 68% and 8%, respectively, whereas the intensity of $[M+6H+SA]^{6+}$ ions increases by 11%. The signal decrease in $[M+4H+3SA]^{4+}$ and $[M+5H+2SA]^{5+}$ ions is presumably a result of decreased reaction rates of $[M+5H+2SA]^{5+}$ and $[M+6H+SA]^{6+}$ ions, suggesting that the displacement caused by dipolar DC affects the reaction rates of more than one product. Similarly, 4.6 V dipolar DC inhibits the reaction rates of $[M+6H+SA]^{6+}$ and $[M+7H]^{7+}$ ions, causing signal accumulation in both species (Figure 7.5c). If more dipolar DC potential is applied, the reaction stops at the formation of the first SA adduction due to the reduction in overall reaction rate.

Unlike ion parking in the resonance excitation mode, adjustment of the LINAC potential does not seem to help increase in the parking efficiency. Intrinsically, the parallel ion parking in a linear ion trap is limited by the fact that multiple reaction products are affected by the same dipolar DC field. If the ion cloud displacement can be accurately tune in such way that the reaction rate of only one product is diminished while all the lower *m/z* ions are not affected, parallel ion parking can then be achieved. According to Equation 7.6, the higher

ratio between r_e and *m/z* is desired so that ion cloud displacement of different *m/z*'s will be more distinguishable at certain V_{DDC}. Therefore, the quadrupole inscribed radius (r_0) and drive frequency (Ω) should be increased, whereas the RF amplitude (V_{RF}) should be decreased. However, at the given instrumentation condition in our lab, the only parameter we can change is the RF amplitude (V_{RF}). The V_{RF} can only be lowered to a certain point where the ions can no longer be trapped due to shallow pseudo potential well depth. Even in those extremes, effective parallel ion parking still cannot be achieved.

7.4 Conclusions

Ion parking in resonance excitation mode has been demonstrated in a linear ion trap with improved efficiency. This approach has potential to increase the ion/ion reaction efficiency by selectively accumulating ion signal on a particular reaction product. The utilization of LINAC potential to maximize overlapping and constrain ions in the Z-dimension is the key to achieve high ion parking efficiency. For different reactions, the LINAC potential has to be tuned accordingly with respect to initial reactant ion positions along the Z-dimension. The excitation amplitude needs to be high enough to accelerate the target ions but should not be too high to induce fragmentation or radial ejection.

Parallel ion parking by dipolar DC has been shown to be possible in principle. The ion reaction rate has been reduced by the displacement of ion clouds caused by the dipolar DC field. However, the result obtained is not comparable to the ion parking in resonance excitation mode due to the

instrumentation constraints. Linear ion traps with larger inscribed radii and driving frequencies are needed in order to achieve parallel parking on a specific product ion species. The trapping efficiency and electronic technique issues should also be considered in terms of increasing the size and frequency of the quadrupole.

7.5 References

[1] Herron, W. J.; Goeringer, D. E.; McLuckey, S. A. Product Ion Charge State Determination via Ion/Ion Proton Transfer Reactions. *Anal. Chem.* **1996,** *68,* 257-262.

[2] Stephenson, J. L. Jr.; McLuckey, S. A. Ion/Ion Reactions in the Gas phase: Proton Transfer Reactions Involving Multiply-Charged Proteins. *J. Am. Chem. Soc.* **1996,** *118,* 7390-7397.

[3] Stephenson, J. L. Jr.; McLuckey, S. A. Ion/Ion Proton Transfer Reactions for Protein Mixture Analysis. *Anal. Chem.* **1996,** *68,* 4026-4032.

[4] Wu, J.; Hager, J. W.; Xia, Y.; Londry, F. A.; McLuckey, S. A. Positive Ion Transmission Mode Ion/Ion Reactions in a Hybrid Linear Ion Trap. *Anal. Chem.* **2004,** *76,* 5006-5015.

[5] Xia, Y.; Wu, J.; Londry, F. A.; Hager, J. W.; McLuckey, S. A. Mutual Storage Mode Ion/Ion Reactions in Hybrid Linear Ion Trap. *J. Am. Soc. Mass Spectrom.* **2005,** *16,* 71-81.

[6] Xia, Y.; Chrisman, P. A.; Erickson, D. E.; Liu, J.; Liang, X.; Londry, F. A.; Yang, M. J.; McLuckey, S. A. Implementation of Ion/Ion Reactions in a Quadrupole/Time-of-Flight Tandem Mass Spectrometer. *Anal. Chem.* **2006,** *78,* 4146-4154.

[7] Stephenson, J. L. Jr.; McLuckey, S. A. Charge Manipulation for Improved Mass Determination of High Mass Species and Mixture Components by Electrospray Mass Spectrometry. *J. Mass Spectrom.* **1998,** *33,* 664-672.

[8] Schaaff, T. G.; Cargile, B. J.; Stephenson J. L. Jr.; McLuckey, S. A. Ion Trap Collisional Activation of the $(M+2H)^{2+}$- $(M+17H)^{17+}$ Ions of Human Hemoglobin -Chain. *Anal. Chem.* **2000,** *72,* 899-907.

[9] Wells, J. M.; Stephenson, J. L. Jr.; McLuckey, S. A. Charge Dependence of Positive Insulin Ion Decompositions. *Int. J. Mass Spectrom.* **2000,** *203,* A1-A9.

[10] Reid, G. E.; Wu, J.; Chrisman, P. A.; Wells, J. M.; McLuckey, S. A. Charge State Dependent Sequence Analysis of Protonated Ubiquitin Ions via Ion Trap Tandem Mass Spectrometry. *Anal. Chem.* **2001,** *73,* 3274-3281.

[11] Syka, J.E.; Coon, J.J.; Schroeder, M.J.; Shabanowitz, J.; Hunt, D.F. Peptide and protein sequence analysis by electron transfer dissociation mass spectrometry. *Proc. Natl. Acad. Sci. U.S.A.* **2004**, *101*, 9528–9533.

[12] Han, H.; McLuckey, S. A. Selective Covalent Bond Formation in Polypeptide Ions via Gas phase Ion/Ion Reaction Chemistry. *J. Am. Chem. Soc.* **2009,** *131,* 12884-12885.

[13] Mentinova, M.; McLuckey, S. A. Covalent Modification of Gaseous Peptide Ions with N-Hydroxysuccinimide Ester Reagent Ions. *J. Am. Chem. Soc.* **2010,** *132,* 18248-18257.

[14] Compton, P.D.; Strukl, J.V.; Bai, D.L.; Shabanowitz, J.; Hunt, D. F. Optimization of Electron Transfer Dissociation via Informed Selection of Reagents and Operating Parameters. *Anal. Chem.* **2012,** *84,* 1781-1785.

[15] McAlister, G.C.; Berggren, W.T.; Griep-Raming, J.; Horning, S.; Makarov, A.; Phanstiel, D.; Stafford, G.; Swaney, D.L.; Syka, J.E.P.; Zabrouskov, V.; Coon, J.J. A proteomics grade electron transfer dissociation-enabled hybrid linear ion trap-orbitrap mass spectrometer. *J. Proteom. Res.* **2008,** *7,* 3127-3136.

[16] McLuckey, S. A.; Reid, G. E., Wells, J. M. Ion Parking During Ion/ion Reactions in Electrodynamic Ion Traps. *Anal. Chem.* **2002,** *74,* 336-346.

[17] Grosshans, P. B.; Ostrander, C. M.; Walla, C. A. Methods and Apparatus to Control Charge Neutralization Reactions in Ion Traps. U.S. Patent 6,570,151 B1, May 27, **2003**.

[18] Grosshans, P. B.; Ostrander, C. M.; Walla, C. A. Methods and Apparatus to Control Charge Neutralization Reactions in Ion Traps. U.S. Patent 6,674,151 B5, January 6, **2004.**

[19] Xia, Y.; Chrisman, P.A.; Erickson, D.E.; Liu, J.; Liang, X.; Londry, F.A.; Yang, M.J.; McLuckey, S.A. Implementation of Ion/Ion Reactions in a Quadrupole/Time-of-Flight Tandem Mass Spectrometer. *Anal. Chem*. **2006**, *78*, 4146-4154.

[20] Xia, Y.; Liang, X.; McLuckey. S.A. Pulsed Dual Electrospray Ionization for Ion/Ion Reactions. *J. Am. Soc. Mass Spectom*. **2005**, *16*, 1750-1756.

[21] Webb, I. K.; Londry, F.; McLuckey, S. A. Implementation of dipolar direct current (DDC) collision induced dissocliation in storage and transmission modes on a quadrupole/time-of-flight tandem mass spectrometer. *Rapid Commun. Mass Spectrom.* **2011,** *25,* 2500-2510.

[22] March, R.E.; An introduction to quadrupole ion trap mass spectrometry. *J. Mass Spectrom.* **1997**, *32*, 351-369.

[23] March, R. E.; Hughes, R. J. Quadrupole Storage Mass Spectrometry; John Wiley & Sons: New York, **1989**.

[24] March, R. E.; Londry, F. A. In Practical Aspects of Ion Trap Mass Spectrometry, Vol. I: Fundamentals of Ion Trap Mass Spectrometry; March, R. E., Todd, J. F. J., Eds.; CRC Press: Boca Raton, FL, **1995**; Chapter 2, pp 25-48.

[25] Louris, J. N.; Cooks, R. G.; Syka, J. E. P.; Kelley, P. E.; Stafford, G. C.; Todd, J. F. J. Instrumentation, applications, and energy deposition in quadrupole ion trap tandem mass spectrometry. *Anal. Chem.* **1987**, *59*, 1677-1685.

[26] March, R.E.; Tkacyzk, M.; Londry, F.A.; Alfred, R.L. Mass selective isolation of ions stored in a quadrupole ion trap. 2. A simulation study of consecutive isolation. *Int. J. Mass Spectrom Ion Processes.* **1993**, *125*, 9-32.

[27] Loboda, A.; Krutchinsky, A.; Loboda, O.; McNabb, J.; Spicer, V.; Ens, W.; Standing, K. Novel Linac II electrode geometry for creating an axial field in a multipole ion guide. *Eur. J. Mass Spectrom.* **2000**, *6*, 531-536.

[28] Goeringer, D. E.; Viehland, L. A.; Danailov, D. M. Prediction of Collective Characteristics for Ion Ensembles in Quadrupole Ion Traps without Trajectory Simulations. *J. Am. Soc. Mass Spectrom.* **2006,** *17,* 889-902.

[29] Prentice, B. M.; McLuckey, S. A. Dipolar DC Collisional Activation in a “Stretched” 3-D Ion Trap: The Effect of Higher Order Fields on RF-heating. *J. Am. Soc. Mass Spectrom.* **2012,** *23,* 736-744.

[30] Tolmachev, A.V.; Vilkov, A.N.; Bogdanov, B.; Păsa-Tolić, L.; Masselon, C.D.; Smith, R.D. Collisional activation of ions in RF ion traps and ion guides: the effective ion temperature treatment. *J .Am. Soc. Mass Spectrom.* **2004**, *15***,** 1616-1628.

[31] Michaud, A.L.; Frank, A.J.; Ding, C.; Zhao, X.-Z.; Douglas, D.J. Ion excitation in a linear quadrupole ion trap with an added octopole field. *J. Am. Soc. Mass Spectrom.* **2005**, *16*, 835-849.

[32] Webb, I.K.; Gao, Y.; Londry, F. A.; McLuckey, S.A. Trapping mode dipolar DC collisional activation in the RF-only ion guide of a linear ion trap/time-of-flight instrument for gaseous bio-ion declustering. *J. Mass Spectrom.* **2013**, *48*, 1059-1065.

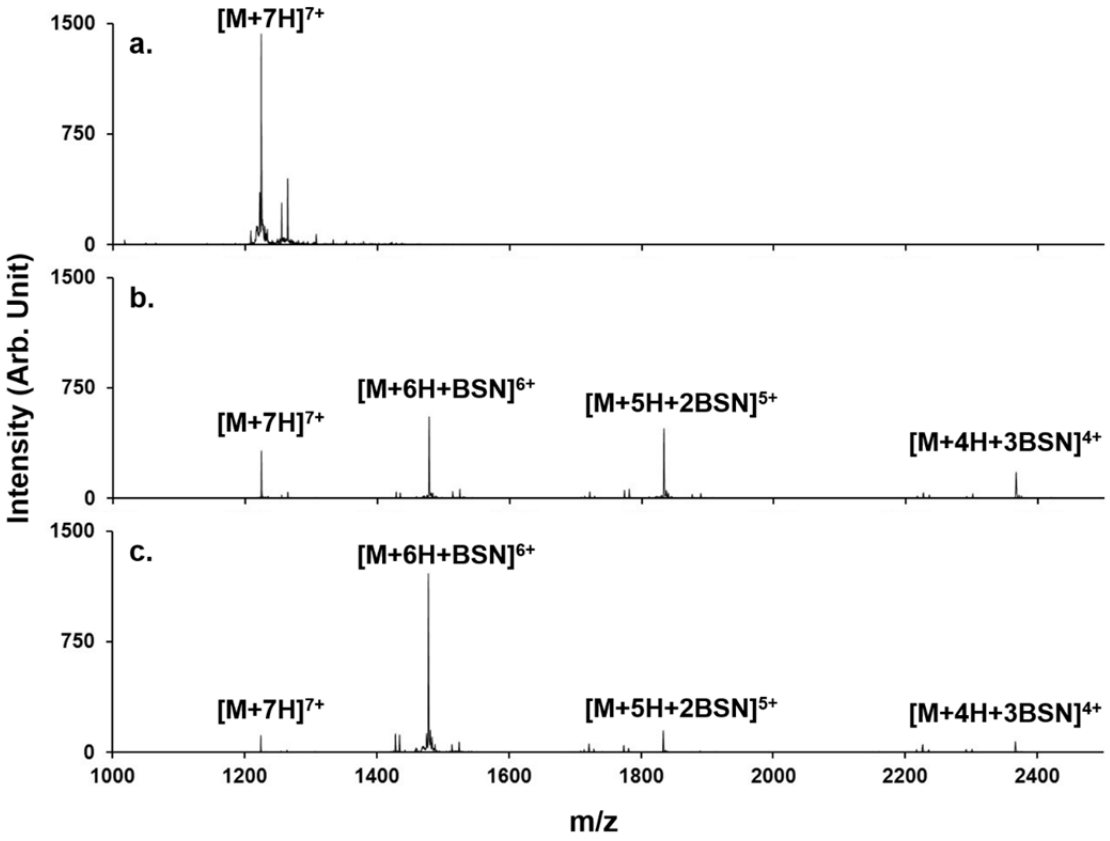

Figure 7.1 Mass spectra of bovine ubiquitin ions acquired in (a) pre-ion/ion mode, (b) post-ion/ion mode and (c) ion parking mode with 81.77Hz_300mV dipolar RF excitation in mutual storage period.

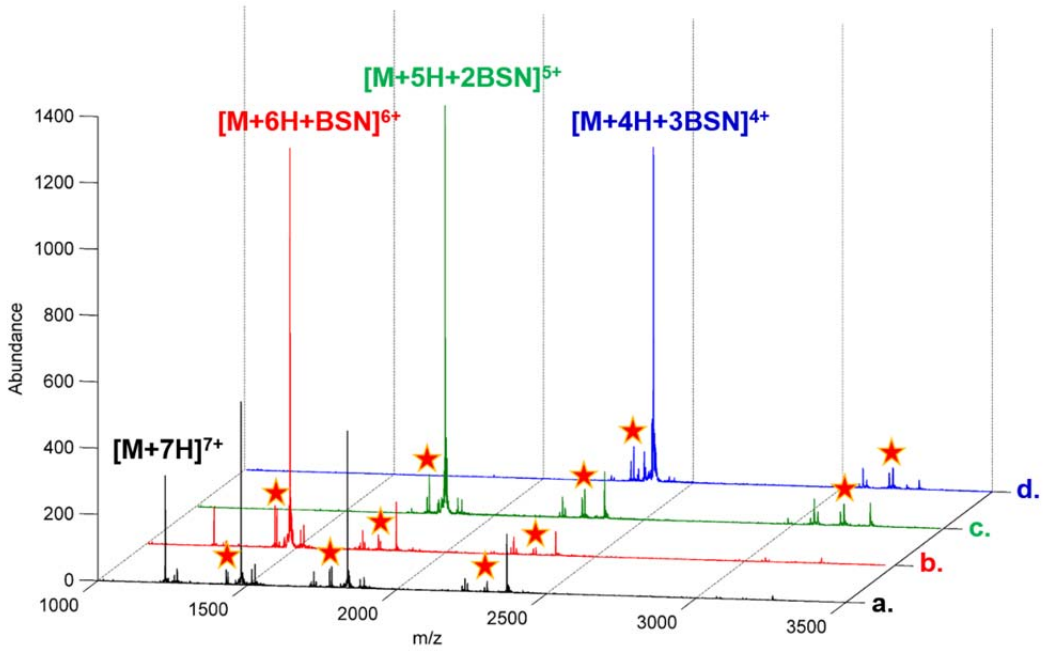

Figure 7.2 Post ion/ion reaction mass spectra of bovine ubiquitin $[M+7H]^{7+}$ and $[BSN-H]^{-}$. (a) Post ion/ion reaction without ion parking; (b) ion parking on $[M+6H+BSN]^{6+}$ with 81.77Hz_300mV; (c) ion parking on $[M+5H+2BSN]^{5+}$ with 65.72Hz_300mV; (d) ion parking on $[M+4H+3BSN]^{4+}$ with 50.95Hz_400mV. The "stars" represent first neutral sulfo-NHS losses from the electrostatic complexes.

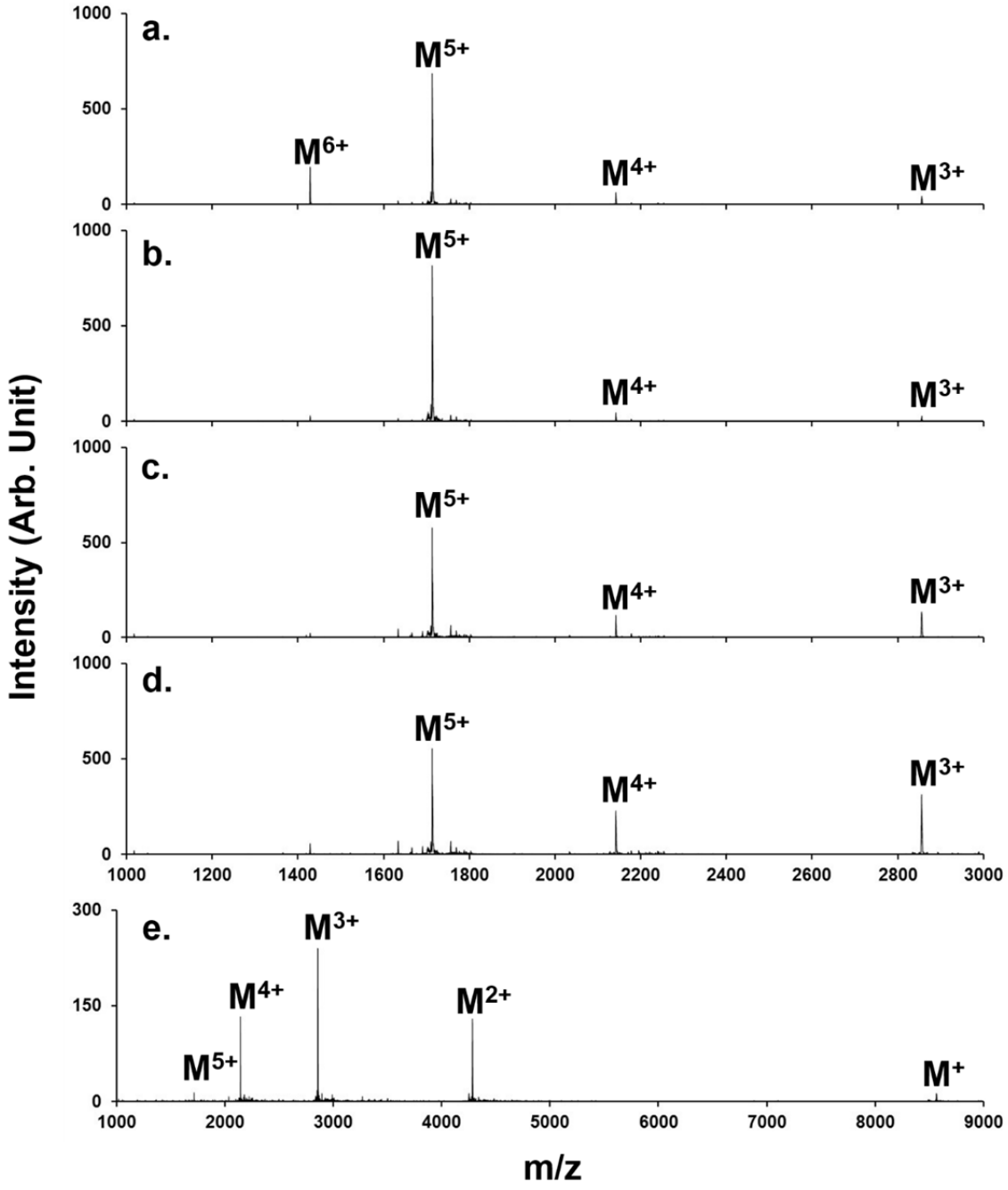

Figure 7.3 LINAC effect on ion parking efficiency demonstrated using proton transfer reaction: $[ubiquitin]^{6+}$+$[PFO-H]^{-}$. (a)~(d) are under the same ion parking frequency (47.23kHz) and amplitude (250mV). The only variable is the LINAC potential: (a) LINAC=-5V; (b) LINAC=0V; (c) LINAC=10V; (d) LINAC=16V. (e) shows the post ion/ion reaction spectrum without ion parking.

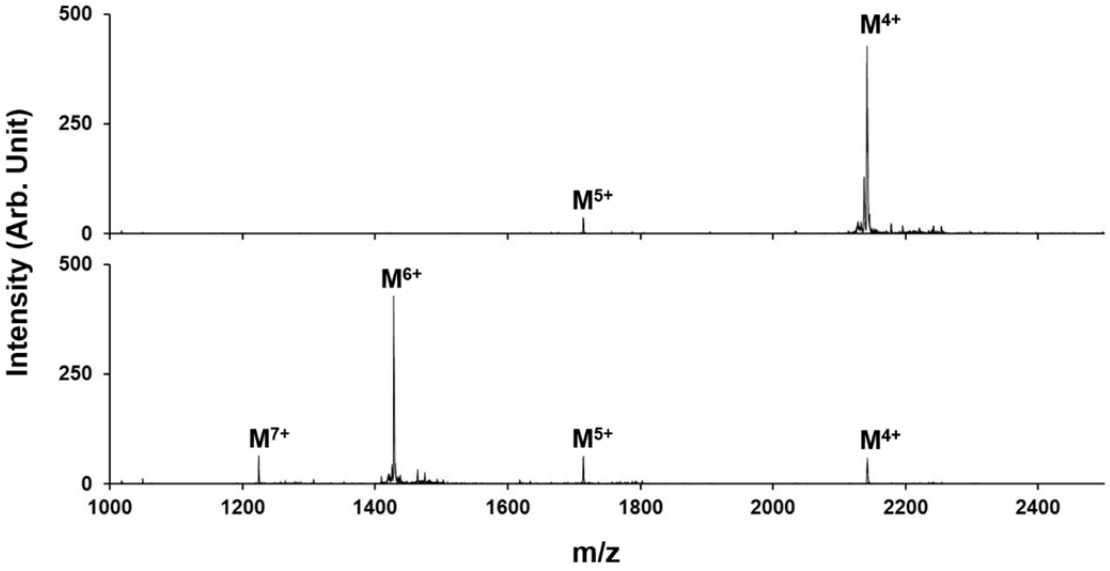

Figure 7.4 Post ion/ion reaction spectra from $[ubiquitin]^{7+}$+$[PFO-H]^{-}$. (a) ion parking at 4+ charge state, with 37.9kHz, 350mV and 60ms PFO injection, LINAC=5V; (b) ion parking at 6+ charge state, with 56.9kHz, 300mV and 30ms PFO injection, LINAC=15V.

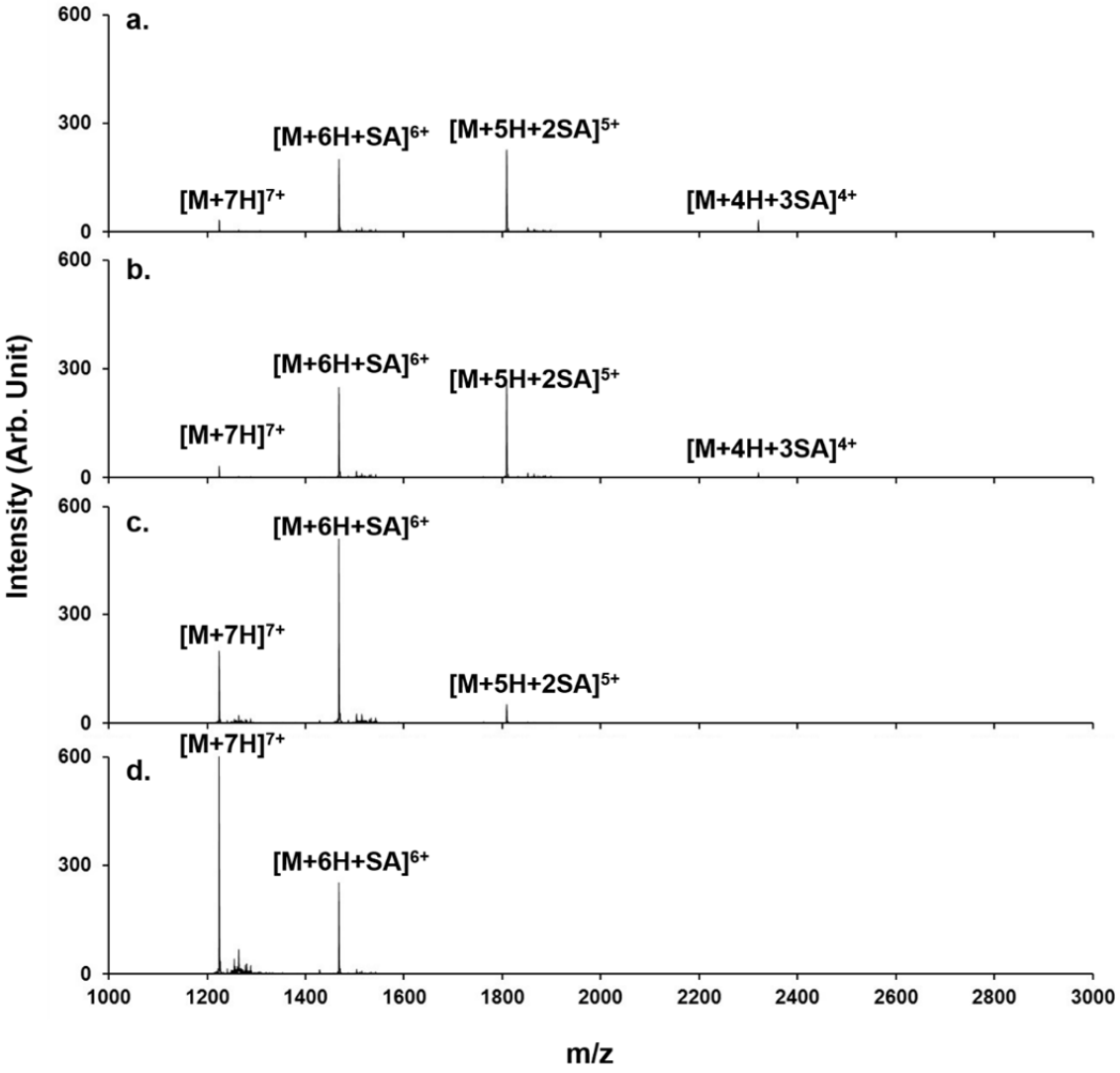

Figure 7.5 Parallel parking of the ion/ion reaction between ubiquitin 7+ and deprotonated sulfo-NHS acetate (SA) in mutual storage mode. (a) 0 V, (b) 2 V, (c) 4.6 V and (d) 6 V dipolar DC are applied to allow ion parking at 6+ charge state.

VITA

VITA

Yang Gao was born on November 16, 1987, in Zhumadian City, Henan Province, China. He spent his first 13 years there, graduating from Zhumadian No.2 Junior High School. Then he went to Henan Experimental High School, Zheng Zhou, and spent 3 years there for senior high school education. He took his first college entrance examination in the year 2004 and missed the recruiting line of Tsinghua University by 1 point. He tried taking the college entrance examination in the following year and got accepted by Peking University Health Science Center, which he attended from September 2005 to July 2009 majoring in pharmaceutical sciences. In 2009, he defended his bachelor degree thesis and graduated from Peking University Health Science Center.

Yang began attending Purdue University in August 2009 and joined Dr. Scott A. McLuckey's research group in the first semester. He has studied top down interrogation and characterization of large biomolecules including nucleic acids, proteins, and protein complexes. His graduate research includes method development for bioanalytical assays using ion/ion reaction and gas phase unimolecular dissociations. He defended his dissertation in November 2013.

PUBLICATION

analytical chemistry

Article

pubs.acs.org/ac

Top-Down Interrogation of Chemically Modified Oligonucleotides by Negative Electron Transfer and Collision Induced Dissociation

Yang Gao,[†] Jiong Yang,[‡] Mark T. Cancilla,[§] Fanyu Meng,*[,‡] and Scott A. McLuckey*[,†]

[†]Department of Chemistry, Purdue University, West Lafayette, IN 47907-2084, United States

[‡]Merck & Co., Inc., 126 E. Lincoln Avenue, Rahway, NJ 07065-0900, United States

[§]Merck & Co., Inc., 770 Sumneytown Pike, West Point, PA 19486-0004, United States

Supporting Information

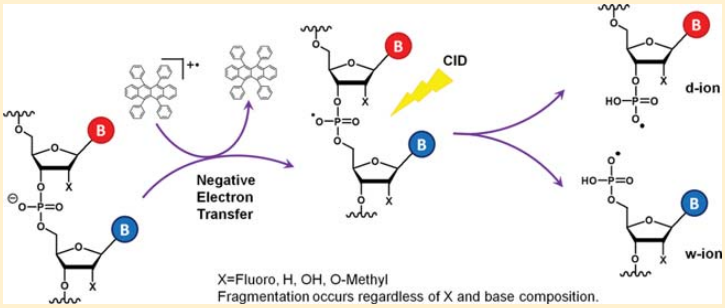

ABSTRACT: Two sets of synthetic 21−23mer oligonucleotides with various types of 2′-position modifications have been studied with tandem mass spectrometry using ion trap collision-induced dissociation (IT-CID) and negative electron transfer (NET)-CID. A systematic study has been conducted to define the limitations of IT-CID in sequencing such 2′-chemically modified oligonucleotides. We found that IT-CID is sufficient in characterizing oligonucleotide sequences that do not contain DNA residues, where high sequence coverage can be achieved by performing IT-CID on multiple charge states. However, oligonucleotides containing DNA residues gave limited backbone fragmentation with IT-CID, largely due to dominant fragmentation at the DNA residue sites. To overcome this limitation, we employed the negative electron transfer to strip an electron from the multiply charged oligonucleotide anion. Then, the radical anion species formed in this reaction can fragment via an alternative radical-directed dissociation mechanism. Unlike IT-CID, NET-CID mainly generates a noncomplementary d/w ion series. Furthermore, we found that NET-CID did not show preferential dissociations at the DNA residue sites and thus generated higher sequence coverage for the studied oligonucleotide. Information from NET-CID of different charge states is not fully redundant such that the examination of multiple charge states can lead to more extensive sequence confirmation. This work demonstrates that the NET-CID is a valuable tool to provide high sequence coverage for chemically modified oligonucleotides, and such detailed characterization can serve as an important assay to control the quality of therapeutic oligonucleotides that are produced under the good manufacture practice (GMP) regulations.

Synthetic oligonucleotides have been extensively researched as drug candidates[1−3] and diagnostic agents.[4] Various chemical modifications have been introduced into such molecules to improve their stability and efficacy as well as to minimize toxicity.[5−7] Among them, modification of the 2′ position on the pentose ring is widely applied in numerous synthetic oligonucleotides and has proved to be reliable and robust.[8] However, such sugar modifications on oligonucleotides also complicate their characterization, an important part of the quality control for oligonucleotides as therapeutics.[9] Specifically for chemically modified oligonucleotides, the structures of base and sugar groups, as well as the order in which the nucleosides are arranged, needs to be thoroughly confirmed using robust analytical methods.

To address this challenge, both enzymatic digestion[10−13] and chemical degradation procedures[14,15] have been described, and they showed good success toward confirming the primary structure of purified synthetic oligonucleotides. Overall, these approaches are analogous to the bottom-up method used in proteomics, where a large biomolecule is first chemically or enzymatically degraded into smaller components before characterization by mass spectrometry. An alternative way to address such a challenge is the ever more popular top-down strategy, where an oligonucleotide pseudomolecular cation or anion is subjected to fragmentation in the mass spectrometer

Received: February 10, 2013
Accepted: March 27, 2013
Published: March 27, 2013

   dx.doi.org/10.1021/ac400448t | *Anal. Chem.* 2013, 85, 4713−4720

Table 1. Summary of the Oligonucleotide Sequences Used in This Study

name	sequence[a]
2′-H 55664	5′-iBdCdCdAdGdGdGdCdGdAdUdGdCdCdUdUdCdCdAdUdTdTiB-3′
2′-OH 55664	5′-iBrCrCrArGrGrGrCrGrArUrGrCrCrUrUrCrCrArUrTrTiB-3′
2′-F 55664	5′-iBfCfCfAfGfGfGfCfGfAfUfGfCfCfUfUfCfCfAfUfTfTiB-3′
2′-OMe 55664	5′-iBmCmCmAmGmGmGmCmGmAmUmGmCmCmUmUmCmCmAmUmTmTiB-3′
2′-H 55665	5′-dAdUdGdGdAdAdGdGdCdAdUdCdGdCdCdCdUdGdGdUdU-3′
2′-OH 55665	5′-rArUrGrGrArArGrGrCrArUrCrGrCrCrCrUrGrGrUrU-3′
2′-F 55665	5′-fAfUfGfGfAfAfGfGfCfAfUfCfGfCfCfCfUfGfGfUfU-3′
2′-OMe 55665	5′-mAmUmGmGmAmAmGmGmCmAmUmCmGmCmCmCmUmGmGmUmU-3′
2′-(F, H) 55664	5′-iBfCfCdAdGdGdGfCdGdAfUdGfCfCfUfUfCfCdAfUdTdTiB-3′
2′-(H, OH) 55664	5′-iBrCrCdAdGdGdGrCdGdArUdGrCrCrUrUrCrCdArUdTdTiB-3′
2′-(H, OMe) 55664	5′-iBmCmCdAdGdGdGmCdGdAmUdGmCmCmUmUmCmCdAmUdTdTiB-3′
2′-(F,OH, OMe) 55665	5′-rArUrGmGmAmAmGmGfCmAfUfCmGfCfCfCfUmGmGmUmU-3′

[a]The modifications on the 2′ of sugar moiety are indicated: "m" represents the 2′-O-methyl modification, "f" stands for the 2′-fluoro modification, "d" indicates a deoxyribonucleotide, "r" indicates a ribonucleotide, and iB stands for inverted abasic (Figure 4 of the Supporting Information).

and sequence information is derived from the masses of fragment ions. A number of reports have appeared describing the successful sequencing and characterization of modified oligonucleotides of various types.[16−19] In principle, direct sequencing of oligonucleotides by tandem mass spectrometry is favored over a digestion approach because of potential advantages in speed, sensitivity, as well as its capability to analyze minor components in a complex mixture. However, in a previous study of the collision-induced dissociation (CID) patterns of 2′-modified mix-mer models, we observed strong differences in the gas-phase fragmentation behavior that arise from the various modification sites.[19] Fragmentation of the phosphodiester linkage at the 3′-side of the modified pentose, for example, was not observed with collisional activation when present with DNA residues. Rather, fragmentation tended to dominate at the DNA residue sites. This represents a complicating factor for use of the top-down method to characterize the primary structure of oligonucleotides. Therefore, it is desirable to fully understand the effects of various 2′-modifications on the relative gas-phase stabilities of the nucleotide residues (in conventional CID) along the oligomer. Moreover, dissociation approaches that generate sequence information that are not affected by the 2′-modifications are highly desirable.

It has been demonstrated that the 2′-modification plays an important role in the oligonucleotide CID process.[19] The gas-phase unimolecular dissociation of DNA gives rise to a-B/w ions,[20] which are generated by a facile base loss process followed by the 3′ C−O bond cleavage.[21−23] This pathway is favored because the base loss channel requires lower activation energy as opposed to any other backbone cleavages. The mechanism involves a 1,2-elimination step that requires the 2′-position to be a hydrogen. Once the 2′-position is substituted with other functional groups, this low energy pathway is inhibited. For the CID of RNA where the 2′-position is an OH group, the low-energy base loss channel is inhibited, but there is a c/y-fragmentation channel that arises from the 5′ P−O bond cleavage, involving the 2′-OH functionality.[24-26] Likewise, this channel is no longer preferred if the 2′-OH is replaced by other functional groups.[24] In accordance with the previous study of model oligonucleotide mix-mers, fragmentation at the DNA residues outcompetes fragmentation at the phosphodiester linkage to the 3′-side of the 2′-modified ribose to the point that the latter is not observed.[19] When there are no DNA residues, backbone cleavages from the 2′-modified residues are observed even when RNA residues are present.[24] Therefore, characterization of chemically modified oligonucleotides containing DNA residues is particularly challenging.

It has been shown that fragmentation of odd-electron (radical) oligonucleotide anions does not favor the base loss channel under similar activation conditions.[27] Therefore, the gas-phase dissociation of the radical species is promising in generating more informative backbone fragmentation. The electron photodetachment dissociation (EPD),[28] electron transfer followed by CID (ET-CID),[18] and negative electron transfer followed by CID (NET-CID)[29] experiments have shown that supplemental activation of odd-electron (radical) oligonucleotide species is effective in the sequence determination of 2′-modified model oligonucleotides. There is also evidence that electron detachment dissociation (EDD)[30] generates similar fragmentation patterns as EPD and NET-CID, namely d/w ions.

In this study, we set out to develop and evaluate a procedure for the identification and characterization of heavily modified oligonucleotides. Several oligonucleotides that mimic the length and chemical modifications as those of potential therapeutic siRNAs[31] have been synthesized. We applied the ion trap CID (IT-CID) and NET-CID to analyze these samples. Specifically, a set of oligonucleotides with uniform 2′ chemical modification on the sugar moiety were subjected to IT-CID to identify the fragmentation patterns for the corresponding even-electron anions. Then, a set of even-electron oligonucleotide mix-mers was studied by IT-CID to identify the relative gas-phase stabilities of different 2′-modified nucleotide backbones. Finally, NET-CID was applied to these mix-mers to demonstrate the utility of using NET-CID to generate high sequence coverage for these highly modified oligonucleotide molecules.

METHOD

Methanol, isopropanol, and glacial acetic acid were purchased from Mallinckrodt (Phillipsburg, NJ). Rubrene, acetonitrile, dichloromethane, piperidine, and imidazole were obtained from Sigma-Aldrich (St. Louis, MO). All oligonucleotides were synthesized in house (Rahway, NJ). For the sake of clarity with respect to the nature of the modification on the 2′ of the sugar moiety, "m" represents the 2′-O-methyl modification, "f" stands for the 2′-fluoro modification, "d" indicates a deoxyribonucleotide (Table 1 and Figure 4 of the Supporting Information). The oligonucleotides are based on two complementary sequences

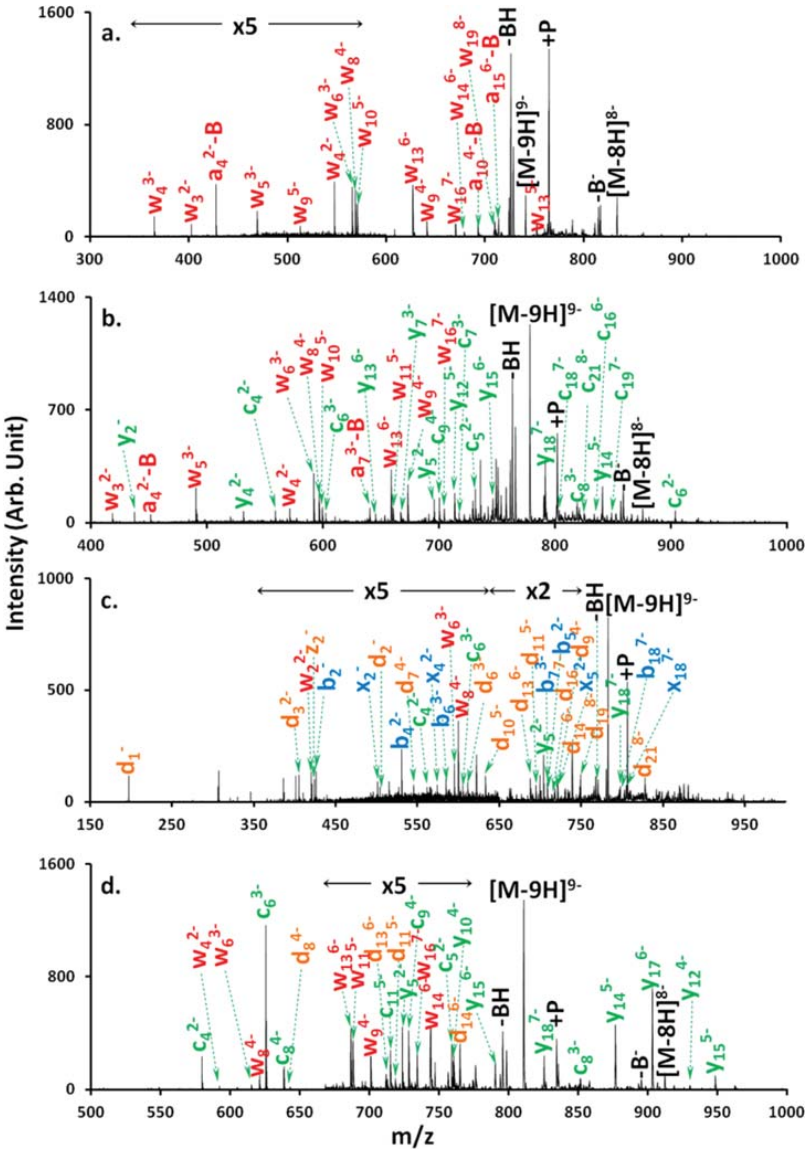

Figure 1. Product spectra from IT-CID of (a) 2′-H 55664, (b) 2′-OH 55664, (c) 2′-F 55664, and (d) 2′-OMe 55664 with 475 mV dipolar excitation at 115 kHz frequency. −BH and $-B^-$ peaks represent neutral and charged base losses. +P peaks indicate $[M - 9H + plasticizer]^{9-}$, which is formed by ion/molecule reactions when the oligonucleotide anions are exposed to the plasticizer present in the vacuum housing.

(55664 and 55665) and different 2′-modifications are incorporated along the backbone.

Preparation of Solutions. Synthetic oligonucleotide samples were desalted before mass spectrometry analysis. Desalting was carried out using a cation-exchange resin. Desalting of oligonucleotides by the cation exchange resin (Amberlite IRN77 hydrogen form) was carried out as described below. The cation exchange resin was rinsed with DEPC−H_2O and then mixed with 100 μL oligonucleotide stock solution of about 200 μM at room temperature for 10 min to reduce the cation adducts (Na^+ or K^+). Oligonucleotide solutions for negative nanoelectrospray (nanoESI) were prepared to ca. 50 μM in 20:80 isopropanol:water (v:v) with the addition of 25 mM piperidine and 25 mM imidazole.[32] Rubrene was dissolved in dichloromethane to a concentration of ca. 4 mM and then diluted to ca. 80 μM in 20:80 dichloromethane:acetonitrile (v:v).

APPARATUS AND PROCEDURES

All MS/MS experiments were performed using a prototype version of a QqTOF tandem mass spectrometer (QSTAR, Applied Biosystems/MDS Sciex, Concord, ON, Canada)

dx.doi.org/10.1021/ac400448t | *Anal. Chem.* 2013, 85, 4713−4720

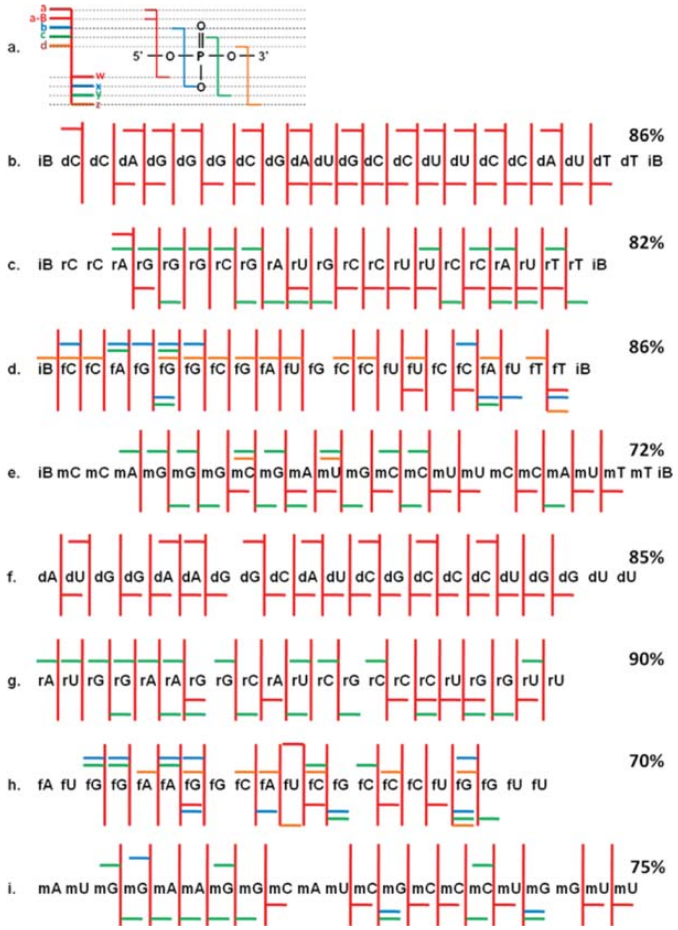

Figure 2. Backbone fragmentation summary for the IT-CID of uniformly 2′-modified oligonucleotides. (a) Fragment nomenclature with color coding. Fragmentation summary for (b) 2′-H 55664, (c) 2′-OH 55664, (d) 2′-F 55664, (e) 2′-OMe 55664, (f) 2′-H 55665, (g) 2′-OH 55665, (h) 2′-F 55665, and (i) 2′-OMe 55665. The percentages are the calculated sequence coverage.

modified to allow for ion/ion reaction studies.[33] A home-built pulsed dual nanoESI source was coupled directly to the nanospray interface to produce ions of both polarities.[34] The multiply charged oligonucleotide anions, $[M - nH]^{n-}$, were generated directly via a nanoESI emitter. Nitrogen was used as the curtain gas as well as the target gas for CID.

In a typical IT-CID experiment, the oligonucleotide anions were generated via nanoESI and the precursor ions were isolated with Q1 RF/DC and directed into the q2 linear ion trap (LIT) at a relatively low kinetic energy. During the trapping time in q2, an RF amplitude was applied in a dipolar manner to one pair of the rods with frequency in resonance of the fundamental secular frequency of the ion of interest. Excitation of the ion of interest led to an increase in orbited trajectory, resulting in higher-energy collisions with the N_2 cooling/bath gas. Conversion of kinetic energy to internal energy subsequently resulted in dissociation. The fragment ions were cooled in q2 and then subjected to mass analysis by the time-of-flight (TOF) detector.

In a typical NET-CID experiment, oligonucleotide anions were introduced into the mass spectrometer via the negative nanoESI source and the ions of interest were isolated and then injected into the q2 LIT. Reagent cations of interest were similarly isolated from the positive nanoESI of the metal complex solution and introduced into the q2 LIT, where ions of both polarities were mutually trapped by applying AC on both entrance and exit lenses of q2. The reaction efficiency was optimized by adjusting the linear accelerator (LINAC) potential[35,36] to allow maximum overlap of the cations and anions. To perform further IT-CID, the products of the ion/ion reaction were sent back to Q1 to isolate the charge-reduced species.[37] Then, the isolated radical anions were introduced to q2 for IT-CID. The theoretical fragment masses were calculated using an in-house developed Excel spreadsheet.

RESULTS

Ion Trap CID of Oligonucleotides with Uniformly Modified Backbones. Previous studies have shown that the 2′-modification can considerably alter the gas-phase fragmenta-

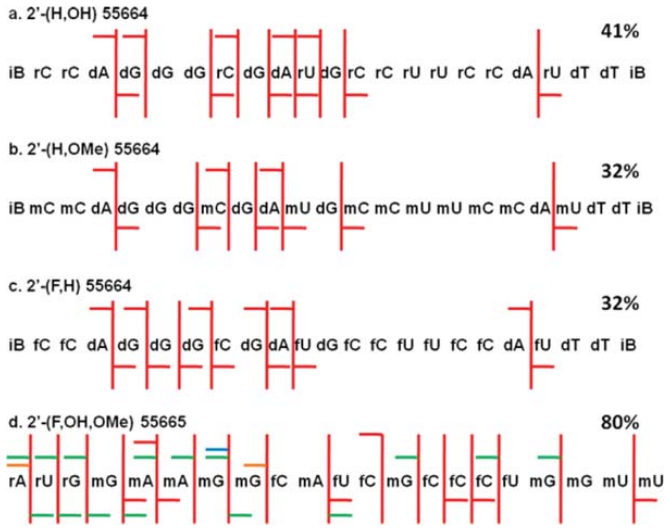

Figure 3. Fragment ion map from IT-CID of $[M - 9H]^{9-}$ of (a) 2′-(H, OH) 55664 and (b) 2′-(H, OMe) 55664. The percentages are calculated sequence coverage. (c) 2′-(F, H) 55664 and (d) 2′-(F, OH, OMe) 55665 with 475 mV dipolar excitation at 115 kHz frequency. (See key in Figure 2 for the fragment types.)

tion patterns of the short-strand oligonucleotide anions.[19,25] To extend this knowledge based on the short oligomers to the longer oligonucleotides (i.e., 21 and 23mers), we have synthesized eight oligonucleotides (Table 1) that are based on 2 basic sequences (named 55664 and 55665) with four different types of 2′ sugar modifications (2′-H, 2′-OH, 2′-F, and 2′-OMe). These molecules were analyzed using a modified Q-TOF instrument (that is capable of performing both IT-CID and NET-CID experiments), and their gas-phase fragmentation behaviors were studied. Ion trap CID was performed on all eight samples with multiply charged anions ($[M - 9H]^{9-}$) as precursors. For 55664 samples, CID of 2′-H oligomers gives rise to a-B/w fragments (Figure 1a), CID of 2′-OH oligomers mainly generates c/y fragments (Figure 1b), CID of 2′-F (Figure 1c) and 2′-OMe (Figure 1d) oligomers produces all possible types of backbone cleavages resulting in a/w, b/x, c/y, and d/z fragments. Similar fragmentation behavior was observed for the 55665 samples. These data suggest that the gas-phase dissociation of the oligonucleotide 21-mers follow the same patterns as those noted for a short model oligomer system.[19] Briefly, the a-B/w fragmentation pattern of the all-DNA oligomer is predicated on the facile base loss channel that involves the 2′-H on the ribose ring;[38,39] the c/y product formation of the all-RNA oligomer results from the 5′ P−O bond cleavages due to a rearrangement mechanism involving the 2′-OH substitution.[24] It is noteworthy that IT-CID of 2′-H 55664 generates relatively poor sequence coverage [defined as the number of cleaved linkage between nucleoside residues divided by the total number of applicable linkages (e.g., 11/22 = 50% in this case)]. This is likely due to relatively little sequential fragmentation following base loss, so we performed supplemental activation on the base loss peaks and successfully improved the sequence coverage to 86% (see Figure 1 of the Supporting Information). When the 2′-position on the pentose ring is substituted by other functional groups, such as 2′-fluoro (2′-F) or 2′-O-methyl (2′-OMe), the low-energy channels are inhibited and therefore other backbone cleavage pathways become competitive. Various fragmentation channels were observed as demonstrated in Figure 1c and 1d. At least 70% sequence coverage is achieved by IT-CID for all of the modification states of 55664 and 55665 samples (Figure 2), indicating that IT-CID may be fairly effective in characterizing oligonucleotides with only one type of sugar moiety.

IT-CID of Oligonucleotide Mix-Mers. It is relatively straightforward to characterize uniformly 2′-modified oligonucleotides due to the simplicity of the backbone. When the oligonucleotide sequences have more than one type of functional sugar groups, it can be expected that preferential cleavages will happen at the modification sites with the most facile dissociation pathways. To confirm this type of cleavage preference, three oligonucleotide mix-mers with DNA moieties and one oligonucleotide mix-mer with no DNA moieties were subjected to IT-CID under the same experimental conditions. Figure 3 shows the fragment ion maps from IT-CID of the four oligonucleotide mix-mers. Backbone cleavages are almost exclusively limited to the 3′-side of the DNA residues when DNA residues are present in the sequence (Figure 3, panels a−c), and the sequence coverage are 41%, 32%, and 32%, respectively. For the oligonucleotide mix-mer with no DNA residues, dissociation is more evenly distributed across the backbone (Figure 3d). Sixteen out of the 20 applicable linkages are cleaved, generating a sequence coverage of 80% for this molecule. This experiment suggests that 2′-OH, 2′-F, and 2′-OMe-modified backbones have comparable fragmentation threshold during the IT-CID event, where the 2′-H backbone is less stable and thus gives rise to a more competitive dissociation pathway. As a summary, we have found that the IT-CID of multiply deprotonated anions is very effective in characterizing oligonucleotides that do not contain any DNA moieties, and for oligonucleotide mix-mers with DNA moieties, IT-CID might not be able to provide good sequence coverage.

NET-CID and IT-CID of Oligonucleotide Mix-Mers. Previous studies have shown that CID of modified oligonucleotide radical anions generates sequence information with little

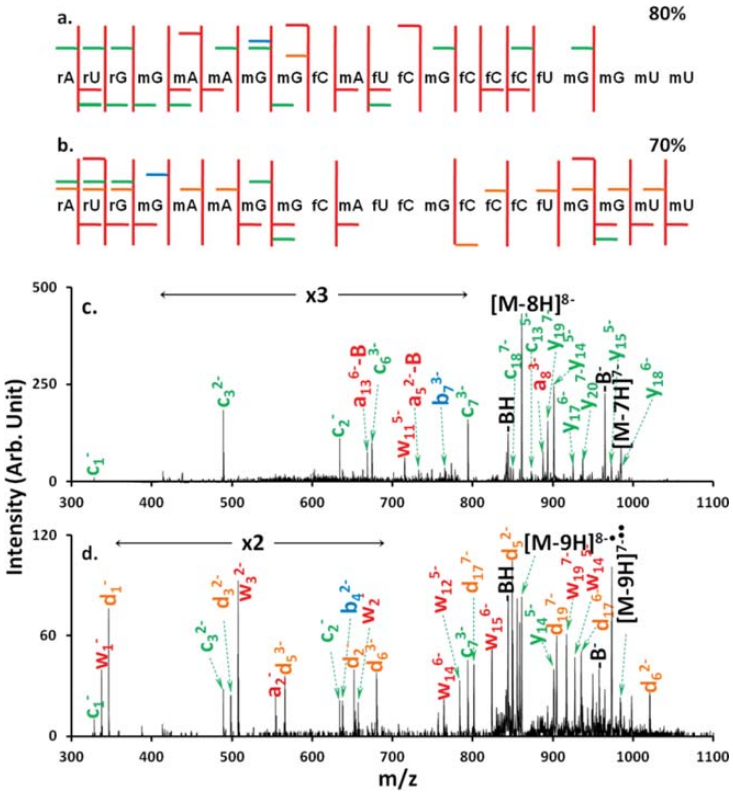

Figure 4. Fragment ion map from IT-CID of (a) $[M - 8H]^{8-}$ and (b) $[M - 9H]^{8-\bullet}$ of 2′-(F, OH, OMe) 55665with 475 mV dipolar excitation at 115 kHz frequency. The percentages are calculated sequence coverage. (c) Product spectrum of $[M - 8H]^{8-}$ of 2′-(F, OH, OMe) 55665. (d) Product spectrum of $[M - 9H]^{8-\bullet}$ of 2′-(F, OH, OMe) 55665. (See key in Figure 2 for the fragment types in A and B.)

apparent preference for modification state,[29] and the radical-directed dissociation mechanism does not involve the 2′-substitution. Therefore, we proceed to examine the utility of NET-CID in characterizing oligonucleotide mix-mers, especially for those that contain DNA moieties. Specifically in this study, we generated radical anions by reacting multiply charged oligonucleotide anions with rubrene radical cations in the gas phase. Rubrene was chosen as the negative electron transfer reaction reagent because it can be generated as a radical cation via electrospray. This significantly simplifies the instrument setup by having both ion sources being nanoelectrospray.

Two representative oligonucleotide mixers, 2′-(F, H) 55664 and 2′-(F, OH, OMe) 55665 (Table 1) were selected to demonstrate the universal fragmentation pattern of the NET-CID process. When 200 ms reaction time was used for the 9-charge state of sequence 55665 that contains 2′-OH, 2′-F, and 2′-OMe in a sugar moiety, we observed multiple charge-reduced products ($[M - 9H]^{8-}$, ...) and rubrene-adducted peaks (see Figure 2 of the Supporting Information). The radical anion generated via single-electron transfer ($[M - 9H]^{8-}$) was selected for collisional activation, and the resulting MS/MS is shown in the Figure 4d. In this case, we observed 102 fragment peaks for NET-CID, where 26 peaks matched theoretical gas phase fragment ions within 100 ppm (see Table 1 of the Supporting Information), and 23 of them matched to the d- and w-typed ions. It is noted that c/y-fragments are also observed in the NET-CID spectrum (Figure 4d), which are most likely generated by exciting the even-electron species from proton transfer processes. Therefore, d/w fragments constitute the major channel for NET-CID fragmentation.

As shown in Figure 4a, the sequence coverage obtained from IT-CID of $[M - 8H]^{8-}$ 55665 is 80%. This number can increase to 85% if multiple charge states are investigated. However, if information from both CID spectra of the even-electron (Figure 4a) and radical species (Figure 4b) are combined, 100% sequence coverage can be achieved. These data suggested that the NET-CID provides additional fragment channels that are complementary to IT-CID. When combining both techniques, we are able to achieve very high (in this case 100%) sequence coverage.

The NET-CID method was also applied to the 2′-(F, H) 55664 oligonucleotide, where only 27% sequence coverage has been achieved when performing the IT-CID study alone (Figure 5a). Totally, 48 peaks were observed in the NET-CID (Figure 5d), where 26 peaks matched theoretical gas-phase fragment ions within 100 ppm (see Table 2 of the Supporting Information), and 14 of them matched expected d/w ions. As shown in Figure 5d, d/w fragments constitute the main dissociation products with randomly distributed a/z fragments also present, and no preferential backbone fragmentation channel is observed. The sequence coverage was improved from 27% (Figure 5a) to 64% (Figure 5b) for the same charge

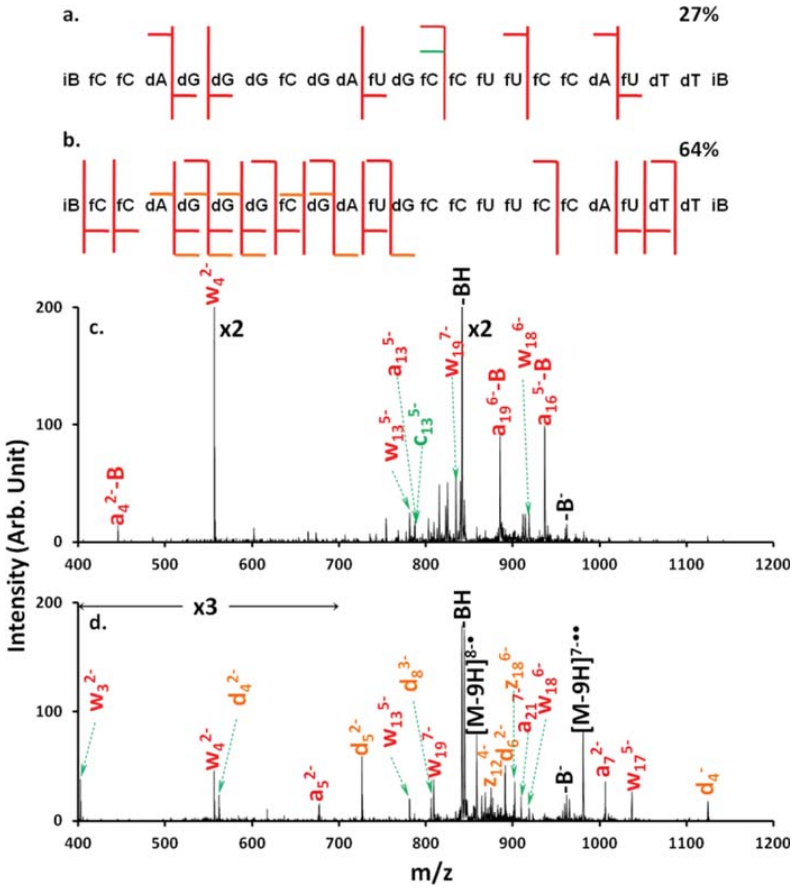

Figure 5. Fragment ion map from ion trap CID of (a) $[M - 8H]^{8-}$ and (b) $[M - 9H]^{8-\bullet}$ of 2′-(F, H) 55664 with 475 mV dipolar excitation at 115 kHz frequency. The percentages are calculated sequence coverage. Product spectra from IT-CID of (c) $[M - 8H]^{8-}$ and (d) $[M - 9H]^{8-\bullet}$ of 2′-(F, H) 55664.

state. Interestingly, the NET-CID of $[M - 7H]^{7-}$, $[M - 8H]^{8-}$, and $[M - 9H]^{9-}$ of 2′-(F, H) 55664 generate 59%, 64%, 64% sequence coverage, respectively, and we found that their cleavage sites are located on different phosphodiester linkages (see Figure 3 of the Supporting Information). This indicates that the NET-CID is affected by the precursor ion charge state, and therefore performing NET-CID on more than one charge states may provide even greater sequence information. To confirm this, we examined the NET-CID of charge states from 5− to 9− and found that combining the information from the 7− to 9− charge states results in a total sequence coverage of 95% (see Figure 3 of the Supporting Information). The 5− and 6− charge states do not provide any additional sequence information.

From the NET-CID of the studied oligonucleotides, it is apparent that the entire sequence of the oligomer usually cannot be generated by simply performing one experiment with a single charge state, despite the lower sensitivity to 2′-modification states in the odd-electron ions. Other variables, such as gas-phase secondary structure and charge site location, may also play important roles. The fact that complementary information is obtained from different charge states strongly suggests that such variables are in play. As there are many variables associated with the size of oligonucleotides, it is hardly surprising that the examination of several ion types (e.g., odd-electron, even-electron, or different charge states) leads to the greatest opportunity for generating higher sequence coverage.

■ CONCLUSION

The identification and complete sequence characterization of highly modified oligonucleotides remains a challenging problem largely due to the diversity of modification states along the backbone. IT-CID, an extensively utilized activation approach for mass spectrometric sequencing, has proved to be limited to some specific modification combinations in even-electron anions, and the achievable sequence coverage is particularly low when DNA residues are present (largely due to the highly favorable base loss channel associated with deoxyribose). In this report, we have shown that the NET-CID (that entails IT-CID of odd-electron anions) is less sensitive to modification states in oligonucleotides with modified sugars. In the case of oligonucleotides mix-mers with DNA residues (55664), NET-CID can serve as an efficient method to break the DNA as well as non-DNA backbone. In contrast to our previous work, where NET-CID provided 100% sequence coverage for comparatively short 2′-modified mix-mer (10-mer),[29] NET-CID on a single

charge state of the 2′-modified 23-mer only provides 56−64% sequence coverage. This significant difference in sequence coverage implicates that longer oligonucleotides are more challenging for top-down characterization due to its complexity in both conformation and chemistry. However, we are able to achieve 95% sequence coverage when combining the MS/MS data from 7-, 8-, and 9- charge states. This demonstrates another major advantage of NET-CID over conventional CID. Specifically, NET-CID on different charge states of DNA-containing oligonucleotides provided complementary sequence information, whereas conventional CID still only generates fragment ions restrained to 3′-cleavage of the DNA residues. Indeed, our data suggest that it is desirable to probe different charge states for both even-electron and odd-electron precursor ions to generate the most complete sequence coverage. Moreover, this technique has similar potential, as shown by Taucher and Breuker,[17] in generating "fragment mass ladders" for chemically modified oligonucleotides by comparing fragment peaks from the dissociation of the odd- and even-electron precursors.

In summary, we found that the even-electron and odd-electron ions fragment along the backbone by distinct mechanisms that showed distinct sensitivities to the 2′-modification states. This work demonstrates that the NET-CID can serve as a part of valuable toolkits to provide high sequence coverage for heavily modified synthetic oligonucleotides. We believe that such detailed characterization will serve as an important assay to control the quality of therapeutic oligonucleotides, especially for those that are produced under GMP regulations and will eventually be used in clinical studies.

■ ASSOCIATED CONTENT

Supporting Information

Additional information as noted in text. This material is available free of charge via the Internet at http://pubs.acs.org.

■ AUTHOR INFORMATION

Corresponding Author

*S.A.M.: address, 560 Oval Drive Department of Chemistry Purdue University West Lafayette, IN 47907-2084, United States; tel, (765) 494-5270, e-mail, mcluckey@purdue.edu. F.M.: 126 E. Lincoln Avenue RY818-B221, Merck & Co., Inc., Rahway, NJ 07065-0900, United States; tel, (732) 594-2188; e-mail, fanyu_meng@merck.com.

Notes

The authors declare no competing financial interest.

■ ACKNOWLEDGMENTS

This research was supported by the New Technology Review and Licensing Committee (NTRLC) of Merck & Co., Inc. and, in part, by the National Science Foundation under CHE-0808380. We want to particularly acknowledge Craig Parish (Merck) for help in synthesizing the oligonucleotide samples, and we also want to thank Chris Welch, Bing Mao, and Zhihong Ge (Merck) for their management support.

■ REFERENCES

(1) Goodchild, J. *Curr. Opin. Mol. Ther.* **2004**, *6*, 120−128.
(2) Opalinska, J. B.; Gewirtz, A. M. *Nat. Rev. Drug. Discov.* **2002**, *1*, 503−514.
(3) Raal, F. J.; Santos, R. D.; Blom, D. J.; Marais, A. D.; Charng, M. J.; Cromwell, W. C.; Lachmann, R. H.; Gaudet, D.; Tan, J. L.; Chasan-Taber, S.; Tribble, D. L.; Flaim, J. D.; Crooke, S. T. *Lancet* **2010**, *375*, 998−1006.
(4) Brody, E. N.; Gold, L. *J. Biotechnol.* **2000**, *74*, 5−13.
(5) Chiu, Y.-L.; Rana, T. M. *RNA* **2009**, *9*, 1034−1048.
(6) Butora, G.; Kenski, D. M.; Cooper, A. J.; Fu, W. L.; Qi, N.; Li, J. J.; Flanagan, W. M.; Davies, I. W. *J. Am. Chem. Soc.* **2011**, *133*, 16766−16769.
(7) Manoharan, M. *Curr. Opin. Chem. Biol.* **2004**, *8*, 570−579.
(8) Chan, J. H.; Lim, S.; Wong, W. S. *Clin. Exp. Pharmacol. Physiol.* **2006**, *33*, 533−540.
(9) Capaldi, D.; Ackley, K.; Brooks, D.; Carmody, J.; Draper, K.; Kambhampati, R.; Kretschmer, M.; Levin, D.; McArdle, J.; Noll, B.; Raghavachari, R.; Roymoulik, I.; Sharma, B. P.; Thürmer, R.; Wincott, F. *Drug Inf. J.* **2012**, *46*, 611−626.
(10) Gao, H.; Liu, Y.; Rumley, M.; Yuan, H.; Mao, B. *Rapid Commun. Mass Spectrom.* **2009**, *23*, 3423−3430.
(11) Li, S.; Limbach, P. A. *Analyst* **2013**, *138*, 1386−1394.
(12) Li, S.; Limbach, P. A. *Anal. Chem.* **2012**, *84*, 8607−8613.
(13) Pomerantz, S. C.; McCloskey, J. A. *Anal. Chem.* **2005**, *77*, 4687−4697.
(14) Farand, J.; Beverly, M. *Anal. Chem.* **2008**, *80*, 7414−7421.
(15) Farand, J.; Gosselin, F. *Anal. Chem.* **2009**, *81*, 3723−3730.
(16) Wang, B. H.; Hopkins, C. E.; Belenky, A. B.; Cohen, A. S. *Int. J. Mass Spectrom. Ion Processes* **1997**, *169/170*, 331−350.
(17) Taucher, M.; Breuker, K. *Angew. Chem., Int. Ed.* **2012**, *51*, 11289−11292.
(18) Smith, S. I.; Brodbelt, J. S. *Anal. Chem.* **2011**, *83*, 303−310.
(19) Gao, Y.; McLuckey, S. A. *J. Mass Spectrom.* **2012**, *47*, 364−369.
(20) McLuckey, S. A.; Van Berkel, G. J.; Glish, G. L. *J. Am. Soc. Mass Spectrom.* **1992**, *3*, 60−70.
(21) McLuckey, S. A.; Vaidyanathan, G.; Habibi-Goudarzi, S. *J. Mass Spectrom.* **1995**, *30*, 1222−1229.
(22) Pan, S.; Verhoeven, K.; Lee, J. K. *J. Am. Soc. Mass Spectrom.* **2005**, *16*, 1853−1865.
(23) Wu, J.; McLuckey, S. A. *Int. J. Mass Spectrom.* **2004**, *237*, 197−241.
(24) Tromp, J. M.; Schürch, S. *J. Am. Soc. Mass Spectrom.* **2005**, *16*, 1262−1268.
(25) Schürch, S.; Bernal-Méndez, E.; Leumann, C. J. *J. Am. Soc. Mass Spectrom.* **2002**, *13*, 936−945.
(26) Andersen, T. E.; Kirpekar, F.; Haselmann, K. F. *J. Am. Soc. Mass Spectrom.* **2006**, *17*, 1353−1368.
(27) McLuckey, S. A.; Stephenson, J. L., Jr.; O'Hair, R. A. J. *J. Am. Soc. Mass Spectrom.* **1997**, *8*, 148−154.
(28) Smith, S. I.; Brodbelt, J. S. *Anal. Chem.* **2010**, *82*, 7218−7226.
(29) Gao, Y.; McLuckey, S. A. *Rapid Commun. Mass Spectrom.* **2013**, *27*, 249−257.
(30) Yang, J.; Håkansson, K. *Eur. J. Mass Spectrom.* **2009**, *15*, 293−304.
(31) Haringsma, H. J.; Li, J. L.; Kenski, D. M.; Flanagan, W. M.; Willingham, A. T. *Nucleic Acids Res.* **2012**, *40*, 4125−4136.
(32) Greig, M.; Griffey, R. H. *Rapid Commun. Mass Spectrom.* **1995**, *9*, 97−102.
(33) Xia, Y.; Chrisman, P. A.; Erickson, D. E.; Liu, J.; Liang, X.; Londry, F. A.; Yang, M. J.; McLuckey, S. A. *Anal. Chem.* **2006**, *78*, 4146−4154.
(34) Xia, Y.; Liang, X.; McLuckey, S. A. *J. Am. Soc. Mass Spectrom.* **2005**, *16*, 1750−1756.
(35) Loboda, A.; Krutchinsky, A.; Loboda, O.; McNabb, J.; Spicer, V.; Ens, W.; Standing, K. *Eur. J. Mass Spectrom.* **2000**, *6*, 531−536.
(36) Liu, J.; Huang, T.-Y.; McLuckey, S. A. *Anal. Chem.* **2009**, *81*, 2159−2167.
(37) Xia, Y.; Thomson, B. A.; McLuckey, S. A. *Anal. Chem.* **2007**, *79*, 8199−8206.
(38) Rodgers, M. T.; Campbell, S.; Marzluff, E. M.; Beauchamp, J. L. *Int. J. Mass Spectrom.* **1994**, *137*, 121−149.
(39) Habibi-Ghoudarzi, S.; McLuckey, S. A. *J. Am. Soc. Mass Spectrom.* **1995**, *6*, 102−113.